AEROSOL GROWTH PROCESSES IN AN ATMOSPHERE CONTAINING A DILUTE, REACTING GAS

by

Peter William Cains B.Sc.(Eng) A.C.G.I.

A Thesis submitted for the degree of Doctor of Philosophy of the University of London.

Imperial College of Science and Technology

1975

ABSTRACT

This thesis comprises a study of the phenomena occurring in an aerosol of manganous sulphate solution droplets in the presence of low concentrations of sulphur dioxide. A quantitative survey has been made of the processes occurring in the system, and the most important of these, particle growth and coagulation, have been considered in some detail. Particle growth occurs due to the catalytic oxidation of sulphur dioxide to sulphuric acid in the droplets and the consequent absorption of water from the ambient atmosphere.

An experimental system was developed to enable the determination of the constitution of the aerosol/gas mixture after a number of contact times varying from 0.7 to 25 mins. Measurements of aerosol nucleus size (by electron microscopy), aerosol droplet size (by light scattering) and of sulphur dioxide concentration in the ambient atmosphere were taken for six different contact times. The aerosol nucleus size measurements were made in the absence of sulphur dioxide, and droplet size determination was carried out in both the absence and presence of reacting gas.

Of the measuring techniques used, the light scattering determination of droplet size yielded the most useful results. The technique used to determine nucleus size was impaired by statistical considerations in the sampling. The results from the measurement of sulphur dioxide concentration were of limited value, owing to absorption of gas into liquid deposited on the apparatus walls.

Experimental results in the absence of sulphur dioxide indicate good agreement with predictions from the theory of Brownian coagulation. In the presence of sulphur dioxide, appreciable growth was observed at the larger aerosol/gas contact times. Given the limitations of the experimental procedure, these results are in reasonable agreement with values obtained from the theoretical analysis.

ACKNOWLEDGEMENTS.

I would like to thank Prof. A. R. Ubbelohde C.B.E. F.R.S. for allowing the work to be carried out in the Dept. of Chemical Engineering and Chemical Technology of Imperial College.

My sincerest thanks go to Dr. M. D. Carabine for his supervision of the project and for his useful suggestions and ideas during the course of the work. I would also like to thank my former colleagues, Dr. J. E. L. Maddock and Dr. A. P. Moore, for helpful discussion during the earlier stages of the work.

Thanks are also due to all members of the technical and support staffs that have assisted during the course of the work. In particular, I would like to thank Mrs. B. A. Robinson for help with the electron microscopy and advice on preparing specimen grids, Mr. P. L. Bird and his staff of the Analytical Services Laboratory for prompt and accurate analysis of samples of manganous sulphate solution, Mr. J. Harris for the design and construction of the reciprocating-head thermal precipitator, Messrs. A. Jones, C. Smith, and K. Gross for their work on the glassware, and Mr. C. Birmingham for advice on the computing involved in the processing of experimental results.

Finally, I would like to thank Mrs. Pam Rowley for her prompt and accurate typing of this thesis.

CONTENTS

ILLUSTRATIONS AND TABLES

Plates

Illustrations

Tables

GLOSSARY OF PRINCIPAL SYMBOLS

a	Particle diameter
a_M	Modal particle diameter
a_m	Median particle diameter
$\bar{a}_3$	Mass mean particle diameter
f	Particle shape factor
i_1, i_2	Mie Coefficients
k	Boltzmann's constant
$k_1, k_2 .. k_7$	Reaction rate constants
k_2', k_6'	Pseudo-rate constants
m	Particle mass
$n(v,t)$	Number density of particles of volume v at time t
p	Vapour pressure of solution
p_o	Saturated vapour pressure of water
p_a	Vapour pressure over droplet of diameter a
$p(a)da$	Particle size distribution density function
r	Particle radius
t	time
$\bar{u}$	mean velocity
v	particle volume
A	Cunningham correction factor
D	Particle diffusivity
$G(v,t)$	Growth rate of particle
H	Henry's constant for sulphur dioxide
I_1, I_2	Scattered light intensity
$I(t)$	Volume-independent growth rate
K_s	Reaction rate constant
N	Particle number concentration
α	Dimensionless particle size
β	Particle collision parameter
θ	Scattering angle
λ	Mean free path of gas molecules

λ_1, λ_2	Mean free path of particles
η	Refractive index; viscosity
μ	Viscosity; dimensionless parameter
σ	Standard deviation
σ_o	ZOLD spread parameter
ϕ	Volume fraction of particles
(Z)	Liquid phase concentration of species Z
[Z]	Gas phase concentration of species Z

Subscript o refers to conditions at t = 0

1. INTRODUCTION

Disperse particulate matter of both natural and anthropogenic origin is normally assumed to be present at all times in the lower atmosphere. Much of this consists of particles in the size range commonly referred to by the term 'aerosol', that is, particles within or just beyond the scope of the optical microscope. Natural aerosols are formed by a number of processes, such as the homogeneous nucleation of water in masses of supersaturated air, or the dispersion of sea water by breaking waves. Fogs, mists and clouds represent regions of high particulate concentration. Anthropogenic aerosols arise largely from the constituents of industrial effluents, either directly, or indirectly via particle forming reactions between gases present in the effluent, e.g. the reaction between ammonia and sulphur dioxide.

The most important processes influencing the number concentration and particle size distribution of atmospheric aerosols are nucleation (formation), particle growth, particle coagulation, and the loss of particles to the earth's surface. In many respects a system of aerosol particles is analagous to a colloidal suspension of solid in liquid; the comparison was made by Schmauss (115) with regard to cloud particles. There are a number of mechanisms by which nucleation of particles may occur. The homogeneous condensation of pure, supersaturated vapours in the absence of foreign particles has been extensively investigated (28, 85). If small particles of foreign substances are present then the process of heterogeneous nucleation takes place with the particles acting as nuclei for condensation (85). Also, nucleation may take place due to chemical interactions of trace substances, often involving natural phenomena such as sunlight or atmospheric electrical discharges (125). An example of this type of process is the photochemical reaction resulting in the formation of so-called 'photochemical smog', which

occurs in atmospheres polluted with oxides of nitrogen and unsaturated hydrocarbons (8). The processes of particle growth and particle coagulation will be dealt with in detail later. The mechanisms by which particles are lost to the earth's surface are principally sedimentation, which is only appreciable for large particles, and washout by precipitation, which is discussed by Junge (62, 64). Extensive measurements of the particle size distribution, number concentration, and chemical constitution of atmospheric aerosols have been reported by Junge (61 - 64), along with attempts to relate the data obtained at various locations to information regarding the sources and dispersion mechanisms of the aerosols.

A constituent of many polluted atmospheres is sulphur dioxide. In particular, high concentrations are to be found in areas where coal is burned as a source of power, since coal invariably contains traces of sulphur (64). Its important atmospheric reactions have been summarised by Carabine (8). The most important products of these reactions, from the point of view of air pollution, are ammonium sulphate and sulphuric acid. The latter is especially important, since the toxicity of sulphuric acid aerosol is greater than that of sulphur dioxide. Moreover, Firket (30), referring to the result of the enquiry into the Meuse Valley disaster of 1930 noted that the physiological effects of the two substances are different; sulphuric acid droplets would be fixed by the superior respiratory ducts, trachea and bronchii, resulting in symptoms of asthma, while sulphur dioxide would penetrate into the cavities of the lungs and produce edema, resulting in symptoms of anoxaemia with acidosis. The report leaves little doubt that the disaster, in which sixty-three people died, was brought about by the presence of a high concentration of sulphur dioxide in the atmosphere, and states that it is probable that part of the sulphur dioxide had been oxidised to sulphuric acid.

Gerhard and Johnstone (40) examined experimentally the photochemical oxidation of sulphur dioxide in the concentration range of 5 - 30 ppm. From their results they predicted that the photochemical oxidation to sulphur trioxide, which would then combine with water vapour present to form droplets of sulphuric acid, would proceed at a rate of 0.1 - 0.2% $hr.^{-1}$ under conditions of intense natural sunlight. This led to the conclusion that other mechanisms, such as oxidation in solution, are probably more effective in oxidising sulphur dioxide to sulphuric acid. This contention is supported by the fact that Coste and Courtier (15) found that the free sulphuric acid content of London air under normal meteorological conditions (i.e. low humidity, low sulphur dioxide concentration of the order of 10^{-3} to 10^{-2} ppm) was very low compared with the concentration of sulphur dioxide. In the Meuse Valley at the time of the disaster (when the humidity and the sulphur dioxide concentration were high) a thick smog was present. Hence, it is probable that the sulphuric acid present in the atmosphere at the time was produced by the oxidation of sulphur dioxide dissolved in smog droplets.

The rate of oxidation of sulphur dioxide in pure water in contact with atmospheric oxygen is slow, however the presence of salts of some transition metals greatly accelerates the reaction. Johnstone (57) investigated the effects of manganous, cupric and ferric salts on the efficiency of absorption of sulphur dioxide into water. He found that the salts of all the above metals increased the absorption rate by increasing the oxidation rate of the sulphur dioxide in solution, and that by far the most efficient catalysts were the manganous salts. Vasil'ev et. al. (124) found that the presence of 0.01% manganous sulphate produced a seven-fold increase in the oxidation rate of sulphur dioxide solutions. It would thus appear reasonable to conclude that transition metal salts present in the atmosphere in aerosol form would greatly increase the amount of sulphuric acid present in a sulphur dioxide polluted environment.

This study is an attempt to monitor changes in the particle size distribution of an aqueous aerosol containing manganous sulphate during the formation of sulphuric acid in the aerosol by the catalytic oxidation of sulphur dioxide at a concentration typical of a polluted atmosphere. An artificially generated aerosol of pure manganous sulphate solution is contacted with air containing such a concentration of sulphur dioxide gas in a series of tubular reaction vessels. Attempts have been made to measure the sulphur dioxide concentration of the contacted gas and the particle size distribution of the aerosol after a series of reaction times. The reaction time is variable up to about twenty-five minutes. The constitution of the aerosol in the absence of sulphur dioxide has also been monitored, since coagulation is expected to account for considerable changes in both the aerosol number concentration and the particle size distribution. A light scattering technique has been used for the monitoring of the particle size distribution in both cases. Also, samples of the aerosol (in the absence of sulphur dioxide) have been taken with the aid of a thermal precipitator, and the dry manganous sulphate 'nuclei' of the aerosol examined under an electron microscope, to determine the number concentration and size distribution changes of the nuclei caused by coagulation. Chapter 2 of this work is devoted to a description and discussion of these methods of measuring particle size.

The changes in the particle size distribution during contact will be influenced by two factors:-

(i) coagulation of the aerosol, and

(ii) growth of the aerosol. The formation of sulphuric acid in a droplet reduces the vapour pressure of the droplet, and consequently a vapour pressure gradient is set up between the droplet surface and the ambient gas. This results in the diffusion of water vapour into the droplets, and hence growth. Both of these phenomena have been studied

in isolation. This work will be reviewed in Chapter 3. However, very little work has so far been carried out on the simultaneous effects of the two together. Recently, Wadden and co-workers (126, 127) have formulated a steady-state model for the combined effects of coagulation and growth due to sulphur dioxide oxidation; the applicability of their results will be discussed in Chapter 3.

Chapter 4 deals with the details of the experimental system, viz. the generation and containment of the aerosol, the sulphur dioxide dosing system, and the attempt to monitor sulphur dioxide concentration. As previously stated, the details of the experimental methods used to determine particle size will be given in Chapter 2. The results of these experiments will be discussed in Chapter 5, with reference to both the performance of the apparatus and theoretical predictions.

2. THE MEASUREMENT OF PARTICLE SIZE

2.1. Monodisperse and Polydisperse Particulate Aggregates

Before discussing methods of determining particle size it is appropriate to make some comments on the characterisation of monodisperse and polydisperse aerosol systems. Clearly, the total amount of dispersed substance present is dependent on the number concentration and mean particulate volume of the aerosol. Monodisperse aerosols do not normally occur naturally and are difficult to generate artificially. The particle size of a polydisperse aerosol is often described by mean diameters with respect to a property such as volume or surface. These are defined by equation of the total volume (or surface, mass, etc) in the dispersion to the product of the total number of particles and the volume (surface, mass, etc.) of the particle of said mean diameter. Thus, for example, the mass mean diameter describes a particle with a mass equal to the average mass of the particles in the dispersion.

The terms used for the characterisation of aerosols in this work will now be formally defined, and the relationships between them will be given.

(i) The number concentration of the aerosol, N, is defined as the total number of particles per unit volume of aerosol. For monodisperse aerosols this quantity together with the particle size is sufficient to describe the aerosol.

(ii) The particle size distribution density function of a polydisperse aerosol is defined as follows:-

$$Pr(\xi_1 \leq \xi \leq \xi_2) = \int_{\xi_1}^{\xi_2} p(\xi)\, d\xi \qquad (2.1)$$

where ξ is a determinant of particle size, normally particle diameter or particle volume.

$p(\xi)$ is the size distribution density function in terms of the size determinant ξ.

$Pr(\xi_1 \leq \xi \leq \xi_2)$ is the probability that ξ lies in the range between and including values ξ_1 and ξ_2 $(\xi_1 < \xi_2)$.

Forms of $p(\xi)$ will be discussed in the next section. The use of a continuous function to describe particle size implies the presence of a large number of particles, such that the discrete intervals between adjacent size groupings of particles may be neglected. If this is not the case, then an equation analagous to (2.1) may be used to describe the particle size distribution in terms of discrete size groupings.

The above quantities, the number concentration and size distribution density function, are sufficient to characterise a polydisperse aerosol. However, it will be useful to introduce two more quantities as follows:-

(iii) The number density distribution of the aerosol, $n(\xi)d\xi$, defined as the number of particles per unit volume of aerosol having a particle size determinant (diameter or volume) between ξ and $\xi + d\xi$

Clearly, since $p(\xi)$ is normalised.

$$n(\xi)d\xi = N \cdot p(\xi)d\xi \quad . \quad . \quad . \quad . \quad . \quad (2.2)$$

(iv) The volume concentration of the aerosol, ϕ, defined as the total volume occupied by the particles per unit volume of aerosol.

$$\phi = \frac{\pi}{6} N \bar{a}_3^3 \quad . \quad . \quad . \quad . \quad . \quad (2.3)$$

where $\bar{a}_3$ is the mass mean diameter of the dispersion. In equation (2.3) it is assumed that the particles are of uniform density. If this is not so, $\bar{a}_3$ must be replaced by the volume mean diameter of the particles. Since, however, in this work, the density of the particulate matter of the aerosol at any given time may be considered

constant, equation (2.3) applies in the form given. $\bar{a}_3$ is normally obtainable from $p(\xi)$, as will be demonstrated in the next section.

2.2. Particle Size Distributions

In this section the form of the particle size distribution density function, $p(\xi)$, defined in the last section, will be discussed. Here, and in the remainder of this chapter, the size determinant of the particles ξ will be taken to be the particle diameter a. If distribution functions are required as a function of particle volume, a simple transformation of variable may be applied to the given functions.

The best known and most universally applied distribution function is the normal distribution. This is a function of two parameters, the mean value and the standard deviation of the population. It is symmetrical about the mean value and admits negative numbers. Since negative particle sizes are inadmissible, the function cannot strictly be used to model particle size distributions. Furthermore, particle size distributions are often positively skewed. A useful form of the particle size distribution function must not only adequately represent particle size distribution data but must also be simple enough for its parameters to be experimentally determinable.

Nakagaki and Shimoyama (101) attempted to devise a method for determining the parameters of a three parameter distribution function by measuring light scattering intensities at three angles. They found, however, that in order to determine the parameters with an accuracy of $\pm$ 4% the experimental accuracy would have to be within $\pm$ 0.2%. Consequently, they recommend that a two parameter function should be used. A well known function containing two parameters and satisfying the constraints outlined in the previous paragraph is the logarithmic normal distribution.

$$p(a)\,da = \frac{1}{2\pi\,\sigma_g\,a}\exp\left[\frac{-(\ln a - \ln a_m)^2}{2\,\sigma_g^2}\right]da \qquad (2.4)$$

where the parameters are:-

a_m, the median diameter. This is equal to the geometric mean diameter.

σ_g, the standard deviation of $(\ln a)$. Its antilogarithm is the geometric mean standard deviation. Orr (104) stated that this form of distribution function often adequately describes droplet size distribution, particularly when the particles are formed by pneumatic atomisation. Also, Matteson and Stöber (86) reported particle size distributions of logarithmic normal form for aerosols produced from a generator similar to the one used in this work (see Section 4.2).

In their studies of sulphur sols, Kerker et. al. (70) used a modified form of the classical logarithmic normal distribution function. It has been analysed by Espenscheid et. al. (29) and has been named the Zeroth Order Logarithmic Distribution, or ZOLD.

$$p(a)da = Z(a_M, \sigma_o)da$$

$$= \frac{1}{\sqrt{2\pi}\, a_M \sigma_o \exp\left(\frac{\sigma_o^2}{2}\right)} \exp\left[\frac{-\left(\ln a - \ln a_M\right)^2}{2\sigma_o^2}\right] da \quad . \quad (2.5)$$

The parameters of this function are as follows:-

a_M is the modal particle diameter, and

σ_o is the zeroth order logarithmic standard deviation, often referred to simply as the spread parameter or spread of the distribution. The mean diameter, $\bar{a}$, and the standard deviation, σ, of the distribution are related to these parameters as follows:-

$$\ln \bar{a} = \ln a_M + \frac{3}{2}\sigma_o^2 \quad . \quad . \quad . \quad (2.6)$$

$$\sigma = a_M\left[\exp(4\sigma_o^2) - \exp(3\sigma_o^2)\right]^{1/2} \quad . \quad . \quad (2.7)$$

Note that σ_o is dimensionless. The advantage that the form of equation (2.5) has over the conventional logarithmic normal function is that σ_o represents solely the spread and skewness of the distribution. Hence

it is possible to explore the effects of changing the spread of the distribution while keeping the mode invariant. The form of the ZOLD function for $a_M = 0.2$ μm. and various values of σ_o is illustrated in Fig. 2 - I.

Espenscheid et. al. (29) also give the useful mathematical relation

$$\int_0^\infty a^n \exp\left[\frac{-(\ln a - \ln a_n)^2}{2\sigma_n^2}\right] da = \sqrt{2\pi}\,\sigma_n a_n^{n+1} \exp\left[\frac{(n+1)^2}{2}\sigma_n^2\right] \quad . \quad (2.8)$$

where a_n, σ_n represent constant parameters. This enables the following quantities to be calculated:-

(i) The moments of the distribution. The most important of these is the mass (or volume) mean diameter, $\bar{a}_3$, for which n=3. Using equations (2.5) and (2.8).

$$\bar{a}_3 = \left[\frac{\int_0^\infty a^3 Z(a_M, \sigma_o) da}{\int_0^\infty Z(a_M, \sigma_o) da}\right]^{1/3} = a_M \exp(2.5\sigma_o^2) \quad . \quad (2.9)$$

(ii) A normalised distribution density function for the volume distribution of the aerosol, $p_v(a)$, may be found. This represents the distribution of volume, or quantity of matter, through the particle size range.

$$p_v(a)da = \frac{1}{\sqrt{2\pi}\,\sigma_o a_M^4 \exp(8\sigma_o^2)} a^3 \exp\left[\frac{-(\ln a - \ln a_M)^2}{2\sigma_o^2}\right] da \quad . \quad (2.10)$$

It is important to note that the function $p_v(a)$, describing distribution of volume, and the function $p(v)$, the number distribution of the particles with respect to the particle volumes, are entirely different in meaning. It is also possible to define a function $p_v(v)$,

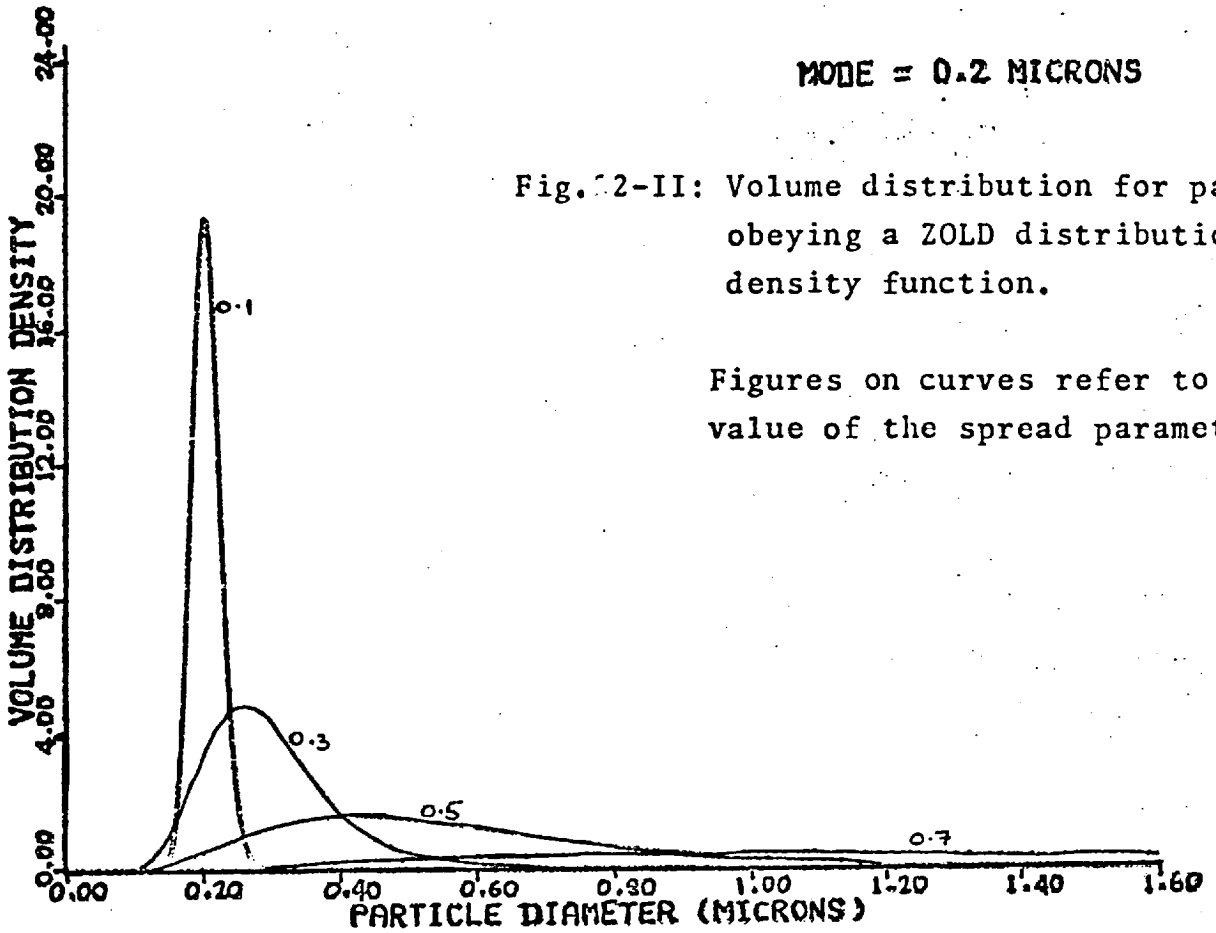

Fig. 2-II: Volume distribution for particles obeying a ZOLD distribution density function.

Figures on curves refer to the value of the spread parameter.

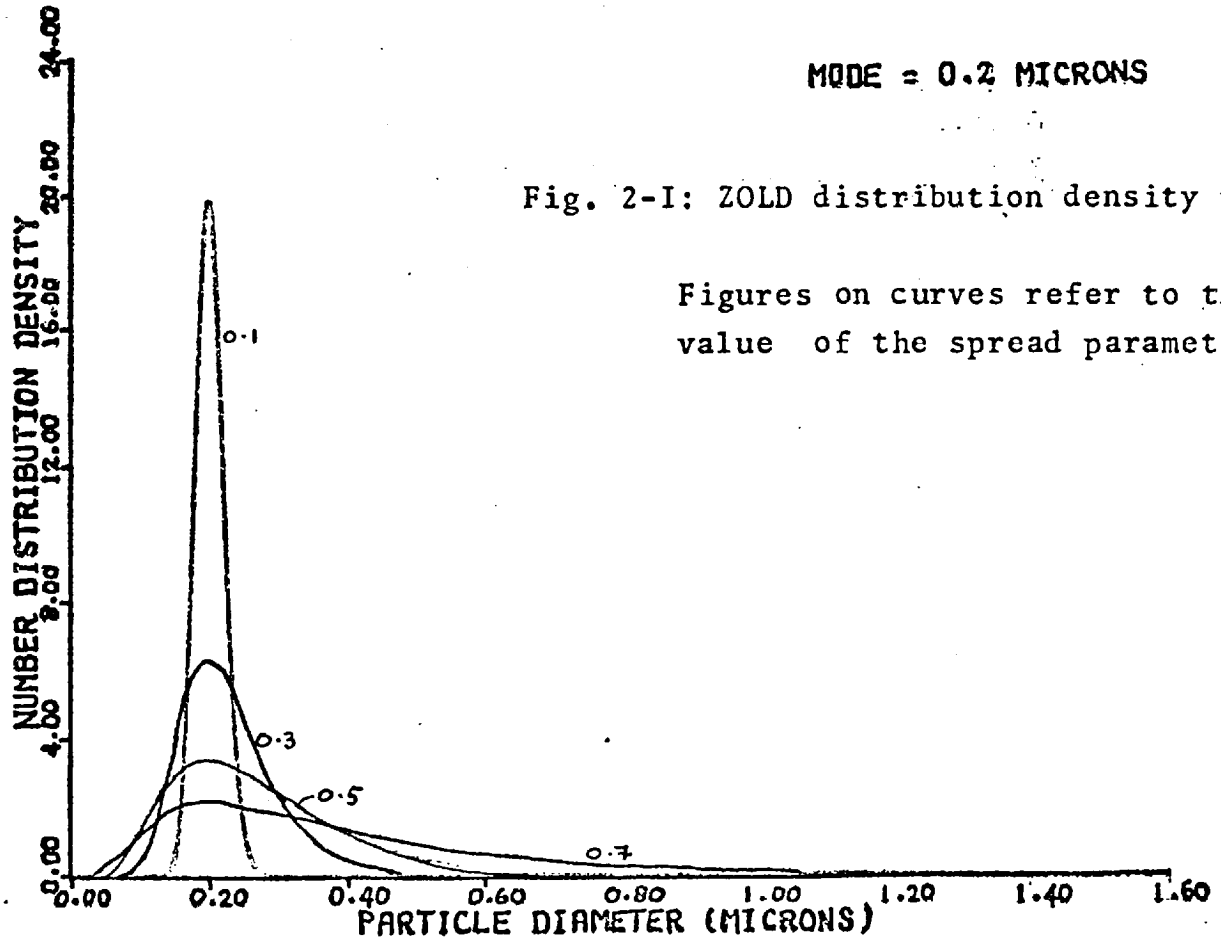

Fig. 2-I: ZOLD distribution density function.

Figures on curves refer to the value of the spread parameter.

the volume distribution of the aerosol with respect to the particle volumes. Analysis of equation (2.10) shows that the value of $p_v(a)$ is a maximum at $a = a_M \exp(3\sigma_o^2)$. The function $p_v(a)$ of equation (2.10) is illustrated in Fig. 2 - II using the values of the parameters (a_M, σ_o) used to plot the ZOLD number distribution function (equation (2.5)) in Fig. 2 - I.

Whereas logarithmic normal type distribution functions appear to be generally accepted for use in experimental situations involving artificially generated aerosols and hydrosols, a brief account will now be given of other distribution functions that have been proposed. Junge (62, 63) found that atmospheric aerosols are generally distributed according to the relationship.

$$p(a) = \frac{\text{constant}}{a^{\beta}} \quad \text{for} \quad 0.2\,\mu\text{m.} < a < 20\,\mu\text{m.} \qquad (2.11)$$

where β is about 4.

For particles with diameters less than 0.2 μm. the curves of $p(a)$ versus a flatten off, and the contribution of these particles to the total atmospheric aerosol volume becomes negligible. Sedunov (119) gives the 'gamma distribution' as the function best describing the particle size distribution in clouds, for the range 4 μm.$<a<$30 - 40 μm.

$$p(a) = \frac{1}{\Gamma(\mu+1)} \cdot \frac{a^{\mu}}{\beta^{\mu+1}} \exp\left(-\frac{a}{\beta}\right) \qquad (2.12)$$

where μ and β are parameters (no details given) and Γ is the gamma function. Sedunov also gives the logarithmic normal function of equation (2.4) as a useful approximating formula in this case.

2.3. Methods of Measuring Particle Size

In Sections 2.1 and 2.2 the representation of polydisperse aerosols in terms of distribution functions was discussed. The rest of this chapter will be devoted to a description of the methods of particle size measurement used in this work. In this section a general review of available techniques and their applicability to the measurements required will be given, whilst in Sections 2.4 and 2.5 a full description of the methods used will be undertaken. It should be noted that this section does not represent a comprehensive survey of methods available for particle size evaluation, but is merely a review of methods applicable to this study.

Firstly, it is necessary to consider exactly what information is required from particle size analysis. In this study, particles of manganous sulphate solution are generated and held for various lengths of time in the absence or presence of traces of sulphur dioxide gas. For complete particle size distribution and concentration determination the following scheme is proposed:-

(a) The measurement of the dry, manganous sulphate nuclei. If the aerosol particles are collected, they may be dried, and particle size determination may be carried out on the manganous sulphate residues. From this data the actual shape of the particle size distribution of the aerosol in the absence of sulphur dioxide and sulphuric acid may be found, and the applicability of distribution functions checked. Further, it should be possible to obtain the number concentration of the aerosol and the distribution parameters of the dry manganous sulphate nuclei.

(b) The measurement of the solution droplets. If the actual droplets could be sized kinetically in terms of parameters of a distribution function (checked from the data obtained from (a)), then a complete range of aerosol properties would be obtainable, viz. the number concentration, the particle size distribution and the mean concentration of manganous sulphate in the droplets. Data obtained from (b) would

enable the monitoring of the effects on particle size of sulphur dioxide in the atmosphere containing the particles, and thus, possibly, of the extent of sulphuric acid formation within the droplets.

A number of methods are commonly described (19, 44, 48, 61, 105) for the collection of samples of aerosol particles and their consequent analysis. The methods normally applied in the 0.1 - 10 μm. range involve impaction (44, 61, 105), or thermal or electrostatic precipitation (44). The most common appliances utilising impaction are the Cascade Impactor and the Konimeter. The Konimeter is not suitable for the measurements required by (a), since it is likely that large, liquid particles may be induced to rupture into smaller ones when subjected to the inertial force by which the instrument operates. Furthermore, Junge (61) found that different adhesive substances used on the sampling slide produced different results. The Cascade Impactor sorts the particles into four different, but overlapping, size ranges, and is clearly not suitable for the measurements required by (a). Thermal precipitation involves no large interial forces. It also has a high efficiency in precipitating submicron particles (44). (The aerosol under examination will probably consist mainly of submicron particles). Electrostatic precipitation has been used to sample submicron aerosols (32), but high voltage gradients are required, and investigation has not been nearly as extensive as that of thermal precipitation. Thus, a method utilising thermal precipitation will be used to collect samples, from which the information outlined in (a) should be obtainable. The most useful instrument for the analysis of samples containing submicron particles is the electron microscope. The details of the construction and functioning of the thermal precipitator, together with the method of analysis applied to the samples, will be given in Section 2.4.

To obtain the data outlined in (b), a method is required whereby no physical interference with the aerosol is incurred. The concentration

of manganous sulphate in the aerosol particles is dependent on the humidity of the surrounding air (see Sections 3.1 and 3.3), and any attempt to extract the aerosol into an environment of a different humidity will cause evaporation from, or condensation on to, the particles, changing their size. Recently, much work has been carried out on light scattering methods of determining particle size. These have the great advantage of not interfering with the physical environment or the aerosol (with the possible exception of photochemical effects). A review of methods of particle size determination utilising light scattering will be given in Section 2.5, together with a description of the method to be used in this work.

2.4 The Thermal Precipitator

This section contains a description of the methods of sampling and measurement used to obtain information about the aerosol particle nuclei. Firstly, a description of the thermal precipitator used to sample the deposit will be given, and then the methods of preparing and treating the specimens will be discussed. For particles in the submicron size range, measurement of samples by optical microscopy is almost impossible, therefore a technique utilising electron microscopy has been developed.

The standard, or fixed-head thermal precipitator was originally developed by Green and Watson (45), who required an instrument to enable the estimation of dust hazards in industry. The instrument used for this work was obtained from Casella Ltd., and is almost identical to that described by Drummond (27). The most important part, the sampling head, is shown in profile and section in Fig. 2 - III. The aerosol to be sampled is drawn through the rectangular channel C, 0.508 mm. deep and 1 cm. wide, past a heated wire W. The sample flowrate of 7 cm^3 min^{-1} is maintained by means of an aspirator connected to the downstream end of the head. The water flowing from the aspirator vessels is collected and measured, such that the total volumetric throughput of the aerosol at any time is known. The heated wire carries a constant current of 1.3 amp. which is supplied by an Oldham type M lead/acid cell fitted with a specially designed output rheostat. The temperature of the wire is maintained about 100°C higher than that of the surroundings. The particles flowing past the wire experience a thermophoretic force arising from the thermal gradient between the wire and the channel walls which causes them to accelerate towards the channel walls. The channel walls contain the sampling surface, normally a glass cover slip or a coated electron microscope grid. If a cover slip (S in diagram) is used to collect the sample, normally the case when optical

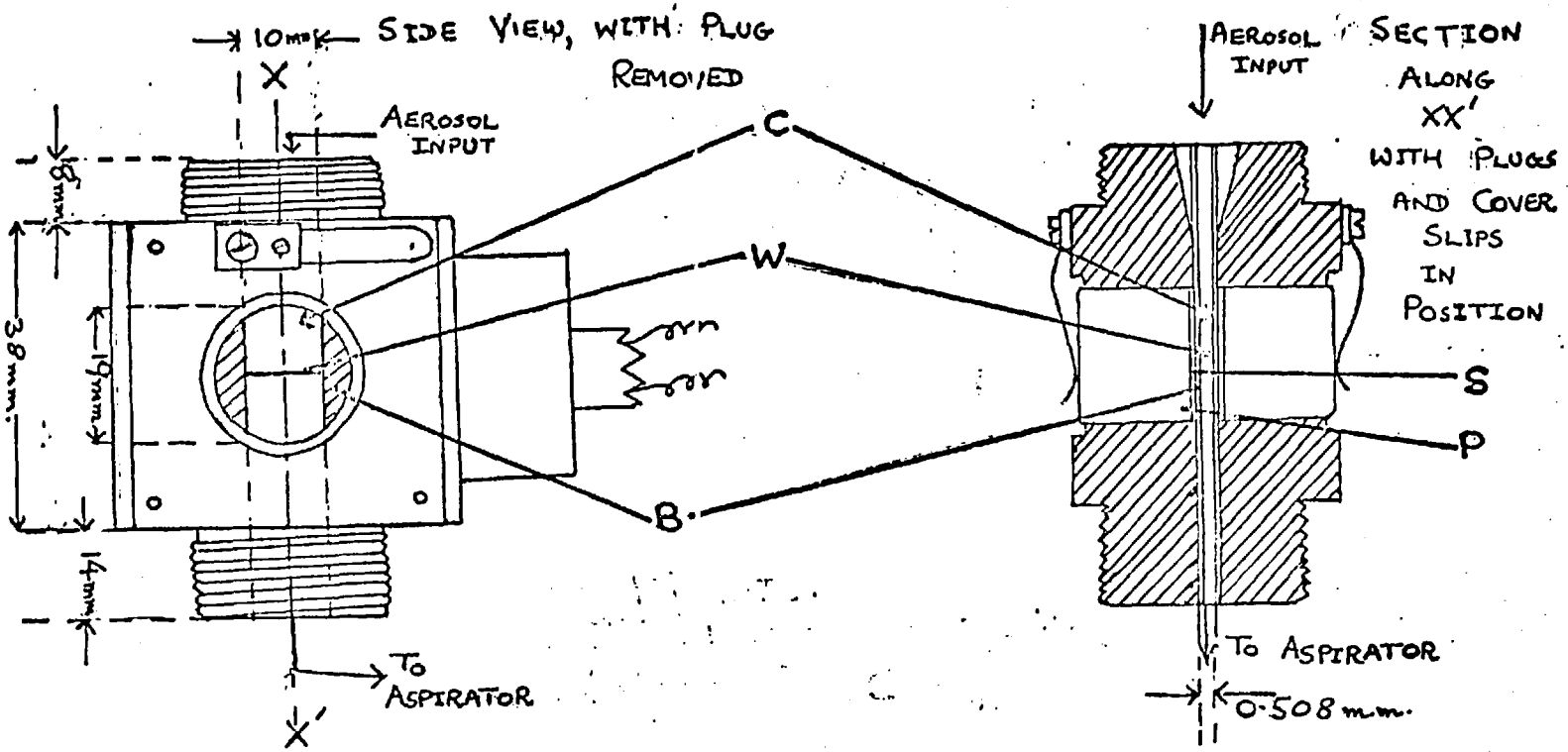

Fig. 2-III: Fixed-head thermal precipitator
(obtained from Cassela Ltd.)

microscopy is to be used to analyse the sample, it is located by a removable plug P. Bakelite spacers B support the slip at a distance of 0.127 mm. from the wire. If it is required to analyse samples using electron microscopy, then a modified plug with recesses into which the grids may be located must be used, with the machined plug face resting on the bakelite spacers and the grid surfaces flush with the plug face. The method of sampling 7 cm^3 min^{-1} from the aerosol will be discussed in Section 4.1.

It has been found, as mentioned in Section 2.3, that the thermal precipitator is very efficient for sampling particles in the submicron size range. Walton (131) found that the sampling efficiency was 100% down to the smallest particle that could then be detected by an electron microscope, about 0.01 μm. in diameter. For larger particles, however, the efficiency is lower. Watson (133) has calculated the loss percentage of particles sampled, i.e. the percentage of particles not precipitated by the instrument, for particle diameters between 2.5 and 30 μm. For 2.5 μm. particles the loss was 1.7%, for 5 and 10 μm. particles 10.6%, and for 30 μm. particles 74.2%. Thus, low experimental values may be expected for particles larger than about 3 μm.

The main drawback of the fixed-head thermal precipitator is that the particle size and number distribution of the sample varies with the distance from the wire. This is illustrated in Fig. 2-VI(a), reproduced from the work of Drummond (27). This inhomogeneity is explained by the fact that different sized particles are deposited along different trajectories, owing to variations in the relative effects of the inertial and thermophoretic forces acting on them. Drummond (27) states that the size distribution of the particles in the region between A and B in Fig. 2-VI(a), about 0.14 - 0.35 mm. upstream of the heating wire, is fairly representative of that of the whole sample, though no data on the number concentration may be obtained from examination of this region. If

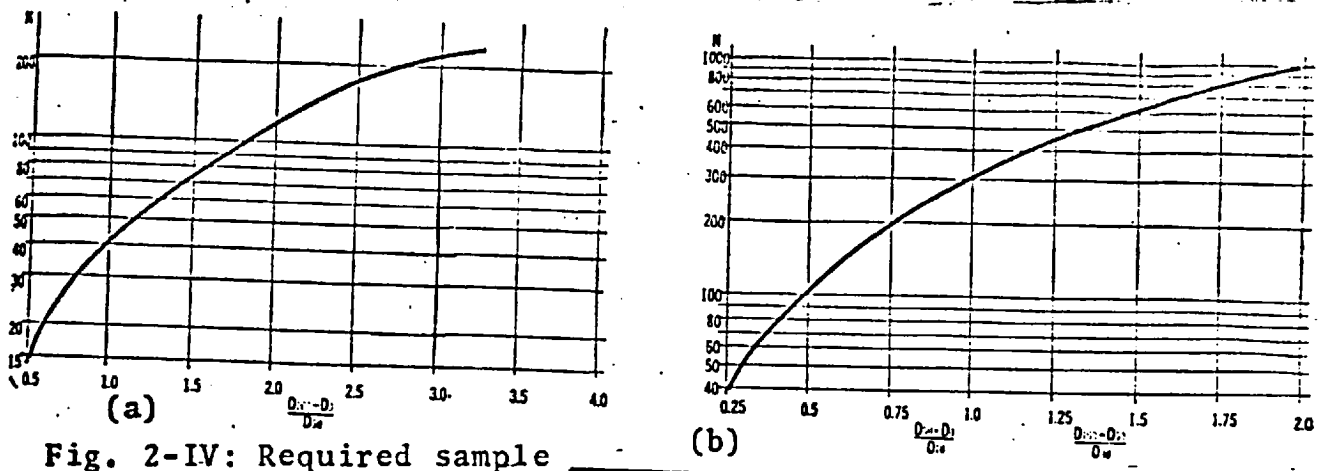

Fig. 2-IV: Required sample size for 99% certainty that (a) the mean particle size, and (b) the particle size distribution is known within 10%. (reproduced from (95))

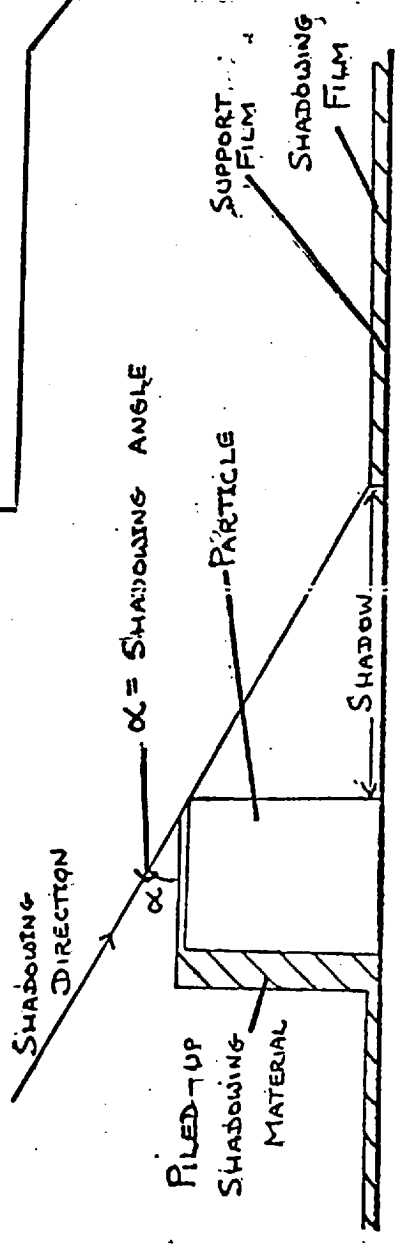

Fig. 2-V: Diagrammatic representation of a shadowed particle (reproduced from (68))

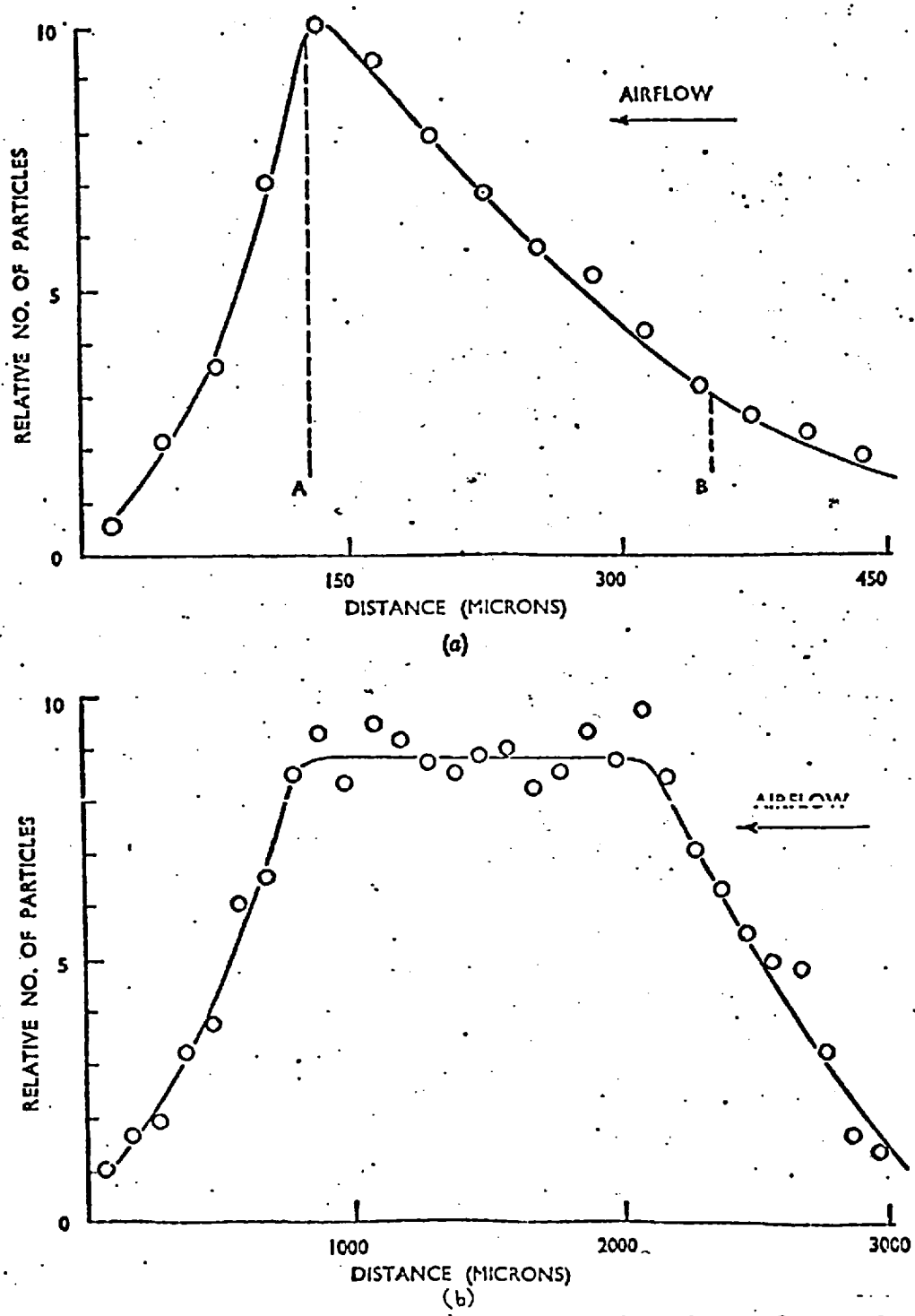

Fig. 2-VI: Variation of number density of sample deposit with distance upstream of the heated wire for
(a) the fixed-head thermal precipitator,
(b) the reciprocating-head thermal precipitator.
(reproduced from (27))

optical microscopy is used to analyse the sample a technique of measuring strips of sample taken perpendicularly to the direction of the precipitator wire may be used to obtain a complete set of data. If electron microscopy is to be used this method cannot be applied, since the area of the sample is restricted to the area of the microscope grid (about 3 mm. in diameter), and also because of the large number of particles that would have to be considered if an entire strip of grid were examined.

To overcome the problem of the inhomogeneity of thermal precipitator samples for electron microscopic examination two methods have been formulated. The first is to modify the instrument such that the sampling stage containing the grid oscillates within the region of precipitating particles (27, 131). Normally, the oscillating sampling stage has an amplitude of about 2 mm. and a period of about 5 s., the velocity of movement being uniform in both directions. The distribution of deposit density for this instrument is shown in Fig. 2-VI(b). It may be seen that the deposit contains an area of constant density about 1 mm. long with the density rapidly falling off on either side of the peak region. The size distribution of the particles in the central uniform area is exactly representative of the sample as a whole, and the number concentration of the particles may be estimated by counting the number of particles in a known area of deposit. The second method advocated to ensure a representative sample is to replace the heated wire of the standard instrument with a heated band or strip, giving a larger region in which the thermal gradient is uniform (128). Walkenhorst (128) describes a precipitator containing two heated bands, 1.5 mm. wide, set 1 cm. apart. Using this instrument, a deposit density curve almost identical to that given by the oscillating, or reciprocating, instrument has been obtained (128), with a central uniform region about 1 mm. wide.

For investigations in this work, an instrument of the first type has been developed, to be compatible with the aspiration and heating current supply facilities of the Casella instrument. The details of the sampling head are illustrated in Fig. 2-VII. The design is almost

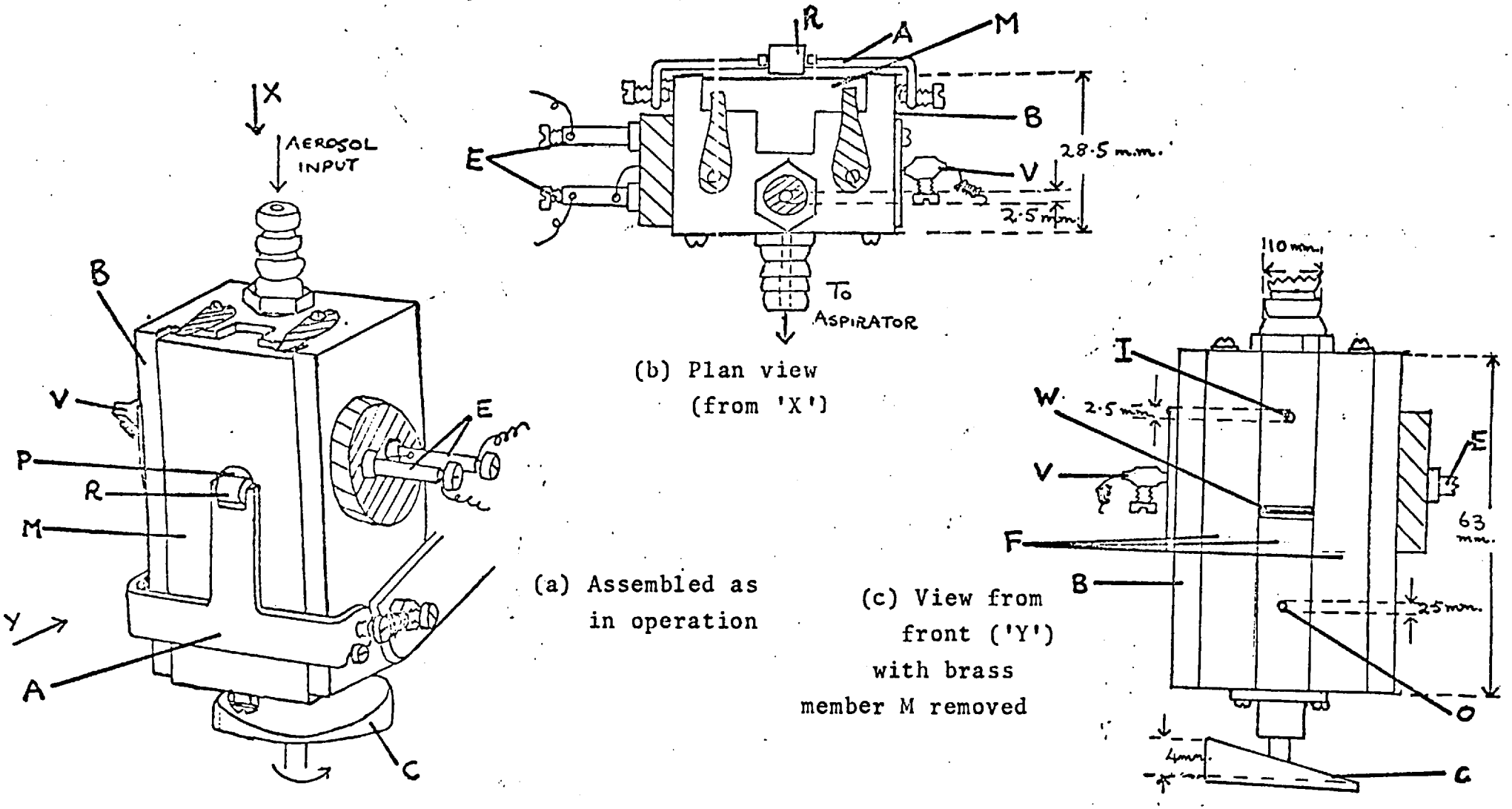

(a) Assembled as in operation

(b) Plan view (from 'X')

(c) View from front ('Y') with brass member M removed

Fig. 2-VII: Reciprocating-head thermal precipitator.

Fig. 2-VII (continued)

(d) Detail of member M: front and side views

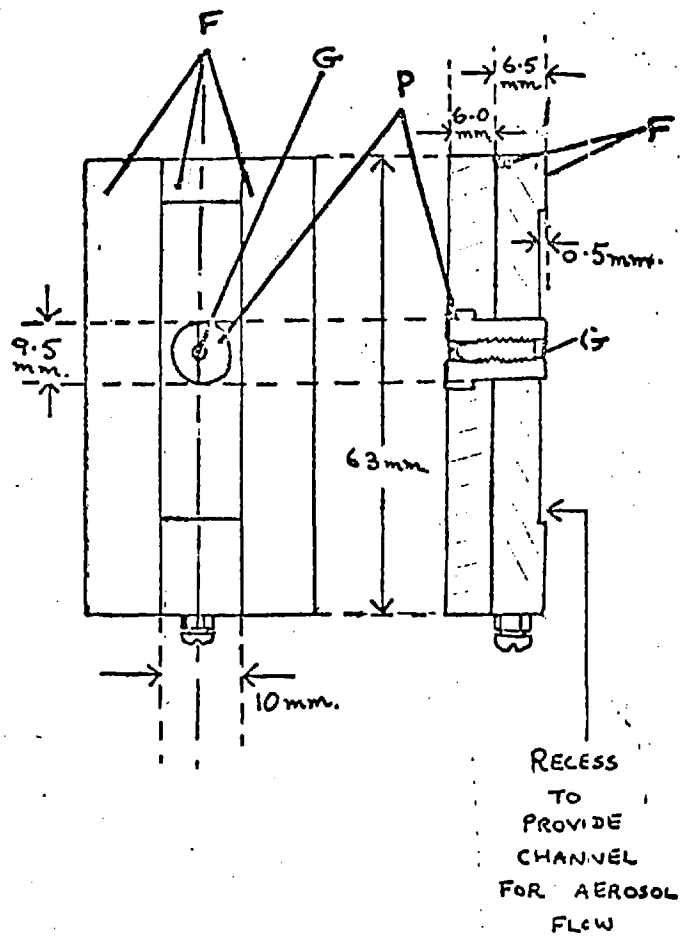

(e) Detail of plug P

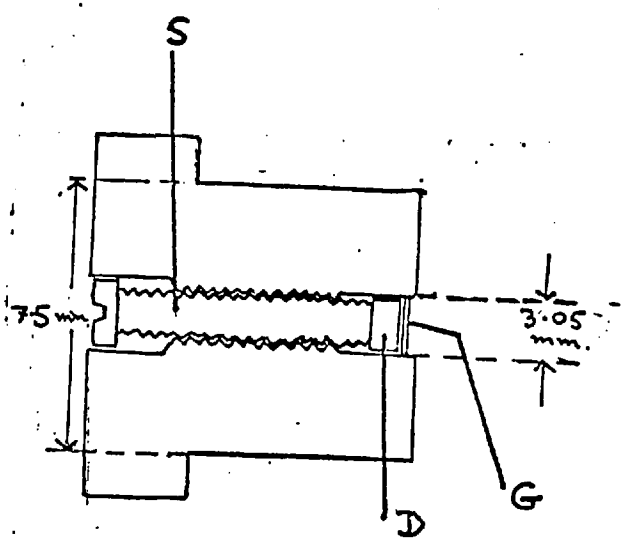

identical to that given by Drummond (27). A plug P, containing the mounted electron microscope grid G, fits into a brass member M, which fits into the main body of the instrument B. The main body of the instrument contains the heated wire W and the aerosol inlet and outlet ports, I and O respectively. The base of the instrument body B is attached to a rotating cam C which actuates the reciprocating motion of the member M. The member slides along machined faces F. the aerosol flowing through a channel provided by a recess in its inner face, as shown in Fig. 2-VII(d). The plug and member are held in place by a spring-loaded arm A, at the top of which is a rotatable cylinder R. The cylinder presses the plug and member in position while the oscillation proceeds. The cam C, which produces a reciprocating motion of 2 mm. amplitude, is rotated by a 5 R.P.M. electric motor. The current to the heated tungsten wire W is transmitted via electrodes E. The small hollow brass cylinder V into which the end of the wire is connected is separate from the instrument body and acts as a weight to ensure that thermal expansion does not distort the wire out of its location. The electron microscope grid G is attached to a small circular cylinder D in the plug P using a trace of silver dag as adhesive. The position of the cylinder D can be adjusted with screw S such that the grid surface is flush with the plug face.

The grids used were standard 400 mesh copper grids, 3.05 mm. in diameter, obtained from Polaron Ltd. Before sampling, it was necessary to coat the grids with a sample support film. The commonest substances used for preparing support films are formvar and collodion. However, these both have the disadvantage of being unstable at high temperatures. Consequently, carbon was selected as the best substance for producing sample support films, since it is more stable at the high temperatures involved in the sampling and subsequent treatment of the grids. A floation method was employed to coat the grids. A film of carbon, approximately 10 mμm. thick, was deposited on to mica strips by vacuum

evaporation and recondensation. The deposited films were then floated off the mica on to the surface of a vessel of water in which a number of grids had been previously immersed. The grids were then lifted through the floating film, which adhered to the grid surfaces, and were subsequently dried and stored in a vacuum dessicator.

After the sampling in the thermal precipitator had taken place, the sampling grid was removed and placed in an oven at 105°C for one hour to ensure that the sample particles were dry. (For discussion of this procedure see Section 5.1(a)). They were subsequently examined under a transmission electron microscope (JEOL 7 or JEM 100B) and sample photographs were taken. Examples of these results are given in Section 5.1(a). The plates obtained were then projected on to the screen of a PCD Projector Analyser/Digital Reading System and the particle images were sized. Each particle was characterised by a pair of co-ordinates, one for each end of the diameter of the particle. The pairs of co-ordinates were punched on to paper tape by the instrument, ready for computer analysis. Normally, about five sample grids were taken for each set of conditions, and all plates taken from these were considered together as a single sample of aerosol.

The plates obtained from the straightforward examination of samples with a transmission electron microscope only yield a two-dimensional image of the particles on the grids. Since we require the volumes of the manganous sulphate particle nuclei we need to obtain some information about the third dimension of the sampled particles. For this purpose, some samples were shadow-casted before examination. The technique of shadow-casting is described by Bradley (68), and is represented diagrammatically in Fig. 2-V. A layer of electron dense material is deposited, by vacuum evaporation and recondensation, on to the specimen, which is tilted at an angle α to the direction of incidence or shadowing. From Fig. 2-V it can be seen that areas shielded by sample particles from the impinging beam of atoms will appear more transparent on examination, and will thus produce shadows. Hence, the third dimension of the

particle may be obtained by measurement of the shadow dimension. The material chosen for shadowing was a gold/palladium alloy (60% gold, 40% palladium) since this produces a high contrast and is relatively cheap as a shadowing material. Its only disadvantage is its tendency to granulate on the sample, limiting resolution to 5 - 10 nm. (68). This is considerably less than the expected size of the smallest particles to be considered in this work. Samples were shadowed at $\alpha = 25^{\circ}$ (Fig. 2-V), the calculations involved being carried out using formulae and data given by Bradley (68), and examples of the plate obtained, with discussion, are given in Section 5.1(a). For these plates, the ratio of the measured thickness of the dry particles to their dimensions, as obtained by measuring the size of the particles perpendicular to the shadowing direction, was calculated and averaged, the result being considered a 'shape factor' for the particles. The results of this analysis are given in Section 5.1(a).

Finally, the data obtained from the samples and stored as described in the last paragraph but one was analysed to check the applicability of the ZOLD particle size distribution function. For this, a computer programme developed by Moore (96) was used. This programme fits the parameters of the ZOLD function, the modal diameter and the spread parameter, to the particle size data using a method of nonlinear least squares, and plots the ZOLD function together with a histogram of the experimental data. The number concentration of the aerosol was also estimated from this data, using the relationship (27)

$$N_A = \frac{N_T}{l\,D} \qquad (2\,13)$$

where N_A is the number of particles per unit area of deposit;

N_T is the total number of particles deposited;

D is the amplitude of the reciprocating motion;

l is the width of the deposit.

If w is the length of the deposit on a stationary slide (i.e. in the direction of aerosol flow) the number of particles deposited per unit area in the region of width $(D-w)$ in the centre of the deposit will be roughly constant. Hence, N_A and consequently N_T and the aerosol particle number concentration may be determined by counting the number of particles on the plates and comparing with the areas of the grids containing the particles counted. For these analyses it is necessary to know the number of particles that must be considered in order that the sample constitutes a fair representation of the population from which it is derived, that is, that the results obtained from the sample represent the conditions in the aerosol from which it was taken. In general, the fractional standard error incurred in sample sizing is proportional to the reciprocal of the square root of the number of particles considered (44). Hence, if number concentration estimates are required it is normal to count about four hundred particles to reduce the standard error to 5%. Walkenhorst (128) states that, for an assessment of particle number concentration free of statistical errors, five hundred to a thousand particles should be counted. Chapman (12) has devised a short-cut method for counting a large number of particles, however, it cannot be used here, since particle size data is also required. If particle size distributions are being considered it is necessary, strictly speaking, to maintain the same level of accuracy over the entire size range. Montgomery (95) has plotted curves giving the number of particles that need to be counted to be 99% certain that (a) the mean particle size and (b) the distribution are known within 10%. These curves are reproduced here as Fig. 2-IV (a) and (b) respectively. Along the abscissa of these curves is plotted the ratio of the diameter of the maximum sized particle minus the diameter of the minimum sized particle to the diameter of the average sized particle,

while the ordinate represents the number of particles counted. It may be seen that, as polydispersity increases, the required sample size increases.

2.5. Determination of Particle Size by Light Scattering

In recent years, much study has been devoted to the development of light scattering techniques to measure the size distribution of aerosols and hydrosols. So far, the particles studied have been mainly spherical, or assumed spherical, since the theory of light scattering by aerosol-sized particles of other shapes has only been developed for a few special cases of limited application. These will not be discussed here, since the droplets under consideration in this work can be assumed to be constantly spherical due to the action of the surface tension of the liquid.

The general solution of the problem of the scattering of a linearly polarised electromagnetic wave by an isotropic, homogeneous sphere was obtained by Mie (90). The derivation of these results is given in a number of standard references, e.g. (5, 69). The light scattered by a particle in a single plane, normally horizontal, is usually considered. The scattering angle, θ , denotes the angle between the direction of the scattered light and the direction of the transmitted light, as illustrated in Fig. 2 - VIII. The incident radiation is assumed to be polarised either perpendicularly to the scattering plane (vertical polarisation) or parallel with it (horizontal polarisation). The formulae giving the scattered radiation intensities will not be given here; it will suffice to say that they are composed of infinite series of Ricatti-Bessel functions and Legendre polynomials. The complexity of these solutions explains the fact that most of the work utilising the Mie Theory has been carried out in recent years, since the development of high-speed digital computers.

The results from the Mie Theory will here be denoted in terms of so-called Mie Coefficients, $i_1(\theta,\alpha)$ and $i_2(\theta,\alpha)$. Here, the subscript 1 denotes that the incident radiation is vertically polarised, while

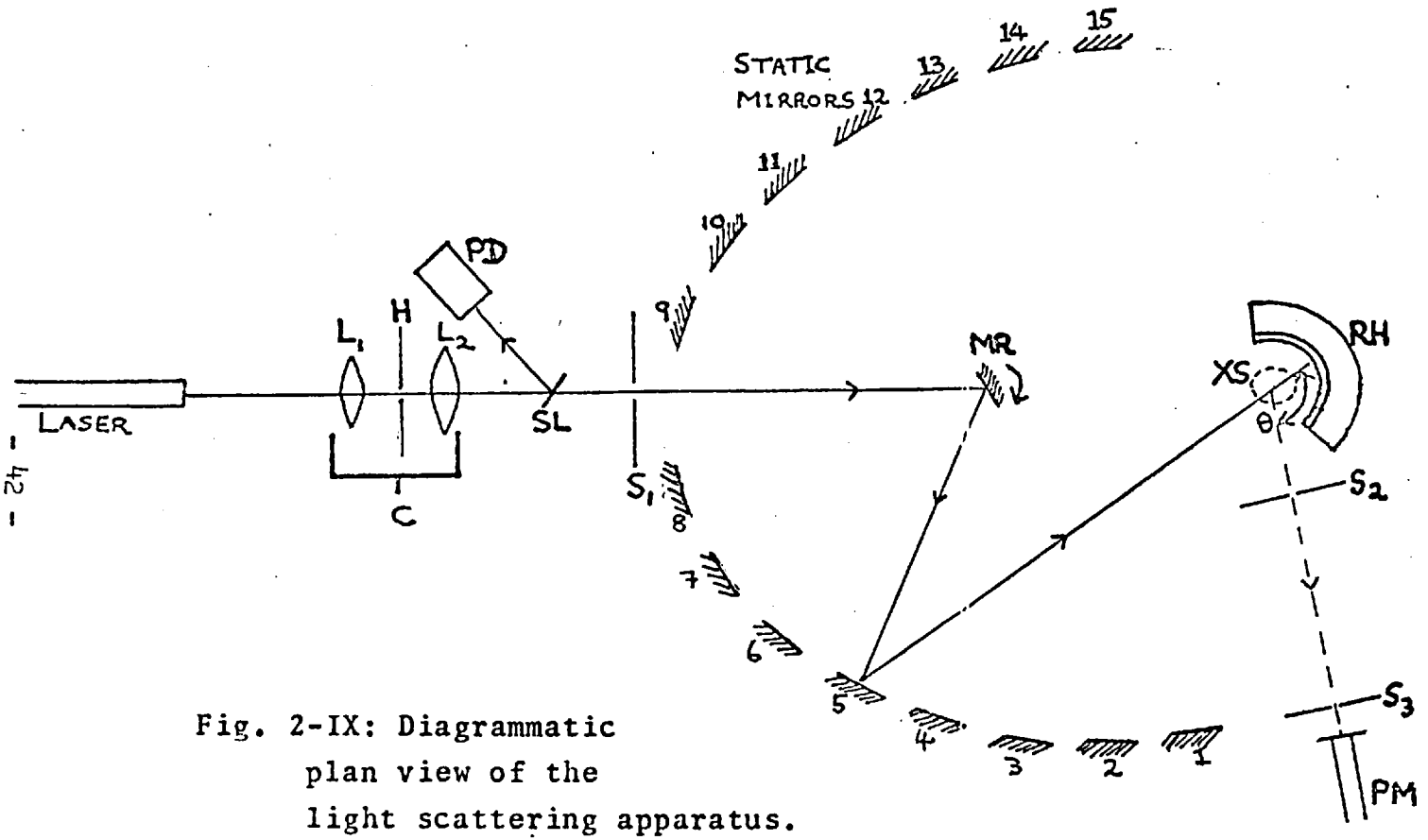

Fig. 2-IX: Diagrammatic plan view of the light scattering apparatus. Arrows denote path of incident laser beam.

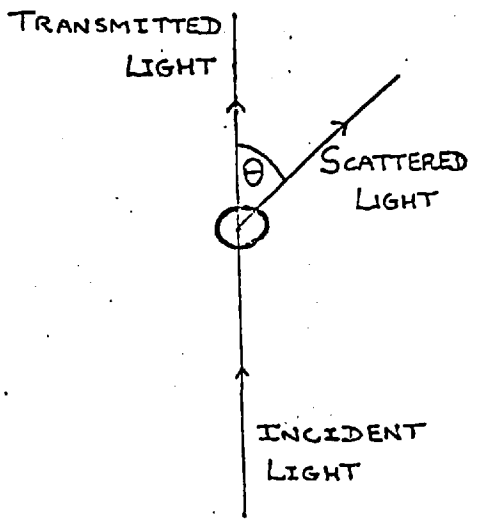

Fig. 2-VIII: Definition of scattering angle .

2 denotes horizontal polarisation, or polarisation in the plane of the scattering plane. θ is the scattering angle, and α is a dimensionless parameter representing particle size, given by

$$\alpha = \frac{\pi a}{\lambda} \quad . \quad . \quad . \quad (2.14)$$

where a is the particle diameter, and

λ is the wavelength of the incident radiation.

Methods of evaluating i_1 and i_2, which represent the relative intensity of light scattered at angle θ by a particle of size characterised by α, are given by Maddock (77) and Moore (96). Both of these authors have presented diagrams showing the relative intensity of light scattered as a function of scattering angle for different values of α. It should be noted at this stage that i_1 and i_2 are also functions of the relative refractive index of the particle with respect to the medium. Since the medium is gaseous, its refractive index may be considered to be unity, and the refractive index of the particle in vacuo, η, may be taken as equal to the required relative refractive index. It is assumed in this work that the particles are non-absorbing, and hence that η is real.

Examination of the scattering patterns of Maddock (77) and Moore (96) show that, if the particles are very small, i.e. $\alpha \leq 0.1$, they give patterns symmetrical about $\theta = 90^\circ$, identical to those predicted by the Rayleigh Theory (56, 110) which treats particles as dipole oscillators. As the particle size increases the patterns become less symmetric, more forward-scattering, and at larger sizes develop a fine structure. In the range $0.1 < \alpha < 2.0$, the minimum in i_2 moves to obtuse angles, with some radiation scattered in the direction of minimum intensity. For $0.1 < \alpha < 1.6$, i_1 is always larger than i_2, and a minimum in i_1 occurs in the backward direction ($\theta > 90^\circ$). At $\alpha = 1.6$, there occurs a strong minimum in i_1, such that i_2 is greater in the backward direction. This minimum moves forward as α increases from 1.7 to 2.2.

At $\alpha = 2.4$ a second minimum in i_1 occurs, slightly forward of the first one and, at about $\alpha = 2.5$, a maximum develops between the two minima. At $\alpha = 2.7$ a second minimum in i_2 forms, and at $\alpha = 3.1$ a third minimum in i_1 occurs. Fourth and fifth minima in i_1 are seen at $\alpha = 3.9$ and 4.1 respectively, while the curve for i_2 becomes more and more complex for $3.0 \leq \alpha \leq 5.0$. Beyond $\alpha = 5$, the numbers of maxima and minima increase rapidly, and the scattering becomes more and more forward-directed until the particle acts as an optical lens with diffraction at the edges, causing a diffraction pattern in the forward direction.

Using the Mie Coefficients defined above, the light scattering patterns of polydisperse aerosols may also be evaluated. If an aerosol has a particle size distribution density function p(a), the light scattered from the aggregate at a scattering angle θ, for vertically polarised light, is

$$I_1(\theta) = \int_0^\infty p(a) i_1(\theta, \alpha) da \quad . \quad . \quad . \quad (2.15)$$

where I_1 is the light scattered. This formula neglects any effects due to multiple scattering, and assumes that it is possible to rigidly define an angle θ which correctly describes the direction of the scattered signal from all particles present. An analagous formula exists for I_2 the light scattered using horizontally polarised incident radiation.

Given that it is possible to calculate the light scattering pattern for either a single particle or an aggregate of particles of known size distribution, the converse problem, i.e. the determination of particle size data from information about the light scattering pattern, will be considered. Reviews of methods available for the measurement of particle size are given by Kerker (69) and Maddock (77, 78). Earlier methods applied to the sizing of monodisperse latexes, such as the location of the first intensity minimum (79), the measurement of the

first red and green orders of the higher order Tyndall Spectra (HOTS) (80), the location of further maxima and minima in the scattering pattern (82), disymmetry at forward-scattering angles (81), and disymmetry between forward and back-scattering angles (26), were found to be unsuitable for the analysis of polydisperse systems. A successful method of sizing polydisperse systems has been developed by Kerker and co-workers (69). This method involves the measurement of the polarisation ratio of the light scattered by the aerosol (i.e. the ratio of the scattered intensity of horizontally polarised light, I_2, to the scattered intensity of vertically polarised light, I_1) at nineteen angles, from $\theta = 40^\circ$ to 130° at 5° intervals. Extensive arrays of theoretical data were generated for different combinations of the ZOLD parameters, a_M and σ_0 (see Section 2.2), at appropriate refractive indices. Hence, values of the ZOLD parameters for an aerosol or hydrosol could be obtained by comparing the experimental values, obtained at each of the nineteen angles, with the stored theoretical values. The combination of a_M and σ_0 giving polarisation ratios that best fit the experimental data were taken as those best describing the size distribution of the system. This method has been used to measure the size distribution of sulphur hydrosols (70), sulphuric acid aerosols (17), and to monitor changes in the size distribution of an aerosol during coagulation (102, 103).

The major drawback of the polarisation ratio method is that, for a ZOLD particle size distribution, $\sigma_0 = 0.3$ represents the upper limit of polydispersity for which the method is applicable, since all distributions more polydisperse than this give polarisation ratio versus scattering angle curves of identical form. That is to say, if the incident light were natural, the scattered light would be nearly completely unpolarised in all directions (69). Wallace and Kratohvil (130), by analysis of errors, determined that, generally, it is only possible to fit a unique pair of ZOLD parameters to a set of light scattering data if $\sigma_0 \leq 0.2$, for particles in the submicron range. A method has been recently developed

in this laboratory (9, 96) which utilises a direct comparison between scattered light intensities, using either vertically or horizontally polarised light, and those predicted by equation (2.15). Light scattered from a laser source is measured at fifteen angles, from about 15° to 165°, and the results obtained by using a least squares method to minimise the function

$$S = \sum_{i=1}^{m} \left[\frac{I_{ne}(\theta_i) - I_n(\theta_i)}{I_{ne}(\theta_i)} \right]^2 \quad . \qquad (2.16)$$

where n = 1 or 2, describing the polarisation of the incident radiation.

I_n is the light scattering intensity for a ZOLD distribution. function, obtained from equation (2.15)

$I_{ne}(\theta_i)$ is the experimentally determined intensity of scattered light at angle θ_i ;

m is the number of angles at which readings are taken.

Moore (96) has developed a computer programme, called SEARCH, which determines values of the ZOLD parameters, a_M and σ_o, such that the function S of equation (2.16) is minimised. Mie Coefficients, $i_n(\theta, \alpha)$ are determined at the fifteen angles at which measurements will be taken, for 1680 values of α, corresponding to particle sizes between 0.001 μm. and 0.6 μm. in 0.001 μm. steps, and between 0.605 μm. and 6.0 μm. in 0.005 μm. steps. These values, for a required refractive index are stored on magnetic tape. The programme SEARCH uses these values to determine $I_n(\theta_i)$ from equation (2.15), and hence to obtain S from equation (2.16). Tests with theoretically derived data and with latexes have shown that, for vertically polarised light, good results for the prediction of ZOLD parameters were obtained with σ_o as high as 0.6 (96). Poor results were only obtained for large particles ($a_M \gtrsim 2.0$, $\sigma_o \approx 0.3$), which showed some dependence on the starting

point used for SEARCH, i.e. the initial guesses of a_M and σ_o required to start the programme. Also, the procedure was not drastically affected by the imposition of 5% random fluctuations on the data. Carabine and Moore (9) claim that, in this case, it should be possible to predict a_M and σ_o to within 4% and 10% respectively. The results obtained using horizontally polarised light were not so successful, however, since local minima is the error function S (equation (2.16)) tended to occur more frequently than in cases using vertically polarised light. This result has been confirmed by Maddock (78) who used a similar method to determine the particle size distribution of generated sulphuric acid droplets.

The instrument developed by Carabine and Moore (9) has been used to obtain light scattering measurements in this work. Details of the construction and operation of this instrument have been given (9, 96), and therefore only a brief review is intended here. A plan view of the instrument is illustrated in Fig. 2 - IX. The light from a helium-neon laser source (wavelength 632.8 nm.) is passed through a collimator C which expands the beam to a diameter of about 4 mm. The collimator consists of a condensing lens L_1, a pinhole H, and a second condensing lens L_2, which is set to give a parallel beam into the scattering apparatus. The beam is then incident on a stationary slide, SL, set at an angle, which reflects part of the beam on to a photodiode PD. This photodiode enables fluctuations in laser intensity to be monitored. The light transmitted by the slide then passes through aperture S_1, 5 mm. in diameter, on to a rotating mirror MR. This mirror is rotated stepwise by a synchronous motor such that the incident beam is reflected on to each of the static mirrors 1 to 15 in turn. The static mirrors are positioned on the circumference of an ellipse, with the rotating mirror and the sampling cell located on the foci. The positioning of the rotating mirror is controlled by an infra-red source and detector

system under the instrument body, and an automatic electronic system controls the mirror rotation and data acquisition of the apparatus. Circuit diagrams are given by the above mentioned authors. The light reflected from the static mirrors then passes through the sampling cell XS. The sampling cell of Moore (96) has been replaced for this work by a flow sampling system similar to that used by Maddock (78), described in Section 4.1. A Rayleigh Horn RH similar to that used by Maddock (78) is placed behind the scattering cell, such that light transmitted through the aerosol at back-scattering angles is not reflected back through the sample, complicating the readings with additional forward-scattered light. The scattered signal is detected by a photomultiplier PM, through apertures S_2 and S_3, S_2 having a slightly smaller diameter than the diameter of the incident laser beam. This is to reduce the angular field of view of the photomultiplier to a half-angle of approximately 0.4°, and to reduce the effect of marginal vertical misalignment of the mirrors. The photomultiplier is an EMI Type 9658 Modified S20 having a quantum efficiency of about 10% at the helium-neon wavelength. It is operated by a regulated high-voltage d.c. power supply at - 900 V. and housed in a specially designed casing, incorporating a mu-metal shield and a collecting telescope, the dimensions of which define the field of view of the detector. As the mirror MR rotates, the signal from the photomultiplier is integrated at a frequency of 60 Hz by a Hewlett-Packard 3450A Multi-function meter, which acts as an analogue-digital converter, and the integrated signal is hence punched on to paper tape. The number of such readings taken at each mirror position is adjustable, and is automatically controlled by the electronics once the scanning cycle is started.

The data obtained from the instrument, after averaging, must be corrected for the optically effective scattering volume. Also, the problems of beam extinction and multiple scattering must be considered (96). Both of these problems are negligible if the aerosol number

concentration is not too high. The experimentally determined scattering signals are related to the quantity $I_{1e}(\theta_i)$ of equation (2.16) as follows (9):-

$$I_{1e}(\theta_i) = C \sin\theta_i \cdot \left[\frac{S_{\theta_i}}{S_o} - \frac{S'_{\theta_i}}{S'_o}\right] \quad . \quad . \quad . \quad . \quad (2.17)$$

where $\sin\theta_i$ represents the correction for the optically effective scattering volume;

C is a constant, proportional to the aerosol number concentration;

S_{θ_i} is the photomultiplier signal from the aerosol at angle θ_i;

S'_{θ_i} is the correction term for background light, e.g. stray light, scattering from the edges of stops, etc. obtained by taking measurements in the absence of aerosol:

S_o, S'_o are the incident beam intensities at the time of measurement of S_{θ_i} and S'_{θ_i}.

Normally it is assumed that $S_o = S'_o$, and the unknown constant of equation (2.17), C, may be eliminated by considering relative scattered signals, i.e. by normalising the data. It should be noted that this procedure eliminates any information that might be obtained about the number concentration of the aerosol. The scattering angles are measured with the aid of a specially designed goniometer (96), attached in the position of the scattering cell. Measurement is accurate to $\pm 0.1^{\circ}$. The angles used in this study, determined as the mean of three goniometer readings, are given in Table 2-1.

Since the application of light scattering methods to polydisperse aerosols with spread parameters greater than 0.3 has hitherto been considered dubious (130) a thorough testing of the SEARCH method for distributions with large spreads has been undertaken. Preliminary results from electron microscopy (see Section 5.1) indicate that the aerosol is likely to consist of a polydisperse distribution of fairly

small particles. Mie Coefficients have been generated for refractive indices of 1.335 (corresponding to a dilute solution of manganous sulphate) and 1.370 (corresponding to a 30% w/w solution of sulphuric acid), and stored on magnetic tape. This data was integrated, according to equation (2.15) for the following ZOLD functions.

(i) $a_M = 0.05$ m., $\sigma_o = 0.4\ (0.1)\ 1.0$

(ii) $a_M = 0.1$ m., $\sigma_o = 0.4\ (0.1)\ 1.0$

(iii) $a_M = 0.2$ m., $\sigma_o = 0.4\ (0.1)\ 0.8$

(iv) $a_M = 0.4$ m., $\sigma_o = 0.4\ (0.1)\ 0.7$

for each refractive index. It should be noted that for $a_M = 0.2\ \mu m.$ a value of σ_o greater than 0.8 would give a combination of parameters outside the range of the SEARCH programme, as would values of σ_o greater than 0.7 if $a_M = 0.4\ \mu m.$ (96). The light scattering patterns that would be produced in each case are given in Figs. 2-X to 2-XVII. It may be seen that virtually no change occurs in the qualitative shape of the curves with the change in refractive index. Increasing polydispersity at the small sizes results in increasing forward-scattered intensity. It also causes the relative intensity of light scattered at the most back-scattering positions to increase, an effect most marked in the cases of larger modal diameter. (Figs. 2-XIV to 2-XVII). These curves may provide useful references to compare with experimental curves (Chapter 5).

The results of the attempt to invert the data presented in Figs. 2-X to 2-XVII are given in Tables 2-2 and 2-3, for a number of SEARCH starting points. It may be seen that, generally, fairly consistently correct results are obtained for the larger modal diameters, but when $a_M = 0.1$ or $0.05\ \mu m.$ the results are dependent on the SEARCH starting points. The results for low values of both a_M and σ_o in Tables 2-2 and 2-3 clearly indicate the presence of a second minimum in the function S of equation (2.16). Thus, it is not possible to uniquely determine the ZOLD parameters of a distribution of this type using light scattering data alone.

Fig. 2-X: Light scattering patterns obtained from ZOLD distributions of modal diameter 0.05μm. with spread parameters 0.4 (0.1) 1.0 (runs 1 to 7 respectively). Refractive index = 1.335

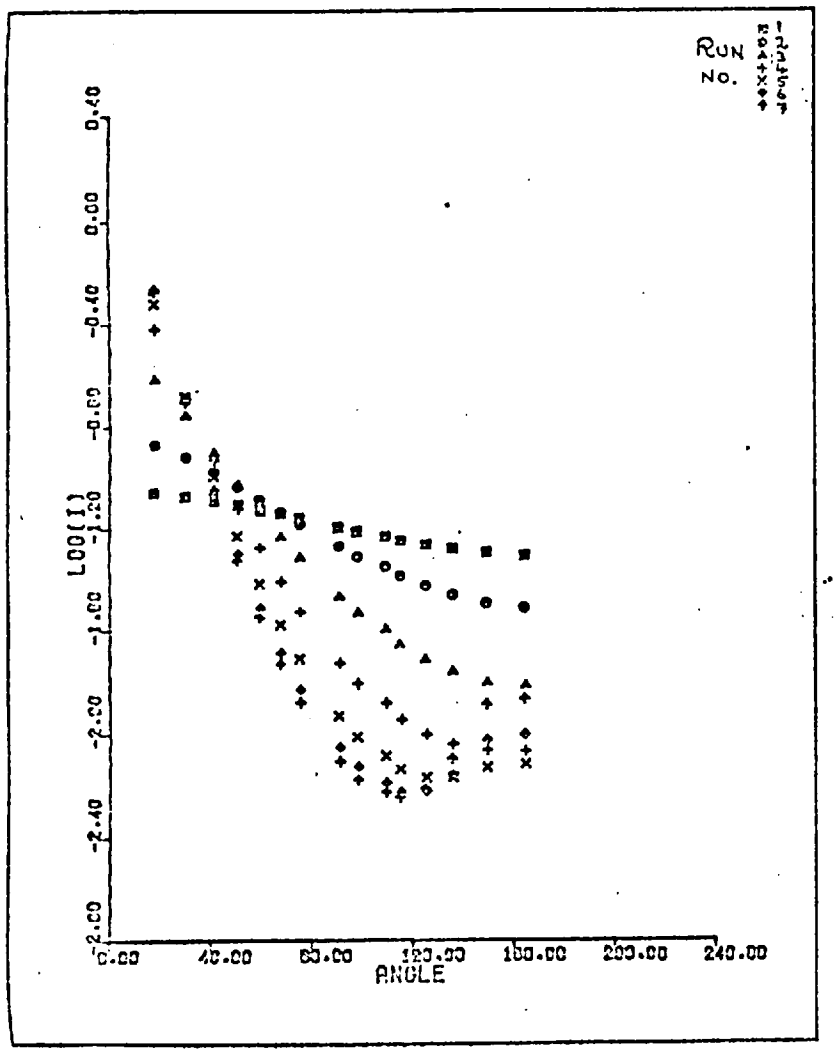

Fig. 2-XI: Light scattering patterns obtained from ZOLD distributions of modal diameter 0.1μm. with spread parameters 0.4 (0.1) 1.0 (runs 1 to 7 respectively). Refractive index = 1.335

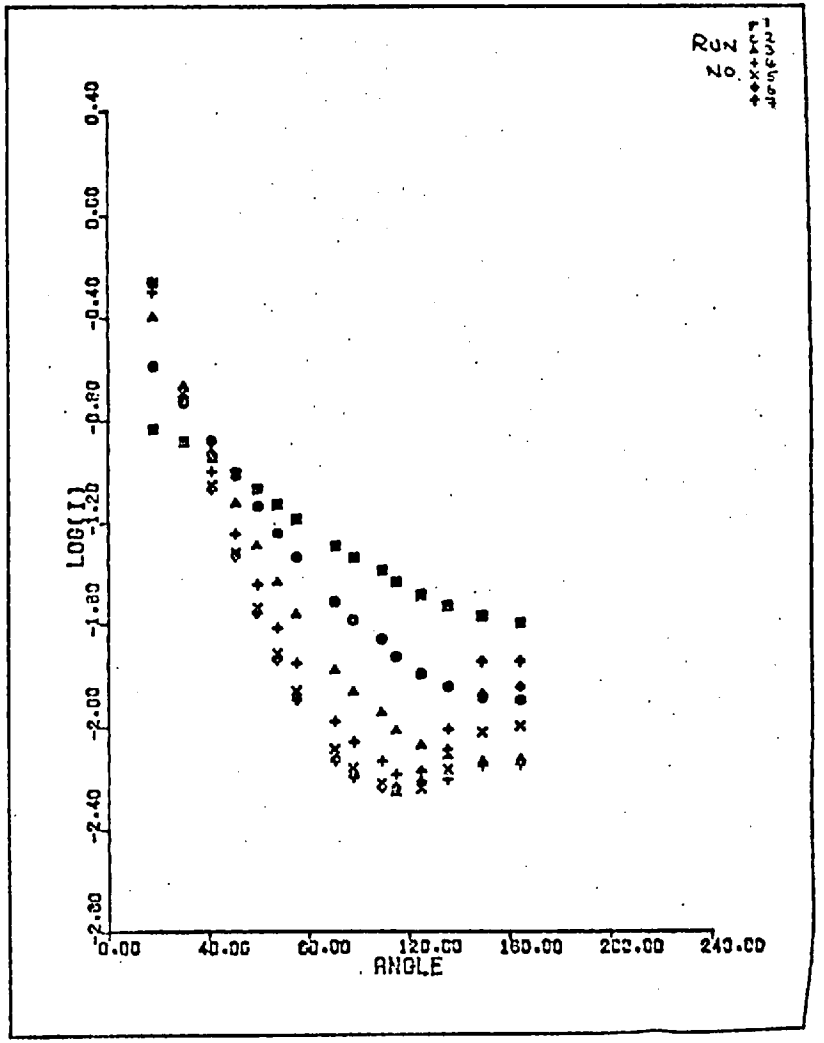

Fig. 2-XII: Light scattering patterns obtained from ZOLD distributions of modal diameter 0.05 μm. with spread parameters 0.4 (0.1) 1.0 (runs 1.to 7 respectively). Refractive index = 1.370

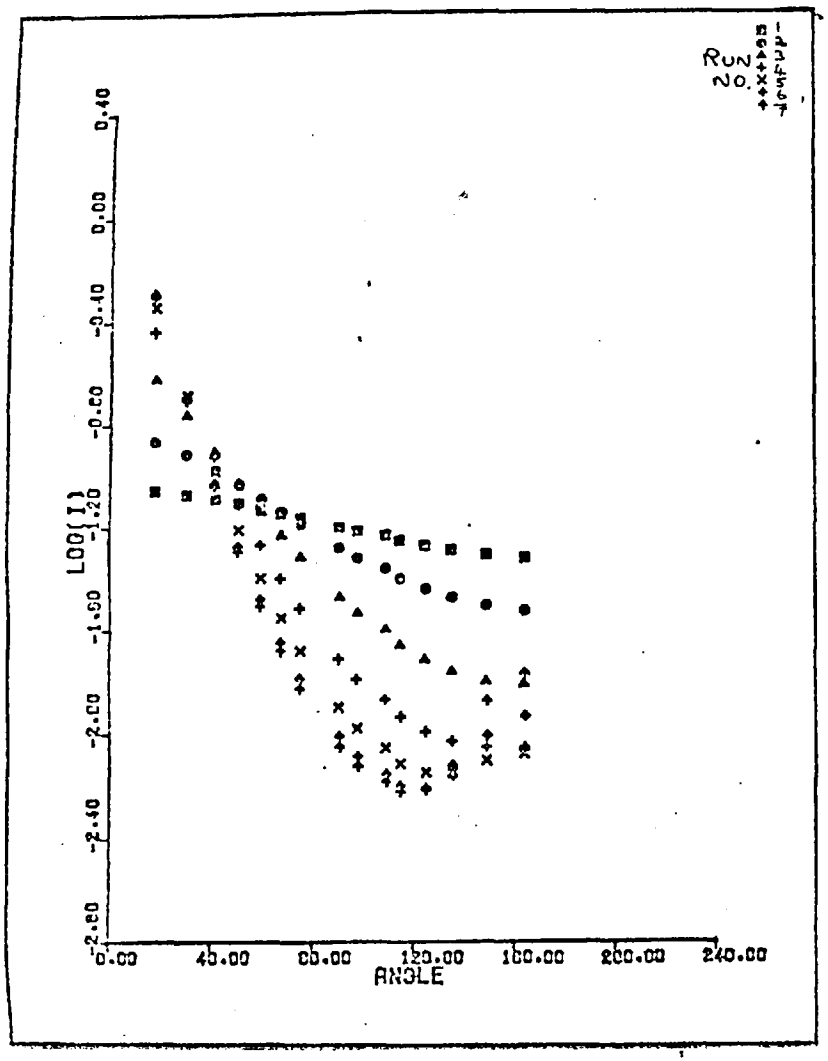

Fig. 2-XIII: Light scattering patterns obtained from ZOLD distributions of modal diameter 0.1 μm. with spread parameters 0.4 (0.1) 1.0 (runs 1 to 7 respectively). Refractive index = 1.370

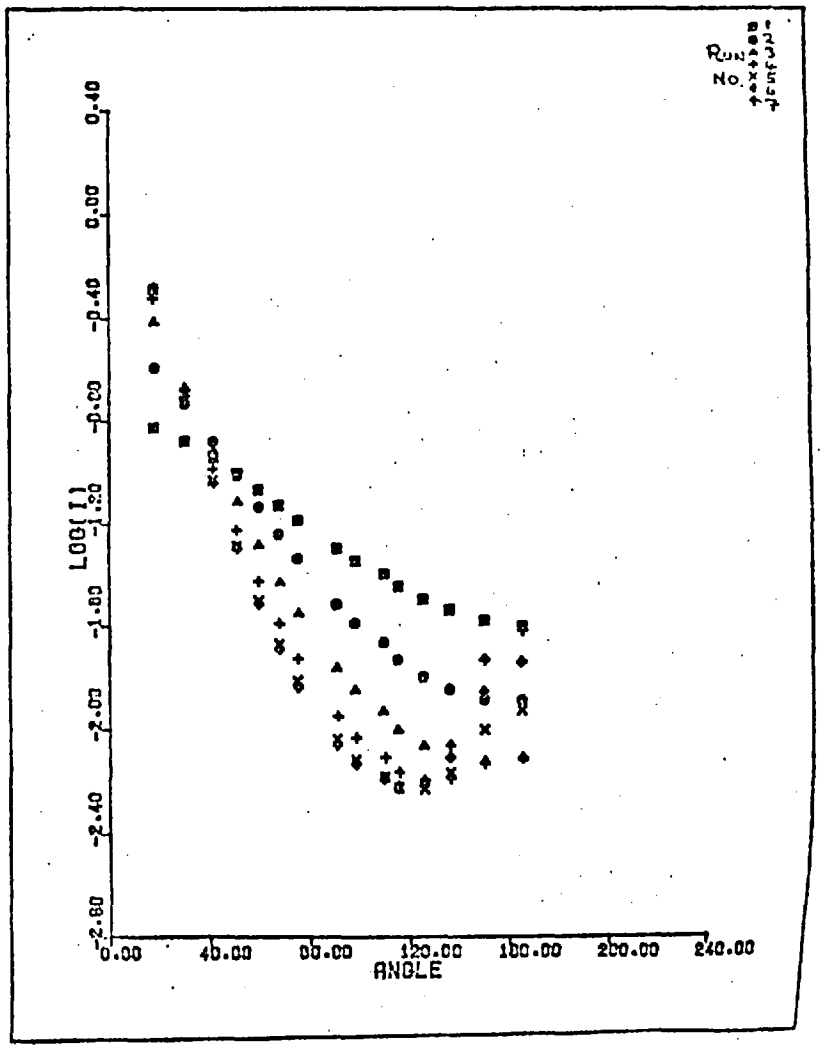

Fig. 2-XIV: Light scattering patterns obtained from ZOLD distributions of modal diameter 0.2μm. with spread parameters 0.4 (0.1) 0.8 (runs 1 to 5 respectively). Refractive index = 1.335

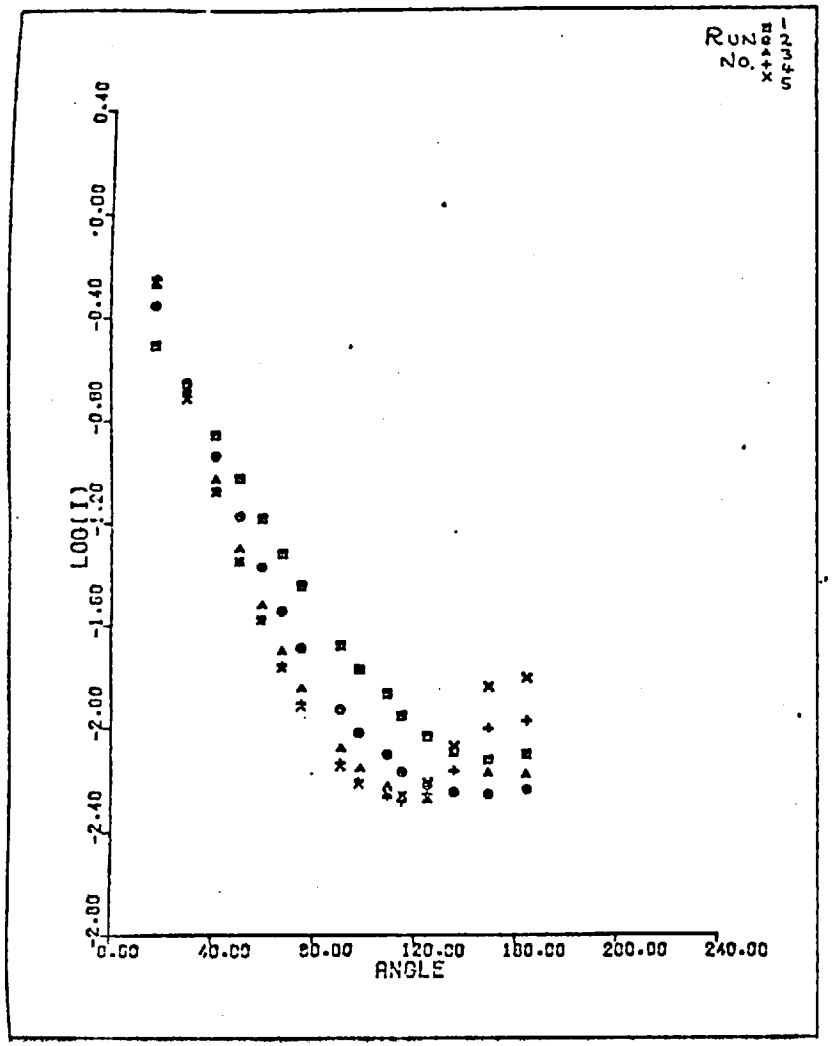

Fig. 2-XV: Light scattering patterns obtained from ZOLD distributions of modal diameter 0.4μm. with spread parameters 0.4 (0.1) 0.7 (runs 1 to 4 respectively). Refractive index = 1.335

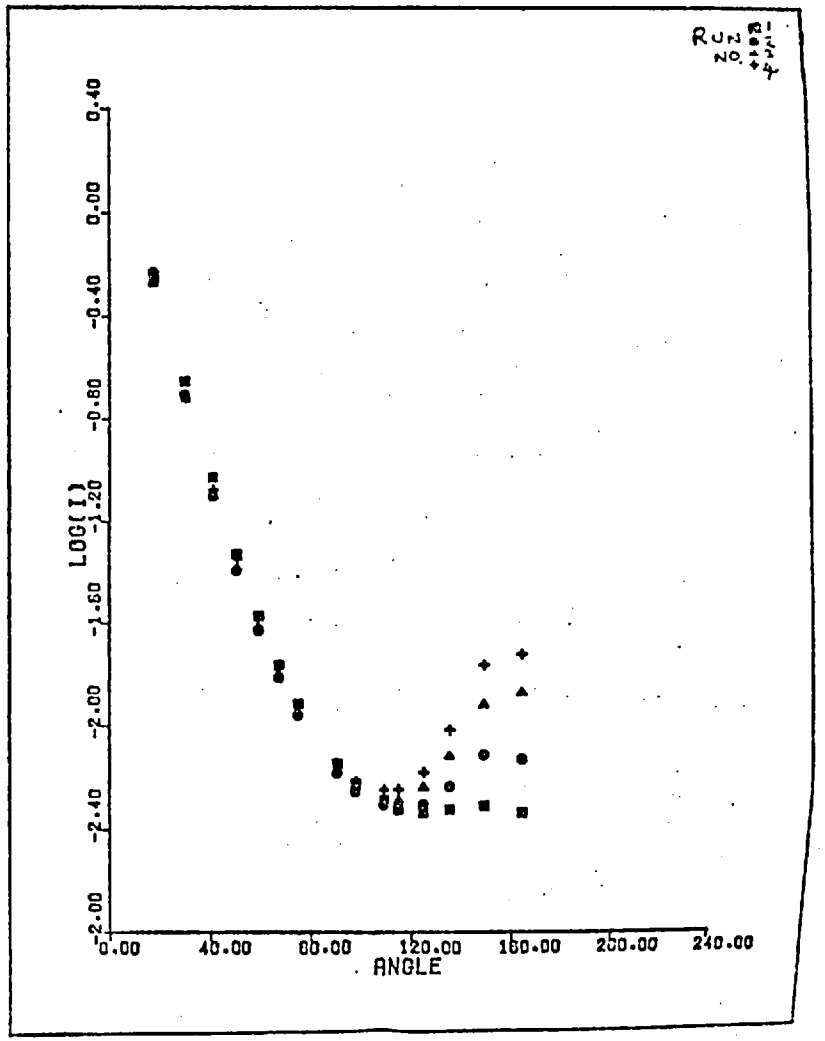

Fig. 2-XVI: Light scattering patterns obtained from ZOLD distributions of modal diameter 0.2 m. with spread parameters 0.4 (0.1) 0.8 (runs 1 to 5 respectively). Refractive index = 1.370

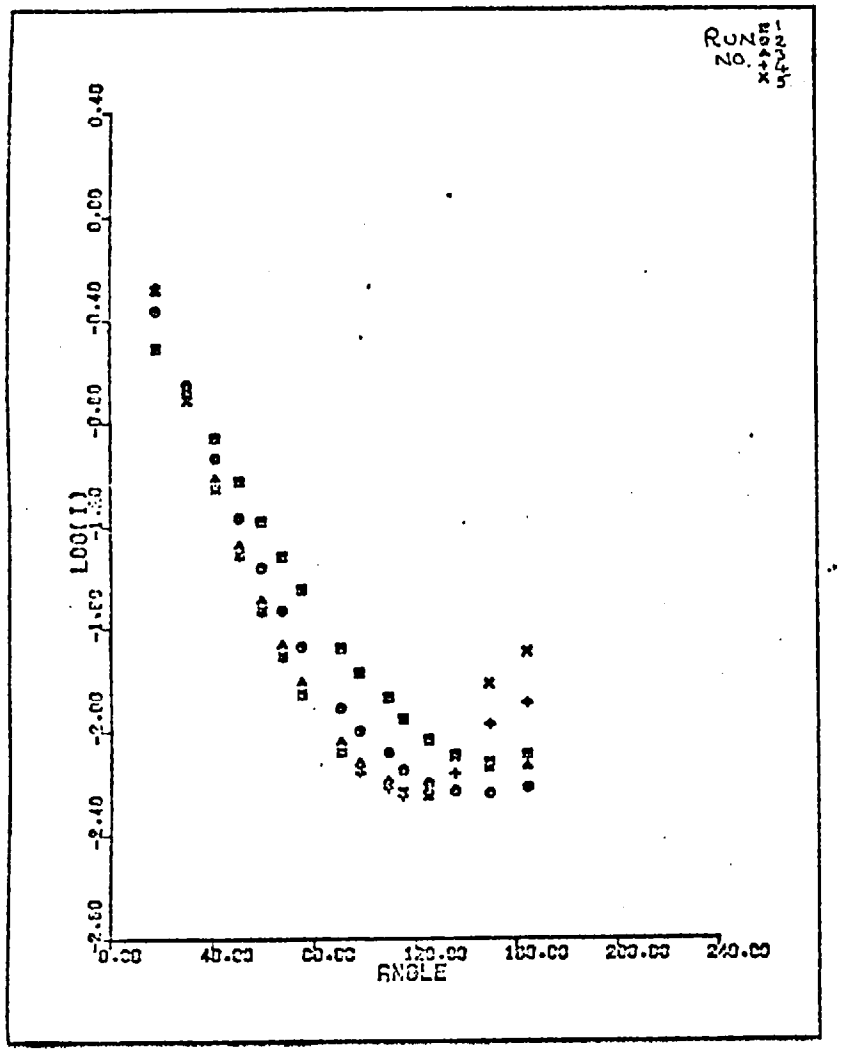

Fig. 2-XVII: Light scattering patterns obtained from ZOLD distributions of modal diameter 0.4 m. with spread parameters 0.4 (0.1) 0.7 (runs 1 to 4 respectively). Refractive index = 1.370

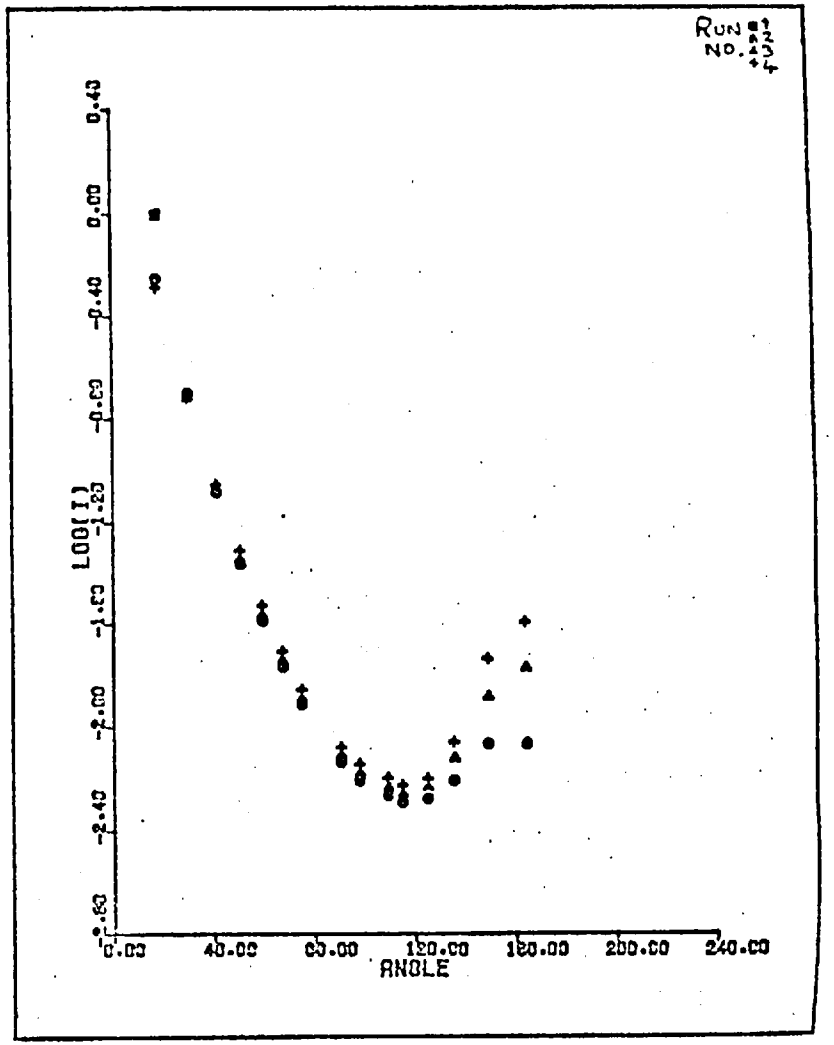

Since experimental data is likely to have errors associated with it, the effects of artificially introducing errors into the data of Figs. 2-X to 2-XVII has been investigated. Only the most successful of the SEARCH starting points have been used, viz. the combinations $(a_M, \sigma_0) = (0.2, 0.7)$ and $(0.1, 0.5)$. The following four cases are considered, and the results are presented in Tables 2 - 4 to 2 - 11.

(i) The effect of a large inaccuracy in the refractive index has been examined. Moore (96) has stated that an accuracy of 0.02 in the refractive index is desirable. In the present study, the refractive index of the particles is not always accurately known, since the exact extent of the chemical reaction occurring in the particles would have to be known for the determination of the particle composition, and hence its refractive index, at any given time. Here, the effect of an error of 0.035 is examined (a larger error than any likely to be incurred in practice). 'Experimental' data in Figs. 2-X, 2-XI, 2-XIV and 2-XV, obtained at $\eta = 1.335$, is inverted using Mie Coefficients obtained at $\eta = 1.370$. The results are given in Table 2-4. The corresponding results obtained by inverting 'experimental' data in Figs. 2-XII, 2-XIII, 2-XVI and 2-XVII ($\eta = 1.370$) using Mie Coefficients obtained at $\eta = 1.335$ are given in Table 2-5. Generally, the results are little affected when σ_0 is comparatively small, especially if a_M is also small. However, large discrepancies occur at large values of σ_0.

(ii) The effect of removing the three most forward-scattering angles, and inverting the data obtained from the remaining twelve has been investigated. In practice it was found (see Section 5.1(c)) that in many cases not all the angular readings taken could be used, especially those taken at the most forward-scattering angles. The results for $\eta = 1.335$ are given in Table 2-6, and those for $\eta = 1.370$ in Table 2-7. The effect generally appears to be to make the results much less reliable and more dependent on the starting position of the SEARCH procedure.

(iii) The effect of a $\pm$ 5% random fluctuation in the data has been examined. The deviation of each of the fifteen data points is exactly 5%, the sign of the displacement being determined randomly. The results are presented in Tables 2-8 (for $\eta = 1.335$) and 2-9 (for $\eta = 1.370$). Generally, the effect of these errors is to displace the predicted values of the ZOLD parameters by up to 33%. Excepting four or five cases, the procedure still locates the correct area of the (a_M, σ_o) surface, but the values of the parameters are almost invariably subject to an error of at least $\pm$ 20%. It should be noted that, in most cases, if the predicted value of one parameter deviates on the high side, the predicted value of the other will err on the low side; thus, the effects on the mean diameters will tend to cancel out rather than accumulate.

(iv) A combination of effects (ii) and (iii) was tried, viz. the inversion of a set of twelve data points each with a random fluctuation of $\pm$ 5%. The results are given in Tables 2-10 ($\eta = 1.335$) and 2-11 ($\eta = 1.370$). It appears that the unreliability and dependence on SEARCH starting point of (ii) is combined with the inaccuracy incurred in (iii). The consequence is that, in this case, the information obtained by inverting light scattering data is of very dubious significance.

As a conclusion to these tests, it may be said that the inversion of light scattering data for particle size distributions described by a ZOLD function, with modal diameter a_M in the range 0.05 - 0.4 μm. and spread parameter σ_o in the range 0.4 - 1.0, may yield useful information if:-

(a) Some information about the particle size distribution is already known, e.g. in this case, the ZOLD parameters of the aerosol particle nuclei may be known from electron microscopy, giving a guide to what would constitute a reasonable pair of parameters obtained from light scattering data.

(b) The light scattering data obtained is not too inaccurate, and sufficient readings have been taken, including some in the forward-scattering zone. For a discussion of results obtained, see Chapter 5.

Table 2-1: Scattering angles used in this study.

Mirror Position i (Fig. 2-IX)	Scattering angle θ_i (°)
1	164.4
2	149.3
3	135.6
4	125.1
5	115.0
6	106.3
7	98.0
8	90.7
9	75.3
10	67.7
11	59.6
12	50.9
13	41.4
14	30.2
15	17.9

Table 2-2: Testing of SEARCH method of inverting light scattering data for highly polydisperse distributions. Pairs of figures indicate ZOLD parameters (a_M,%) for the distribution. (see section 2.2) Refractive index = 1.335

Data generated from / Initial guess	0.050,0.400	0.050,0.500	0.050,0.600
0.2,0.7	0.050,0.400	0.061,0.466	0.051,0.595
0.1,0.5	0.053,0.400	0.050,0.499	0.051,0.597
0.5,0.4	0.053,0.389	1.883,0.075	0.057,0.578
0.4,0.9	2.027,0.062	2.018,0.063	1.893,0.077
1.0,0.3	2.027,0.062	1.885,0.075	1.892,0.077
0.8,0.1	0.050,0.400	2.018,0.063	2.001,0.066

Table 2-2 (continued)

Data generated / Initial guess from	0.050,0.700	0.050,0.800	0.050,0.900	0.050,1.000	0.100,0.400	0.100,0.500	0.100,0.600
0.2,0.7	0.050,0.698	0.050,0.800	0.061,0.870	0.051,0.994	0.100,0.400	0.100,0.500	0.100,0.600
0.1,0.5	0.051,0.697	0.052,0.793	0.052,0.894	0.051,0.994	0.100,0.400	0.100,0.500	0.100,0.600
0.5,0.4	0.050,0.700	0.051,0,796	0.053,0.891	0.051,0.994	1.878,0.074	0.100,0.500	0.100,0.600
0.4,0.9	1.990,0.081	1.631,0.127	0.061,0.869	0.051,0.994	1.878,0.074	1.903,0.077	2.104,0.084
1.0,0.3	1.989,0.081	1.631,0.127	0,052,0.891	0.051,0.994	3.041,0.028	1.903,0.077	2.104,0.084
0.8,0.1	1.992,0.080	1.631,0.126	0.073,0.840	0.051,0.994	0.100,0.400	1.903,0.077	0.100,0.600

Data generated / Initial guess from	0.100,0.700	0.100,0.800	0.100,0.900	0.100,1.000	0.200,0.400	0.200,0.500	0.200,0.600
0.2,0.7	0.100,0.700	0.100,0.800	0.097,0.903	0.104,0.987	0.197,0.403	0.200,0.500	0.200,0.600
0.1,0.5	0.100,0.700	0.100,0.800	0.101-0.896	0.101,0.993	0.200,0.400	0.197,0.503	0.200,0.600
0.5,0.4	0.100,0.700	0.100,0.800	0.101,0.896	0.104,0.987	0.197,0.403	0.200,0.500	0.197,0.603
0.4,0.9	1.566,0.131	0.100,0.800	0.097,0.903	0.104,0.987	1.953,0.078	0.200,0.500	0.197,0.603
1.0,0.3	0.100,0.700	0.100,0.800	0.097,0.903	0.104,0.987	1.953,0.078	1.667,0.134	0.200,0.600
0.8,0.1	1.556 0.130	0.100,0.800	0.101,0.896	0.101,0.993	0.200,0.400	1.667,0.134	0.200,0.600

Table 2-2 (continued)

Data generated / Initial guess from	0.200,0.700	0.200,0.800	0.400,0.400	0.400,0.500	0.400,0.600	0.400,0.700
0.2,0.7	0.200,0.699	0.200,0.798	0.400,0.400	0.400,0.500	0.396,0.602	0.409,0.692
0.1,0.5	0.200,0.699	0.196,0.802	0.400,0.400	0.400,0.500	0.400,0.600	0.408,0.694
0.5,0.4	0.200,0.699	0.196,0.802	0.398,0.401	0.400,0.500	0.400,0.600	0.409,0.692
0.4,0.9	0.200,0.699	0.200,0.798	0.398,0.401	0.400,0.500	0.396,0.602	0.409,0.692
1.0,0.3	0.196,0.703	0.196,0.802	0.400,0.400	0.398,0.501	0.400,0.600	0.409,0.692
0.8,0.1	0.196,0.703	0.200,0.798	0.400,0.400	0.398,0.501	0.400,0.600	0.408,0.694

Table 2-3: Testing of SEARCH method of inverting light scattering data for highly polydisperse distributions. Pairs of figures indicate ZOLD parameters (a_m, σ_a) for the distribution (see section 2.2) Refractive index = 1.370

Data generated / Initial guess from	0.050,0.400	0.050,0.500	0.050,0.600	0.050,0.700	0.050,0.800	0.050,0.900	0.050,1.000
0.2,0.7	0.050,0.400	0.050,0.500	0.050,0.600	0.050,0.700	0.050,0.800	0.067,0.852	0.052,0.994
0.1,0.5	0.051,0.396	0.050,0.499	0.051,0.596	0.050,0.700	0.050,0.799	0.051,0.899	0.050,0.999
0.5,0.4	0.078,0.317	0.051,0.496	1.805,0.074	0.050,0.700	0.058,0.772	0.057,0.878	0.052,0.993
0.4,0.9	1.791,0.061	1.789,0.059	1.804,0.074	1.959,0.082	1.494,0.135	0.052,0.894	0.051,0.995
1.0.0.3	1.791,0.061	1.789,0.059	0.057,0.576	1.959,0.082	1.494,0.135	1.376,0.143	1.267,0.211
0.8,0.1	0.167,0.024	0.051,0.495	1.804,0.074	1.959,0.082	1.494,0.135	0.059,0.873	0.050,0.999

Table 2-3 (continued)

Data generated / Initial guess from	0.100,0.400	0.100,0.500	0.100,0.600	0.100,0.700	0.100,0.800	0.100,0.900	0.100,1.000
0.2,0.7	0.100,0.400	0.100,0.500	0.100,0.600	0.100,0.700	0.100,0.800	0.100,0.900	0.107,0.985
0.1,0.5	0.100,0.400	0.100,0.500	0.100,0.600	0.100,0.700	0.100,0.800	0.100,0.900	0.050,0.664
0.5,0.4	0.100,0.400	2.872,0.039	0.100,0.600	0.100,0.700	0.100,0.800	0.100,0.900	0.107,0.985
0.4,0.9	1.789,0.059	0.100,0.500	1.987,0.083	1.439,0.133	0.100,0.800	0.100,0.900	0.258,0.806
1.0,0.3	1.789,0.059	0.100,0.500	1.987,0.083	1.439,0.133	0.100,0.800	0.100,0.900	1.210,0.267
0.8,0.1	0.100,0.400	0.100,0.500	2.836,0.063	1.439,0.133	0.100,0.800	0.100,0.900	0.107,0.985

Data generated / Initial guess from	0.200,0.400	0.200,0.500	o.200,0.600	0.200,0.700	0.200,0.800	0.400,0.400	0.400,0.500
0.2,0.7	0.200,0.400	0.200,0.500	0.200,0.600	0.200,0.700	0.200,0.800	0.400,0.400	0.400,0.500
0.1,0.5	0.200,0.400	0.200,0.500	0.200,0.600	0.200,0.700	0.200,0.800	0.400,0.400	0.400,0.500
0.5,0.4	0.200,0.400	0.200,0.500	0.200,0.600	0.200,0.700	0.200,0.800	0.400,0.400	0.400,0.500
0.4,0.9	1.914,0.083	1.516,1.149	0.200,0.600	0.200,0.700	0.200,0.800	0.400,0.400	0.400,0.500
1.0,0.3	1.914,0.083	1.661,0.321	0.200,0.600	0.200,0.700	0.200,0.800	0.400,0.400	0.400 0.500
0.8,0.1	0.200,0.400	0.200,0.500	0.200,0.600	0.200,0.700	0.200,0.800	0.400,0.400	0.400,0.500

Table 2-3 (continued)

Data generated / Initial guess from	0.400,0.600	0,400,0.700
0.2,0.7	0.399,0.600	0.416,0.689
0.1,0.5	0.399,0.600	0.052,0.635
0.5,0.4	0.399,0.600	0.416,0.689
0.4,0.9	0.399,0.600	0.416,0.689
1.0,0.3	0.399,0.600	0.416,0.689
0.8,0.1	0.399,0.600	0.416,0.689

Table 2-4: Testing of the SEARCH method. Inversion of data generated with η=1.335 using Mie coefficients obtained with η=1.370.

Data generated / Initial guess from	0.050,0.400	0.050,0.500	0.050,0.600	0.050,0.700	0.050,0.800	0.050,0.900	0.050,1.000
0.2,0.7	0.050,0.398	0.087,0.400	0.056,0.582	0.051,0.703	0.081,0.729	0.142,0.721	0.276,0.699
0.1,0.5	0.052,0.390	0.050,0.497	0.052,0.593	0.051,0.704	0.081,0.729	0.142,0.721	0.276,0.699

Table 2-4 (continued)

Data generated / Initial guess from	0.100,0.400	0.100,0.500	0.100,0.600	0.100,0.700	0.100,0.800	0.100,0.900	0.100,L.000
0.2,0.7	0.100,0.399	0.097,0.505	0.103,0.601	0.147,0.634	0.230,0.636	0.420,0.578	1.142,0.267
0.1,0.5	0.100,0.399	0.097,0.505	0.103,0.601	0.147,0.634	0.230,0.636	0.420,0.578	1.142,0.267

Data generated / Initial guess from	0.200,0.400	0.200,0.500	0.200,0.600	0.200,0.700	0.200,0.800	0.400,0.400	0.400,0.500
0.2,0.7	0.199,0.402	0.220,0.483	0.282,0.525	0.400,0.532	0.713,0.440	0.460,0.353	0.531,0.414
0.1,0.5	0.199,0.402	0.220,0.483	0.282,0.525	0.400,0.532	0.714,0.440	0.460,0.353	0.531,0.413

Data generated / Initial guess from	0.400,0.600	0.400,0.700
0.2,0.7	0.682,0.420	1.030,0.318
0.1,0.5	0.682,0.420	1.030,0.318

Table 2-5: Testing of the SEARCH method. Inversion of data generated with η=1.370 using Mie coefficients obtained with η=1.335.

Data generated / Initial guess from	0.050,0.400	0.050,0.500	0.050,0.600	0.050,0.700	0.050,0.800	0.050,0.900	0.050,1.000
0.2,0.7	0.054,0.387	0.052,0.496	0.052,0.592	0.052,0.687	0.054,0.767	0.050,0.898	0.050,0.999
0.1,0.5	0.054,0.387	0.052,0.496	0.052,0.592	0.052,0.687	0.050,0.780	0.050,0.898	0.051,0.999

Data generated / Initial guess from	0.100,0.400	0.100,0.500	0.100,0.600	0.100,0.700	0.100,0.800	0.100,0.900	0.100,1.000
0.2,0.7	0.102,0.396	0.102,0.496	0.097,0.599	0.062,0.771	0.050,0.911	0.061,1.000	0.201,0.870
0.1,0.5	0.102,0.396	0.102,0.496	0.097,0.599	0.063,0.771	0.050,0.911	0.059,1.000	0.050,0.640

Data generated / Initial guess from	0.200,0.400	0.200,0.500	0.200,0.600	0.200,0.700	0.200,0.800	0.400,0.400	0.400,0.500
0.2,0.7	0.198,0.402	0.180,0.517	0.127,0.686	0.056,0.934	0.074,1.000	0.327,0.457	0.242,0.624
0.1,0.5	0.198,0.402	0.180,0.517	0.126,0.687	0.056,0.934	0.083,0.997	0.327,0.457	0.242,0.624

Table 2-5 (continued)

Data generated / Initial guess from	0.400,0.600	0.400,0.700
0.2,0.7	0.104,0.904	0.149,0.994
0.1,0.5	0.104,0.904	0.050,0.636

Table 2-6: Testing of the SEARCH method. Inversion of data, omitting the three most forward - scattering angles. Refractive index = 1.335

Data generated / Initial guess from	0.050,0.400	0.050,0.500	0.050,0.600	0.050,0.700	0.050,0.800	0.050,0.900	0.050,1.000
0.2,0.7	0.739,0.086	0.729,0.108	0.711,0.164	0.051,0.689	0.054,0.790	0.055,0.886	0.065,0.995
0.1,0.5	0.062,0.362	0.057,0.477	0.057,0.576	0.051,0.689	0.050,0.797	0.052,0.893	0.050,0.518

Table 2-6 (continued)

Data generated / Initial guess from	0.100,0.400	0.100,0.500	0.100,0.600	0.100,0.700	0.100,0.800	0.100,0.900	0.100,1.000
0.2,0.7	0.772,0.129	0.699,0.175	0.506,0.299	0.089,0.718	0.082,0.834	0.134,0.842	0.148,0.913
0.1,0.5	0.108,0.381	0.106,0.484	0.098,0.597	0.089,0.718	0.054,0.563	0.053,0.496	0.050,0.469

Data generated / Initial guess from	0.200,0.400	0.200,0.500	0.200,0.600	0.200,0.700	0.200,0.800	0.400,0.400	0.400,0.500
0.2,0.7	0.200,0.395	0.190,0.508	0.186,0.614	0.213,0.686	0.236,0.760	0.411,0.392	0.408,0.495
0.1,0.5	0.200,0.395	0.190,0.508	0.186,0.614	0.057,0.525	0.050,0.490	0.411,0.392	0.051,0.577

Data generated / Initial guess from	0.400,0.600	0.400,0.700
0.2,0.7	0.417,0.588	0.430,0.676
0.1,0.5	0.081,0.410	0.052,0.450

Table 2-7: Testing of the SEARCH method. Inversion of data, omitting the three most forward - scattering angles. Refractive index = 1.370

Data generated / Initial guess from	0.050,0.400	0.050,0.500	0.050,0.600	0.050,0.700	0.050,0.800	0.050,0.900	0.050,1.000
0.2,0.7	0.728,0.177	0.714,0.170	0.676,0.176	0.050,0.700	0.066,0.761	0.050,0.900	0.059,0.971
0.1,0.5	0.083,0.300	0.050,0.500	0.057,0.575	0.054,0.686	0.086,0.718	0.050,0.576	0.050,0.504

Data generated / Initial guess from	0.100,0.400	0.100,0.500	0.100,0.600	0.100,0.700	0.100,0.800	0.100,0.900	0.100,1.000
0.2,0.7	0.707,0.164	0.684,0.183	0.100,0.600	0.100,0.700	0.099,0.801	0.112,0.878	0.158,0.903
0.1,0.5	0.100,0.400	0.100,0.500	0.100,0.600	0.100,0.700	0.050,0.568	0.050,0.495	0.052,0.443

Data generated / Initial guess from	0.200,0.400	0.200,0.500	0.200,0.600	0.200,0.700	0.200,0.800	0.400,0.400	0.400,0.500
0.2,0.7	0.200,0.400	0.200,0.500	0.200,0.600	0.198,0.702	0.217,0.781	0.400,0.400	0.400,0.500
0.1,0.5	0.200,0.400	0.200,0.500	0.200,0.600	0.050,0.539	0.050,0.472	0.400,0.400	0.050,0.577

Table 2-7 (continued)

Data generated from / Initial guess	0.400,0.600	0.400,0.700
0.2,0.7	0.398,0.601	0.434,0.675
0.1,0.5	0.050,0.492	0.057,0.418

Table 2-8: Testing of the SEARCH method. Inversion of data with ±5% random deviations from predicted values. Refractive index = 1.335

Data generated from / Initial guess	0.050,0.400	0.050,0.500	0.050,0.600	0.050,0.700	0.050,0.800	0.050,0.900	0,050,1.000
0.2,0.7	0.109,0.216	0.068,0.444	0.067,0.555	0.067,0.645	0.053,0.794	0.067,0.847	0.079,0.917
0.1,0.5	0.149,0.076	0.054,0.486	0.067,0.555	0.055,0.680	0.052,0.797	0.067,0.847	0.079,0.917

Table 2-8 (continued)

Data generated / Initial guess from	0.100,0.400	0.100,0.500	0.100,0.600	0.100,0.700	0.100,0.800	0.100,0.900	0.100,1.000
0.2,0.7	0.125,0.352	0.075,0.550	0.075,0.660	0.091,0.715	0.135,0.742	0.056,0.986	0.203,0.828
0.1,0.5	0.125,0.352	0.075,0.550	0.075,0.659	0.091,0.715	0.135,0.742	0.056,0.986	0.203,0.828

Data generated / Initial guess from	0.200,0.400	0.200,0.500	0.200,0.600	0.200,0.700	0.200,0.800	0.400,0.400	0.400,0.500
0.2,0.7	0.208,0.384	0.199,0.495	0.235,0.562	0.159,0.739	0.299,0.693	0.379,0.412	0.458,0.459
0.1,0.5	0.208,0.384	0.199,0.495	0.235,0.562	0.159,0.739	0.299,0.693	0.379,0.412	0.458,0.459

Data generated / Initial guess from	0.400,0.600	0.400,0.700
0.2,0.7	0.310,0.657	0.533,0.595
0.1,0.5	0.310,0.657	0.533,0.595

Table 2-9: Testing of the SEARCH method. Inversion of data with ±5% random deviations from predicted values. Refractive index = 1.370

Data generated from / Initial guess	0.050,0.400	0.050,0.500	0.050,0.600	0.050,0.700	0.050,0.800	0.050,0.900	0.050,1.000
0.2,0.7	0.066,0.332	0.061,0.464	0.067,0.554	0.140,0.494	0.050,0.804	0.069,0.842	0.083,0.909
0.1,0.5	0.070,0.320	0.060,0.468	0.067,0.554	0.050,0.696	0.050,0.806	0.069,0.842	0.083,0.909

Data generated from / Initial guess	0.100,0.400	0.100,0.500	0.100,0.600	0.100,0.700	0.100,0.800	0.100,0.900	0.100,1.000
0.2,0.7	0.122,0.358	0.077,0.548	0.075,0.662	0.094,0.710	0.138,0.738	0.055,0.994	0.221,0.812
0.1,0.5	0.122,0.358	0.077,0.548	0.075,0.662	0.094,0.710	0.138,0.739	0.055,0.994	0.051,0.649

Data generated from / Initial guess	0.200,0.400	0.200,0.500	0.200,0.600	0.200,0.700	0.200,0.800	0.400,0.400	0.400,0.500
0.2,0.7	0.211,0.382	0.201,0.492	0.236,0.562	0.159,0.740	0.308,0.687	0.381,0.411	0.454,0.461
0.1,0.5	0.211,0.382	0.202,0.492	0.236,0.562	0.159,0.740	0.308,0.687	0.381,0.411	0.454,0.461

Table 2-9 (continued)

Data generated from / Initial guess	0.400,0.600	0.400,0.700
0.2,0.7	0.304,0.664	0.565,0.577
0.1,0.5	0.304,0.664	0.050,0.649

Table 2-10: Testing of the SEARCH method. Inversion of data with ±5% random deviations from predicted values, omitting the three most forward - scattering angles. Refractive index = 1.335

Data generated from / Initial guess	0.050,0.400	0.050,0.500	0.050,0.600	0.050,0.700	0.050,0.800	0.050,0.900	0.050,1.000
0.2,0.7	0.739,0.085	0.730,0.107	0.710,0.153	0.636,0.226	0.050,0.800	0.076,0.829	0.253,0.684
0.1,0.5	0.081,0.293	0.115,0.333	0.119,0.429	0.051,0.693	0.051,0.799	0.050,0.584	0.050,0.521

Table 2-10 (continued)

Initial guess \ Data generated from	0.100,0.400	0.100,0.500	0.100,0.600	0.100,0.700	0.100,0.800	0.100,0.900	0.100,1.000
0.2,0.7	0.729,0.136	0.694,0.179	0.509,0.303	0.132,0.655	0.100 0.797	0.084,0.914	0.107,0.961
0.1,0.5	0.146,0.311	0.095,0.501	0.074,0.674	0.132,0.655	0.050,0.574	0.050,0.507	0.050,0.470

Initial guess \ Data generated from	0.200,0.400	0.200,0.500	0.200,0.600	0.200 0.700	0.200,0.800	0.400,0.400	0.400,0.500
0.2,0.7	0.221,0.348	0.179,0.504	0.116,0.694	0.110,0.809	0.160,0.832	0.296,0.478	0.375,0.512
0.1,0.5	0.221,0.348	0.179,0.504	0.116,0.694	0.050,0.548	0.160,0.832	0.285,0.487	0.060,0.553

Initial guess \ Data generated from	0.400,0.600	0.400,0.700
0.2,0.7	0.375,0.608	0.420,0.666
0.1,0.5	0.050,0.503	0.050,0.460

Table 2-11: Testing of the SEARCH method. Inversion of data with ±5% random deviations from predicted values, omitting the three most forward - scattering angles. Refractive index = 1.370

Data generated from / Initial guess	0.050,0.400	0.050,0.500	0.050,0.600	0.050,0.700	0.050,0.800	0.050,0.900	0.050,1.000
0.2,0.7	0.730,0.180	0.717,0.163	0.696,0.163	0.614,0.239	0.050,0.798	0.079,0.822	0.169,0.774
0.1,0.5	0.051,0.383	0.104,0.356	0.113,0.442	0.050,0.703	0.050,0.798	0.053,0.570	0.052,0.504

Data generated from / Initial guess	0.100,0.400	0.100,0.500	0.100,0.600	0.100,0.700	0.100,0.800	0.100,0.900	0.100,1.000
0.2,0.7	0.714,0.157	0.089,0.517	0.077,0.670	0.153,0.628	0.063,0.873	0.119,0.856	0.107,0.966
0.1,0.5	0.138,0.327	0.089,0.517	0.077,0.670	0.153,0.628	0.050,0.568	0.050,0.494	0.052,0.455

Data generated from / Initial guess	0.200,0.400	0.200,0.500	0.200,0.600	0.200,0.700	0.200,0.800	0.400,0.400	0.400,0.500
0.2,0.7	0.220,0.352	0.184,0.502	0.133,0.672	0.050,0.943	0.188,0.898	0.339,0.455	0.369,0.517
0.1,0.5	0.220,0.455	0.184,0.502	0.132,0.673	0.050,0.542	0.054,0.462	0.339,0.455	0.064,0.532

Table 2-11 (continued)

Data generated / Initial guess from	0.400,0.600	0.400,0.600
0.2,0.7	0.317,0.653	0.398,0.686
0.1,0.5	0.050,0.489	0.050,0.438

3. THEORETICAL ANALYSIS OF THE PROPERTIES OF THE AEROSOL/GAS SYSTEM

3.1 Factors Determining Changes in Aerosol Particle Size in an Interacting Aerosol/Gas System

In Chapter 1, the two main processes by which particle growth occurs were outlined. In this chapter, the theoretical bases of these growth mechanisms will be examined in some detail, and reference will be made to other processes occurring in aerocolloidal systems that are of importance here. Sections 3.2 and 3.3 deal with the growth of the manganous sulphate solution droplets, arising from the formation of sulphuric acid in the liquid phase of the aerosol. In Section 3.4 the process of particle coagulation is discussed. A brief account of the effects of sedimentation is given in Section 3.5. Finally, in Section 3.6, an attempt is made to draw together information obtained from the consideration of single processes, and to formulate predictions of the behaviour of real systems in which all the processes may occur simultaneously.

By way of introduction, a general survey of these important processes will be given here. The aerosol droplets in their initial condition at the outlet point of the generator system are considered to be at equilibrium with the surrounding gas. This introduces a requirement that the relative humidity of the gas phase must be high, in order that droplets of solution may exist in the equilibrium condition. If the relative humidity of the ambient gas falls below a critical level, then the droplets of solution will evaporate leaving dry, solid manganous sulphate particles, and hence no reaction will take place. A full analysis of the phenomenon of solution concentration/humidity equilibrium is given in Section 3.3 and in the appendix.

If the aerosol particles are contacted with an atmosphere containing sulphur dioxide, transfer of matter from the gas phase (water vapour and sulphur dioxide) to the bulk of the particulate liquid phase results

from a combination of five processes:-

(i) Diffusion of sulphur dioxide molecules from the bulk of the surrounding gas to the droplet surfaces. The absorption of sulphur dioxide at the surface of the droplet sets up a concentration gradient between the bulk of the gas phase and the droplet surface. This provides the driving force for the gas phase diffusion.

(ii) Diffusion of dissolved sulphur dioxide, including any that may be oxidised to sulphuric acid, from the droplet surfaces into the bulk of the droplets.

(iii) The rate of oxidation of sulphur dioxide to sulphuric acid in the droplets. This is increased by the catalytic effect of the manganous sulphate in the droplets. The formation of sulphuric acid has the effect of reducing the water vapour pressure at the droplet surfaces. The composition of the droplets also determines the vapour pressure of sulphur dioxide at the surfaces, at any given time.

(iv) Diffusion of water vapour molecules from the bulk of the surrounding gas to the droplet surfaces. The changing water vapour pressure at the droplet surfaces (during the formation of sulphuric acid within the droplets) causes a water vapour concentration gradient to be set up. Hence, diffusion takes place.

(v) Diffusion of condensed liquid water from the droplet surfaces into the bulk of the droplets.

All of the above five factors may influence the transfer of matter from the bulk of the gas phase to the bulk of the liquid phase, but the actual transfer rate will be controlled by the slowest of the processes. In fact, as will be shown in Section 3.3, the third factor, i.e. the reaction rate in the liquid phase, is rate controlling in this case. Thus, Section 3.2 deals with the prediction of the rate of sulphuric acid formation within the bulk of the droplets. The results of this analysis, obtained from the reaction kinetics, will then be used in Section 3.3 to calculate actual droplet growth and its effect on the

particle size distribution.

Aerosol coagulation may be influenced by many factors, such as the Brownian motion of the particles, the nature of the particle surfaces, the presence of shear forces in the suspending medium, the presence of electric charges on the particles, and external force fields. In Section 3.4, a quantitative treatment of coagulation due to Brownian motion will be given followed by a qualitative discussion of other factors, all of which are considered relatively unimportant in this case.

Sedimentation of aerosol particles is negligible for small particles, but is appreciable as particles become large. The implication that sedimentation rates control the upper limit of particle size in the aerosol is discussed in Section 3.5.

Finally, in Section 3.6, the results obtained by considering the above named processes are compared, and an attempt is made to predict the effects of their simultaneous occurrence. Also, the results and applicability of other workers' attempts to model the system will be discussed.

3.2. The Catalytic Oxidation of Sulphur Dioxide to Sulphuric Acid in the Presence of Transition Metal Salts

In the previous section, it was pointed out that the oxidation rate of sulphur dioxide to sulphuric acid within the droplets is the rate-determining (i.e. slowest) step occurring during droplet growth. If that is the case, then the liquid phase sulphur dioxide concentration in the particles at any time may be considered to be at equilibrium with the concentration of the ambient gas, and the growth rate determined by the rate of production of sulphuric acid inside the droplets. In this section, the prediction of the oxidation rate from the reaction kinetics will be discussed, and calculations of the increase in the sulphuric acid content of the droplets will be made.

Firstly, it is necessary to determine the partition relationship between sulphur dioxide in the aqueous and gas phases, in order that, given an initial gas phase concentration, the amount of oxidizable sulphur dioxide in the liquid phase may be obtained. Johnstone and Leppla (59) have shown that, over a range of gas phase concentrations between about 260 and 17,000 ppm., a Henry's Law relationship is valid, i.e. at equilibrium

$$(SO_2) = H[SO_2] \qquad (3.1)$$

where (SO_2) represents the liquid phase concentration of sulphur dioxide (unit m.mol. cm^{-3})

$[SO_2]$ represents the gas phase concentration of sulphur dioxide (unit m.mol. m^{-3})

H is Henry's constant for the system. Since the gas phase concentrations used in this work are considerably lower than those used by Johnstone and Leppla (59) it would be reasonable to assume the validity of equation (3.1) in this case. The above authors found the average value of H at 25°C to be 2.6×10^{-5} m^3 cm^{-3}. The value of the ionisation constant of the dissolved gas was also calculated, and found to be about 0.013, in agreement with values obtained earlier by Sherril and Noyes

(120). Johnstone and Leppla (59) also found that the absolute solubility of sulphur dioxide decreases as the concentration of sulphuric acid increases; a liquid phase sulphuric acid concentration of 0.08 m.mol.cm^{-3} serves to decrease the solubility by about a third.

Studies of the reaction kinetics of the conversion of dissolved sulphur dioxide to sulphuric acid have been extensive. Earlier workers noted that the presence of manganese, iron or copper salts greatly accelerated the oxidation process in bulk solutions. Johnstone (57) has noted that, of these metals, manganese is by far the most vigorous catalyst. Johnstone (57) and Copson and Payne (14) found that, in the absence of inhibitors, 30% w/w acid solutions were readily obtainable. Vasil'ev et. al. (124) found that the introduction of 0.01% manganous sulphate increased the liquid phase oxidation rate by more than sevenfold, and produced a ratio of 70% oxidised to 30% dissolved sulphur dioxide in the resulting mixture. In the absence of catalyst only 25% of the sulphur dioxide was found to be oxidised, all other factors being the same. The authors postulated that the oxidation rate in the presence of the catalyst is determined by the rate of reaction of an intermediate compound. Kaštanov and Ryžov (67) studied the oxidation in a solution containing various quantities of added sulphuric acid. They found that the reaction rate tended to decrease as the sulphuric acid concentration increased, until, at a sulphuric acid concentration of about 20%, the effects of the catalyst were negated. At higher concentrations the absolute reaction rate appeared to remain constant, but the decreasing solubility of the sulphur dioxide caused the actual rate of acid production to decrease. Grodzovskij (46) noted that the linear fall-off of reaction rate with sulphuric acid concentration up to 30% correlates with the fall of the absorption coefficient of oxygen in the solution. A catalysis mechanism was proposed (46) in which a complex between the Mn^{2+} ion and sulphur dioxide is first formed. This is then oxidised to Mn^{3+} by dissolved oxygen, which in turn oxidises the sulphite component to sulphate, itself

being reduced to Mn^{2+}. Using this scheme, Grodzovskij (46) was able to ascribe reasons for the sharp fall-off in oxidation rate as the sulphuric acid concentration rises above 30%. These include the tendency for a relatively stable complex to form between Mn^{3+} and SO_4^{2-} ions, reducing the active catalyst concentration, and the increasing difficulty with which the $Mn^{2+}-SO_2$ complex formation and oxidation takes place. This scheme received support when Kaštanov and Guljanskaja (66) extracted in ether a compound of empirical formula $MnSO_4.SO_2$ from the reacting mixture.

The most comprehensive work on the mechanism of the catalytic oxidation of sulphur dioxide solutions has been given by Basset and Parker (4). These authors propose a mechanism similar to that of Grodzovskij (46), in which a $Mn(SO_3)_2^{2-}$ or similar ion adds an oxygen molecule very readily, either by addition or by depriving $O_2 \rightarrow SO_3^{2-}$ and similar complexes of their oxygen, viz.

$$O_2 \rightarrow SO_3^{2-} + Mn(SO_3)_2^{2-} \longrightarrow SO_3^{2-} + O_2 \rightarrow Mn(SO_3)_2^{2-}$$

The new complex will then undergo rapid rearrangement:-

$$O_2 \rightarrow Mn(SO_3)_2^{2-} \longrightarrow Mn(SO_4)_2^{2-}$$

and since ions of low electroaffinity, such as SO_3^{2-}, will replace ions of high affinity, such as SO_4^{2-}, the sulphate complex will break up and fresh sulphite complexes will be formed. This explains the apparent suppression of dithionate formation in solutions catalysed by Mn^{2+} salts, and also the somewhat lower oxidation rate achieved in the presence of solutions of manganous chloride, where the formation of stable chloride complexes interferes with the formation of the sulphite complexes.

A mathematical analysis of this type of reaction scheme, for aerosols of manganous sulphate solution in an atmosphere containing sulphur dioxide, has been developed by Matteson et. al. (87). The mechanism is regarded as consisting of four stages, corresponding to the equations below,

$$Mn^{2+} + SO_2 \underset{k_2}{\overset{k_1}{\rightleftharpoons}} Mn.SO_2^{2+} \quad \cdots \quad (I)$$

$$2Mn.SO_2^{2+} + O_2 \underset{k_4}{\overset{k_3}{\rightleftharpoons}} (Mn.SO_2^{2+})_2 \leftarrow O_2$$

$$\underset{k_5'}{\overset{k_5}{\rightleftharpoons}} 2\,Mn.SO_3^{2+} \quad \cdots \quad (II)$$

$$2Mn.SO_3^{2+} + H_2O \underset{k_7}{\overset{k_6}{\rightleftharpoons}} 2Mn^{2+} + HSO_4^- + H^+ \quad \cdots \quad (III)$$

$$HSO_4^- + H^+ \rightleftharpoons H_2SO_4 \quad \cdots \quad (IV)$$

the rate constants $k_1 \ldots k_7$ being defined as shown. From this scheme Matteson et. al. derive the three essential differential equations that mathematically describe the reaction.

$$\frac{d}{dt}[SO_2] = -k_1 H \phi \left\{ (MnSO_4)_o - (X) \right\} [SO_2]_o + k_2' \phi (X) \quad \cdots \quad (3.2)$$

$$\frac{d}{dt}(H_2SO_4) = k_6'(X) - 2k_7 \left\{ (MnSO_4)_o - (X) \right\} (H_2SO_4)^2 \quad \cdots \quad (3.3)$$

$$\frac{d}{dt}(X) = \left\{ k_1 H \left\{ [SO_2]_o - \phi (H_2SO_4) \right\} + 2k_7 (H_2SO_4)^2 \right\} (MnSO_4)_o$$

$$- \left\{ k_1 H \left\{ \phi \left\{ (MnSO_4)_o - (X) - (H_2SO_4) \right\} + [SO_2]_o \right\} \right.$$

$$\left. + k_2' + k_6' + 2k_7 (H_2SO_4)^2 \right\} (X) \quad \cdots \quad (3.4)$$

where (Z) refers to the liquid phase concentration of species Z

$[Z]$ refers to the gas phase concentration of species Z

(X) is the liquid phase concentration of all intermediates:

$$(X) = (Mn.SO_2^{2+}) + \frac{1}{2}\left((Mn.SO_2^{2+})_2 \leftarrow O_2 \right) + (Mn.SO_3^{2+}) \quad \cdots \quad (3.5)$$

subscript o refers to initial conditions

H is Henry's constant for sulphur dioxide

ϕ is the volume fraction of the aerosol, defined in Section 2.1.

The above equations are derived on the assumption that, as the reaction proceeds, the concentrations of complexes $Mn.SO_2^{2+}$ and $Mn.SO_3^{2+}$ may be taken as proportional to the total complex concentration (X). The pseudo-rate constants k_2' and k_6' are defined as

$$k_2' = \frac{k_2(Mn.SO_2^{2+})}{(X)} \qquad (3.6)$$

$$k_6' = \frac{k_6(Mn.SO_3^{2+})(H_2O)}{(X)} \qquad (3.7)$$

(The water concentration (H_2O) is not expected to vary significantly).

Matteson et. al. (87) obtained experimental values for the key rate constants k_1, k_2', k_6', k_7, by analysing the system under the assumption that the concentration of intermediate compounds (X) does not vary significantly from its steady state value $(X)_e$, once the reaction has started. It is also assumed that the terms in (H_2SO_4) and $(X)^2$ in equation (3.4) are negligible. Hence, setting the derivative on the left hand side of equation (3.4) to zero, the following expression for $(X)_e$ is obtained.

$$(X)_e = \frac{[SO_2]_o (MnSO_4)_o}{[SO_2]_o + \phi(MnSO_4)_o + K_s} \qquad (3.8)$$

where

$$K_s = \frac{k_2' + k_6'}{k_1 H} \qquad (3.9)$$

If this is true, then equations (3.2) and (3.3) may be solved separately. If we make the further assumption that $\phi(MnSO_4)_o << [SO_2]_o + K_s$, justified for aerosols of fairly dilute solutions of manganous sulphate, the following analytical solutions of equations (3.2) and (3.3) respectively can be obtained.

$$[SO_2] = \frac{k_2'}{k_1 H K_s}[SO_2]_o + \left\{1 - \frac{k_2'}{k_1 H K_s}\right\}[SO_2]_o \cdot \exp\left\{-\left\{\frac{k_1 H K_s \phi\,(MnSO_4)_o}{[SO_2]_o + K_s}\right\}t\right\} \qquad (3.10)$$

$$(H_2SO_4) = \frac{(H_2SO_4)_o \sqrt{\frac{k_6'}{2k_7K_s}[SO_2]_o} + \frac{k_6'}{2k_7K_s} \cdot \tanh\left\{\frac{(MnSO_4)_o}{[SO_2]_o + K_s}\sqrt{2k_6'k_7K_s[SO_2]_o}\,t\right\}}{\sqrt{\frac{k_6'}{2k_7K_s}[SO_2]_o} + (H_2SO_4)_o \cdot \tanh\left\{\frac{(MnSO_4)_o}{[SO_2]_o + K_s}\sqrt{2k_6'k_7K_s[SO_2]_o}\,t\right\}} \qquad (3.11)$$

Numerical results obtained in this work from equations (3.10) and (3.11), using the rate constants of Matteson et. al. (87), are given in Table 3-1 (a)(i). Comparison of (X)e, obtained from equation (3.8), with values of (X) computed from the equation of conservation of sulphur.

$$[SO_2]_o = [SO_2] + \phi\{(X) + (H_2SO_4)\} \qquad (3.12)$$

show large deviations. Therefore a numerical solution of equations (3.2), (3.3) and (3.4) was evaluated and the results are presented in Table 3-1 (a)(ii) and Fig. 3-I. The most striking features of these results are the very low equilibrium concentration of sulphuric acid, the high equilibrium concentration of intermediates, and the rapid attainment of equilibrium. The low yield of sulphuric acid is especially notable, since it contrasts starkly with results of other workers, reviewed previously, that maintain that sulphuric acid concentrations

Table 3-1: Results from attempts to solve the reaction kinetics equations.

Conditions: $(MnSO_4)_o$ = 0.347 m.mol.cm^{-3} (5%w/w)

Φ = 1.596 cm^{3}m^{-3}

$[SO_2]_o$ = 63 ppm.

(a) Using rate constants of Matteson et.al. (87)

(i) Analytical solutions using equations (3.10) and (3.11)

Time (mins.)	$[SO_2]$ ppm.	(H_2SO_4) mmol.cm^{-3}	(X) from (3.12) m mol. cm^{-3}	%Error $\left\|\frac{(X)-(X)_e}{(X)}\right\|$
0.5	53.9	0.021	0.234	16.7
2.5	46.3	0.059	0.408	52.3
5.0	45.9	0.063	0.415	53.1
10.0	45.9	0.063	0.415	53.1
25.o	45.9	0.063	0.415	53.1

(ii) Numerical solutions from equations (3.2) to (3.4)

Time (mins.)	$[SO_2]$ ppm.	(H_2SO_4) mmol.cm^{-3}	(X) from diff. mmol.cm^{-3} eqtn.*	(X) from $\frac{mmol}{cm^3}$ (3.12)
0.5	58.5	0.022	0.201	0.104
2.5	53.5	0.064	0.207	0.194
5.0	53.2	0.068	0.207	0.207
10.0	53.2	0.068	0.207	0.207
25.0	53.2	0.068	0.207	0.207

(b) Using rate constants of Wadden (126), and those derived from the data of Johnstone & Coughanowr (58)

(i) Analytical solutions

Time (mins.)	$[SO_2]$ ppm.	(H_2SO_4) mmol.cm^{-3}	(X) from (3.12) m mol cm^{-3}	%Error $\left\|\frac{(X)-(X_e)}{(X)}\right\|$
0.5	60.53	0.084	-0.015	647
2.5	54.24	0.420	-0.175	297
5.0	50.83	0.835	-0.495	117
10.0	48.99	1.632	-1.24	107
25.0	48.66	3.537	-3.14	103

Table 3-1 (continued)

(ii) Numerical solutions

Time (mins.)	$[SO_2]$ ppm.	(H_2SO_4) $mmol.cm^{-3}$	(X) from diff. eqtn. $mmol.cm^{-3}$	(x) from (3.12) $mmol.cm^{-3}$
0.5	57.9	0.065	0.077	0.077
2.5	48.0	0.354	0.066	0.066
5.0	37.6	0.655	0.055	0.055
10.0	23.0	1.082	0.036	0.036
25.0	7.11	1.548	0.014	0.014

* Note: The initial deviations in the values of (X) arise from the fact that the initial condition was taken to be $(x)_o = (x)_e$, obtained from equation (3.8), instead of $(x)_o = 0$, as in all other cases.

Table 3-2: Values of the reaction rate constants.

Rate Constant	Units	Value of Matteson et. al.	Value used here	Source of value used here
k_6'	$min.^{-1}$	0.22	2.025	
k_7	$mmol.^{-2}cm.^{6}min.^{-1}$	35	1.064 $x10^{-2}$	Wadden (126)
K_S	$mmol.m^{-3}$	2.2	8.92	
k_1	$cm^3.mmol.^{-1}.min.^{-1}$	2.4 $x10^5$	3.54 $x10^4$	derived as described
k_2'	min^{-1}	10	6.18	

of around 30% should be obtainable. It is suspected that the most probable reason for these peculiar results is error in the evaluation of the rate constants.

Wadden (126) has considered the simple case, using the assumptions outlined above, where the sulphur dioxide concentration in the gas phase remains constant throughout the reaction. In this case, the kinetics reduce to equation (3.3) with (X) replaced by (X)e, which may be substituted from equation (3.8). In the analysis Wadden (126) neglects the $\Phi(MnSO_4)_o$ term in the denominator of equation (3.8). Using this simplified scheme values of k_6', k_7 and K_5 have been obtained (126) by numerically fitting data from the literature to the resultant form of equation (3.3). These values, tabulated in Table 3-2, deviate considerably from those obtained by Matteson et. al. (87). Perhaps the most significant difference is between the relative values of k_6' and k_7 which, as may be seen from the reaction scheme, determine the conversion rate of the complex $Mn.SO_3^{2+}$ to sulphuric acid.

If it is assumed that the rate constants of Wadden (126) are reasonably correct, and that those of Matteson et. al. (87) are in error, it will be necessary to recalculate values of k_1 and k_2' since the values determined by Matteson et. al. are inter-related with the values of k_6' and K_5. However, k_1 and k_2' can be very easily calculated from data obtained in the literature. Matteson et. al. (87) have pointed out that, if the catalyst concentration is much lower than the sulphur dioxide concentration, i.e. $(MnSO_4)_o << H[SO_2]_o$ the first step of the mechanism (I) becomes rate-controlling, and the kinetics follow the equation

$$\frac{d}{dt}(SO_2) = -k_1(MnSO_4)_o^2 \qquad \ldots \qquad (3.13)$$

i.e. the reaction rate becomes independent of the sulphur dioxide concentration and proportional to the square of the catalyst concentration. This result has been observed experimentally, both in bulk solutions (16, 54), and in droplets (58). Therefore it has been possible to utilise the data of these workers to determine a value of k_1.

Only the data of Johnstone and Coughanowr (58) and Coughanowr and Krause (16) have been used, since their experimental points show rather less scatter than do those of Hoather and Goodeve (54). A linear fit of $(MnSO_4)_o^2$ versus reaction rate was made for the data of the two above-mentioned works. In the former case a value of 3.54×10^4 cm^3 $mmol^{-1}$ min^{-1} was obtained for k_1, while in the latter case the value was 2.73×10^4 cm^3 $mmol^{-1}$ min^{-1}. These values are in reasonable agreement with each other, and disagree with the value quoted by Matteson et. al. (87) by about a factor of ten. The value obtained from the results of Johnstone and Coughanowr (58) will be used in this work, though numerical experiments showed that the use of the other value produces little discrepancy.

Finally, a value of k_2' may be obtained from equation (3.9), since k_1, k_6', K_s and H are known. The values of the rate constants used in this work, together with those obtained by Matteson et. al. (87) for comparison, are given in Table 3-2.

Some results obtained using the new rate constants in the analytical solutions (equations (3.10) and (3.11)) are given in Table 3-1 (b)(i). Although more reasonable sulphuric acid concentrations are now produced, the discrepancy between the steady-state value of (X)e and the value (X) calculated from equation (3.12) is extremely large. This suggests that the assumption that (X)e remains approximately constant, as given by equation (3.8), is probably invalid. Therefore, a computer programme to numerically integrate equations (3.2), (3.3) and (3.4) simultaneously was developed, using the initial condition (X)o = 0. This, as shown by the values in Table 3-1 (b)(ii) produces sulphuric acid concentrations of the expected order, and low concentrations of (X) which agree exactly with values obtained from equation (3.12).

Finally, the results of the numerical solution of equations (3.2), (3.3) and (3.4), using the constants in the second column of Table 3-2,

are presented in Figs. 3-II, 3-III and 3-IV, for different initial conditions. These results show all the expected trends; a gradual reduction in sulphur dioxide concentration in the gas phase, an increase in the sulphuric acid concentration to a value of the order anticipated, and an initial jump in the concentration of intermediates, followed by a steady decrease as the concentration of sulphuric acid increases and the reaction rate decreases. It should be noted that these predictions take no account of solution dilution due to water condensation, or of the reduction in the solubility of sulphur dioxide as the concentration of sulphuric acid in the liquid phase increases. The effects of droplet growth, due to the condensation of ambient water vapour and its effects on the solution concentration, will be considered in the next section, and in Section 3.6.

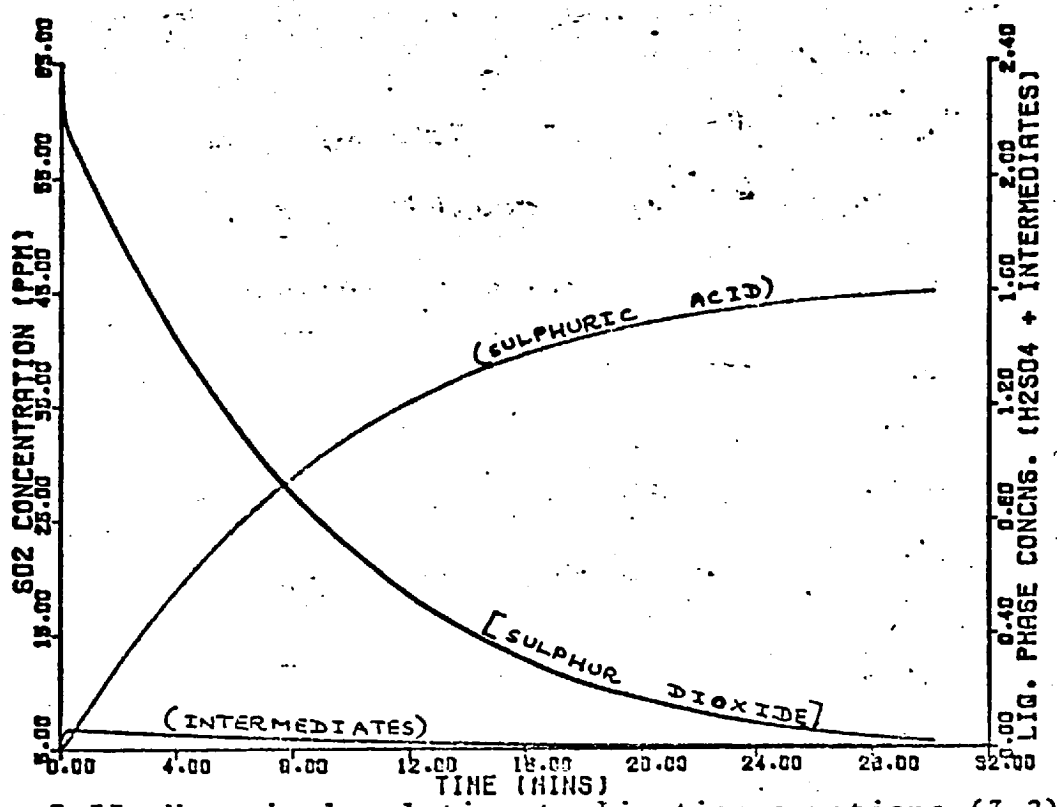

Fig. 3-II: Numerical solution to kinetics equations (3.2) to (3.4) using rate constants of Wadden (126) and Johnstone & Coughanowr (58).

$(MnSO_4)_o$ = 0.347 m.mol.cm.$^{-3}$; $[SO_2]_o$ = 63 ppm.

ϕ = 1.596 cm.^{3}m.$^{-3}$

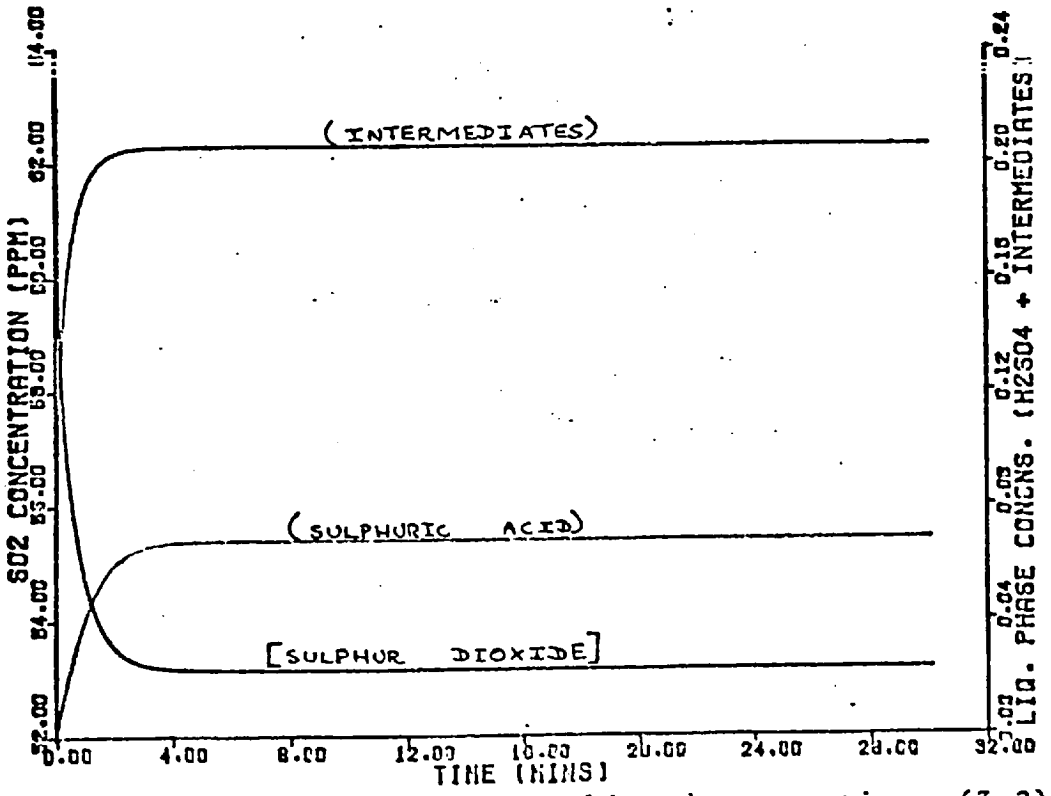

Fig. 3-I: Numerical solution to kinetics equations (3.2) to (3.4) using rate constants of Matteson et al. (87)

$(MnSO_4)_o$ = 0.347 m.mol.cm.$^{-3}$; $[SO_2]_o$ = 63 ppm.

ϕ = 1.596 cm.^{3}m.$^{-3}$

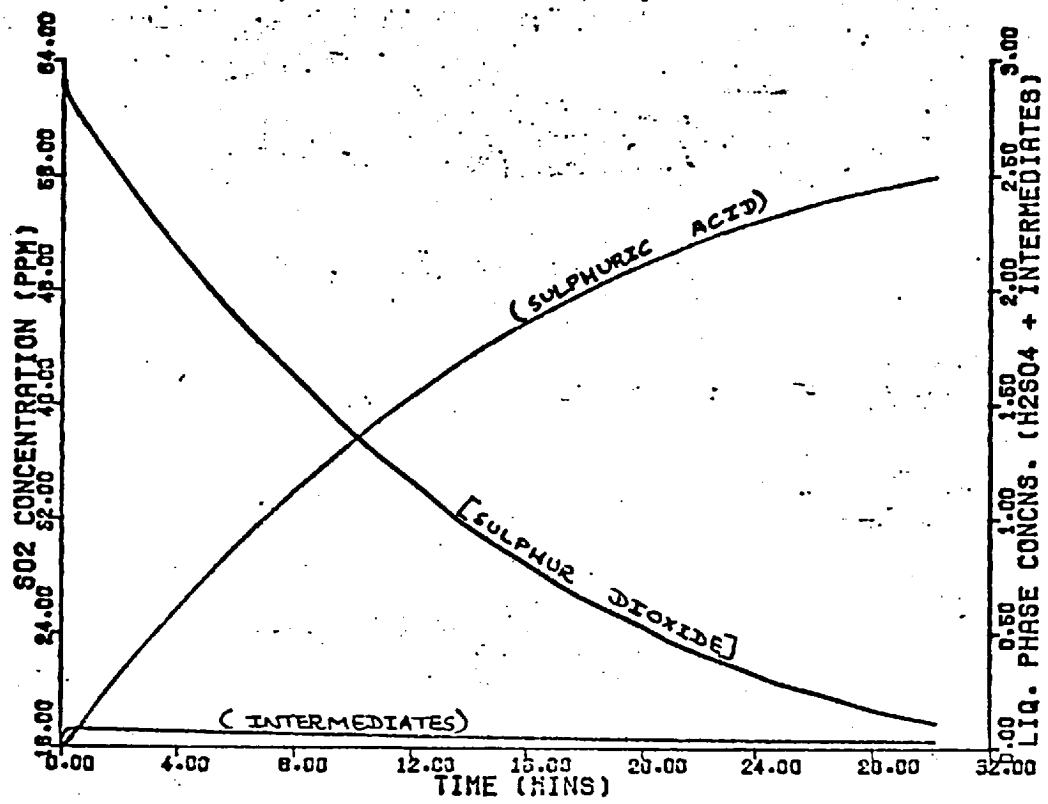

Fig. 3-III: Numerical solution to kinetics equations

$(MnSO_4)_o$ = 0.347 m.mol.cm.$^{-3}$; $[SO_2]_o$ = 63 ppm.

ϕ = 0.698 cm.^{3}m.$^{-3}$

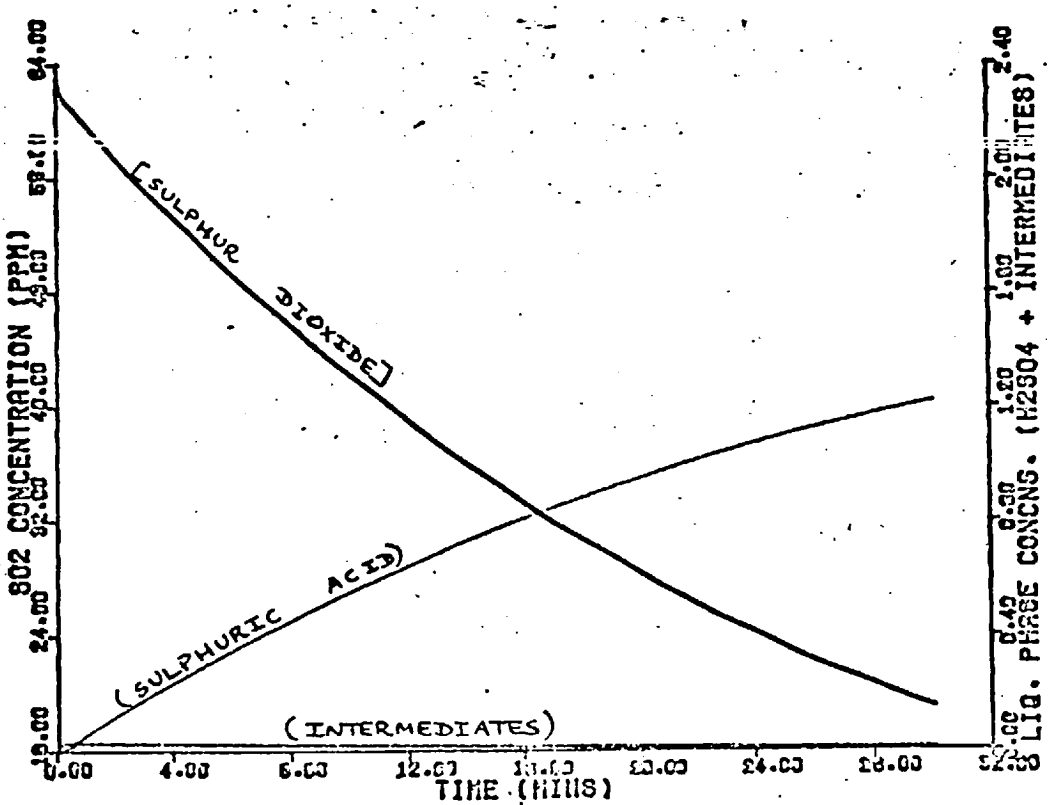

Fig. 3-IV: Numerical solution to kinetics equations

$(MnSO_4)_o$ = 0.135 m.mol.cm.$^{-3}$; $[SO_2]_o$ = 63ppm.

ϕ = 1.595 cm.^{3}m.$^{-3}$

3.3. Particle Growth Occurring due to the Reaction Described in Section 3.2

The five contributory steps that affect droplet growth occurring as a consequence of reaction within the droplets have already been outlined in Section 3.1. It was also asserted that the reaction may be considered the rate-controlling step for the mechanism of particle growth. In this section, some justification for this assertion will be presented, and a quantitative account of the effects of particle growth will be given.

Maddock (78) has studied, both theoretically and experimentally, the growth of droplets of concentrated sulphuric acid in atmospheres containing water vapour. In this case, only two transfer mechanisms come into play, viz. the diffusion of water vapour molecules from the ambient atmosphere to the droplet surfaces (gas phase diffusion) and the diffusion of liquid water from the droplet surface throughout the bulk of the droplet. Maddock (78) numerically solved both the steady-state Maxwell equation for gas phase diffusion and the non-steady-state form (these equations are given by Fuchs (30)) for the case of a particle with an outwardly moving boundary, into the bulk of which liquid phase diffusion is taking place. The results indicated that, in the gas phase diffusion situation, equilibrium between the aerosol and the gas phase was attained in a period of the order of 10^{-3}s., while uniformity of concentration in the liquid phase was achieved in even shorter times (10 - 100 μs.) Experimentally, Maddock (78) found that no significant variation of particle size with time occurred once the acid particles and humid air had been contacted, indicating that equilibration had probably taken place in a very short time, i.e. less than the shortest aerosol/humid air contact time used in the experiment (about 6s.)

It has been shown in the previous section that the time scale over which the catalytic oxidation of sulphur dioxide to sulphuric acid in the droplets takes place may be considered to be of the order of tens

of minutes. Thus, from the results of Maddock (78), it may be assumed that the liquid phase reaction controls the aerosol growth rate, despite the fact that the diffusion of sulphur dioxide is rather slower than that of water vapour. Matteson et. al. (87) make this assumption in their work, concerned with aerosols of about the same size as those used in this work. Results for larger particles, however, have been analysed somewhat differently; Johnstone and Coughanowr (58), working with droplets of 0.7 to 0.9 mm. diameter, considered the diffusion of sulphur dioxide within the droplets and the inhomogeneities in sulphur dioxide concentration throughout the droplets. Here, however, the liquid diffusion field is much larger than in the droplets considered in this work.

Estimates in the literature of the extent of droplet growth due to the reaction vary enormously. Foster (31) has calculated, using particle composition and humidity data obtained by Johnstone and Moll (60), that an aerosol, with a manganous sulphate 'nuclei' concentration of 2 mg. m^{-3} and an initial particle diameter of 0.65 μm. in an atmosphere of 95% relative humidity, will grow to 2.75 μm. after three minutes exposure in an atmosphere containing 250 ppm. of sulphur dioxide, a liquid phase sulphuric acid concentration of 1.38 mmol. cm^{-3} having been attained. Matteson et. al. (87), however, predict a maximum size increase of 5% by volume for their particles, given that the initial relative humidity of the surrounding atmosphere is 100%. This figure must, however, be considered in the context of the above authors' very low apparent yields of sulphuric acid, obtained using their apparently erroneous rate constants (see Section 3.2).

Starting with the assumptions that the growth of the particles is controlled by the liquid phase reaction rate, and that the kinetics given in Section 3.2 adequately represent the reaction, an analysis of particle growth will now be attempted. To begin, it is necessary to know something of the relative rates of increase in size for particles

of different sizes, and hence the effects of growth on the dispersity of the aerosol. For diffusion controlled processes, Reiss (111) has deduced that the rate of increase of the square of the particle radius is constant for all particles, and hence the aerosol tends to become more monodisperse. This is a rather different situation from that in which growth is reaction rate controlled. In this case, since the initial solute concentration is uniform (provided the particles are not so small that surface tension effects become important), droplet volumes will be proportional to the mass (or volume) of the manganous sulphate 'nuclei' of the particles. If diffusional processes are considered rapid, then vapour pressure equilibrium may be considered to exist between the bulk of the liquid phase and the bulk of the gas phase, with respect to both water vapour and sulphur dioxide. Thus, at any given time all reactant concentrations are the same throughout the liquid phase of the aerosol. Therefore, the ensuing sulphuric acid concentrations will be the same throughout all the droplets. Now, in order for droplet concentrations to remain equal during particle growth, the growth must take place at such a rate that the increase in particle volume is proportional to the particle volume at any given time. Thus, at any given time t, the growth function $G(v,t)$ may be represented by

$$G(v,t) \equiv \frac{dv}{dt} = v.\ I(t) \qquad \ldots \qquad (3.14)$$

where v is the particle volume at time t

$I(t)$ is the particle growth rate, a function of time only, defined by equation (3.14).

It will be proved later that the effect of this assumption is that the ZOLD spread parameter remains constant throughout droplet growth, i.e. the polydispersity of the distribution remains unchanged.

The growth rate of the aerosol $I(t)$ can be calculated from a knowledge of the solute concentration/humidity relationship between the droplets and the ambient atmosphere. Before this is discussed, the

variation of the vapour pressure above a droplet with droplet size will be considered. Values of p_a/p_∞, where p_a is the equilibrium vapour pressure over a droplet of diameter a and p_∞ is the equilibrium vapour pressure over a plane surface of the same composition as the droplet, are given in Table 3-3 for water droplets at 25°C. These results have been calculated from the Kelvin equation (84). From Table 3-3 it may be seen that it is possible to neglect surface tension effects for the droplets considered in this work, for which the modal particle diameter is expected to lie in the 0.1 - 0.5 μm. size range.

Many different approaches have been applied to the formulation of the equation for the equilibrium relationship between the solute concentration in the droplets and the humidity of the ambient atmosphere. Classically, a Raoult's Law relationship is applied. The thermodynamic aspects of changes in the droplet concentration/humidity equilibrium in the atmosphere have been presented by Köhler (72), in the theory of condensation on to hygroscopic nuclei. In the application of Raoult's Law to electrolyte solutions, care must be taken to ensure that the effects of solute dissociation are considered; McDonald (100) has pointed out that errors in much U.S. meteorological literature have been due to neglect of this factor. Mason (84) derived a formula for expressing vapour pressure as a function of solute concentration by considering the effects of the osmotic pressure of the solution on its free energy. It has been decided, however, to use the approach of Low (76) in this work, since this treatment has a very sound theoretical basis, and data is readily available in a convenient form. The derivation of the concentration/humidity relationships, using this approach, for solutions of manganous sulphate and of sulphuric acid is given in the appendix to this work. Some values of p/p_o, where p is the vapour pressure over a solution containing electrolyte and p_o is the saturated vapour pressure of pure water at the same temperature and pressure, have been calculated, and are given in Table 3-4 (i) and (ii) for solutions of

Table 3-3: Effect of droplet surface curvature on vapour pressure for water droplets at 25°C.

Particle diameter a (μm.)	$\frac{p_a}{p_\infty}$	Particle diameter a (μm.)	$\frac{p_a}{p_\infty}$
1.000	1.00052	0.050	1.01055
0.500	1.00105	0.010	1.05386
0.100	1.00526	0.005	1.11063

Table 3-4: Vapour pressure lowering of solutions of manganous sulphate & sulphuric acid.

(i) Manganous sulphate solution.

Solution concentration mmol.cm.$^{-3}$	Calculated relative humidity $\frac{p}{p_o}$	Solution concentration mmol.cm.$^{-3}$	Calculated relative humidity $\frac{p}{p_o}$
0.1	0.99798	1.1	0.97842
0.2	0.99609	1.2	0.97650
0.3	0.99416	1.3	0.97461
0.4	0.99221	1.4	0.97275
0.5	0.99023	1.5	0.97091
0.6	0.98824	1.6	0.96910
0.7	0.98626	1,7	0.96731
0.8	0.98428	1.8	0.96556
0.9	0.98231	1.9	0.96384
1.0	0.98035	2.0	0.96216

Table 3-4 (continued)

(ii) Sulphuric acid solutions

Solution concentration mmol.cm.$^{-3}$	Calculated relative humidity $\frac{p}{p_o}$	Solution concentration mmol.cm.$^{-3}$	Calculated relative humidity $\frac{p}{p_o}$
0.1	0.99636	1.4	0.94572
0.2	0.99317	1.6	0.93571
0.3	0.98999	1.8	0.92514
0.4	0.98671	2.0	0.91404
0.5	0.98330	2.5	0.88414
0.6	0.97975	3.0	0.85149
0.7	0.97604	3.5	0.81652
0.8	0.97218	4.0	0.77966
0.9	0.96815	4.5	0.74132
1.0	0.96397	5.0	0.70192
1.2	0.95515		

manganous sulphate and sulphuric acid respectively. It may be seen that quite large changes in droplet composition would be expected to result in quite small changes in the equilibrium relative humidity, or, conversely, small fluctuations in the humidity of the atmosphere suspending the aerosol particles may have drastic effects on the concentration of the droplets, and hence their size. Also, it may be conjectured that, if the humidity were to fall below a critical level, corresponding to the equilibrium value for a saturated solution of manganous sulphate, then the water in the droplets will tend to evaporate off, leaving dry manganous sulphate nuclei. Orr and co-workers (106) noted that small nuclei, less than 1 μm. in diameter, have solubilities in excess of those predicted by the theory of Köhler (72) (which predicts that the solution should become supersaturated at lower humidities). However, one of the problems involved in the experimental part of this work was the maintenance of high humidities throughout; this will be discussed further in Chapter 4.

Knowing the solute concentration/humidity relationship between the droplets and the surrounding gas, and the chemical kinetics of the oxidation process (Section 3.2) it is possible to formulate the relationship between the droplet growth rate $I(t)$, defined by equation (3.14), and the aerosol/gas contact time t. The increase in the bulk of the particles arises from two sources:-

(i) The increase in sulphuric acid concentration within the droplet. The uptake of sulphur dioxide and oxygen results in the formation of one molecule of sulphuric acid from one molecule of water. Since one mole of pure sulphuric acid would occupy a greater volume than one mole of water, the droplet volume should tend to increase.

(ii) As the sulphuric acid concentration increases, the equilibrium vapour pressure at the droplet surface decreases, and water is transferred to the droplet from the surrounding atmosphere. In the calculations, it is assumed that the water and sulphuric acid added to

the particles by droplet growth occupy the same volume as they would if they existed in the pure state. This is not very satisfactory, since solutions of sulphuric acid in water are known to have volumes slightly smaller than that which the constituents would occupy in pure form. However, it is felt that this approximation is likely to lead to a smaller error than the alternative simple approximation that the volume increase due to (i) is negligible. It should be noted that the assumption made may cause the predicted growth rates to be larger than those observed in practice.

A computer programme has thus been developed to predict the rate of growth of the particles, and their solute concentrations, as a function of time. The programme will also predict the reduction in the sulphur dioxide concentration of the ambient atmosphere. The scheme of the calculation, similar to that adopted by Wadden et. al. (127) is as follows.

(a) The initial conditions of the system are read in, viz.

(i) The ZOLD parameters of the size distribution of the manganous sulphate nuclei in the system.

(ii) The concentration of manganous sulphate in the droplets.

(iii) The concentration of sulphur dioxide in the gas phase.

(iv) The number concentration of the aerosol particles.

Thus, the following quantities are calculated:-

1. The total mass per unit volume of the dry manganous sulphate nuclei.
2. The initial volume fraction of particles in the aerosol.
3. The equilibrium relative humidity of the surrounding atmosphere at $t = 0$. This is calculated from the initial manganous sulphate concentration using the method given in the appendix of this work.

(b) Increment time t by Δt (0.1 min.) Calculate new values of the gas phase concentration of sulphur dioxide and of the liquid phase concentrations of both sulphuric acid and the intermediate reaction compounds (X) described in Section 3.2.

(c) Calculate the new equilibrium vapour pressure of the surrounding atmosphere, using the new concentration data, as described in the appendix.

(d) Does this new equilibrium vapour pressure agree with the previous value within a specified tolerance level (10^{-6})? If it does, then proceed to step (e). If it does not, calculate the amount of water vapour condensing on to, or evaporating from, the droplets such that the equilibrium vapour pressure of the ambient gas changes from its current to its previous value, as given by step (c) (or (a) 3). Recalculate the solution concentrations of manganous sulphate, sulphuric acid, and the reaction intermediates. Go back to step (c).

(e) Check that the total water content of the system, considering both liquid and gas phases, has remained unchanged, to within a specified tolerance level (10^{-3}). If this condition is satisfied, proceed to step (f). If not, scale the current value of the relative humidity such that the condition is satisfied and return to step (d).

(f) Calculate the increase in volume of the liquid content due to the formation of sulphuric acid (process (i) above), ΔV_a, and that due to the accretion of water from the gas phase (process (ii) above), ΔV_w. Hence calculate the total change of the volume of liquid in the system, $\Delta V = \Delta V_a + \Delta V_w$ in the time increment Δt. Calculate and store a finite-difference approximation of I(t) over the time increment as $I(t) = \left(\frac{1}{V}\right)\left(\frac{\Delta V}{\Delta t}\right)$ where V is the volume of liquid in the system at the beginning of the time step.

(g) Does the current t value equal or exceed the specified maximum value? If it does, write out required values, and terminate. If it does not, return to step (b).

Results from this computation are illustrated in Figs. 3-V to 3-VII, for input conditions identical to those used in the previous section to produce Fig. 3-II. It should be noted, at this stage, that these input conditions correspond to a fairly large volume fraction of particles, larger than any observed during the experimental work, and therefore the predicted growth in this case is rather less than would be expected in a more dilute aerosol (see Sections 3.6 and 5.3). It may be seen that Figs. 3-II and 3-IV are almost identical, showing that, in this case, particle growth has a negligible effect on the predicted gas phase sulphur dioxide concentration and liquid phase sulphuric acid concentration. Fig. 3-VI shows the growth rate I(t) as a function of time, and Fig. 3-VII illustrates the resultant increase in the size of the particles in this case.

Finally, the effect of droplet growth according to the above mechanism on a particle size distribution initially obeying a ZOLD function (Section 2.2), with modal diameter $a_m(t=0)$ and spread parameter σ_0 will be considered. If growth proceeds in a manner satisfying equation (3.14), then, at time t

$$v(t) = v_0 \exp\left[\int_0^t I(t)\,dt\right] \qquad \cdots (3.15)$$

where $v(t)$ is the volume of a given particle at time t

v_0 is the volume of the same particle at t = o

This relationship is used to predict the ratio $v(t)/v_0$, illustrated in Fig. 3-VII. Now, if the number density of particles of volume v at time t (i.e. the number of particles per unit volume of aerosol - see Section 2.1) is represented by $n(v,t)$, the distribution function would be expected to change as

$$n\left\{v \exp\left[\int_0^t I(t)\,dt\right], t\right\} = \frac{n(v,0)}{\exp\left[\int_0^t I(t)\,dt\right]} \qquad \cdots (3.16)$$

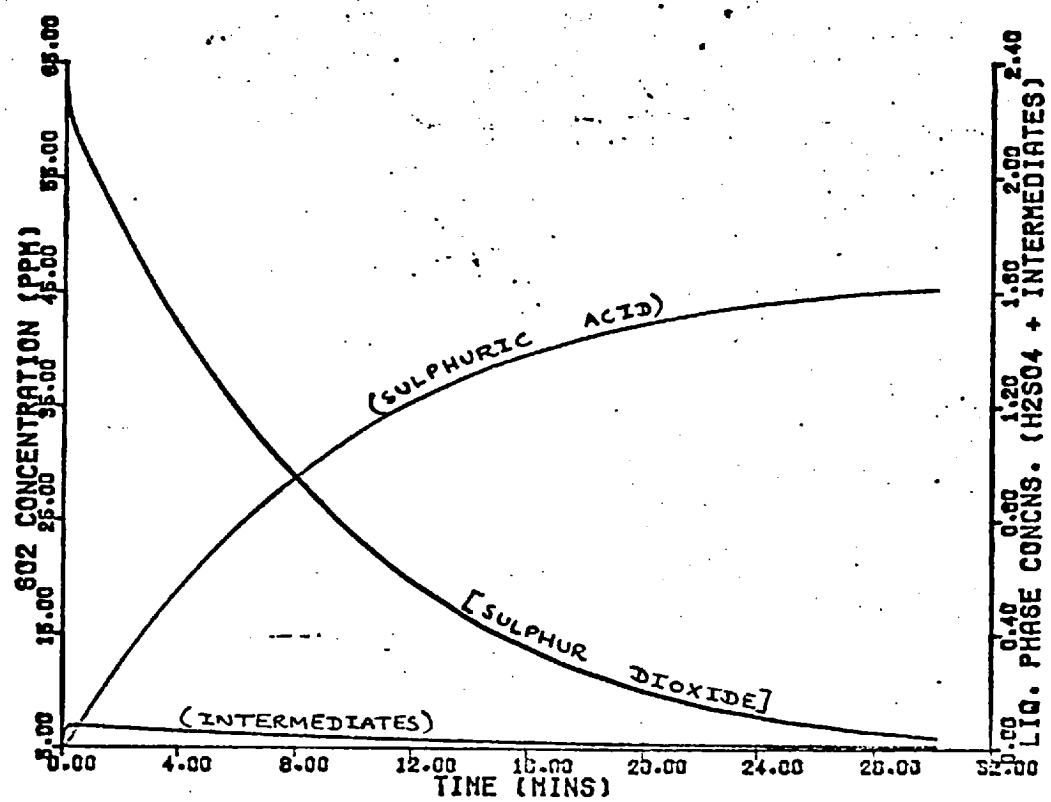

Fig. 3-V: Numerical solutions to kinetics equations for the case of a growing aerosol.

$(MnSO_4)_o = 0.347$ m.mol.cm.$^{-3}$; $[SO_2]_o = 63$ ppm.

$\phi = 1.596$ cm.^{3}m.$^{-3}$

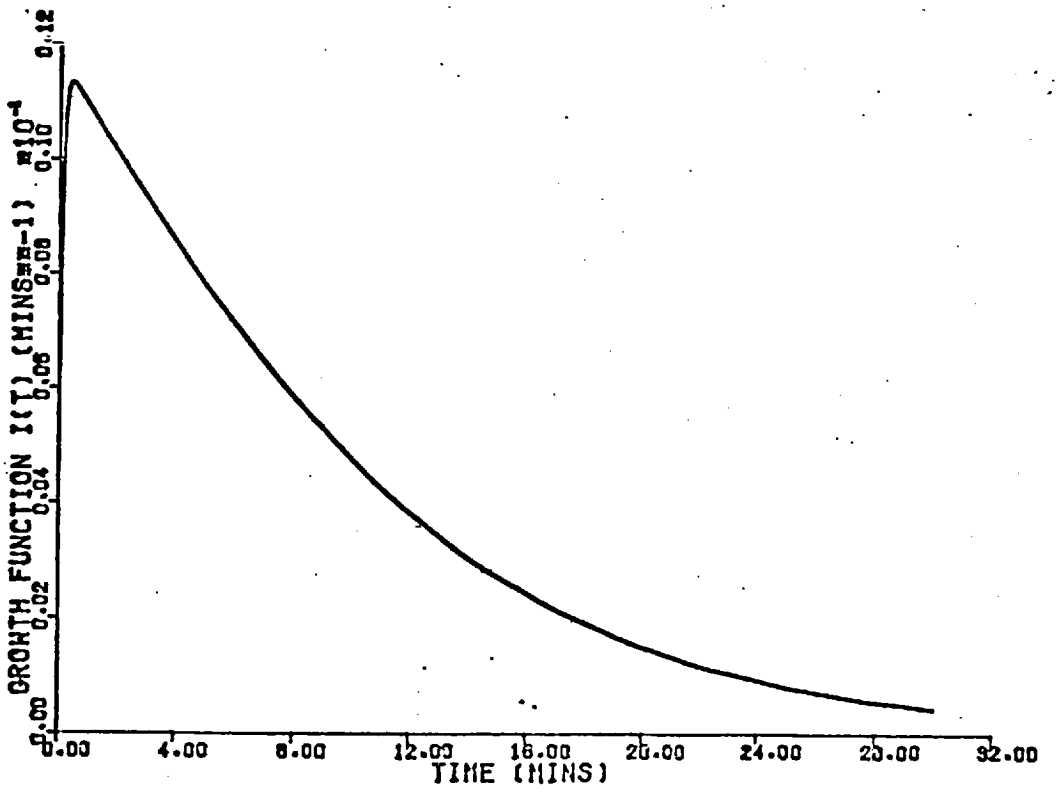

Fig. 3-VI: Particle growth rate $I(t)$ for system with initial conditions given in Fig. 3-V.

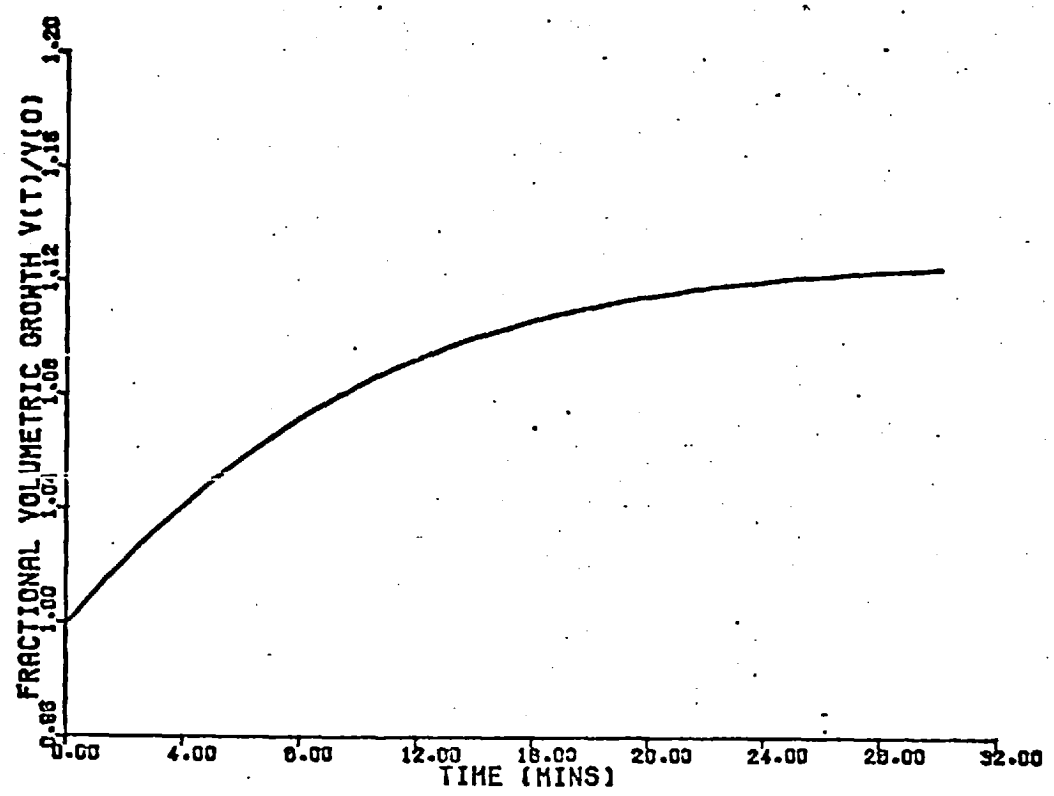

Fig. 3-VII: Volumetric growth rate of particle $v(t)/v_0$ with initial conditions given in Fig. 3-V.

The most general equation for droplet growth, in the absence of particle/particle interactions (coagulation) or particle/wall interactions (e.g. sedimentation).

$$\frac{\partial}{\partial t}\left[n(v,t)\right] + \frac{\partial}{\partial v}\left[n(v,t)\, G(v,t)\right] = 0 \qquad (3.17)$$

where $G(v,t)$ is the particle growth function $\frac{dv}{dt}$ given in equation (3.14)

If $G(v,t)$ is of the form given by equation (3.14), equation (3.17) reduces to

$$\frac{\partial}{\partial t}\left[n(v,t)\right] + v\, I(t) \frac{\partial}{\partial v}\left[n(v,t)\right] + I(t) n(v,t) = 0 \qquad (3.18)$$

Now, if equation (3.16) represents a solution to the general equation (3.18), then it should be possible, via substitution to transform equation (3.18) to an ordinary differential equation in one independent variable. Introducing the new independent variable

$$\eta = v \exp\left[\int_0^t I(t)\, dt\right] \qquad (3.19)$$

assume that

$$\psi(\eta) = n(v,t) \qquad (3.20)$$

Substitution of equations (3.19) and (3.20) into equation (3.18) leads to the result

$$2\eta \frac{d\psi}{d\eta} = -\psi \qquad (3.21)$$

Equation (3.21) is an ordinary differential equation with independent variable η. The fact that equation (3.18) can be transformed into this form indicates that solutions of the type given by equation (3.16) satisfy the general requirement for particle growth of equation (3.18).

Solution of equation (3.21) should produce an equation which, given the validity of equation (3.16), should characterise the growth process at all $t \geq 0$. Thus

$$\frac{\psi}{\psi_0} = \left(\frac{\eta}{\eta_0}\right)^{-1/2} \qquad (3.22)$$

where η_o is a chosen reference point, and

$$\psi_o = \psi(\eta_o),$$

gives the variation of the number density of the particles with the new independent variable η.

Equation (3.16) states that all particles increase by a factor of

$$\exp\left[\int_o^t I(t)\,dt\right]$$

after time t. Now, from the properties of the ZOLD function, this would have the effect of increasing the modal diameter of the function by a factor of the cube root of this value, the spread parameter remaining constant, i.e.

$$a_m(t) = a_m(t=0)\,\exp\left[\frac{1}{3}\int_o^t I(t)\,dt\right] \qquad (3.23)$$

where $a_m(t)$ is the modal diameter at time t

$a_m(t=o)$ is the modal diameter at t = o

It is of interest to note that the form of the distribution continues to conform to the ZOLD function. Use of this fact, and equation (3.23) will be made in Section 5.3, where comparison with experimental results will be undertaken.

3.4. Coagulation of the Aerosol

In Sections 3.2 and 3.3 the mechanism of droplet growth occurring due to reaction with an ambient gaseous specie was considered. In this section, the changes in the particle size distribution due to particle/particle interactions will be discussed. A quantitative account of coagulation due to the Brownian motion of the particles will be given, since, as will be demonstrated, this appears to be the dominant mechanism occurring under the conditions in which the experiments took place. Firstly, the formulation of the theory will be considered, followed by a brief review of methods that have been applied to obtain solutions. The authors attempt to solve the equations for the conditions under consideration will then be given. Finally, the effect of other factors, as mentioned in Section 3.1, will be briefly and qualitatively discussed.

The basic theory of Brownian coagulation was developed by Smoluchowski (121) from a quantitative treatment of Brownian motion. Smoluchowski (121, 122) obtained analytical solutions predicting the changes in the particle size distribution occurring in the early stages of coagulation of an initially monodisperse colloidal suspension. Later, Müller (97, 98) produced a slightly more generalised result describing the behaviour of an initially bidisperse distribution. This solution was applied to explain the observed fact that polydisperse particulate distributions coagulate more rapidly than monodisperse ones. The validity of the results of both Smoluchowski (121, 122) and Müller (97, 98) for hydrosols of colloidal gold was demonstrated experimentally by Wiegner and Tuorila (135). In a later paper Müller (99) gives a general equation for the coagulation of a polydisperse colloidal suspension:

$$\frac{\partial}{\partial t}\left[n(v,t)\right] = \frac{1}{2}\int_0^v \beta(v_1, v-v_1)\, n(v_1,t)\, n(v-v_1,t)\, dv_1 - n(v,t)\int_0^\infty \beta(v,v_1)\, n(v_1,t)\, dv_1 \quad . \qquad (3.24)$$

where $n(v,t)$ is the number density of particles of volume v at time t, as defined in Section 2.1.

$\beta(v_1,v_2)$ is the collision parameter, denoting the probability of a collision occurring between a particle of volume v_1 and a particle of volume v_2.

Equation (3.24) is also conventionally applied to aerosols. In a hydrosol, however, the medium suspending the particles may always be considered to represent a continuum, however small the particles become. The mean free path of the molecules in a gas, the suspending medium for aerosols, is of the order of a few hundredths of a micron, under normal temperatures and pressures. Thus, it is quite common for aerosol particles to be of diameters comparable to the mean free path of the suspending gas molecules. If this is the case, then the conventional Continuum Hypothesis treatment for evaluating β breaks down, and alternative approaches need to be used. Normally, the dependence is expressed in terms of the Knudsen number of the particle, Kn, defined as the ratio of the mean free path of the surrounding gas molecules to the radius of the particle, i.e.

$$Kn = \frac{\lambda}{r} \qquad (3.25)$$

where λ is the mean free path of the gas molecules, and

r is the particle radius.

The approach to the evaluation of β is thus determined according to the value of Kn.

1. $Kn \leq 0.1$.

This is the case of the classical Continuum Hypothesis, in which the particles are large enough compared with the mean free path of the suspending gas molecules to assume that a no-slip condition exists at the particle surfaces. The form of β, expressed as a homogeneous function of the particle radii, r_1 and r_2, is as given by Smoluchowski (121, 122) and by Müller (99) with reference to hydrosols.

$$\beta(r_1,r_2) = 4\pi (\mathcal{D}_1 + \mathcal{D}_2)(r_1 + r_2) \quad . \quad . \quad . \quad (3.26)$$

where $\mathcal{D}_1$ and $\mathcal{D}_2$ are the Stokes-Einstein particle diffusivities of the particles of radii r_1 and r_2 respectively:

$$\mathcal{D}_i = \frac{kT}{6\pi\mu r_i} \quad . \quad . \quad (3.27)$$

where T is the absolute temperature of the suspending medium.

μ is the viscosity of the suspending medium.

k is Boltzmann's constant.

2. $0.1 < Kn \leq 1$

The above form of equation (3.26) is applicable in this case, providing a 'slip-flow' correction factor is employed in the evaluation of the particle diffusivity (134). The 'slip-flow' effect was first analysed by Cunningham (18). Subsequently, Knudsen and Weber (71) and Millikan (91) determined that the form of the so-called Cunningham correction factor that best fit experimental results is

$$\mathcal{D}_i = \frac{kT}{6\pi\mu r_i}\left[1 + A_i \frac{\lambda}{r_i}\right] \quad . \quad . \quad (3.28)$$

where

$$A_i = a + b \exp\left[-c \frac{\lambda}{r_i}\right]$$

a, b, and c being constants.

Knudsen and Weber (71) and Millkan (91) independently measured values of a, b, and c. These values have been reviewed by Davies (23), who has re-defined their values in terms of the currently accepted Chapman-Enskog definition of the mean free path of a gas. According to Davies (23), the best values of the constants are:

$$a = 1.125$$

$$b = 0.400$$

$$c = 1.10$$

It may be seen from equations (3.26) and (3.28) that the application of the above leads to an increase in the probability of two particles colliding as the particle size decreases.

3. $Kn > 10$.

In this size range the particles are so small that they may be considered comparable with the molecules of the suspending gas. Hence, a Kinetic Theory approach may be used for the evaluation of β. Hidy and Brock (50) give for this case

$$\beta(r_1, r_2) = \left[\frac{8\pi kT(m_1+m_2)}{m_1 m_2}\right]^{\frac{1}{2}} [r_1 + r_2]^2 \quad . \qquad (3.29)$$

where m_1 and m_2 are the masses of the particles of radii r_1 and r_2 respectively.

4. $1 < Kn < 10$.

No satisfactory general theory of particle collision mechanism exists for this region owing to the lack of knowledge of the statistical mechanical properties of dense gases. The Kinetic Theory approach has been extended by Hidy and Brock (50, 51) by applying a first collision correction, in which the collisional process for two particles is conceived as if the particles only interact through streams of gas molecules being reflected from each particle. The resultant equation, however, is only applicable for $Kn \geq 7$. The most useful results for application in this region are those obtained from Fuchs' semi-empirical Concentration Jump theory. Fuchs (37) envisaged a region of discontinuity in concentration near the boundary of the spherical particle, with a thickness of the order of the mean free path of the approaching particles. Thus, it was argued that the Continuum treatment applies over distances large compared with the mean free path of the particles, but at distances within a radial distance of the mean free path of a particle, particles will move as though in a vacuum. Thus, in the form given by Hidy and Brock (51)

$$\beta(r_1, r_2) = \frac{2kT}{3\mu}\left[\frac{1}{r_1} + \frac{1}{r_2}\right][r_1 + r_2] \cdot \Phi_c \quad . \qquad (3.30)$$

where

$$\Phi_c = \frac{r_1 + r_2}{r_1 + r_2 + (\lambda_1^2 + \lambda_2^2)^{1/2}} + \frac{2kT}{3\pi\mu}\left[\frac{1}{r_1} + \frac{1}{r_2}\right] \cdot \frac{\prod_{i=1}^{2}\left[1 + A_i \frac{\lambda}{r_i}\right]}{(\bar{u}_1^2 + \bar{u}_2^2)^{1/2}(r_1 + r_2)}$$

where $\bar{u}_1, \bar{u}_2$ are the mean velocities of motion of the particles of radii r_1 and r_2 respectively, obtained from Kinetic Theory considerations, i.e.

$$\bar{u}_i = \left[\frac{8kT}{\pi m_i}\right] \quad . \quad . \quad . \quad (3.31)$$

λ_1, λ_2 are the mean free paths of the particles of radii r_1 and r_2 respectively, obtained from the Stokes-Einstein particle diffusivity (equation (3.27))

$$D_i = \frac{\pi}{8} \bar{u}_i \lambda_i \quad . \quad . \quad (3.32)$$

A_i is the Cunningham correction factor, given in equation (3.28)

λ is the mean free path of the gas molecules.

Astakhov (2) has examined Smoluchowski's diffusion problem in the light of solutions to the steady-state Fokker-Planck equations, in an attempt to construct a more accurate theory of coagulation in the region of $Kn \approx 1$. Values of Φ_c obtained from Fuchs' theory are compared with those of Astakhov, for equal sized particles, by Hidy and Brock (51). The latter authors note good agreement up to $Kn \approx 5$.

The above outline of the different mechanical models used to determine the collision parameter for interacting particles gives an indication of the complexity of the coagulation problem. More comprehensive reviews and discussion of the formulation of the theory are given, e.g. by Zebel (24), Hidy and Brock (51) and Drake (52). The variation of β with increasing Knudsen number is illustrated in Fig. 3-VIII, taken from

Hidy and Brock (51). The ordinate represents β/β_{class}, the ratio of the predicted value of β to that which would be obtained by application of the classical Smoluchowski treatment, for equal sized particles. Experimental points (10, 25, 39, 107) are also indicated.

The solution of equation (3.24), for a given set of initial and boundary conditions, is a problem that has received much attention. Solution methods are reviewed by Hidy and Brock (51), and a comprehensive review of mathematical considerations in the solution of the coagulation equation has recently been given by Drake (52). Only a brief review, with emphasis on applicability, of some methods employed to obtain solutions of equation (3.24) will be given here.

The application of a Laplace Transform method by Schumann (117) and Melzak (89) has led to analytical solutions for the case of β being assumed to be constant over the range of particle size. Moreover, Melzak (89) asserted that his method was also applicable to situations in which β is of the forms $\beta(v_1,v_2) = a(v_1 + v_2)$ and $\beta(v_1,v_2) = b v_1 v_2$, a and b being constants. Scott (118) has applied a similar method to obtain solutions in these cases. Martynov and Bakanov (83) have suggested that a complete solution of equation (3.24) may be expressed as a power series, however application of these series is only really practicable in the case of fairly monodisperse distributions. Hidy and Brock (51) have found that the above three simple cases that have been solved by the Laplace Transform method are inapplicable to practical situations, except that the case of constant β gives reasonable results for fairly monodisperse distributions over short times.

A rather different approach that has been used to obtain analytical solutions of equation (3.24) is the so-called Similarity Transformation (33, 34, 35, 75, 123, 132). This involves the reduction of equation (3.24) to an ordinary differential equation via the substitution of a trial function, in one independent variable, for $n(v,t)$. This trial function is assumed to represent the form of the function $n(v,t)$ with respect to the new independent

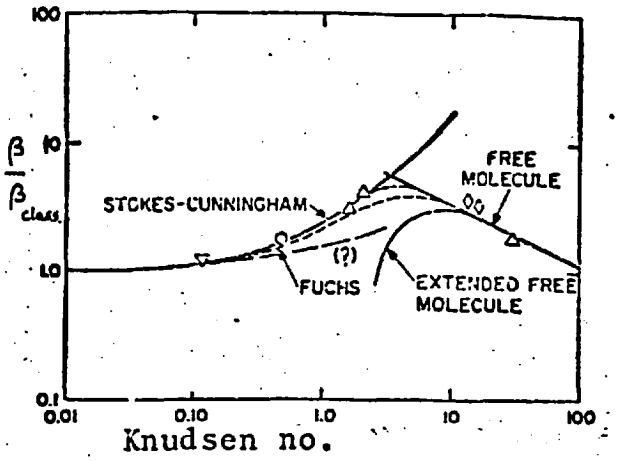

Fig. 3-VIII: Variation of β , with increasing Knudsen no. from value predicted by the classical Continuum theory. (reproduced from (51)).
Experimental points given from the following references:-
o (107) ; △ (10) ; ▽ (25) ; ◇ (39)

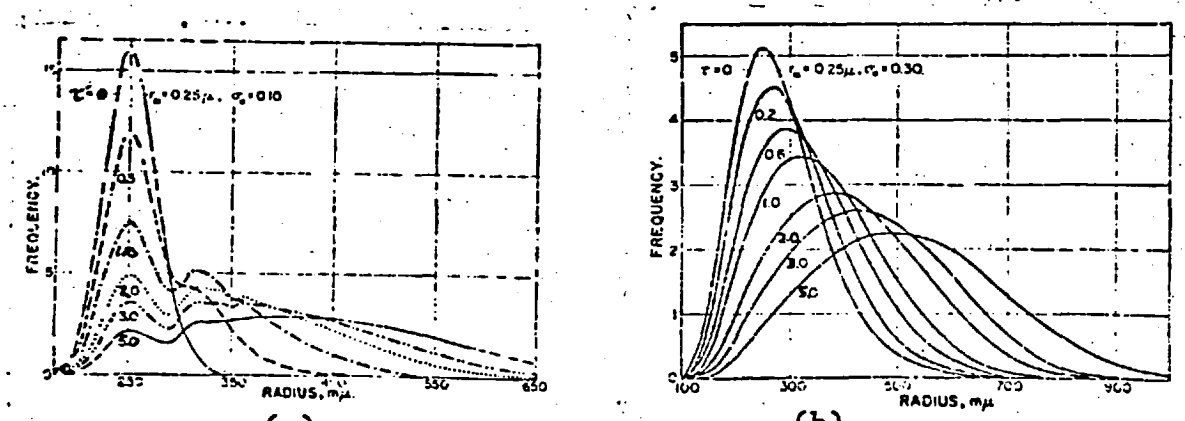

(a) (b)

(a) Modal radius = 0.25 m.
Spread = 0.1
Number concentration=10^7cm.$^{-3}$
$t'_{\frac{1}{2}}$= 3.94 min.

(b) Modal radius = 0.25 m.
Spread = 0.3
Number concentration=10^7cm.$^{-3}$
$t'_{\frac{1}{2}}$= 3.72 min.

Fig. 3-IX: Particle size distributions arising from initial ZOLDs. The numbers on the curves refer to the dimensionless coagulation time $\tau' = \frac{t}{t'_{\frac{1}{2}}}$ (reproduced from (137)).

variable is comprised of system variables which may themselves be functions of particle size and time. This method was firstly applied to explain regularities observed in the size distribution of tropospheric aerosols (33), and of stratospheric aerosols (34). Subsequently, a transformation function was found that reduces equation (3.24) to an ordinary differential equation in one variable (123). The transformed equation was then solved numerically over the whole particle size spectrum, and analytically for its extreme upper and lower ends, for the form of β corresponding to the classical Smoluchowski treatment, given by equations (3.26) and (3.27) (35). These results were in fairly good agreement with the numerical solutions of Hidy (49). A similar approach has been used to obtain a similarity solution for the case where the Stokes-Einstein diffusivity is modified by the Cunningham correction (132). Recently, a Similarity Transform has been applied to the coagulation of aerosols in the molecular regime, the mechanics of which are given by equation (3.29) (75). Clark and Whitby (13) have made measurements on atmospheric aerosols that show considerable agreement with the Similarity Transformations, but Junge (65) has pointed out that the work of Clark and Whitby (13) constitutes a necessary, but not a sufficient condition for the acceptance of the Similarity Hypothesis, applied to atmospheric aerosols. The numerical work of Hidy (49) indicates that, theoretically, an aerosol should approach a self-preserving form (predicted by the Similarity Theory) at around $\tau_1 = 3$, where τ_1 represents dimensionless time, defined by

$$\tau_1 = \frac{kT N_o t}{3\mu} \qquad (3.33)$$

where No is the number concentration of particles at t = o

t is time.

For the aerosol considered in this work, the value of t corresponding to $\tau_1 = 3$ is of the order of at least 250 min. Thus, it is not proposed to apply the Similarity Hypothesis in this work.

By far the commonest method of obtaining solutions of equation (3.24) appears to be via numerical approximation. Normally, equation (3.24) is replaced by a series of ordinary differential equations by assuming that the particles fall into discrete size groupings. The coagulation problem has been formulated in these terms by Müller (99) and Chandrasekhar (11). If there are n such groupings into which the particles may fall, n simultaneous ordinary differential equations result. It is also common practice to replace the derivatives in these equations by finite -difference approximations. These are generally forward-difference forms, since conditions are generally postulated for zero time. The forward-difference approximation of the derivative is then used to calculate the conditions at an incremented time. The new conditions enable conditions to be predicted after a further time increment, and so on. The first attempt at the computer solution of equation (3.24), or its derived discrete particle form, appears to be that of Zebel (139), who obtained a solution predicting the effects of coagulation on an initially trapezoidal distribution of particles. Hidy (49) developed a computer programme to test the validity of the Similarity Theory when applied to aerosols formed from the coagulation of monodisperse, bidisperse, and discretely polydisperse distributions. Hidy and Lilly (53) substituted Smoluchowski's simple results into the Similarity Transform relationships of Swift and Friedlander (123) and obtained a useful simple relationship describing the form of the distribution at large values of the transformed independent variable. Quon and Mockros (109) and Mockros et. al. (92) have obtained solutions for a coagulating aerosol that is continuously reinforced by the addition of a feed term. Perhaps the most useful numerical results from the point of view of this work are those obtained by Willis et. al. (137). These workers have calculated the form of the distribution, for various coagulation times, of aerosols initially having ZOLD distributions. Initial distributions having a modal radius of 0.25 μm. and spread

parameters of 0.1 and 0.3 have been used, the initial number concentration of the aerosol being taken as 10^7 cm^{-3}. The coagulated distribution curves obtained by these workers are here reproduced as Fig. 3-IX. The numbers on the curves refer to the dimensionless coagulation time $t/t'_{\frac{1}{2}}$, where $t'_{\frac{1}{2}}$ is given for each case. It may be seen that, in the case of the more monodisperse aerosol, a second peak tends to form after moderate coagulation times (about 4-8 mins.), whereas the more polydisperse aggregate remains unimodal, and keeps its shape throughout. Subsequent experimental work, with the aid of a light scattering technique, produced support for such numerical results, both for results in the 'slip-flow' regime ($0.1 < Kn \leq 1$) (103) and in the Continuum regime (102).

Since the aerosols in this work appear to have an initial modal diameter around 0.2 μm. and a spread parameter of about 0.32 (see chapter 5), it would be expected that the pattern of coagulation in this work should be similar to that predicted by Willis et. al. (137). However, since the particle number concentration used in this work is rather lower than that used by Willis et. al. (137), a technique for the estimation of the change in the particle size distribution occurring due to Brownian coagulation has been developed. This consists of splitting the distribution into 100 particle size divisions such that the increments defining the boundaries of the divisions occur at equal volume intervals. Thus, if a particle in group i coagulates with a particle in group j the resultant particle would fall into group $(i + j)$. The maximum particle diameter, a_{max}, is taken such that $p(a_{max}) \leq 10^{-3}$, i.e. the ZOLD function is truncated at that point, and the size groups are formed by calculating the volume intervals as one hundredth of the volume of the particle of diameter a_{max}. Each group is characterised, for the purpose of calculating β the collision parameter between two particles, by the mean of the radius boundaries at the lower and upper ends of the size group. This treatment is rather crude (Hidy (49), for example, advocates the use of at least 600 intervals), however the computation time required rises approximately as the square of the number of intervals

considered, and also, since the form of the result expected is known from the work of Willis et. al. (137), only a rough approximation of the expected changes is required. $\sigma_o = 0.32$ represents about the most polydisperse distribution that may be handled using this number of intervals, since the number of particles included in the first interval needs to be relatively small. (This is because, in this region, the ratio of any two particle diameters may vary enormously, hence to take the characterising radius of the interval as representing each of two particles in the group may lead to errors in the prediction of β. For intervals other than the first, the diameter ratio between the largest and the smallest particle is at the most a factor of two, which should produce a fairly insignificant error in the value of β. This has been demonstrated for hydrosols, using a Continuum approach, by Wiegner and Tuorila (135).)

Figs. 3-X and 3-XI show the histograms obtained from this computation, representing the aerosol after coagulation times of 0.7 min. and 21.0 min. Fig. 3-X shows how the number densities of the smaller particles decrease as coagulation proceeds. The position of the modal diameter appears to shift to a slightly larger particle size, but the representation is too crude to place an accurate quantitative value on this change. Also, the number of large particles in the system increases, thus making the distribution appear more polydisperse. This increase in the number densities of the large particles is best illustrated in Fig. 3-XI. Here, it may be seen that the basic logarithmic-normal shape of the distribution is maintained. Fig. 3-XII shows the decrease of the total number concentration of the aerosol with coagulation time.

Finally, the effects of factors other than Brownian motion will be briefly discussed, and an attempt will be made to justify their exclusion in the quantitative consideration of coagulation occurring in this system.

1. The effects of electric charges present, or induced, on the particles.

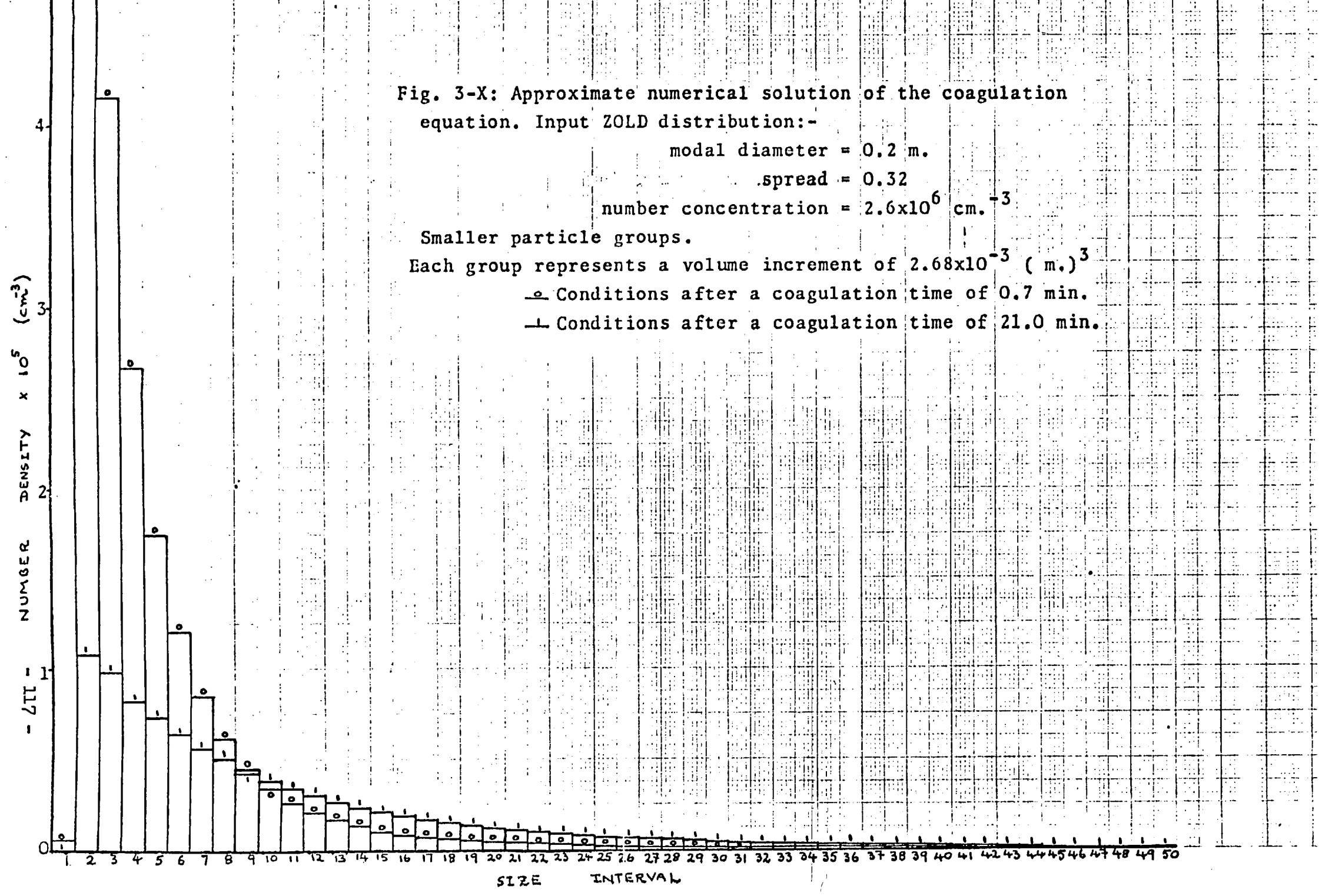

Fig. 3-X: Approximate numerical solution of the coagulation equation. Input ZOLD distribution:-

modal diameter = 0.2 m.

spread = 0.32

number concentration = 2.6×10^6 $cm.^{-3}$

Smaller particle groups.

Each group represents a volume increment of 2.68×10^{-3} $(m.)^3$

o Conditions after a coagulation time of 0.7 min.

⊥ Conditions after a coagulation time of 21.0 min.

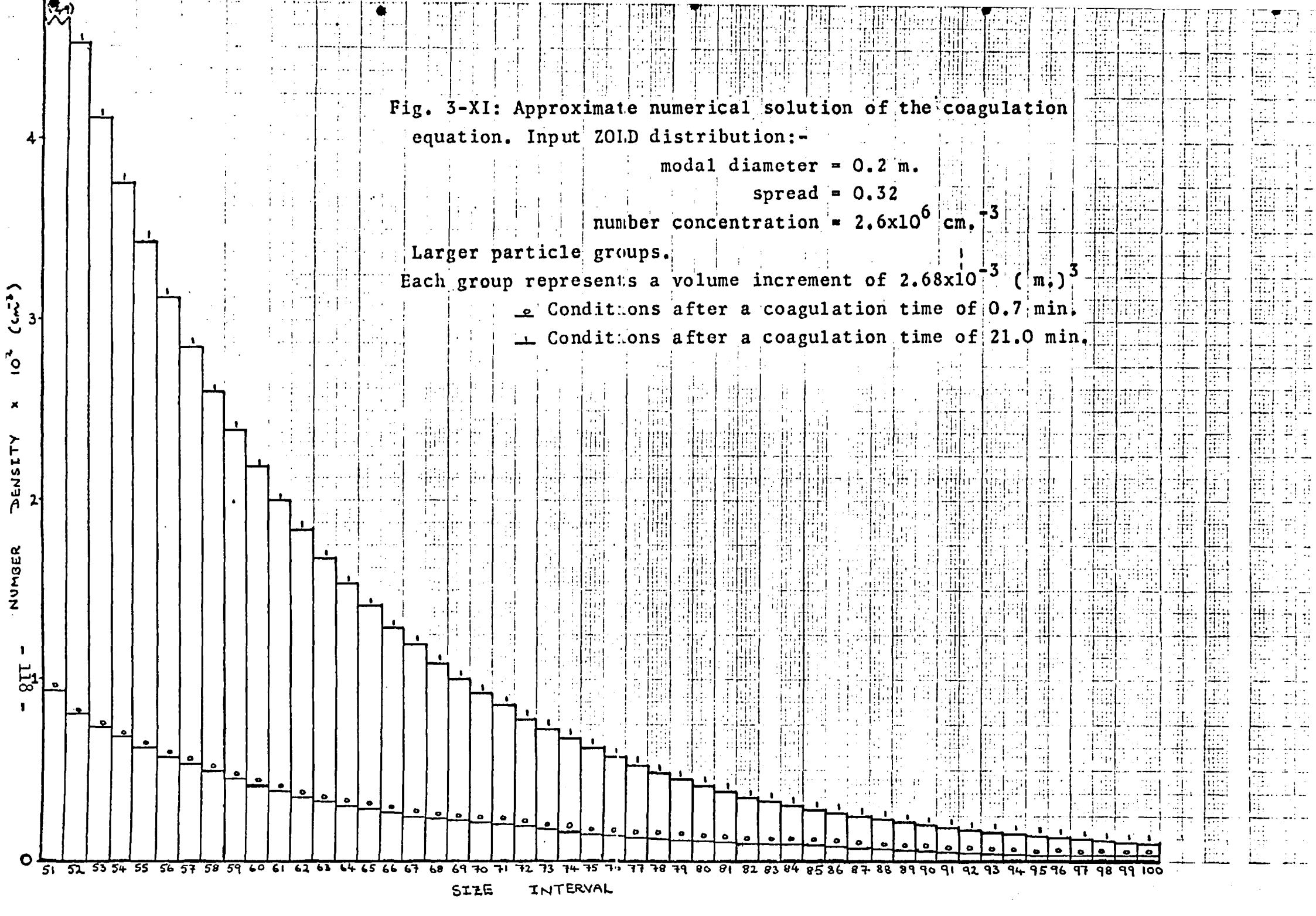

Fig. 3-XI: Approximate numerical solution of the coagulation equation. Input ZOLD distribution:-

modal diameter = 0.2 m.

spread = 0.32

number concentration = 2.6×10^6 $cm.^{-3}$

Larger particle groups.

Each group represents a volume increment of 2.68×10^{-3} $(m.)^3$

o Conditions after a coagulation time of 0.7 min.

| Conditions after a coagulation time of 21.0 min.

Fig. 3-XII: Coagulation. Change of aerosol number concentration with time. From approximate numerical solution illustrated in Figs. 3-X and 3-XI.

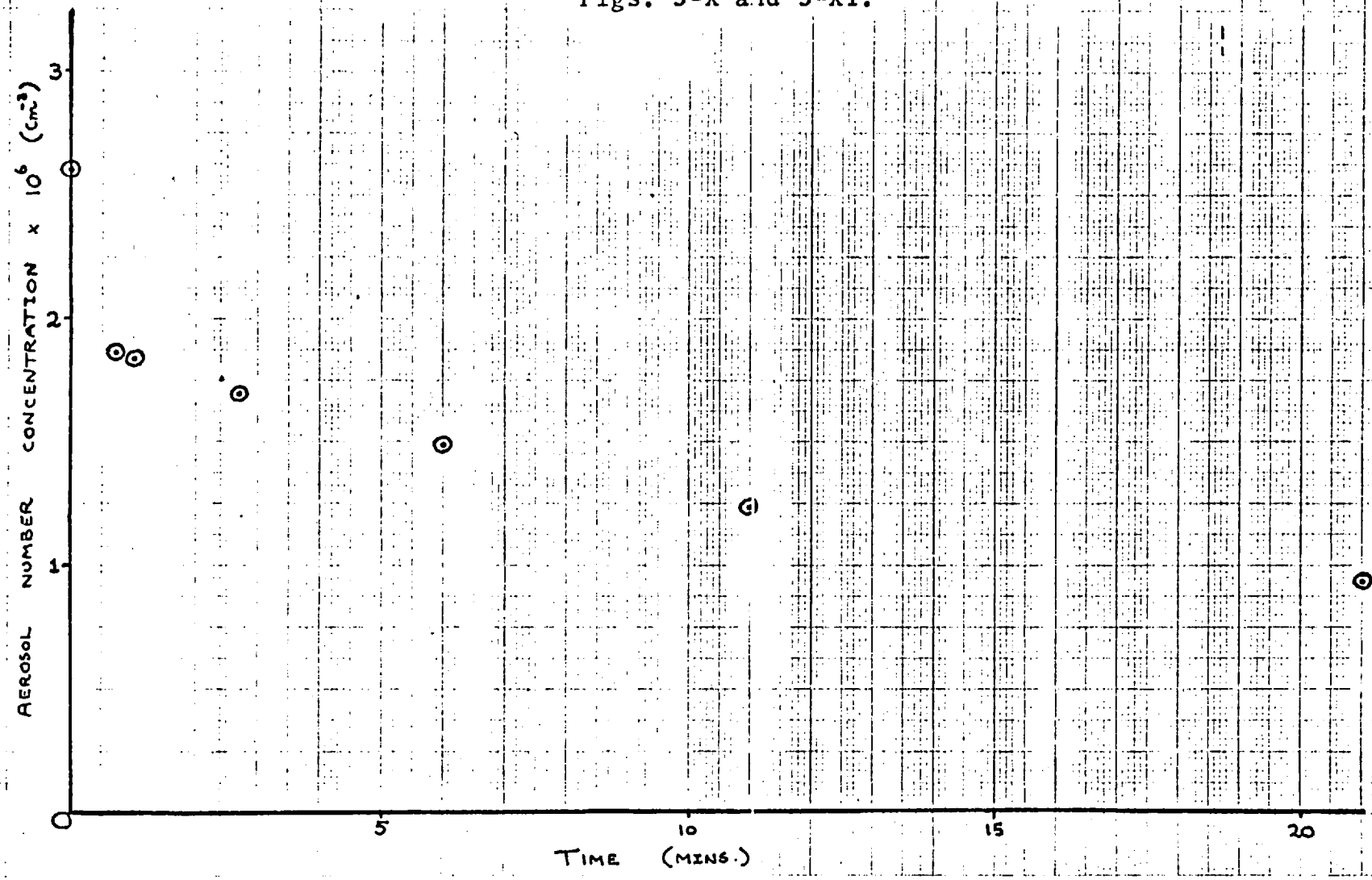

Fuchs (36) has applied the Smoluchowski theory of coagulation to aerosols carrying electric charges, and found that unipolar charges impede coagulation, but that the presence of very small bipolar charges increases the coagulation rate. Gillespie (41) has experimentally shown that the rate of coagulation and surface loss of an aerosol may be appreciably affected by the presence of electric charges on the particles. An integrodifferential equation describing the general case of the coagulation of a distribution of charged particles has been developed by Zebel (139). Although Zebel's treatment of the mechanics of the situation in which the 'slip-flow' extension of the Continuum Theory breaks down has been criticised (50) the numerical solutions obtained give insight into the effects of charging. Firstly, Zebel (139) solved the equation for particles in the absence of charge, producing curves similar to those of Willis et. al. (137) for their more monodisperse initial distribution. Then solutions for initially trapezoidal distributions of particles carrying unipolar charges were obtained on the assumption that the charge carried by a particle is proportional to its volume. The results showed that, for moderately or highly charged aerosols, there was markedly less tendency for larger particles, comprising aggregates of the particles in the initial distribution, to form.

The origins of charges on particles may be either due to the dispersion mechanism or to the presence of ionic species in the medium suspending the particles. The intensities of the charge induced by various dispersion mechanisms on a number of dispersates has been investigated by Sachsse (114). A conclusion of these measurements is that aerosols produced by atomisation (see Chapter 4) with air tend to be largely uncharged, and that particles of insoluble and insulating materials show more tendency to become charged than those produced from electrolytes. Thus, we may assume in this work, that the aerosol leaves the generator uncharged. The mechanism of particle charging in highly ionic environments has been studied by Arendt and Kallmann (1), while the charging and discharging of particles in air containing small amounts of ionic matter (i.e. the normal situation in the troposphere) has been

analysed by Kunkel (74). Kunkel (74) concludes that no general solution is possible for the prediction of the amounts of charge present on the particles, except in special cases. It will be assumed, in this work, that the presence of ionic matter in the air used for atomising the dispersate may be neglected.

2. The effects of shear due to the motion of the fluid.

In the apparatus used in this work (see Section 4.1) the particles are entrained in a laminar flowfield. Owing to the velocity gradient across the cross-section of the containing vessel, particles following different streamlines may come into contact, and subsequently coalesce, if the distance between them becomes less than the sum of the particle radii. A mathematical analysis of this situation, along similar lines to that produced for Brownian coagulation, has been presented by Smoluchowski (122). Gillespie (42) has shown, by evaluating average rate constants, that shear coagulation tends to decrease with increasing polydispersity of particle size; the opposite is the case for Brownian coagulation. Huang et. al. (55) considered the effects of shear coagulation on an aerosol possessing the same initial conditions as are given in Fig. 3-IX (a) (137). These workers reached the conclusion that a velocity gradient of 10^4 min^{-1} or greater is required to produce appreciable effects on the coagulation rate; a figure much larger than any expected in the apparatus used in this work.

3. The effects of inter-particle London- Van der Waals forces.

These are only important in the case of very small particles, in regime of coagulation determined by the Kinetic Theory approach. Hamaker (47) has computed the forces between two separated spherical particles as a function of the distance separating them, the result indicating that the London - Van der Waals forces generally cause an attraction. Overbeek (73) has contended that the retardation of these forces becomes large at interaction distances beyond 0.02 μm. Fuchs

and Sutugin (39) have taken account of these factors in their analysis of results obtained from experimental measurements of the coagulation rate of 2.5 nm. and 4.5 nm. particles. In this work, however, very few if any particles are likely to lie in the molecular regime (Kn $\geq$ 10), hence consideration of inter-particle London - Van der Waals forces appears to be unnecessary.

4. Diffusiophoretic forces.

In a system where diffusion is taking place, a small particle may experience a force arising from the motion of the diffusing species. Schmitt and Waldmann (116) have studied experimentally the force exerted on an aerosol of silicon oil in a diffusing gas mixture. A subsequent theoretical analysis has been presented by Brock (6). Since, in the situation of gases diffusing to droplets, it is not generally possible to discern a simple direction of motion for the diffusing matter (as this itself will change when the particles move) it will be assumed that the presence of diffusion in the system does not affect the Brownian motion of the particles.

3.5. The Effects of Sedimentation on The Aerosol

The possible effects of gravitational force on the constitution of a flowing aerosol are twofold. Firstly, a decrease in the number concentration may result from the deposition of particles, particularly the larger ones, on to the walls of the containing vessel. Secondly, the sedimenting motion of a particle may interfere with its random Brownian motion, and consequently may affect the coagulation rate of the aerosol.

Smoluchowski (121) has analysed mathematically the case of particles undergoing Brownian motion in the presence of an external force field, especially for the case of the gravitational force field. The result of this analysis is an equation relating the distribution of particles, in the direction of the gravitational field, to time. Although this approach in principle could be applied to predict the extent of particle sedimentation, it is unnecessary in practice. For the case of an aerosol in laminar flow through a horizontal tube, the loss of particles due to sedimentation on to the lower part has been given by Davies (24):-

$$N = N_o(1 - f) \qquad (3.34)$$

where

$$f = \frac{2}{\pi}\left[2\mu\sqrt{1-\mu^{2/3}} + \sin^{-1}\mu^{1/3} - \mu^{1/3}\sqrt{1-\mu^{2/3}}\right]$$

Here, No is the number concentration of particles at the entrance to the tubular system,

N is the number concentration of particles at the exit of the tubular system,

f represents the fractional particle loss in the system,

μ is a dimensionless parameter, determined by the size and settling mechanism of the particles, and the dimensions of the container tube.

If we assume that the particles are of equal size, characterised by diameter a, and that their deposition rate is determined by Stokes Law, then (24)

$$\mu = \frac{\pi R a^2 \rho_s L}{16 \eta Q} \qquad (3.35)$$

where R is the radius of the tube containing the aerosol,

L is the length of the tube containing the aerosol,

ρ_s is the density of the particulate substance,

a is the particle diameter,

η is the viscosity of the suspending medium,

Q is the aerosol flow-rate through the apparatus.

Values of N have been calculated for conditions corresponding approximately to those used in the experimental work, which give the maximum aerosol hold-up time in the system (see chapter 4), for particle diameters of 0.1 μm., 0.5 μm., and 1.0 μm. From the values obtained, tabulated in Table 3-5, it may be seen that the loss of particles due to sedimentation may be considered negligible for particles in the submicron range.

The second effect of particle sedimentation mentioned above, the effect of sedimenting particles on the Brownian coagulation process, has been analysed by Müller (99). Calculations from formulae given by Müller (99) indicate that, for sedimentation to affect the Brownian coagulation of the particles, particles of a diameter of 3 μm. or larger would need to be present. In any case, particles smaller than about 1.4 μm. would be practically unaffected by the presence of large, sedimenting particles. This analysis is assumed to be accurate within 10%, the accuracy on the conventional ultramicroscope used for experimental work on colloidal systems at the time.

In conclusion, it appears that the aerosols used in this work (see chapter 5) comprise particles too small for the effects of particle sedimentation to be important. Therefore no further treatment of the topic will be attempted.

Table 3-5: Sedimentation of Particles in laminar flow through a horizontal tube

Length of tube (m.)	Particle diameter (m.)	Initial number concentration ($cm.^{-3}$)	Final number concentration ($cm.^{-3}$)
50	0.1	2.600×10^{6}	2.600×10^{6}
50	0.5	2.600×10^{6}	2.598×10^{6}
50	1.0	2.600×10^{6}	2.592×10^{6}
26	0.1	2.600×10^{6}	2.600×10^{6}
26	0.5	2.600×10^{6}	2.599×10^{6}
26	1.0	2.600×10^{6}	2.596×10^{6}

3.6. Overall Model of the Aerosol/Gas System

Having discussed separately the principal factors affecting changes in the size distribution and number concentration of an aerosol of manganous sulphate particles in the presence of a reacting gas, an attempt will now be made to draw them together, and predict the time-dependent characteristics of a real system. The problem of simultaneous particle growth and coagulation has so far received comparatively little attention, presumably because of its complexity.

The basic kinetic equation for simultaneous particle growth and coagulation in a homogeneous system (where particle number densities are independent of position) is (108)

$$\frac{\partial}{\partial t}\left[n(v,t)\right] + \frac{\partial}{\partial v}\left[n(v,t)\,G(v,t)\right] = \frac{1}{2}\int_0^v \beta(v_1, v-v_1)\, n(v_1,t)\, n(v-v_1,t)\, dv_1 - n(v,t)\int_0^\infty \beta(v,v_1)\, n(v_1,t)\, dv_1 \qquad (3.36)$$

where $n(v,t)$ is the number density of particles of volume v at time t, as defined in Section 2.1.

$G(v,t)$ is the droplet growth function of a particle of volume v at time t. Its definition and form are discussed in Section 3.3.

$\beta(v_1,v_2)$ is the collision parameter between particles of volumes v_1 and v_2, as given in Section 3.4.

Pich et. al. (108) have analysed equation (3.36) for the case of Smoluchowski coagulation, with β given by equations (3.26) and (3.27), and simultaneous Maxwellian diffusive condensation (see (38)). A Similarity Transform is applied to the equation, and the resultant ordinary differential equation is solved, analytically for the extreme

upper and lower ends of the particle size spectrum, and numerically over its entire range. Wadden and co-workers (126, 127) have numerically computed some solutions of an equation similar to equation (3.36) for a model of reaction and coagulation similar to that of this work. The model is based on some simplifications, and the results and applicability to this work will be discussed later in this section.

The author has attempted to evaluate a numerical solution to equation (3.36) analagous to that produced for the case of coagulation alone, described in Section 3.4. The form of G(v,t) given by equation (3.14) is substituted, and the left hand side of equation (3.46) becomes identical with that of equation (3.18). A central difference approximation of the derivative with respect to v was introduced, and the computer programme run, as described in Section 3.4, to predict the constitution of the aerosol after time increments of 0.1 min. Values of the aerosol growth rate I(t), defined in equation (3.14), were generated previously for all required values of t and stored. It was found, however, that answers were unobtainable owing to numerical problems in the calculation. These are probably due to the fact that the volume increments are too large for the finite-difference approximation of the $\frac{\partial}{\partial v}$ term to represent the derivative adequately. It is felt that the rectification of such problems is beyond the scope of this work, and that a rather more sophisticated approach to this problem is required.

Finally, a brief discussion of the work of Wadden and co-workers (126, 127) will be given, since, in some respects, their model corresponds to the experimental situation in this work. The model consists of a control volume, into which a constant rate of input is introduced, and out of which all particles larger than a specified volume are deposited. Inside the control volume particles undergo coagulation and growth. The particle collision parameter β is assumed to be constant, and the gas phase sulphur dioxide concentration is assumed not to vary. The input aerosol is either monodisperse, or obeys a logarithmic-normal distribution. Solutions are obtained for the steady-state condition of the system, i.e.

all time derivatives are set to zero. This model was set up in an attempt to interpret phenomena observed in the atmosphere.

The results of Wadden et. al. (127) indicate that, if the sulphur dioxide concentration is above about 3.4 ppm., both droplet growth and coagulation will affect the shape of the resultant particle size distribution. At sulphur dioxide concentrations below this figure, droplet growth stops at the relative size at which a maximum liquid phase sulphuric acid concentration is reached. In the former case, it is presumably true that the effect of droplet growth due to the absorption of water is to keep the acid sufficiently dilute to ensure further reaction. In the latter case, however, the rate of accretion of water may be so slow that the sulphuric acid concentration corresponding to kinetic equilibrium is soon reached, and no further reaction or absorption will take place. Hence, in this case, subsequent changes in the particle size distribution may be accredited to coagulation alone. These results may be applied to the system used in this work. If the ambient sulphur dioxide concentration is sufficiently large compared with the volume fraction occupied by the aerosol particles, sufficient sulphuric acid will be formed initially to produce a relatively large vapour pressure displacement, and thus considerable dilution of the acid will result. This enables the reaction to continue. It should also be noted that this situation requires a high initial relative humidity. If the ambient sulphur dioxide concentration is fairly low compared to the particle volume fraction, then the rate of formation of sulphuric acid will tend to fall off before appreciable droplet growth has taken place, and hence comparatively little acid dilution will occur. This would be the situation in the case of the illustration in Section 3.3, Figs. 3-V to 3-VII, where the droplet growth has little effect on the liquid phase sulphuric acid concentration as compared with that calculated from the kinetics in Section 3.2 and presented in Fig. 3-II. Thus, if either the sulphur dioxide concentration of the ambient gas were to increase somewhat, or the volume concentration of the particles of the aerosol were to

decrease, it is possible for a much greater growth rate to occur, and to take place over a longer period of time. This point will be returned to in Section 5.3.

From their consideration of coagulation Wadden et. al. (127) claim fair agreement between their distribution function and that measured in the atmosphere on days of stable conditions. The slope of their distribution, on a logarithmic scale, is about -1.3 to -1.4. It has been mentioned in Section 2.2, that the work of Junge (62,63) indicates that the slope should be -3 to -4. As pointed out by Wadden et. al. (127) the discrepancy is probably due to the ideality of the model used. It may also involve the assumption that the particle collision parameter is constant. As was pointed out in Section 3.4, this is only rarely an acceptable approximation to the real case (51), and hence may partly explain the discrepancy.

4. EXPERIMENTAL ARRANGEMENTS

4.1. General Description of the Flow System

In this chapter, the development of an experimental system to measure the changes occurring in the aerosol/gas mixture, as discussed in the previous chapter, will be considered. Two items of apparatus concerned with the determination of particle size and number concentration, the thermal precipitator and the light scattering apparatus, have already been dealt with in Sections 2.4 and 2.5. This section deals with the general flow system used to contain the aerosol.

A block diagram of the apparatus is given in Fig. 4-I, showing the various positions at which the monitoring appliances, viz. the temperature and humidity probes, the thermal precipitator, the light scattering apparatus, and the gas sampling syringe, may be placed. Aerosol from the generator, described in Section 4.2, is optionally mixed with a gas stream in the mixer Mx (the input 2 to the mixer may be sealed). The generation of the gas stream, which may or may not contain low concentrations of sulphur dioxide, is described in Section 4.3. From the mixer outlet, the aerosol may be passed into a variable number of tubular vessels, the volume of which determine the length of time for which the aerosol is held up. From the exit of these vessels, the aerosol passes to one of the monitoring devices. By varying the number of tubular vessels used, it is possible to vary the residence time of the aerosol, and thus the reaction/coagulation time before sampling.

The materials used for the construction of apparatus should fulfill two requirements. Firstly, they should not in any way impede the progress of the reaction described in Section 3.2, and, secondly, they should not absorb and/or desorb appreciable quantities of sulphur dioxide. The first requirement excludes any substance that may evolve traces of phenolic vapours. This immediately rules out the use of natural or artificial rubbers. The poisoning of the manganous sulphate catalyst by substances such as those evolved by rubbers has been observed by a number of workers (14, 58). It has been noted (58) that the amounts of vapour

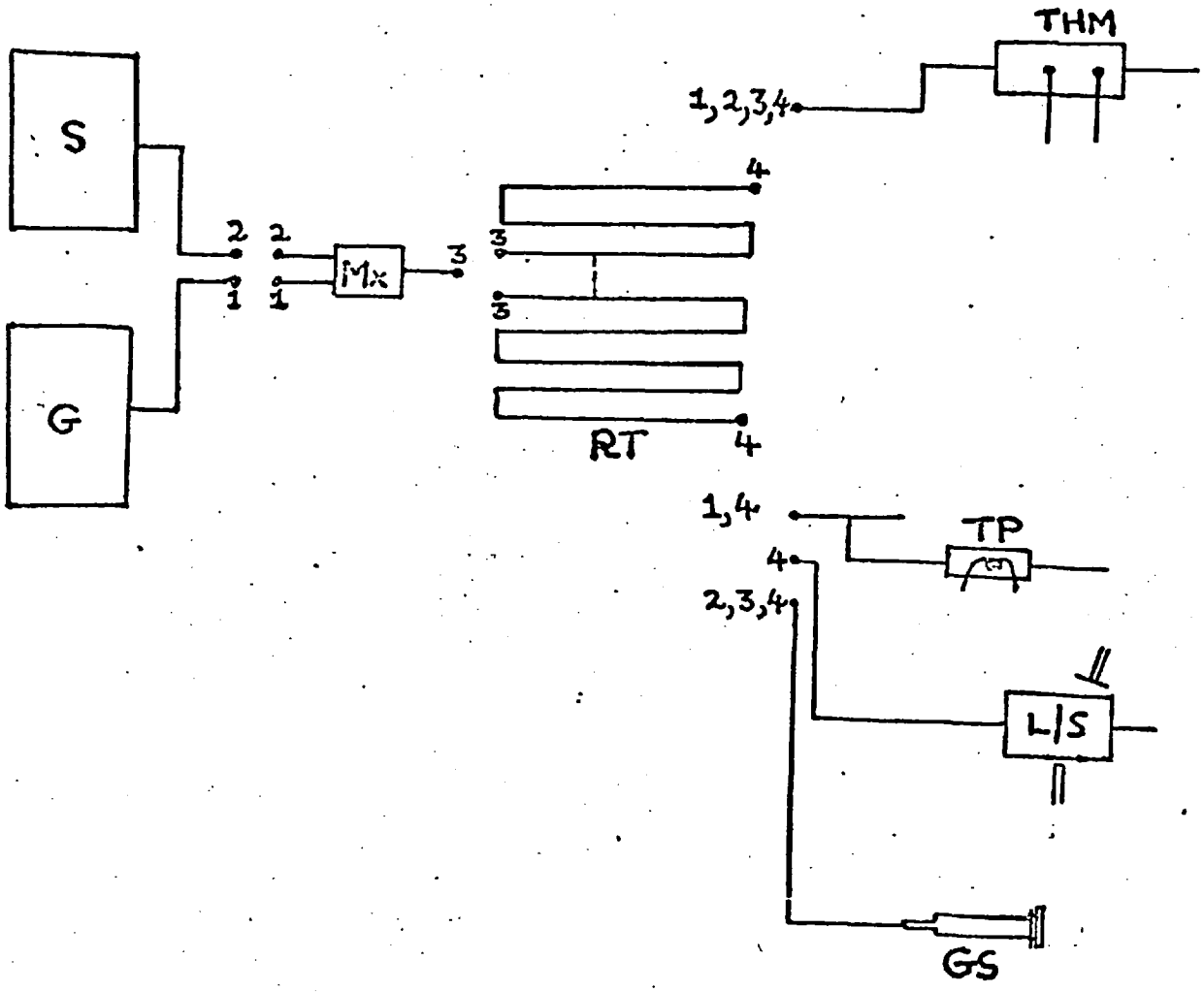

Fig. 4-I: Block diagram of apparatus, showing connection options.

G represents the aerosol generator (section 4.2)

S represents the gas stream containing the sulphur dioxide (section 4.3)

Mx is an aerosol/gas mixer

RT represents the tubular vessels in which the aerosol/gas mixture is held during reaction

TP represents the thermal precipitator (section 2.4)

L/S represents the light scattering apparatus (section 2.5)

GS represents the gas syringe, or other device, used to collect a sample of aerosol/gas mixture for sulphur dioxide concentration determination (section 4.4)

THM represents the vessel in which the temperature and humidity sensors are placed

1,2,3,4 represent the ways in which the apparatus may be connected - connection with matching numbers may take place, e.g. the gas syringe may be connected at points 2,3 or 4.

of organic accelerator contaminating the aerosol after passage through a short length of rubber tubing is sufficient to inhibit the reaction. The transient adsorption of sulphur dioxide on to a selection of materials, and its subsequent desorption, has been investigated experimentally by Wohlers and co-workers (138) for sulphur dioxide concentrations in the 1 - 100 pphm. range. These experiments indicated that no adsorption or desorption occurred with 'Teflon', glass or stainless steel. Thus, for reasons of economy and ease of manipulation, glass was chosen as the substance from which the flow system would be substantially constructed.

The tubular vessels were designed on the basis that the total flowrate through the system would be 5 l/min. This figure is at the upper end of the operating range of the aerosol generator. It may be seen, from Section 3.2, that residence times of up to about 20 - 30 mins. are required in order to monitor the progress of the reaction. Also, it is necessary to minimise the breadth of the residence time distribution at the outlet of the tubular vessels. For this, the ideal situation is that of plug flow through a long, narrow tube. Since this is unattainable in practice, the next best flow pattern will be utilised; laminar flow through a long, narrow tube. Thus, the system illustrated in Fig. 4-III was developed. 26 tubular vessels, about 192 cm. long, with tapers at either end to ball sections of 'Rotulex 41/25' ball and cup joints, were constructed as illustrated in Fig. 4-III(a). These joints were selected because they employ a 'Teflon'-coated sealing ring. The tapers prevent the formation of eddies in the flowing aerosol as the containing tube narrows or widens. 25 of the tubes have an internal diameter of 5 cm., the other an internal diameter of 4 cm. (This tube is denoted 'S'). The tubes were mounted under a laboratory table, in the configuration illustrated in Fig. 4-III(b). The wooden matrix used to hold the tubes was padded to minimise risk of breakage and ensure a snug fit for the tubes. Glass U-bends, as illustrated in Fig. 4-III(a), were then constructed with 'Rotulex 41/25' cup sections at each end, to enable the

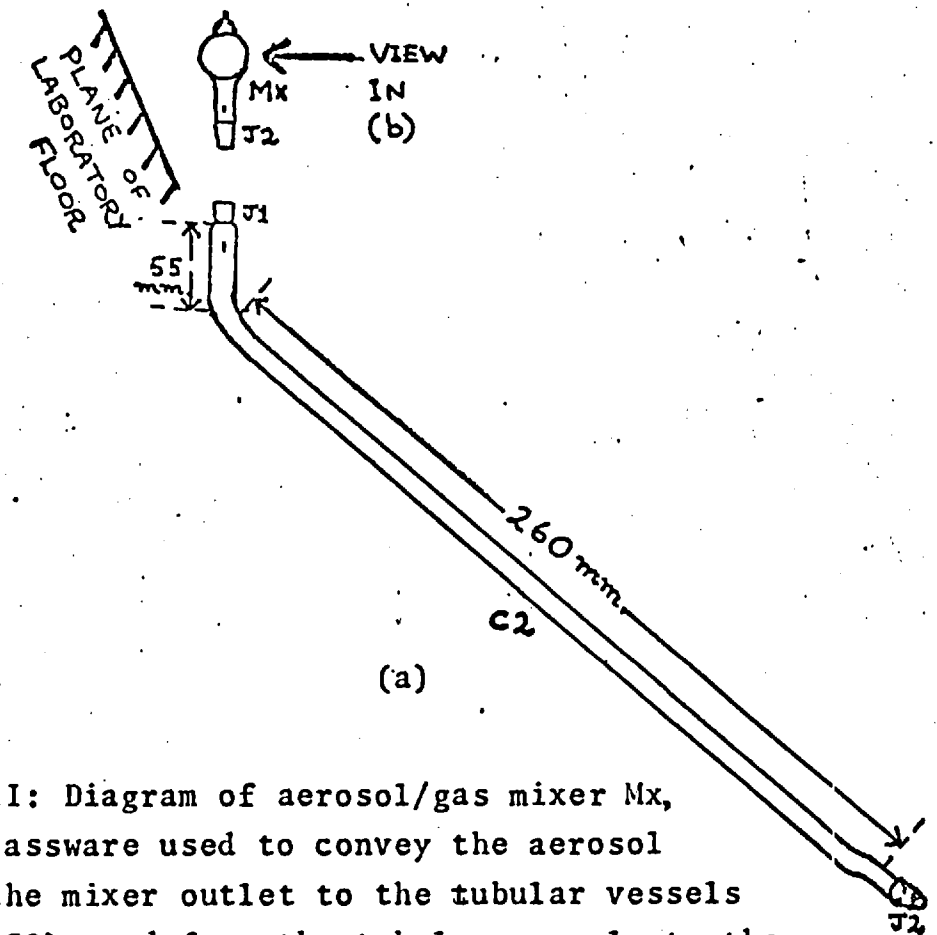

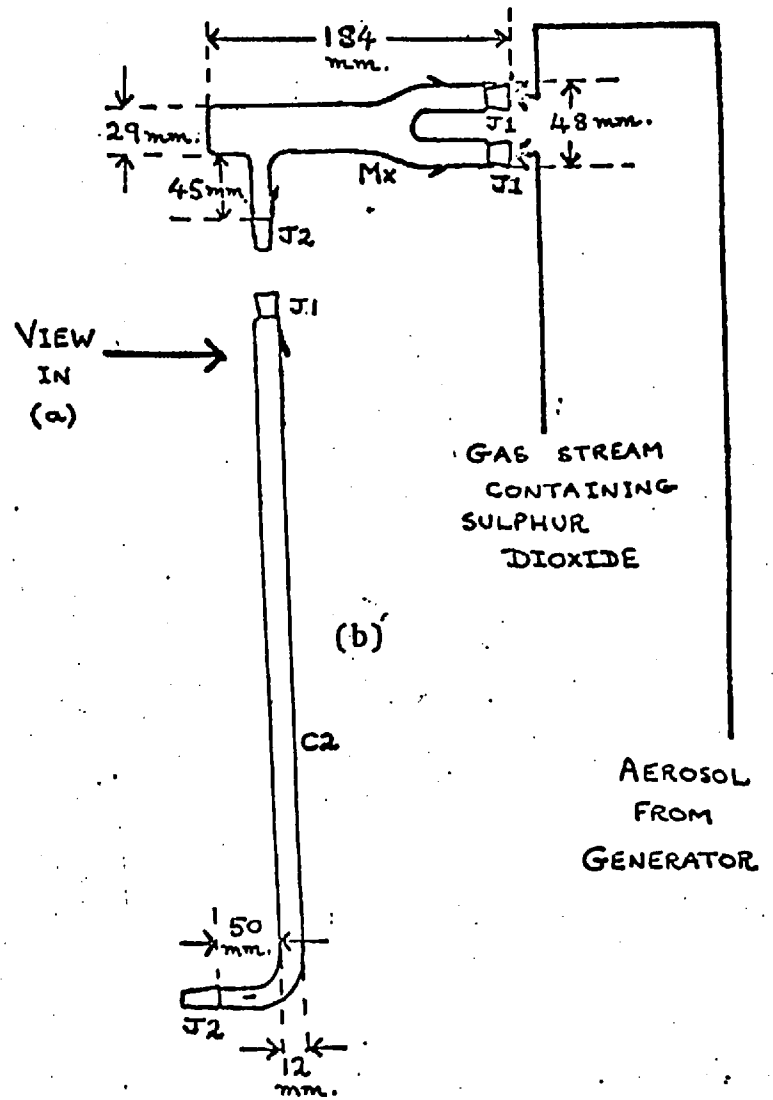

Fig. 4-II: Diagram of aerosol/gas mixer Mx, and glassware used to convey the aerosol from the mixer outlet to the tubular vessels (C1 & C2), and from the tubular vessels to the sampling point (C3).

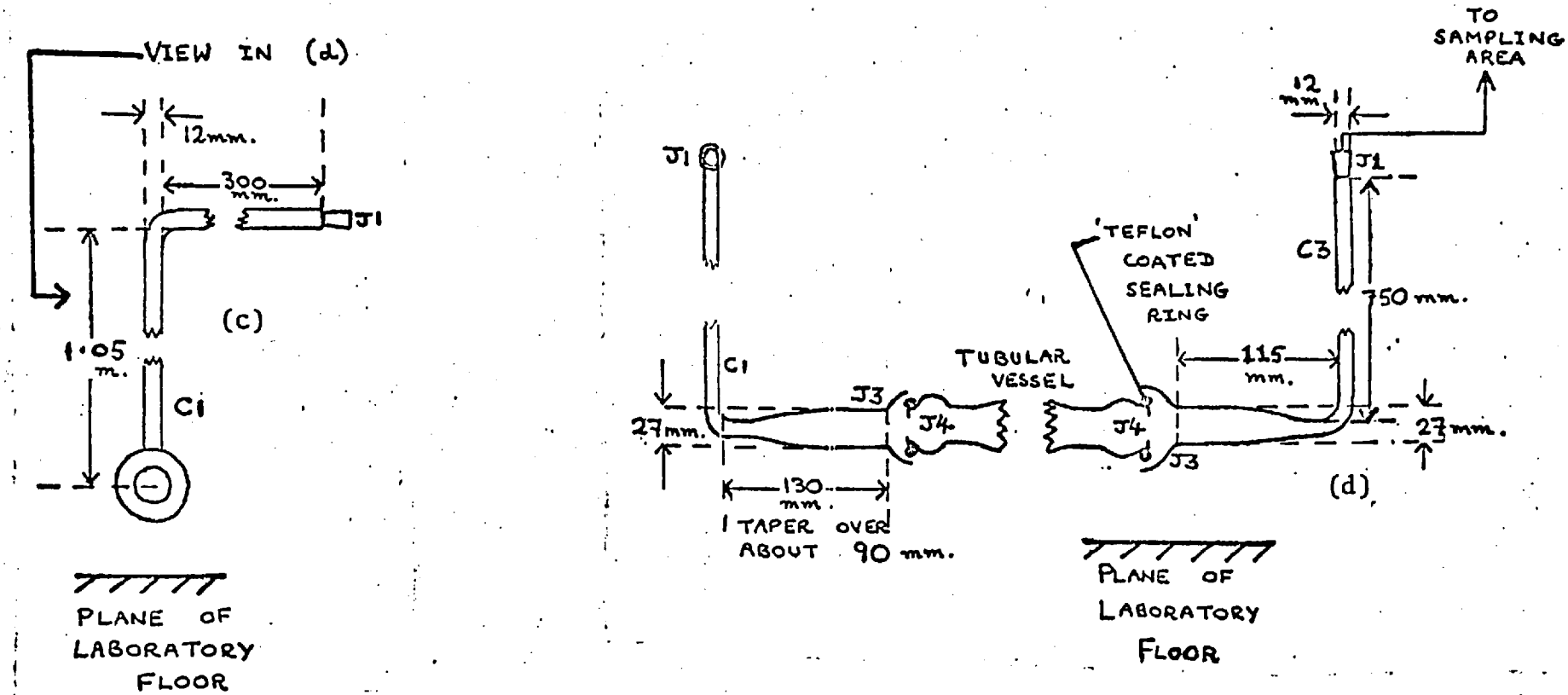

Fig. 4-II (continued)

Joints:- J1. Socket section 'Clearfit KSRB14' joint
J2. Corresponding Cone section 'Clearfit KCNB14'
J3. Cup section 'Rotulex 41/25' joint
J4. Corresponding Ball section 'Rotulex 41/25'

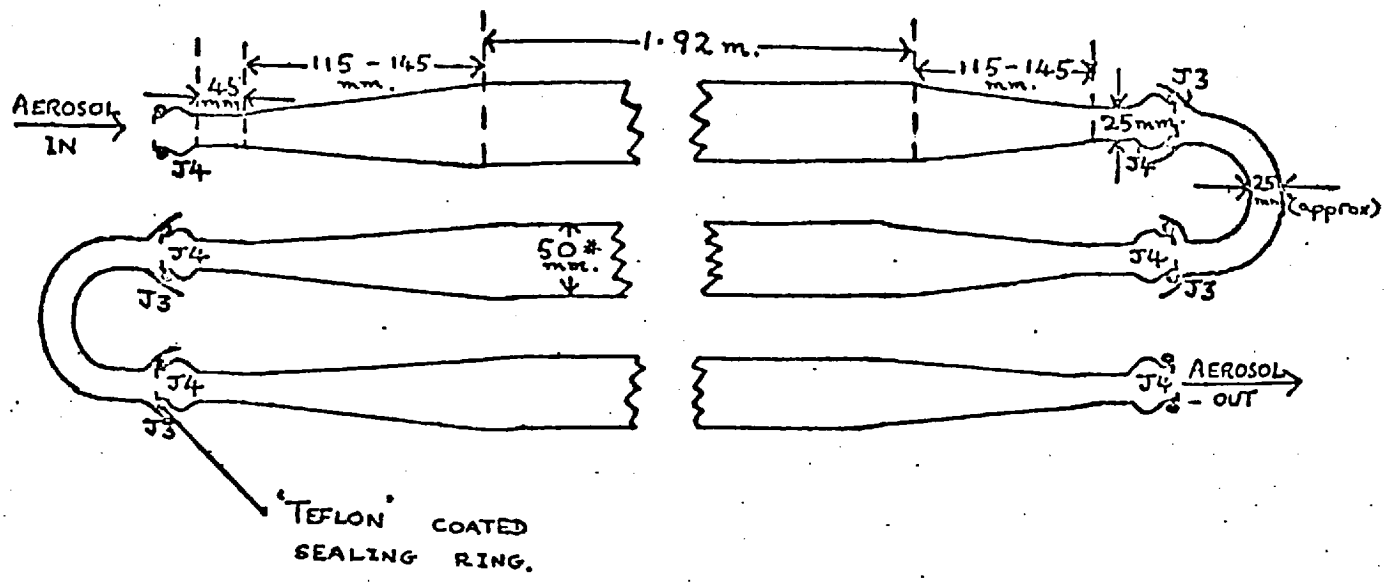

(a) Diagram illustrating the tubular vessels, in which the aerosol/gas reaction takes place, and the method of joining them with U-bends.
(*The normal internal diameter of the tubes is 5cm. In one case, the tube marked 'S', it is 4cm.)
Joints:- J3. Cup section 'Rotulex 41/25' joint
J4. Ball section 'Rotulex 41/25' joint.

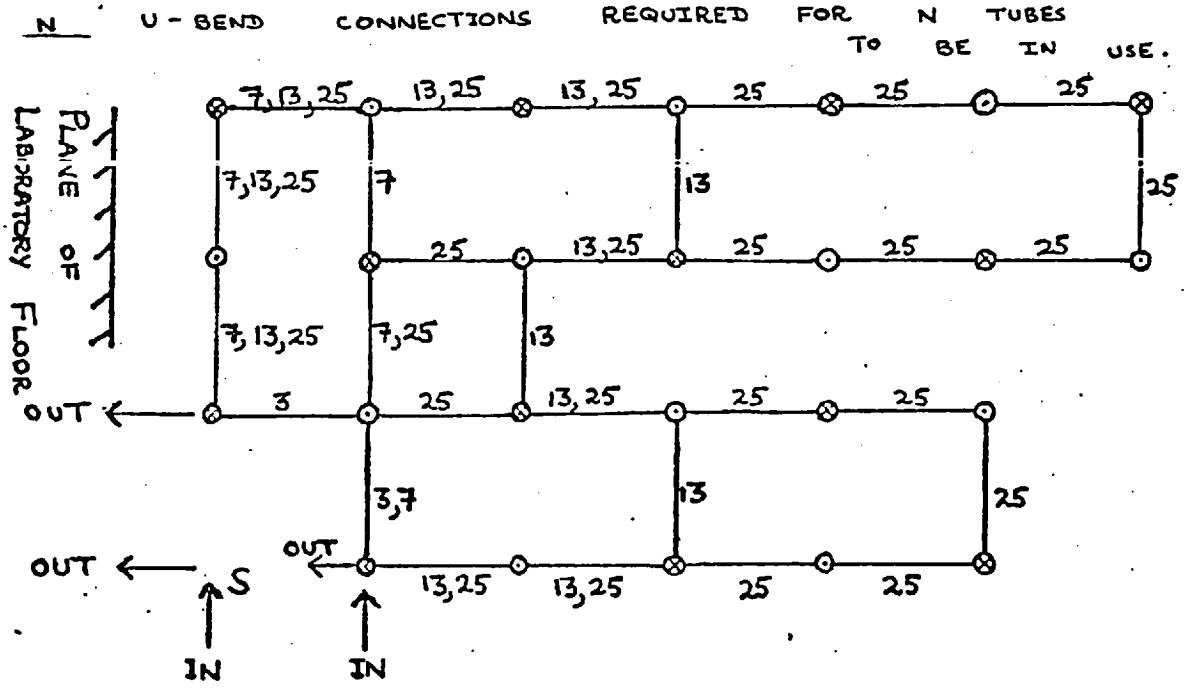

(b) Diagrammatic end-view of the location of the tubular vessels, showing the positions of the U-bends for a required number of vessels to be in use.
'IN' & 'OUT' refer to the possible input & output points for the aerosol.

Fig. 4-III: Diagrams of the tubular vessels, in which the aerosol is held during reaction.

tubes to be connected in series. It was found that the system was sufficiently flexible to allow all twenty-five of the normal tubes to be connected together easily and without leakage.

It was decided to use a series of residence times corresponding to the following numbers of tubes: S, 1, 3, 7, 13, 25. The positioning of the U-bends used to achieve these combinations is illustrated in Fig. 4-III(b). The actual residence times were calculated. These are given in Table 4-I, inclusive of time spent in the connecting tubes and the aerosol/gas mixer (Mx in Fig. 4-I), for each sampling device. The possible entry and exit points of the aerosol to and from the tubular vessels are also shown in Fig. 4-III(b).

The aerosol/gas mixing vessel Mx is illustrated in Fig. 4-II(a) and (b). It is constructed of glass. It is not possible to agitate the aerosol/gas mixture since the creation of turbulence greatly affects the coagulation and stability of an aerosol.

The connecting tubes from the mixer Mx to the tubular vessels are also illustrated in Fig. 4-II (denoted C1 and C2). The main consideration in their design was the maintenance of laminar flow in the system. It was also required to keep the residence time of the aerosol in the connections as small as possible. This connection was constructed in two sections to facilitate assembly. An outlet tube, C3, from the vessels was also designed, with its outlet, a standard 'Clearfit' socket joint, in the proximity of the monitoring devices. 'Clearfit' cone and socket joints were used for all connections (except those to the tubular vessels which require 'Rotulex 41/25' joints) because they require no greasing, and thus no aerosol contamination is involved.

The vessel used for monitoring the temperature and humidity of the aerosol/gas mixture is illustrated in Fig. 4-IV. The instrument used to take these measurements was a YSI Model 91 Dew Point Hygrometer, manufactured by the Yellow Springs Instrument Co. Ohio. The thermo-resistor probes used for measuring dry-bulb and wet-bulb temperatures

Table 4-1: Residence times of aerosol/gas mixture in the apparatus, for each of the sampling devices used.

(a) Aerosol sampled by thermal precipitator

Flowrate through system (l/min.)	Tubular vessels employed	Residence time (min.)
5.0	0	4.486
5.0	S	5.142
5.0	1	5.415
5.0	3	7.089
5.0	7	10.437
5.0	13	15.454
5,0	25	25.501

(b) Aerosol flowing through light scattering apparatus

Flowrate through system (l/min.)	Tubular vessels employed	Residence time (min.)
5.0	S	0.686
5.0	1	0.959
5.0	3	2.633
5.0	7	5.981
5.0	13	11.002
5.0	25	25.501

Table 4-1 (continued)

(c) Aerosol sampled for analysis of sulphur dioxide concentration

Flowrate through system (l/min.)	Tubular vessels employed	Residence time (min.)
5.0	0	0.032
5.0	S	0.688
5.0	1	0.961
5.0	3	2.635
5.0	7	5.983
5.0	13	11.004
5.0	25	21.045

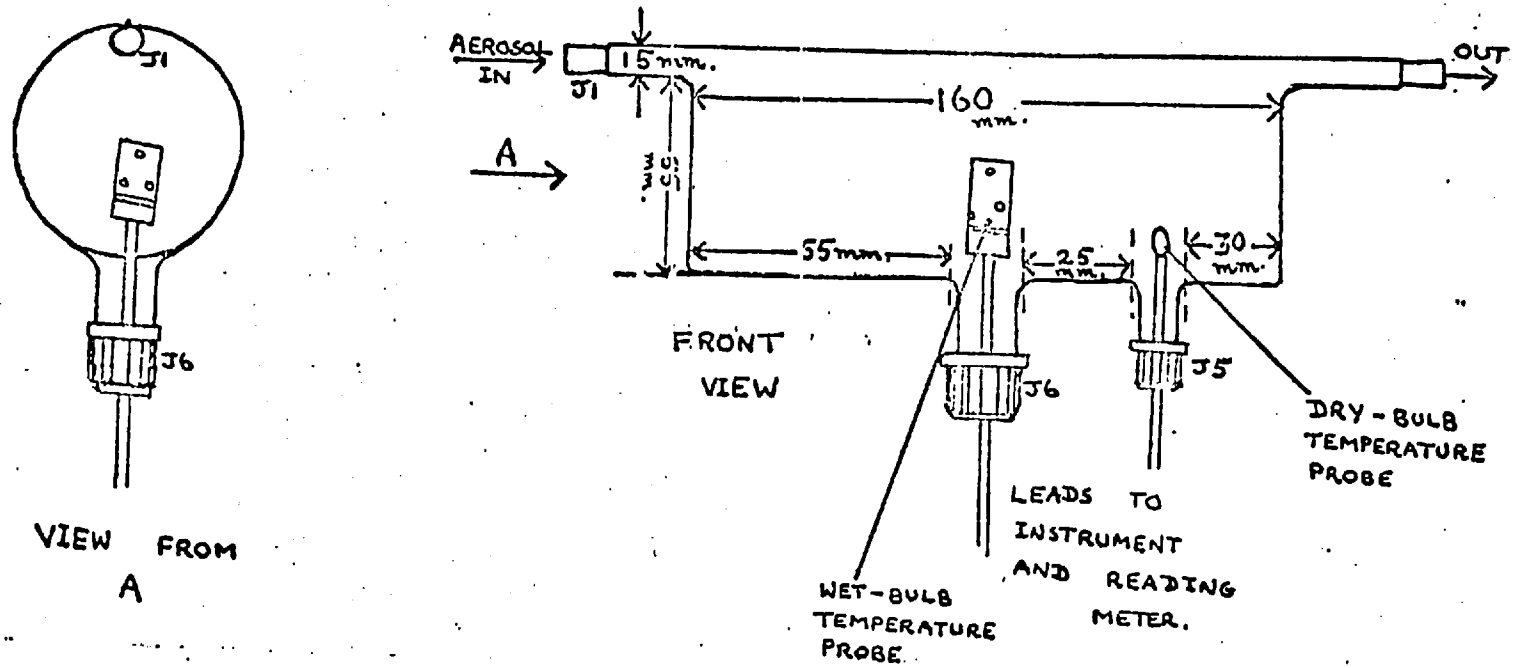

Joints:- J1. Socket section 'Clearfit KSRB14' joint
J5. 'Quickfit SQ18' Screw-cal joint
J6. 'Quickfit SQ28' Screw-cap joint.

Fig. 4-IV: Diagram of the vessel in which the temperature and humidity monitors are placed.

were mounted as shown in Fig. 4-IV. 'Teflon' tape was wrapped carefully around the leads of the probes until it was possible to fit them into the 'Quickfit' screw-cap joints, incorporating a 'Teflon' sealing ring, as illustrated. Using the instrument, it should be possible to measure relative humidities to within about 2% absolute. Only recently, with the application of infra-red detectors, does it appear possible to obtain greater sensitivity in the high humidity areas considered in this work. The wet-bulb temperature probe used in this work requires about five minutes stabilisation time, therefore the gas or aerosol under consideration was allowed to pass for ten minutes before any attempt was made to take a reading. The vessel illustrated in Fig. 4-IV was connected to the required sampling point by a short length of PVC tubing and the usual 'Clearfit' cone and socket joints.

As mentioned in Section 2.4, the thermal precipitator requires an aerosol throughput of about 7 cm^3 min^{-1} for efficient operation. The standard instrument, described in Section 2.4 incorporates an aspirator vessel downstream of the sampling head, out of which water is allowed to flow at 7 cm^3 min^{-1}, drawing aerosol through the head. In order to sample the aerosol, a short tube incorporating a side-arm was constructed. To the end of the side-arm was fitted a 'Quickfit' SQ18 screw-cap joint. A glass tube, concentric with the side arm and 0.5 cm. in diameter was fitted into the screw-cap joint. The use of this joint enabled the end of the inner tube to be moved back and forth across a cross-section of the aerosol flow in the main tube. A length of PVC tubing connected the tube from the screw-cap to the precipitator inlet. The whole appliance was connected to the required sampling position by a 'Clearfit' joint.

The arrangement used to introduce the aerosol into the light scattering apparatus was similar to that employed by Maddock (78), illustrated in Fig. 4-V. The aerosol was contained by a concentric nitrogen 'sheath' in a gap between two container vessels. The incident laser beam passed through the aerosol in this gap. Thus, effects of laser reflection and refraction from aerosol container vessels were avoided.

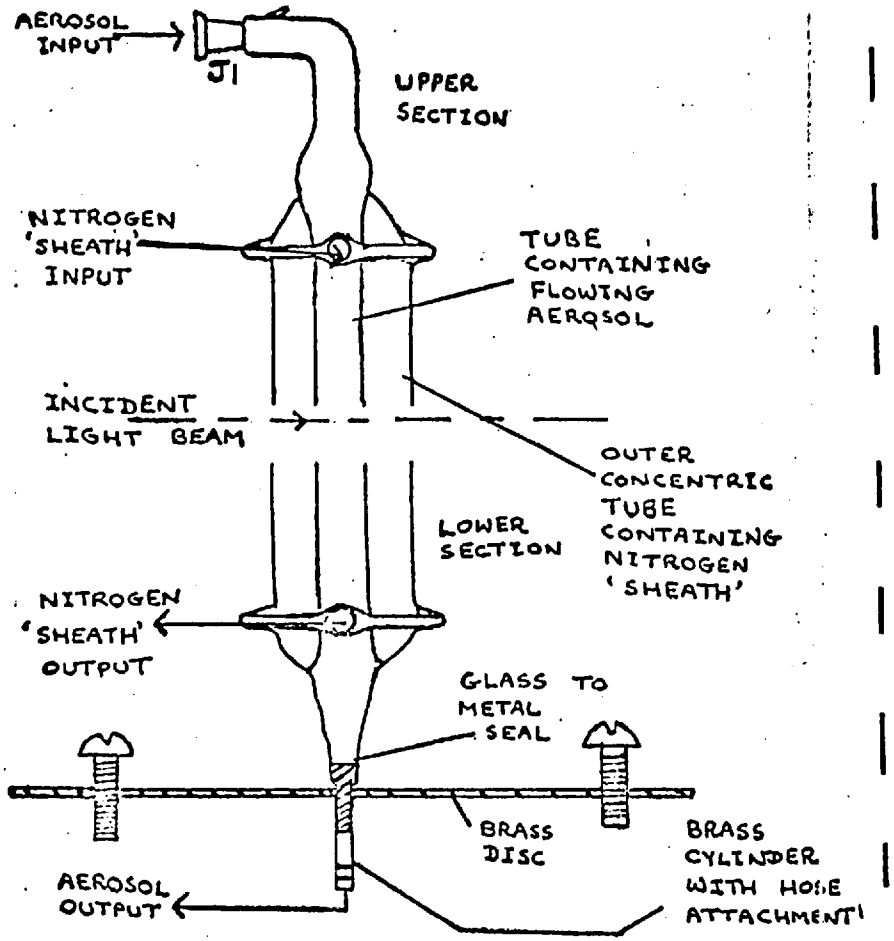

(a) Diagram of the light scattering sampling cell.

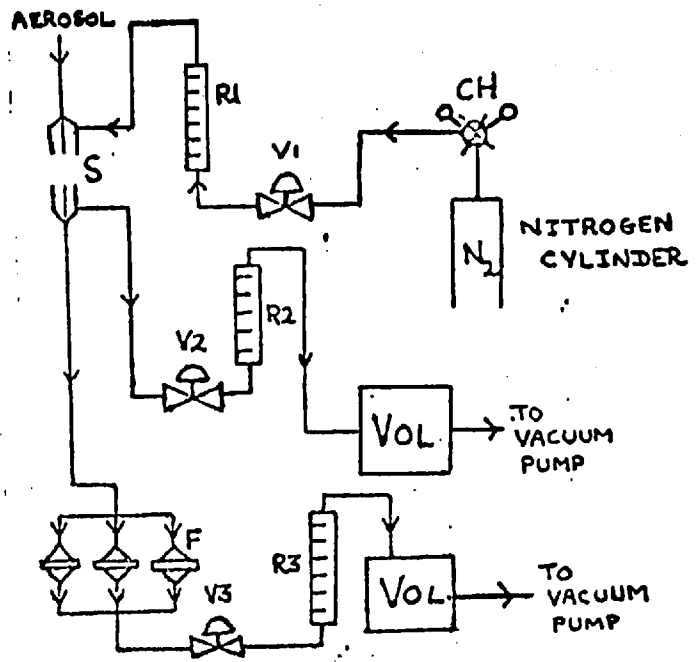

F -- 'Millipore' filters. S - Light scattering cell. CH - Cylinder head. V1,V2,V3 - Flow control valves. R1,R2,R3 - Rotameters. VOL - Ballast volume vessels.

(b) Flow diagram for sampling cell.

Fig. 4-V: The light scattering sampling apparatus.

The lower section of the apparatus was screwed to the base of the light scattering instrument of Carabine and Moore (9) by a brass disc, which was fixed to the metal portion of a glass-to-metal seal with 'Araldite'. A small brass cylinder, which fits into the sampling vessel location hole of the light scattering instrument, was similarly attached to the metal below the disc. The lower section of the arrangement was thus located and locked into position by screws on the brass plate. The upper section was located with clamps, as shown, such that the gap was about 0.8 cm., with the incident light beam passing as near to the upper section as possible. This was to minimise any effects of draughts changing the flow pattern of the aerosol under test. The inner tube, containing the aerosol, has an internal diameter of 2.0 cm., while the outer concentric tube has a diameter of 4.8 cm. Both the aerosol and the nitrogen sheath were drawn out of the lower section by vacuum pumps, each with a 10 l. ballast volume attached. The flowrates of both outlet streams were controlled by needle valves and monitored by rotameters, as shown in Fig. 4-V(b). Upstream of the flow control valve, the aerosol outlet stream was passed through three 'Millipore VS' 4.7 cm. diameter membrane filters, arranged in parallel, to remove the particles present. The nitrogen 'sheath' was introduced from a cylinder using a similar rotameter/flow valve system. It was found, empirically, that optimum results were obtained when both of the outlet flowrates were high (10 l/min. or higher) and the inlet flowrate of the sheath was about half the flowrate of the inlet aerosol stream. It was also found necessary to keep the instrument covered during operation to ensure the exclusion of draughts. The aerosol was introduced into this system via a length of 1.2 cm. i.d. nylon tubing, using the normal 'Clearfit' joints.

Finally, the aerosol or gas can be introduced into a gas syringe, so that a sample may be taken for sulphur dioxide analysis. This procedure is discussed more fully in Section 4.4. The aerosol is communicated to the syringe via 0.8 cm. i.d. PVC tubing. Any effect that the tubing may

have on the reaction at this stage is unimportant, since the aerosol will already have passed through the tubular vessels, and the residence time in the connecting tubing is negligible. However, it is important that no effective adsorption or desorption of sulphur dioxide at the wall of the tubing takes place. Byers and Davis (7) have investigated this phenomenon for PVC, and their results show that the equilibration time is relatively short, rather less than an hour. Since the system was normally run for at least an hour before any readings were taken, it should be possible to neglect any transient adsorption or desorption in the sampling tube. In any case, such phenomena would show in the results, since sulphur dioxide measurements were generally conducted over a period of hours.

4.2. The Aerosol Generator

In this section, the construction and operation of the device used to obtain submicron aerosols will be described. Since the droplets are comprised of a solution of an involatile electrolyte, it was decided to use a dispersion type of generator. Another problem considered in this section is the maintenance of high humidity levels in the system, such that the particles do not evaporate to dry manganous sulphate nuclei before they reach the reaction vessels.

Of the methods commonly used to produce particulate clouds (see, for example (44)) air-blast atomisation appeared to hold out most promise for producing aerosols of the size required in this work. Aerosols produced by air-blast atomisation, however, tend to be very heterogeneous in size. Therefore, some method of reducing polydispersity is required for it to be possible to characterise the particle size distribution by the methods described in chapter 2. A common method of removing large particles from an aerosol produced by air-blast atomisation is by the use of liquid barriers. These are created when an object, such as a glass plate, is placed in the stream of the flowing aerosol. Smaller particles are carried round the obstruction in the streamlines of the suspending gas, but larger particles, by virtue of their greater inertia, leave the flowing stream and collide with the object. In a short time the surface of the object becomes wetted with a layer of liquid from the impacting large particles. This tends to increase the ability of the surface to remove those particles colliding with it from the stream, since there is less chance of a colliding particle rupturing on impact, and the resulting particles returning to the stream.

The effects of up to six such liquid barriers on aerosols produced by air-blast atomisation have been investigated by Dautreband et. al. (22). These workers found that the use of six liquid barriers produced the result that the final particle size obtained was independent of the initial solute concentration of the master solution. (The term 'master

solution' here denotes the solution which is atomised by the air-blast, i.e. the dispersate of the process). It would normally be expected that the particles obtained by atomising a more concentrated master solution should be larger than those obtained from a less concentrated solution. (The particles initially produced from the air-blast would be of roughly equal size, neglecting effects of changes in viscosity and surface tension. However, the particles obtained from the more concentrated solutions possess larger 'nuclei' of the involatile solute. Since, in absolute terms, the ambient humidity is not a sensitive function of solute concentration, the droplets formed in the presence of the larger 'nuclei' should be larger than those formed from the smaller 'nuclei', even though they consist of more concentrated solution). Dautreband et. al. (22) also found that, using between two and five liquid barriers, the final mean particle size becomes less dependent on the initial concentration of the master solution as the number of barriers increases. It was also shown that the output aerosol had a particle size distribution similar to a logarithmic-normal function.

Subsequently, Dautreband and co-workers (20, 21) have developed a series of generators that utilise a combination of air-blast atomisation and liquid barrier filtration. Of these, the so-called 'Dautreband D30' generator appears to have been the most successful. Extensive investigations of the properties of the aerosols produced by this instrument, with changing dispersate viscosity, surface tension, etc., for solutions of sodium chloride have been carried out (129). An interesting fact noted (129) is that the aerosol obtained appeared to be electrically charged, though no quantification or discussion of this fact is given. (refer Section 3.4 of this work). Matteson and Stöber (86) have found that the aerosols obtained from a modified Dautreband D30 generator roughly obey a logarithmic-normal distribution. The latter workers also present an explanation of the observation of charged particles in terms of the theory that an imbalance of molecular and electrical forces at the

air/solution interface of an electrically neutral droplet results in the formation of an electrical double layer at the surface of the droplets.

For the purpose of this work, however, the Dautreband D30 generators produce too large an aerosol throughput (30 l/min.). Therefore, a smaller generator operating along similar principles was designed. The construction of this instrument is illustrated in Fig. 4-VI. The atomiser used is almost identical to that used in Rappaport-Weinstock generator of Maddock (78), which produced aerosols of sulphuric acid. The instrument is 17 cm. high, and has a base diameter (circular cross-section) of 9 cm. The first liquid barrier is incorporated into this device as a glass plate, supported as shown, such that the jet of atomised liquid from the nozzles impinges against it at about 1.2 cm. from the liquid nozzle. The atomising air passes through a nozzle about 0.5 mm. in diameter, across the top of a similar nozzle containing the dispersate. The dispersate is continuously drawn into the liquid nozzle by the Venturi Effect. Fresh master solution may be introduced into the atomiser via the inlet tube in the base while the apparatus is in operation. A reservoir of master solution in a 10l. aspirator is located as shown, and fresh dispersate may be gravity-fed to the atomiser by operating the stopcock. Similarly, the dispersate may be removed via the other tube in the base of the instrument. Thus it is possible to change the master solution in the atomiser without dismantling the apparatus, and, if necessary, while the apparatus is in operation.

On leaving the atomiser, the aerosol passes through an intermediate glass tube, 18 cm. long and 2.4 cm. in diameter, to the aerosol filter. The filtration unit is connected to the intermediate tube via two 'Quickfit SQ28' screw-cap joints, with 'Teflon' sealing rings, as shown.

The filter effectively consists of two more liquid barriers. The inlet tube to the filter is 1.6 cm. in diameter. The top 4.8 cm. of this tube is perforated with holes, 2mm. in diameter, with centre-to-centre spacing of 6 mm. The top end of the tube is sealed by a glass

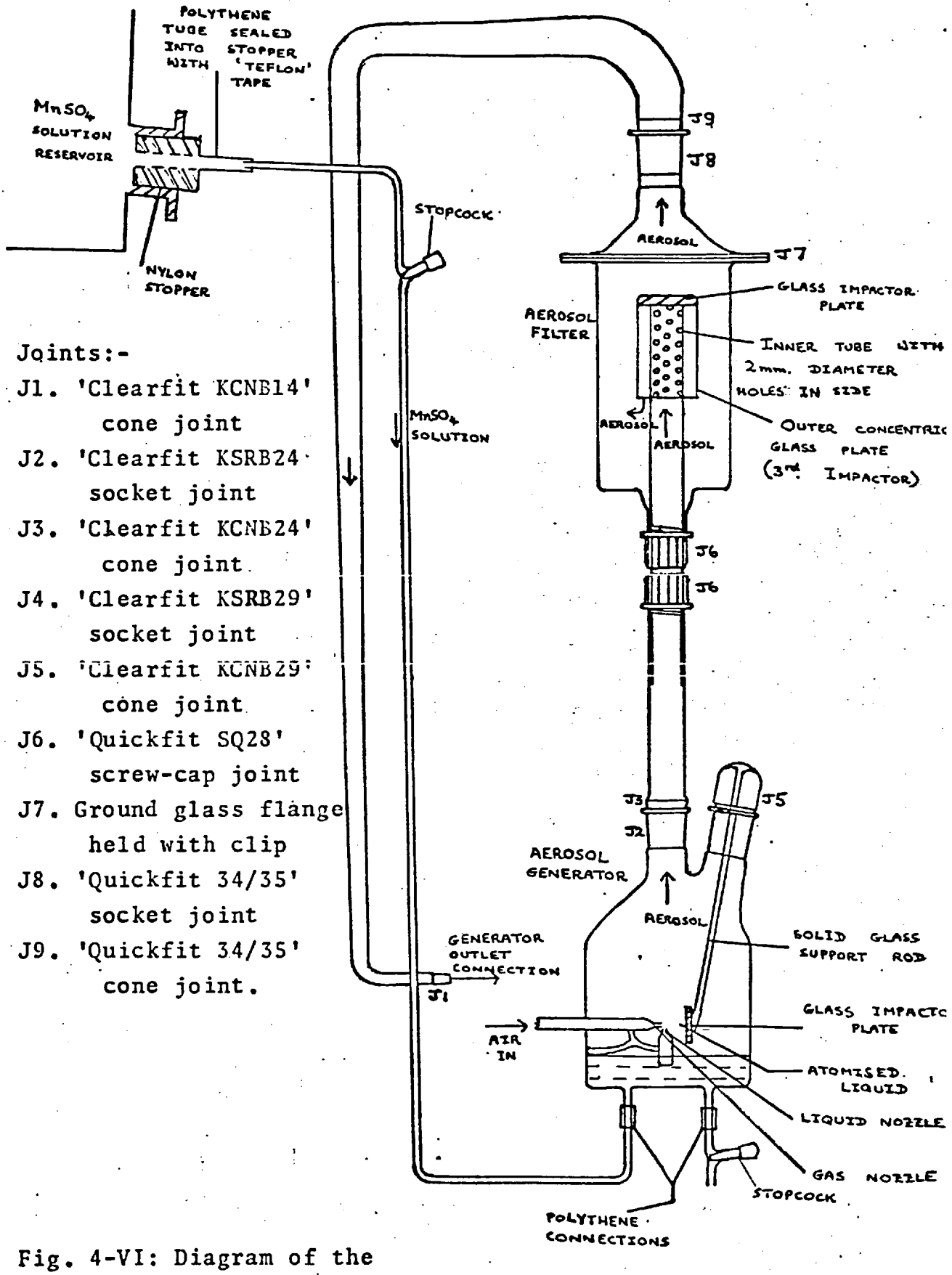

Joints:-

J1. 'Clearfit KCNB14' cone joint

J2. 'Clearfit KSRB24' socket joint

J3. 'Clearfit KCNB24' cone joint

J4. 'Clearfit KSRB29' socket joint

J5. 'Clearfit KCNB29' cone joint

J6. 'Quickfit SQ28' screw-cap joint

J7. Ground glass flange held with clip

J8. 'Quickfit 34/35' socket joint

J9. 'Quickfit 34/35' cone joint.

Fig. 4-VI: Diagram of the construction of the aerosol generator and filter units.

plate. Thus, the aerosol is forced to change direction sharply and exit through the holes, so the glass sealing plate constitutes a second liquid barrier to the aerosol. Concentric with the perforated section of tube is situated an outer tube, unperforated, with an internal diameter 4 mm. larger than the external diameter of the inner tube. This constitutes a third barrier, since the aerosol again has to change direction sharply and exit through the gap at the bottom of the outer concentric tube, as shown in Fig. 4-VI. The flanged attachment allows for easy dismantling, cleaning and drying of the filter unit. The ground glass flanges are lubricated by a 'Teflon' spray, after the application of which care was taken to allow the surfaces to dry thoroughly before the apparatus was assembled. The aerosol leaves the filter unit via a 'Quickfit 34/35' cone and socket joint lubricated by 'Teflon' spray. The tapered aerosol exit tube has three right-angled bends in it, and any large particles present will tend to deposit at these bends, since the aerosol experiences a change of direction. At the outlet end of this tube is a 'Clearfit KCNB 14' cone joint, constituting connection 1 of Fig. 4-I.

The air supply system to the generator is illustrated in Fig. 4-VII. Air from a cylinder is passed to a 'Millipore VS' membrane filter, 9 cm. in diameter. The air is conveyed in a $\frac{1}{4}$ in. diameter copper pipe, and the pressure downstream of the cylinder head is normally 50 psig. The membrane filter is contained in a stainless steel, pressure resistant holder. The filtration is necessary to remove any small particles that may be present in the air supply, in order that no foreign aerosol particles can be nucleated in the high humidity regions of the aerosol generator. From the filter, the air passes through an I.V. Pressure Controllers Ltd. 115/7 pressure controller, to which is fitted a Budenberg P18F pressure gauge, reading 0 - 30 psig. The controller permits a steady, controlled pressure head to be established, as indicated by the gauge, which itself enables run conditions to be duplicated. Then the air passes through a needle valve and a rotameter, to control and monitor flowrate. The stream

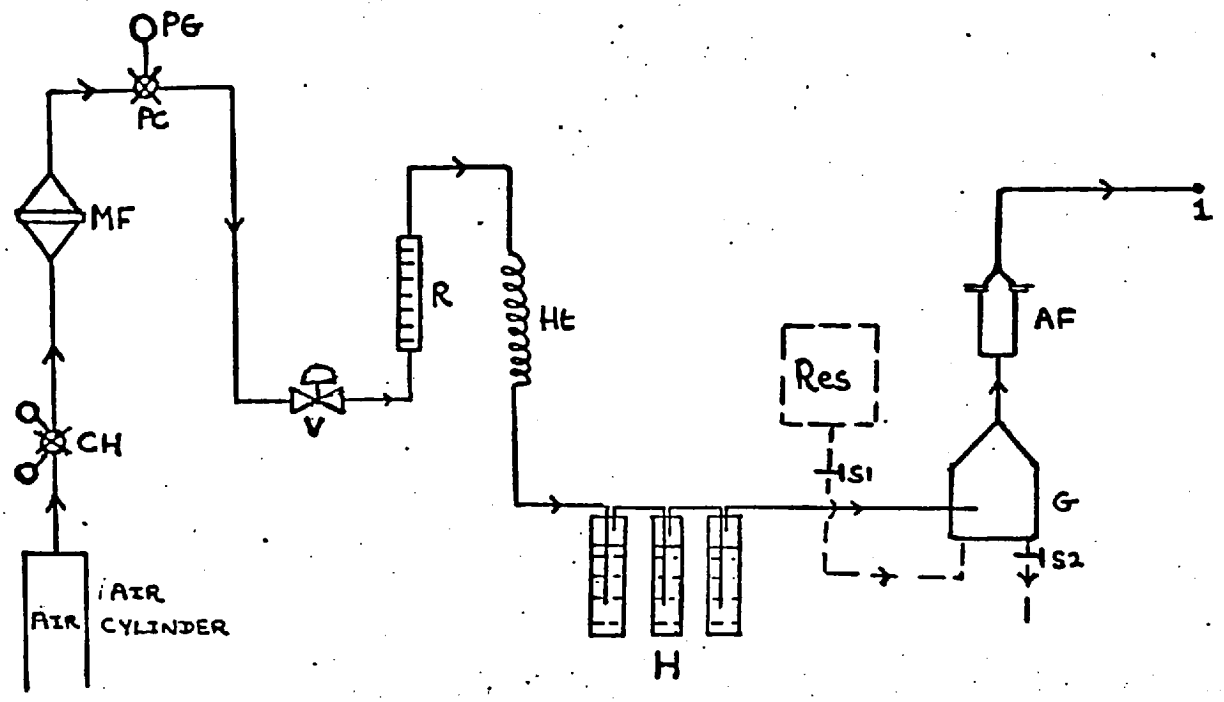

——Gas/aerosol stream

– – -Liquid (master solution) stream

CH - Cylinder head
MF - 'Millipore' filter
PC - Low pressure controller
PG - Low pressure gauge
V - Flow control valve
R - Rotameter
Ht - Heating coil (in water bath)
H - Humidifier (3 Dreschel bottles in series containing aerosol master solution)
G - Aerosol generator
AF - Aerosol filter unit
Res - Master solution reservoir
S1, S2 - Stopcocks

Fig. 4-VII: Diagram of the flow system of the aerosol generator.

then passes through a heating coil, consisting of a coil of copper pipe immersed in a thermostatically controlled water bath, and on, via a metal-to-glass connection, to the humidifier. The humidifier consists of three 500 ml. Dreschel bottles in series, connected together by short lengths of polythene tubing. The bottles contain master solution, identical to that in the generator reservoir, and their tops are lubricated with 'Teflon' spray and clamped in position. Thus, the atomising gas is heated, then bubbled through the dispersate in an attempt to increase the humidity prior to atomisation. In this way, it is hoped to obtain less concentrated droplets than would otherwise occur, and also to retard the increase in the master solution concentration in the generator during atomisation.

The use of master solution in the humidifiers ensures that all aerosol particles present are of manganous sulphate solution. If water were used, it is possible that entrained water droplets may be carried through the atomiser and end up in the aerosol system. However, entrained droplets of master solution from the humidifier go through the same filtration procedures as the droplets produced in the atomiser. There is also the problem that areas of supersaturation may be set up in the flowing aerosol, for example due to a slight temperature drop. It may be argued that this will tend to cause homogeneous nucleation of water droplets to take place. However, Reiss and LaMer (112) have shown that this will not occur unless the number concentration of vapour sinks, i.e. particles or nuclei, present falls to 100 cm^{-3}. The number concentration of particles in this work is expected to be three or four orders of magnitude higher than this. Therefore, it should be possible to assert that the aerosol particles in this work consist entirely of droplets of manganous sulphate solution.

It was originally intended to operate the aerosol generator at a flowrate of 4 l/min., the gas stream described in the next section providing the complimentary 1 l/min. However, for reasons given in the

next section, it was necessary to increase the working flowrate of the generator to 4.9 l/min., while reducing that of the gas stream to 0.1 l/min. Thus, the standard conditions under which the generator was operated involved a flowrate of 4.9 l/min., a gauge pressure of 10.8 psig., and a water bath temperature of 35°C. Except where otherwise stated, it should be assumed that these conditions are used in the experimental work. The manganous sulphate solutions used were prepared by dissolving 'Analar' grade manganous sulphate crystals in distilled water.

4.3. The Sulphur Dioxide Introduction System

It was decided at the outset of the investigation that the sulphur dioxide concentration in the reacting aerosol/gas mixture should be of the order of 60 ppm., as this is likely to show a noticeable change as the concentration of sulphuric acid in the droplets increases from about 0 to 1 m.mol. cm^{-3}, for moderate particle number concentrations. The system for producing a dilute gas stream and introducing it into the aerosol stream is given in this section. The apparatus described here is denoted by block 'S' in Fig. 4-I.

The basic unit used to produce dilute gas mixtures was a Wösthoff dosing pump, obtained from H. Wösthoff oHG., Bochum. This was incorporated into the flow system illustrated in Fig. 4-VIII. The flow system used here is similar, in principle, to the system of Axelrod et. al.(3), using two Wösthoff units, designed to give even lower sulphur dioxide concentrations. A mixer is required downstream of the Wosthoff unit to disperse the impulses of sulphur dioxide into the bulk of the carrier gas. It has been found, experimentally and theoretically (3), that three 500 ml. vessels connected in series will produce an output stream with a homogeneous sulphur dioxide concentration. Thus, the mixer M in Fig. 4-VIII was constructed from three 500 ml. Dreschel bottles, with their ground glass tops clamped in position and sealed with 'Teflon' spray. The bottles were connected together with polythene tubing. The outlet of the last bottle was connected to a 'Clearfit KCNB 14' cone joint, which constitutes connection 2 in Fig. 4-I, by a length of polythene tubing.

The air stream into the Wösthoff cock is filtered, humidified and controlled as follows (see Fig. 4-VIII). Air flows from a cylinder into a humidifier. This consists of three brass vessels, each 500 ml. in volume and containing water, connected in series. The air, conveyed in a copper pipe, is bubbled through each of these vessels in turn. Downstream of the humidifier, the air passes through a coarse, glass-wool filter, which serves to remove any large droplets of water carried over

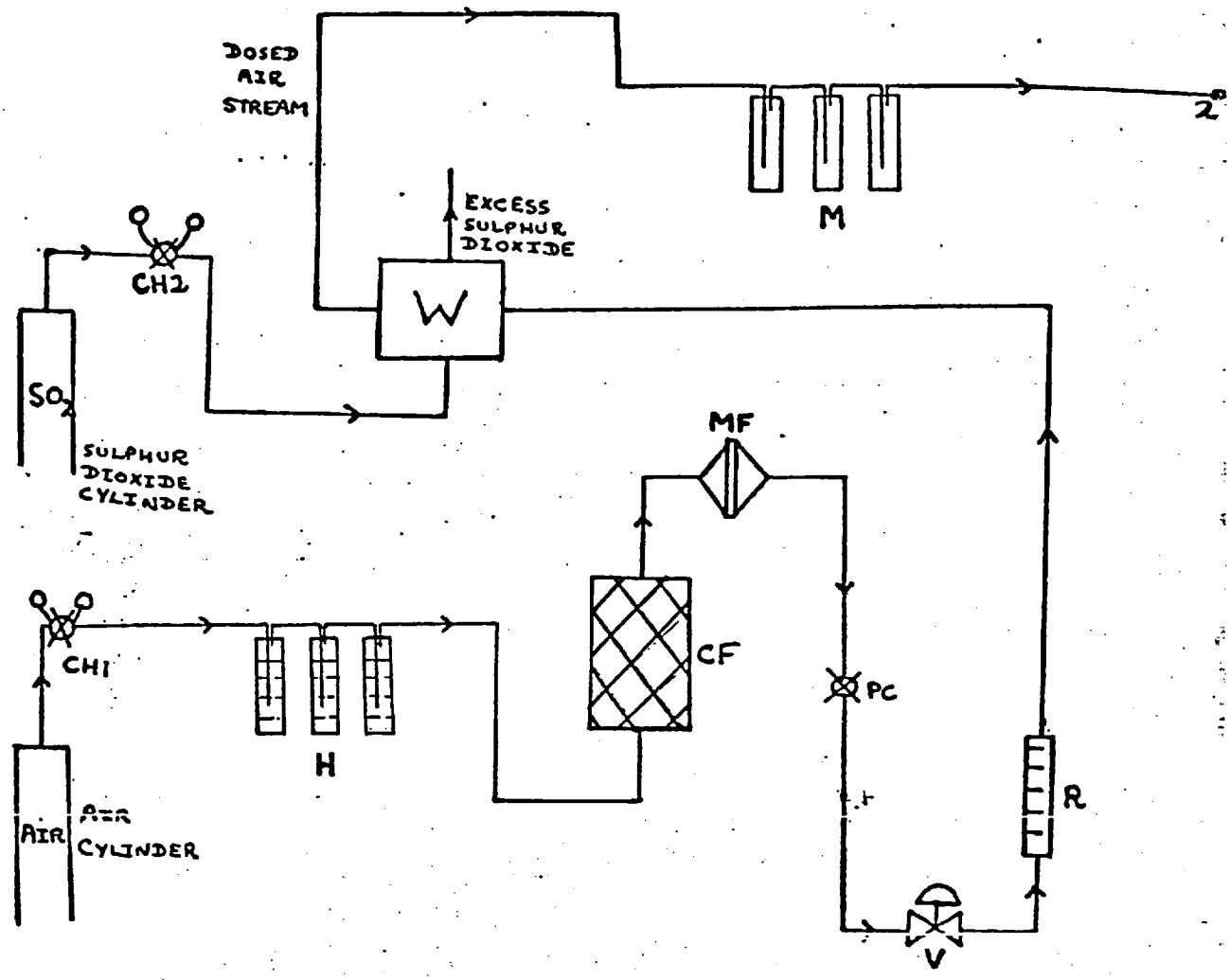

CH1,CH2 - Cylinder heads
H - Humidifier (3 vessels containing water)
CF - Glass wool filter
MF - 'Millipore' filter
PC - Pressure controller
V - Needle valve for flow control
R - Rotameter
W - Wösthoff dosing pump
M - Gas mixer (3 500ml. Dreschel bottles connected in series)

Fig. 4-VIII: Flow diagram of the sulphur dioxide introduction system.

from the humidifier. After passing through the glass-wool filter, the air is filtered by a 4.7 cm. diameter 'Millipore VS' membrane filter (pore size 0.025 μm.) contained in a pressure resisting holder. Then the air passes through a low pressure controller, which ensures a constant pressure head at all points downstream. A needle valve and rotameter control and monitor flowrate. The connection from the rotameter outlet to the input of the Wosthoff unit is a short length of polythene tubing.

In the original design of the apparatus it was envisaged that this stream would have a flowrate of 1 l/min. to complement the 4 l/min. flowrate of the stream from the aerosol generator. (see Section 4.2). However, it was found that the maximum relative humidity attainable using the system described in the previous paragraph was around 46%, even when the humidifier vessels were placed in a water bath at 60°C. This would serve to reduce the humidity of the mixed stream and thus drastically the concentration of the aerosol particles. Therefore the flowrate of the sulphur dioxide introduction stream was reduced to 0.1 l/min., and that of the aerosol stream was increased to 4.9 l/min. Humidity readings were taken in the mixed stream using the new flowrates. These indicated relative humidity values around 96%, proving that the system was adequately humid.

Byers and Davis (7) found that, over periods of about 45 mins., adsorption and desorption of sulphur dioxide on to polythene is considerable. However, after about an hour equilibrium appeared to be attained, with the outlet concentration approaching the inlet concentration. It was decided that the sulphur dioxide introduction system would be run for about $1\frac{1}{2}$ to 2 hours prior to use in any experimental work.

Before use in the aerosol system, the apparatus described in this section was checked titrimetrically to ensure that the gas issuing from connection 2 had the same sulphur dioxide concentration as that calculated from the volume of the duct in the Wösthoff unit and the flowrate

of air through the system. A solution of potassium permanganate of known concentration was made up. A 20 cm^3 portion of this was placed in a Dreschel bottle and made alkaline by the addition of a small amount of sodium hydroxide solution. The gas input into the solution (in the bottle cap) was fitted with a 'Sinta-Glass' distributor to increase the surface area of gas passing through the solution and hence create more efficient absorption conditions. The bottle containing the test solution was connected to point 2 in Fig. 4-VIII. A second Dreschel bottle containing very dilute alkaline potassium permanganate solution was attached downstream of the first bottle to act as an indicator of whether any sulphur dioxide had been carried over from the first bottle. No apparent change occurred in this bottle during the experiment, indicating that all sulphur dioxide present in the stream had been absorbed in the first bottle. The sulphur dioxide introduction system was run for a period of time, the number of sulphur dioxide impulses injected into the stream being measured by a counter incorporated in the Wösthoff pump. After 600 impulses had been counted, the bottle was disconnected and its contents were transferred to a titration flask. The resulting liquid was acidified and an excess of potassium iodide solution was added. The potassium permanganate not reduced by the sulphur dioxide oxidised part of the potassium iodide, producing a dark red solution of iodine in potassium iodide. A solution of sodium thiosulphate of known concentration was titrated against the iodine, using starch as indicator. From the amount of solution used it is possible to calculate the amount of potassium permanganate reduced by the sulphur dioxide, and hence the average amount of sulphur dioxide passing per impulse of the Wösthoff pump. The procedure was repeated using 701 pump impulses. In both cases, the result was that the average quantity of sulphur dioxide emitted per pump impulse corresponds to a volume of 0.0448 cm^3 at standard temperature and pressure. The manufacturer specifies that the volume of the duct in the Wösthoff cock used is 0.045 cm^3. This experiment demonstrates the

reliability of the connections used in the apparatus, and the fact that adsorption and desorption on the polythene tubing is negligible, given that an adequate equilibriation time is allowed for.

Two types of input sulphur dioxide cylinder were used, one consisting of a 7.5% mixture of sulphur dioxide in nitrogen, the other consisting of 99.98% pure sulphur dioxide. The gases were obtained from B.O.C. Special Gases Ltd.

4.4. Determination of Sulphur Dioxide Concentration

In this final section of chapter 4 the method used in an attempt to measure gas phase sulphur dioxide concentrations in the aerosol/gas mixture will be described. By obtaining measurements of the gas phase sulphur dioxide concentration at various points during the progress of the reaction, it may be possible to obtain some insight into the validity of the proposed reaction mechanism (see Section 3.2).

Originally, the idea of building a mask correlation spectrometer, similar to the one described by Williams and Kolitz (136) was considered. This technique has been applied to atmospheric conditions by Moffat and co-workers (93, 94). Ultimately, however, a method employing flame emission spectrophotometry was selected, since this technique has been fairly extensively investigated, and instruments are available on the market. The model chosen was a United Analysts Gas Odorant Chromatograph, incorporating a chromatograph column to separate sulphur dioxide from other gaseous species present that may interfere with readings. This instrument incorporates a hydrogen-rich flame to reduce sulphur compounds present in the sample to sulphur vapour (S_2), and operates in the 1 - 20 ppm. range of sample concentrations.

Before discussing the calibration of the instrument, a few notes on sampling will be given. If the sample is expected to have a sulphur dioxide concentration of between 1 and 20 ppm. (as was the case during calibration) the procedure is relatively simple. The flowing gas was passed through a short length of PVC tubing. Into the wall of this tubing a 2 ml. hypodermic syringe was inserted. The syringe was purged and filled with sample gas. The amount of gas in the syringe was adjusted to the 1.2 ml. graduation mark, and the needle placed in the spectrophotometer input port corresponding to the short chromatograph column. The pressure of the carrier gas was allowed to push the piston of the syringe up for one second, and then the sample was injected over a 2.5 second period. Strict timing of this introduction period was found necessary, since meter readings were found to be fairly dependent on sample input

rate. With relatively high input sulphur dioxide concentrations (when the meter sensitivity was set to either of the two least sensitive values) the meter needle made one impulse, and the maximum value that the needle reached, together with the meter sensitivity, was noted. However, using relatively small sulphur dioxide concentrations, it was found that the meter needle deflected twice. The first impulse occurred immediately after the sample was injected, and was of roughly constant magnitude; the second occurred after a time interval similar to that observed with high concentrations, and was of variable magnitude. It was assumed that the first impulse was due to the pressure fluctuation caused in the flame by the injection of the sample. The second impulse was taken to represent the sulphur dioxide concentration of the sample. In all cases, the needle was left in position with the plunger pushed right in while readings were taken. After a reading had been taken, the syringe was purged with the inlet combustion gas from the sampling port before proceeding to the next sample. This was carried out until the meter needle indicated that no sulphur dioxide remained in the system.

The initial calibration was carried out using the Wösthoff dosing system, described in Section 4.3, with 7.5% sulphur dioxide in nitrogen as the dosing gas. This produced sulphur dioxide concentrations in the range of 1 - 20 ppm. and the method described in the previous paragraph was used to introduce samples into the spectrophotometer. Five spectrophotometer readings were taken for each set of concentration conditions, and the mean and standard deviation of these values were calculated. They are plotted on a log-log plot of ammeter reading versus the concentration of sulphur dioxide in the sample in Fig.4-IX as points 2 to 7. Theoretically, the calibration curve should have a slope of 2 on a log-log plot, since the intensity of radiation emitted from the reduction product S_2 should increase as the square of the concentration. A linear regression line was fitted to points 2 to 7 in Fig. 4-IX, and is represented by the solid line. Its equation was found to be

$$\eta = -1.04 + 1.89\xi \quad . \quad . \quad . \quad (4.1)$$

Fig. 4-IX: Plot of $\log_{10} y$ versus $\log_{10} x$, where x is the concentration of sulphur dioxide in ppm. & y is the converted, corrected spectrophotometer reading in A.

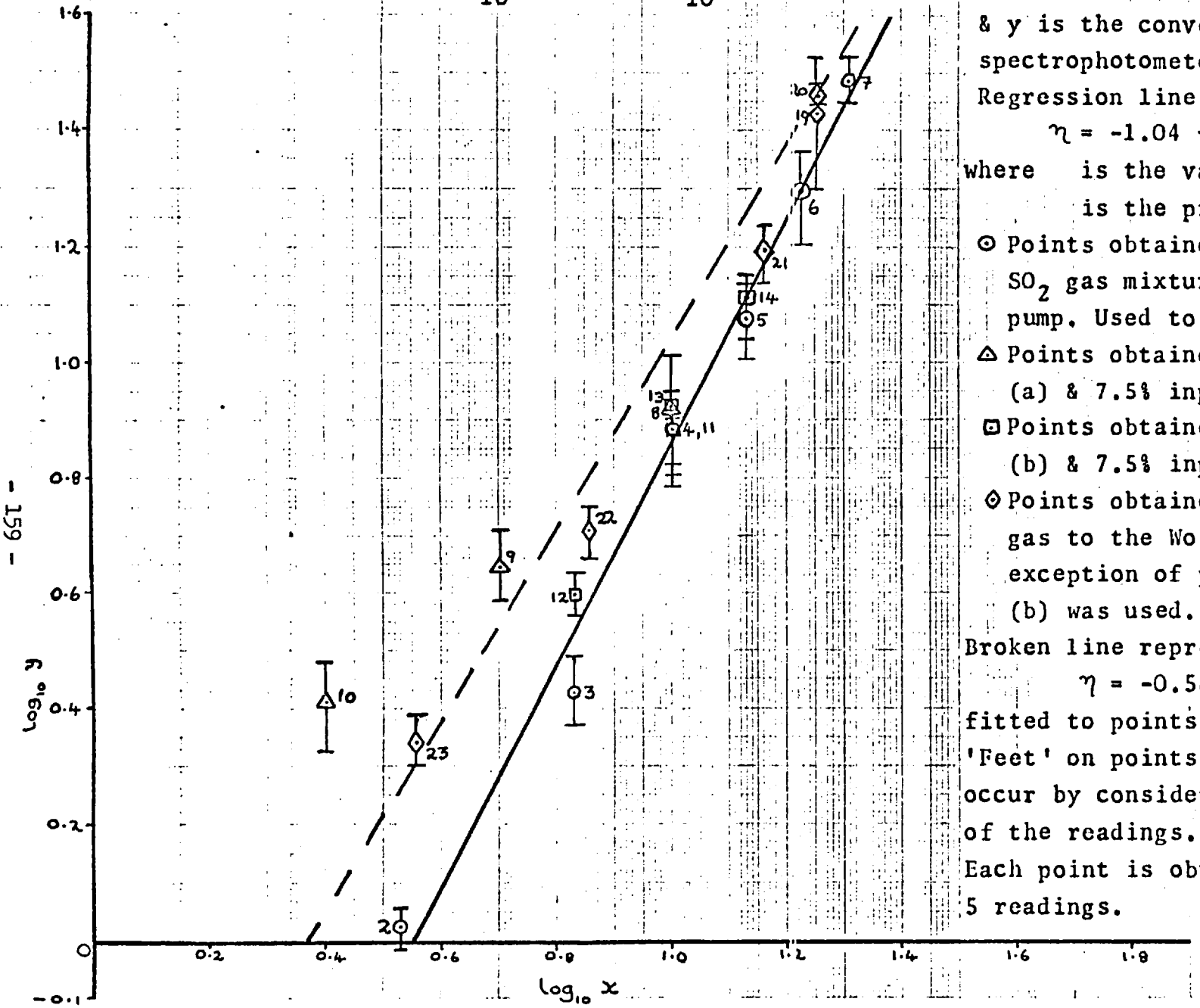

Regression line is

$$\eta = -1.04 + 1.89\xi$$

where ξ is the value of $\log_{10} x$

η is the predicted value of $\log_{10} y$

⊙ Points obtained using no dilution & 7.5% SO_2 gas mixture as input to the Wosthoff pump. Used to obtain regression curve. (2-7)

△ Points obtained using dilution method (a) & 7.5% input gas. (8-10)

⊡ Points obtained using dilution method (b) & 7.5% input gas. (11-14)

◈ Points obtained using pure SO_2 as input gas to the Wosthoff unit. With the exception of point 19, dilution method (b) was used. (19-23)

Broken line represents regression line

$$\eta = -0.580 + 1.58\xi$$

fitted to points 19-23.

'Feet' on points represent deviations that occur by considering the standard deviation of the readings.

Each point is obtained as the average of 5 readings.

where ξ is the logarithm to base 10 of the sulphur dioxide concentration of the sample.

η is the expected value of the logarithm to base 10 of the meter reading, based on a least squares analysis of the data of points 2 to 7.

Since the concentration of the sulphur dioxide used in interaction with the aerosol was expected to be around 63 ppm., it was necessary to develop a method of obtaining diluted samples. The two following methods were tried.

(a) Gas was drawn into the sampling syringe, and the plunger adjusted to a level corresponding to half the gas volume required for the sample. The plunger was then quickly moved to the level corresponding to a full sample. Rapid action is necessary to promote gas mixing. This new sample could then be halved and diluted, and, in principle, the process repeated as many times as desired.

(b) Sample gas was allowed to flow into a gas syringe (calibrated to 100 ml.). The plunger was then pushed in until an appropriate volume e.g. 30 ml. of gas remained. The syringe was then moved, and the plunger withdrawn to the 100 ml. mark, sucking in air. The end of the syringe was sealed by a rubber policeman, and the contents mixed by moving the plunger and shaking the syringe. The sampling (2 ml.) syringe was then introduced through the rubber policeman, flushed, and filled by exerting pressure on the piston of the gas cylinder. Slight pressure is exerted on this piston at all times during sampling to prevent air entering through holes in the policeman and diluting the sample gas. Results obtained from trials of each of these methods are presented in Fig. 4-IX. Points 8, 9 and 10 correspond to tests using dilution method (a), with 1:2, 1:4, and 1:8 gas dilution ratios respectively. The same dosing gas was used here as was used for points 2 to 7. It may be seen that considerable deviations occur as the dilution increases, and it appears

that dilution method (a) is unsuitable. Points 11 to 14 were obtained using dilution method (b), with gas dilution ratios of 3:10, 2:10, 3:10 and 4:10 respectively. It may be seen that these points deviate from the regression line by amounts comparable with points 2 to 7. It therefore appears that dilution method (b) is the best way of diluting samples containing more than 20 ppm. of sulphur dioxide.

Finally, the runs marked 19 to 23 were made using pure sulphur dioxide as the dosing gas in the Wosthoff system. Dilution method (b) was used. It may be seen that these points deviate from the regression line to give rather high meter readings. A second regression line was fitted to this data, which is illustrated as a broken line in Fig. 4-IX. Its equation is

$$\eta = -0.580 + 1.58\xi \qquad (4.2)$$

ξ and η having the same meaning as in equation (4.1). Comparing the two lines, equation (4.1) corresponds closely to the quadratic dependence of the meter readings on the sulphur dioxide concentration, the coefficient of ξ being 1.89. This is much better than the value of 1.6, given by equation (4.2). Furthermore, the seven points 2 to 7 appear to fit the line of equation (4.1) more closely than the five points 19 to 23 fit equation (4.2). Therefore, it appears that best results will be obtained by using equation (4.1) as the calibration line.

In the above experiments, five samples have been taken per point on Fig. 4-IX. In experiments involving gas/aerosol mixtures where dilution method (b) is necessary (i.e. the normal case - see Section 5.3) samples were taken from the gas syringe until the latter was empty. This compensates for any inhomogeneity caused by inadequate mixing, which will show up in the standard deviations of the experimental values. Discussion of results obtained from samples of the aerosol/gas mixture is given in Sections 5.1(b) and 5.3.

5. RESULTS AND DISCUSSION

5.1. Performance of the Apparatus

Before discussing experimental results in the context of the theories outlined in chapter 3, it is appropriate to examine them to assess the accuracy, applicability and limitations of the experimental techniques used.

(a) The Collection of Particles by Thermal Precipitation and their Subsequent Examination and Analysis (See Section 2.4)

The first stage in the development of this technique was to ensure that the particles examined were composed of manganous sulphate nuclei and not of solution droplets. It should be possible to detect solution droplets by the fact that rapid evaporation of water present would take place in the high vacuum of the electron microscope, producing a visible contraction in apparent particle size. Two precautions were taken to ensure that the sample particles on the grids were dry before examination under the electron microscope. Firstly, a heating wire generating about 150 watts was wound around the sampling tube about 6 cm. upstream of the reciprocating head. This should cause the particles to evaporate before deposition. Secondly, the grids were placed in an oven at 105°C. for one hour after removal from the precipitator: apart from ensuring that the particle drying is complete, this fulfills another purpose to be discussed shortly. Examination of particles under the microscope indicated that no water was present after this procedure had been carried out.

Normal transmission examination under the electron microscope indicated that the particles were almost entirely circular in their projected cross-section. Examples of prints obtained are given in Plate 1 (a) to (d), for a range of aerosol residence times in the experimental system. No crystalline structure could be identified. It appears probable that the particles consist of manganous sulphate monohydrate $MnSO_4.H_2O$, which is the stable hydrate between 27°C and 140°C (88). This is probably formed under the conditions in the oven, and observed on the plates,

Plate 1: Examples of electron micrographs obtained.

(i) Transmission examination

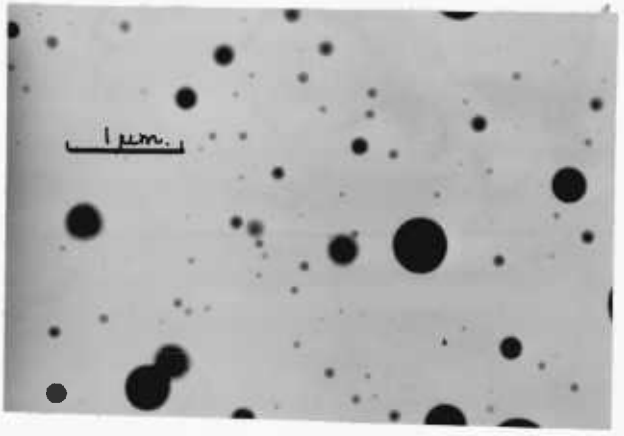

(a) 0 tubes used
15000 X

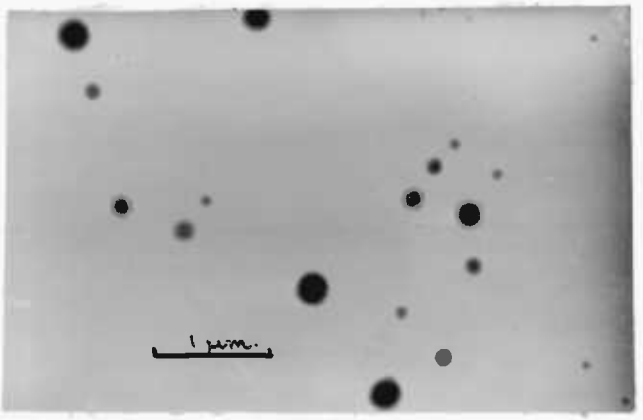

(b) 1 tube used
15000 X

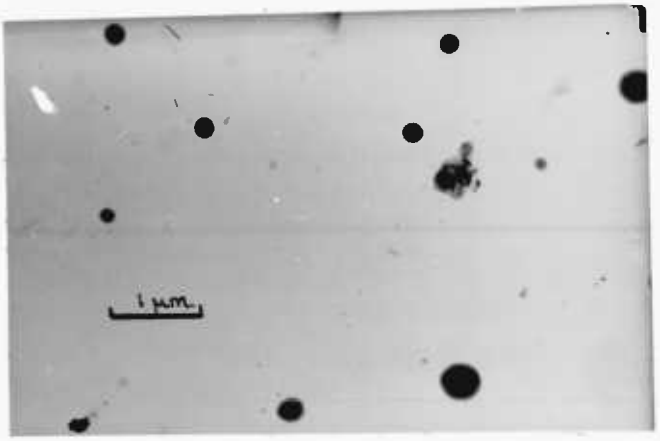

(c) 7 tubes used
12000 X

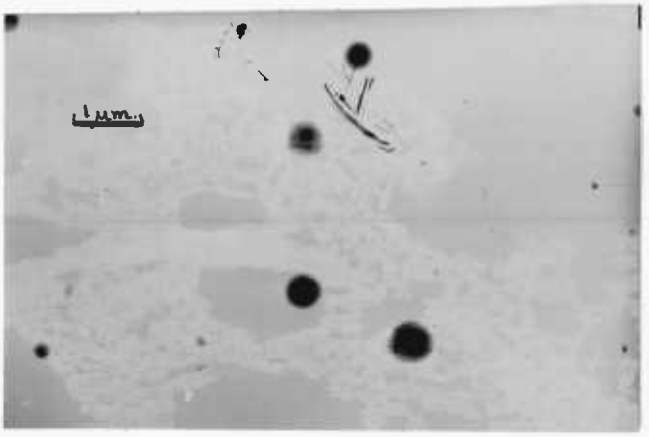

(d) 25 tubes used
9000 X

(ii) Shadowed samples

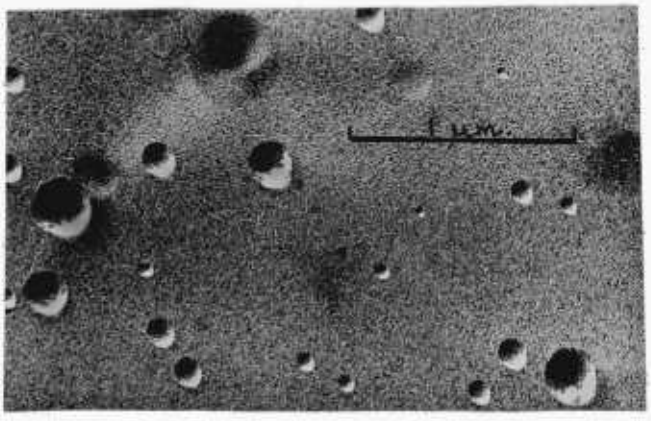

(e) 0 tubes used
30000 X

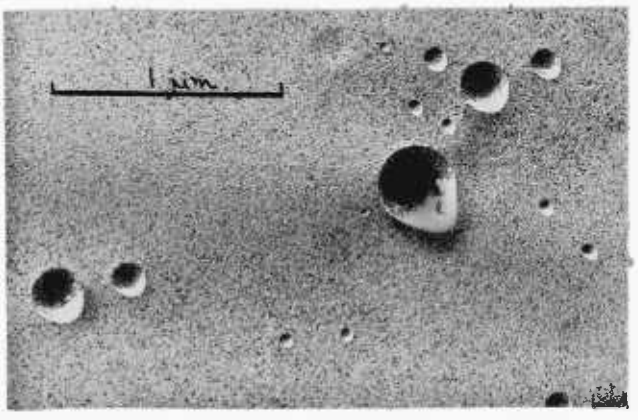

(f) 0 tubes used
30000 X

possibly in its metastable state between 20°C and 27°C. According to Mellor (88), the monohydrate has been prepared and appears as a reddish-yellow or reddish-white deposit. This is consistent with results observed. As a further check, a few drops of manganous sulphate solution were placed on a watch glass and dried in the oven under identical conditions to those used for the sample grids. A reddish-white powdery deposit was obtained, apparently similar to the compound described above.

The appearance of the samples that have undergone shadow-casting is illustrated in Plate 1(e) and (f). The dark areas depict the particles and the light areas the shadows where the gold/palladium layer is rarified. A number of these plates were taken and used to determine the shape factor, f, defined as the ratio of the depth of the particle on the plate (determined from its shadow) to its diameter measured perpendicular to the shadowing direction. These measurements were made on the 174 particles. The mean shape factor was found to be 0.27, with a standard deviation of 0.077. Though this standard deviation value is fairly low, indicating that the value of f is roughly the same for all sample particles, it should be borne in mind that the standard error associated with a single parameter determination from a sample of 174 particles is $1/\sqrt{174}$, i.e. 7.6%. Thus, the value may be considered reasonably representative, though the standard error is outside the normal 5% tolerance limit. The simplest way to employ this factor in the evaluation of particle volumes is to assume that particles may be considered as oblate spheroids, with f representing the ratio of the shorter axis to the longer. This approach has been employed because it was not possible to discern fine structure, and also, it would appear reasonable for an amorphous deposit from an evaporated solution to assume a fairly smooth surface geometry.

The results obtained on fitting a ZOLD distribution density function to particle size distributions obtained from the measurement of particles on the plates will be presented and discussed in sections

dealing with the conditions of the run, i.e. in Sections 5.1(d) and 5.2.

(b) The Monitoring of Sulphur Dioxide Concentration (See Section 4.4)

Before discussing the performance of the spectrophotometer a notation will be introduced by which these experiments will be classified. Each sample taken into the gas syringe, and diluted according to dilution method (b) (Section 4.4) will be referred to in the form X.Y. The value given to X determines the running conditions, e.g. number of reaction tubes used, aerosol flowrate, etc., and a set of experiments for a given value of X will be denoted a 'run'. During each run, a series of samples were taken from the aerosol/gas mixture, the time lapse between the beginning of the run, i.e. the time that the apparatus is switched on, and the withdrawal of sample being noted. The analysis of a sample will be termed an 'experiment', each experiment of run X being differentiated by a value Y. An experiment consists of diluting the gas (if necessary) and introducing portions of sample into the spectrophotometer. Each individual value obtained from the spectrophotometer will be referred to as a 'meter reading' or simply a 'reading'.

It was found that an experiment could comprise any number between four and twenty readings, depending on the condition of the rubber policeman and the position of insertion of the hypodermic needle. (A needle insertion near the glass of the gas syringe led to rapid gas emission). These readings are plotted in Fig. 5-I for three experiments chosen at random. It can be seen that the first sample taken in all three cases yields a low result, and that, normally, the other readings taken from the gas syringe when it is almost full yield readings on the low side of average. This pattern was observed in all cases, and is presumably due to inadequate mixing of the sampled and diluent gas in the gas syringe. The later readings, on the whole, were found to be fairly consistent. The presence of the low values increases the standard deviation calculated for the experiment. This is reflected most strongly in experiments where the number of readings is small. It is felt that

Fig. 5-I: Spectrophotometer performance. Relative meter readings taken from sample gas syringe, from 3 random experiments.

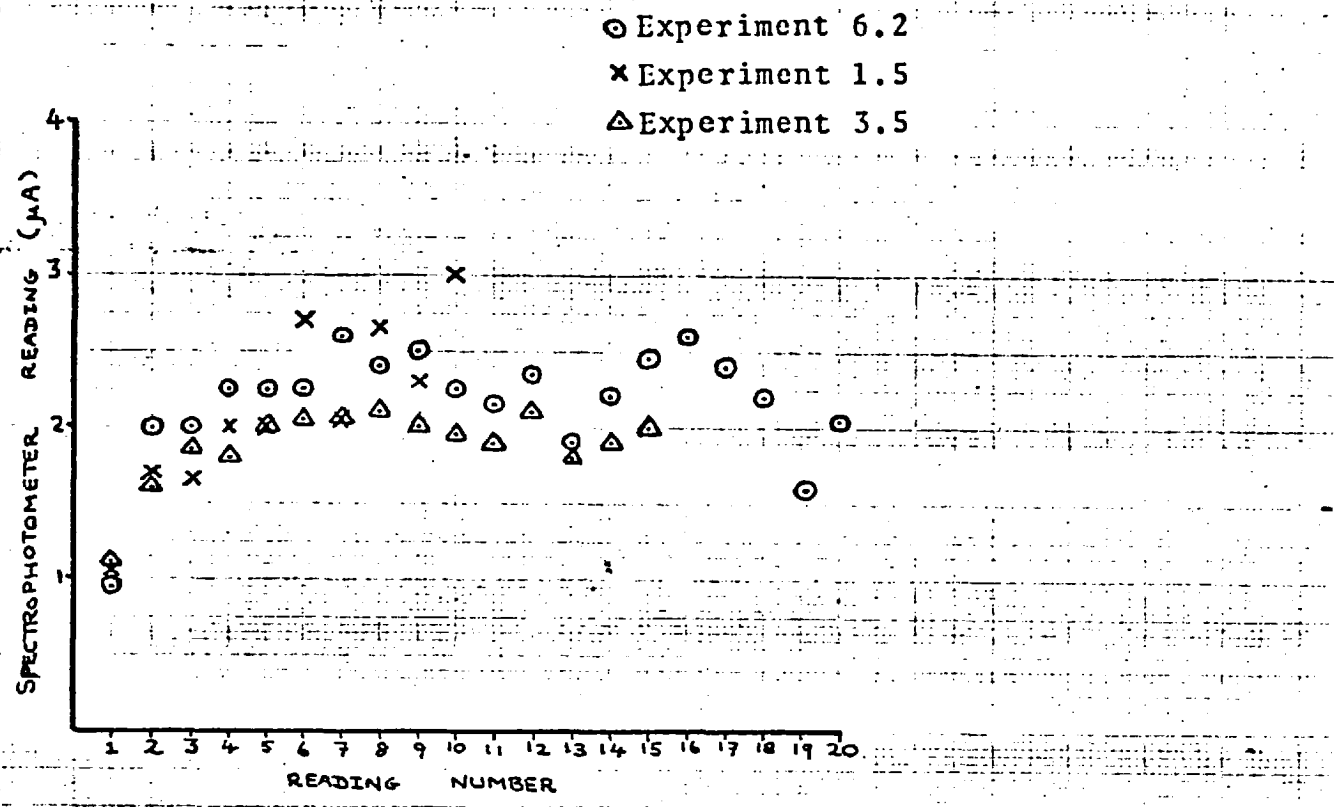

Fig. 5-II: Spectrophotometer performance. Sulphur dioxide concentration values for experiments of run 3, as a function of apparatus running time.

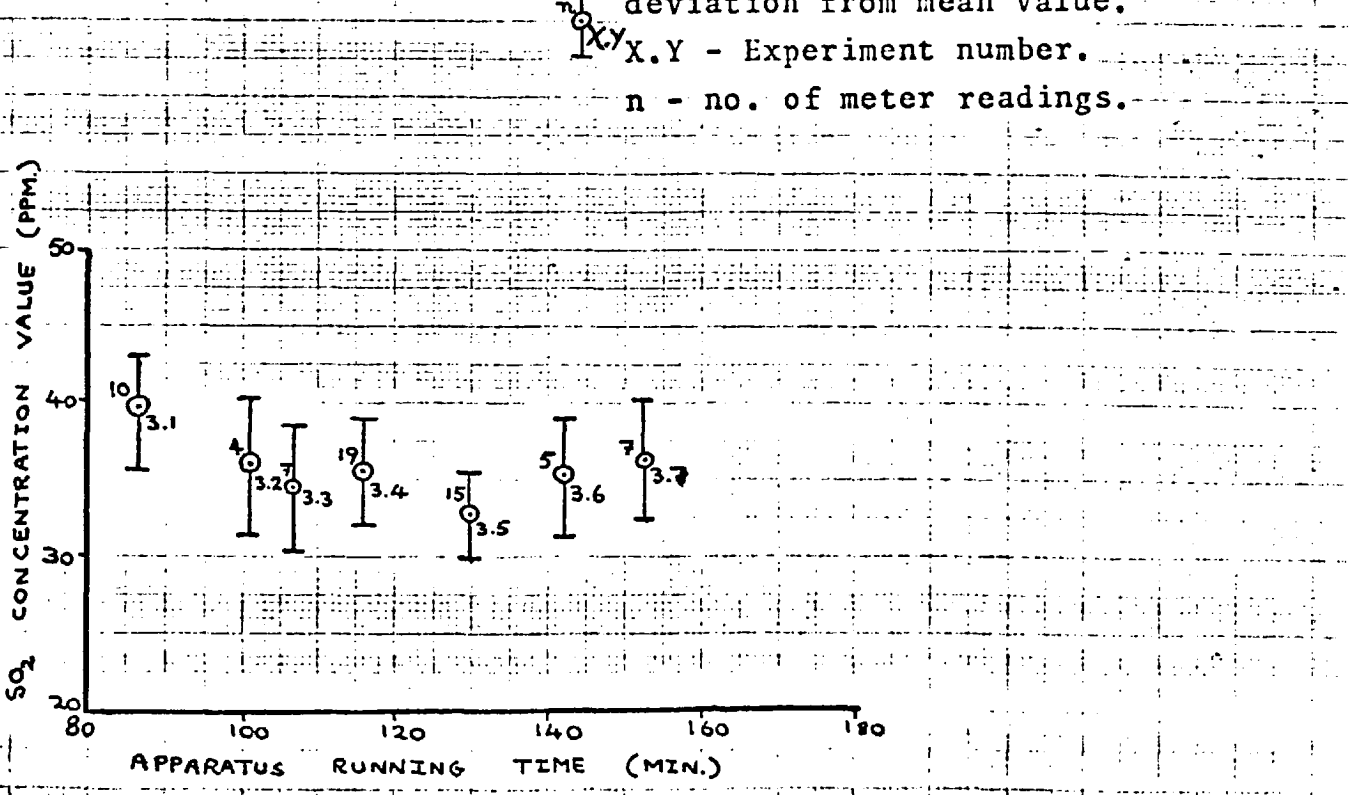

the large standard deviations incurred in these cases given an honest quantification of the possible inaccuracy in the results.

The variation of sulphur dioxide concentration for a typical run with apparatus running time is given in Fig. 5-II. The significance of the run number will be explained in Section 5.3. The experiment number and the number of readings employed are given with each experimental point. The 'feet' of the points represent the effect on the result of adding or subtracting the sample standard deviation of the readings, and thus provide an indication of the sensitivity of the measurements. It may be seen from Fig. 5-II that no regular change in the experimental points can be discerned with increasing running time. From this it may be concluded that, within the limits of experimental sensitivity and accuracy, the apparatus running time does not affect the sulphur dioxide concentration measured by the spectrophotometer for a given set of run conditions.

(c) The Light Scattering Determination of Particle Size (See Section 2.5)

A similar notation to that used to describe the results from the spectrophotometer will be used to classify the light scattering experiments. Experiment X.Y refers to run X with a set of experimental conditions, e.g. aerosol flowrate, number of reactor tubes, etc., with Y distinguishing sets of data collected after various apparatus running times. A 'scan' refers to the values collected after the rotating mirror of the light scattering apparatus has traversed all fifteen static mirrors. A 'reading' refers to one number from the data acquisition system, as punched on to the data collecting paper tape.

As mentioned in Section 2.5, it was not possible to use data acquired at all mirror positions owing to the presence of obviously erroneous values. Fig. 5-III shows two plots of relative scattered intensity, on a logarithmic scale, versus scattering angle, obtained from the apparatus. Diagram (a) represents a normal case, while diagram (b) shows a particularly bad case. Plots of light scattering data in this chapter show a run, the experiments in which are distinguished by the use of separate centred symbols. The effects of a reduced number of mirror

Fig. 5-III: Examples of plots of scattered intensity (uncorrected) versus angle, showing obviously erroneous values.

(a) Normal case. Run 3

■ Blank run values - ignore.

● 3.1
▲ 3.2
+ 3.3
} 4 readings / mirror position/scan, 8 scans / experiment

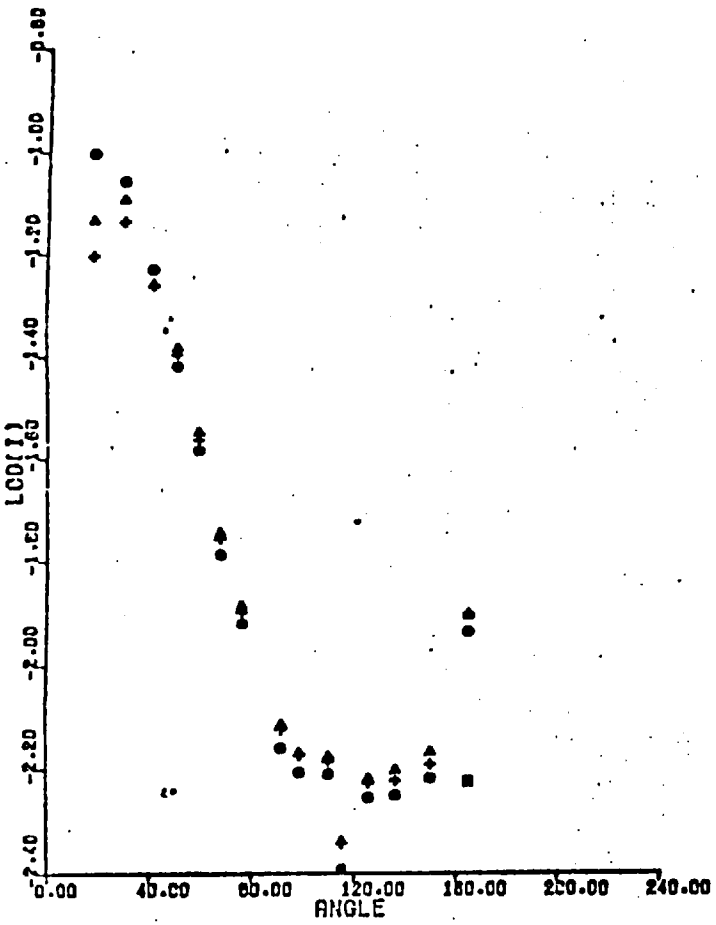

(b) Bad case. Run 18

■ Blank run values - ignore.

● 18.1
▲ 18.2
+ 18.3
} 4 readings / mirror posn./scan, 8 scans/expt.

× 18.4 6 scan expt.
◆ 18.5 as 18.1-18.3

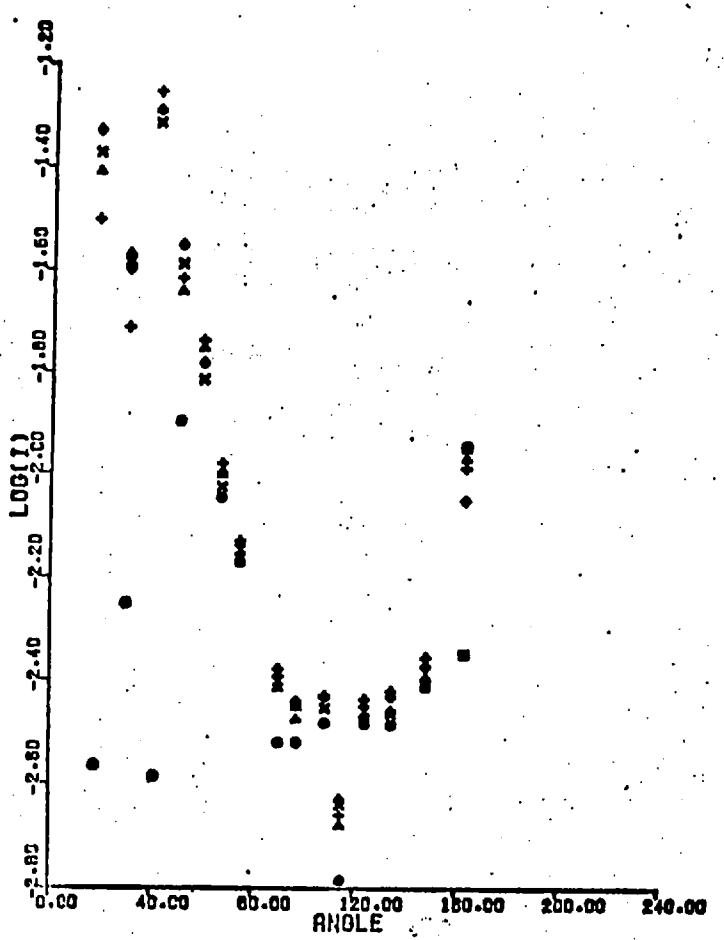

positions on the SEARCH data inversion technique has been discussed in Section 2.5. Now, an attempt to explain the discrepancies will be given.

One factor affecting the light scattering intensities obtained is the accuracy of alignment of the static mirrors. It was found that this procedure had to be carried out very carefully. Also, it is rather inconvenient to alter the alignment since this would necessitate the evaluation of a new set of Mie coefficients at the new scattering angle. Adjustment during a run was very difficult owing to the fact that the instrument needed to be uncovered, with the result that the aerosol flow through the sampling cell (See Section 4.1) was disturbed, causing aerosol to escape into the light scattering box. Once in the box the aerosol was difficult to remove, causing problems with stray scattered light. The fifth most obtuse angle (mirror position 5) of Fig. 5-III(a) and (b) appears to be slightly misaligned as it gives a low consistent reading in both cases. Misalignment is also probably the main cause of the low readings at the most forward-scattering angles in Fig. 5-III(b).

Another important factor affecting the readings is the presence of signal noise. There are three potential sources of noise in the light scattering apparatus; the laser, the photomultiplier, and the aerosol flow through the sampler. Since the analogue-digital converter, which converts the analogue signal from the photomultiplier to the digits that are punched on the paper tape, has a minimum integration time of 1/60 s., only noise in the 1-100 Hz frequency range needs to be considered. It is convenient to represent the effect of noise as noise-to-signal ratio, defined as the ratio of the root mean square magnitude of the noise, as determined from an oscilloscope trace, to the magnitude of the mean d.c. signal. The noise-to-signal ratio for the laser was determined by examining the signal obtained from the photodiode (see Fig. 2-IX). It was found to be of the order of 0.3% after laser stabilisation (i.e. about $1\frac{1}{2}$ hours after switching on) which is negligible compared with the noise

obtained from the photomultiplier and the aerosol flow.

In order to ascertain the importance of noise originating from the operation of the photomultiplier and the flowing aerosol the noise-to-signal ratio was measured for the first six runs (to use each of the combinations of tubular vessels described in Section 4.1), in the presence and absence of aerosol flowing. The results are presented in Tables 5-1 and 5-2 for the absence and presence of flowing aerosol respectively. The values in Table 5-1 provide estimates of the importance of photomultiplier noise. The magnitudes of these signals should be compared with the magnitudes of the d.c. signals obtained with aerosol flowing to determine the relative importance of the photomultiplier and aerosol flow noise components. It may be seen from Table 5-2 that the noise-to-signal ratios obtained at back-scattering angles, and at the less acute forward-scattering angles, are comparable with those obtained in the absence of aerosol, given in Table 5-1. Also, the qualitative appearance of the noise, as a function of time, on the oscilloscope screen is similar in these cases, with very little variation occurring over large time increments (i.e. seconds). The noise appeared to have the same amplitude at all observation times. This indicates that the origin of the noise is probably the photomultiplier, and that the aerosol flow has little or no effect. However, at the more acute forward-scattering angles the noise-to-signal ratio increased, and variations in noise amplitude were observed over periods of seconds. This indicates that inhomogeneities in the aerosol flow are probably affecting the signal. It was found that at the most forward-scattering angle (mirror position 15, see Table 2-1), and in many cases the adjacent angle (mirror position 14), the noise was so great that it was not possible to ascertain a d.c. signal from the oscilloscope trace. The relative increase in noise at small scattering angles is illustrated in Fig. 5-III(a). It may also contribute to the large irregularities in the forward-scattering in Fig. 5-III(b).

Table 5-1: Noise obtained on light scattering measurements in the absence of aerosol.

Run no. 1

Mirror position	d.c.signal (mV.)	Noise-to-signal ratio	Mirror posn.	d.c.signal (mV.)	Noise-to-signal ratio
1	7.3	4%	9	1.7	4%
2	2.3	4%	10	1.7	4%
3	1.8	3%	11	1.7	4%
4	1.9	4%	12	1.7	4%
5	1.8	4%	13	1.7	4%
6	1.7	4%	14	1.7	4%
7	1.7	4%	15	2.0	5%
8	1.7	4%			

Run no. 2

Mirror position	d.c.signal (mV.)	Noise-to-signal ratio	Mirror posn.	d.c.signal (mV.)	Noise-to-signal ratio
1	6.1	8%	9	1.5	6%
2	2.0	9%	10	1.5	7%
3	1.6	6%	11	1.5	8%
4	1.7	7%	12	1.5	8%
5	1.6	8%	13	1.5	7%
6	1.5	9%	14	1.6	8%
7	1.5	7%	15	1.8	9%
8	1.5	8%			

Run no. 3

Mirror position	d.c.signal (mV.)	Noise-to-signal ratio	Mirror posn.	d.c.signal (mV.)	Noise-to-signal ratio
1	5.6	8%	9	1.7	7%
2	2.1	10%	10	1.7	7%
3	1.7	7%	11	1.7	6%
4	1.8(5)	7%	12	1.7	6%
5	1.7(5)	7%	13	1.7	7%
6	1.7	7%	14	1.8	7%
7	1.7	6%	15	2.0	7%
8	1.7	7%			

Table 5-1 (continued)

Run no. 4

Mirror position	d.c.signal (mV.)	Noise-to-signal ratio	Mirror posn.	d.c.signal (mV.)	Noise-to-signal ratio
1	7.9	8%	9	2.9(5)	8%
2	3.5	9%	10	2.9(5)	9%
3	3.0	8%	11	3.0	8%
4	3.2	8%	12	3.0	7%
5	3.0	8%	13	3.0	7%
6	2.9(5)	9%	14	3.0(5)	8%
7	2.9	8%	15	3.4	9%
8	2.9(5)	8%			

Run no. 5

Mirror position	d.c.signal (mV.)	Noise-to-signal ratio	Mirror posn.	d.c.signal (mV.)	Noise-to-signal ratio
1	7.2	10%	9	2.9	7%
2	3.4	9%	10	2.9	8%
3	2.9	9%	11	2.9	8%
4	3.0(5)	9%	12	3.0	8%
5	2.9	9%	13	2.9	8%
6	2.9	8%	14	3.0	8%
7	2.9	8%	15	3.2(5)	9%
8	2.9	7%			

Run no. 6

Mirror position	d.c.signal (mV.)	Noise-to-signal ratio	Mirror posn.	d.c.signal (mV.)	Noise-to-signal ratio
1	7.1	10%	9	2.4	8%
2	3.0	10%	10	2.4	8%
3	2.5	8%	11	2.4	8%
4	2.6(5)	9%	12	2.4(5)	10%
5	2.5	8%	13	2.5(5)	8%
6	2.4(5)	8%	14	2.7(5)	10%
7	2.4	9%	15	3.7	10%
8	2.4	10%			

Table 5-2: Noise obtained on light scattering measurements in the presence of aerosol.

Run no. 1

Mirror position	d.c.signal (mV.)	Noise-to-signal ratio	Mirror posn.	d.c.signal (mV.)	Noise-to-signal ratio
1	31	3%	9	28	3%
2	20	3%	10	40	2%
3	14	3%	11	62	4%
4	12	3%	12	93	5%
5	8.6	3%	13	99	7%
6	13	3%	14	140	11%
7	13	3%	15	--	--
8	16	3%			

Run no. 2

Mirror position	d.c.signal (mV.)	Noise-to-signal ratio	Mirror posn.	d.c.signal (mV.)	Noise-to-signal ratio
1	16	6%	9	17	5%
2	10	7%	10	24	5%
3	8.9	6%	11	37	4%
4	7.8	7%	12	57	3%
5	5.6	8%	13	90	9%
6	8.5	6%	14	120	13%
7	8.7	6%	15	--	--
8	9.8	7%			

Run no. 3

Mirror position	d.c.signal (mV.)	Noise-to-signal ratio	Mirror posn.	d.c.signal (mV.)	Noise-to-signal ratio
1	12	9%	9	12	8%
2	6.1	10%	10	17	8%
3	5.7	9%	11	27	6%
4	5.6	10%	12	39	5%
5	4.2	11%	13	63	7%
6	6.2	10%	14	80	17%
7	6.3	10%	15	--	--
8	6.9	10%			

Table 5-2 (continued)

Run no. 4

Mirror position	d.c.signal (mV.)	Noise-to-signal ratio	Mirror posn.	d.c.signal (mV.)	Noise-to-signal ratio
1	12(.5)	8%	9	14	7%
2	7.8	8%	10	21	7%
3	7.3	9%	11	32	6%
4	7.0	9%	12	48	5%
5	6.9	9%	13	65	14%
6	8.0	9%	14	80	18%
7	8.8	8%	15	--	--
8	10	9%			

Run no. 5

Mirror position	d.c.signal (mV.)	Noise-to-signal ratio	Mirror posn.	d.c.signal (mV.)	Noise-to-signal ratio
1	11	8%	9	11	8%
2	6.5	8%	10	16(.5)	7%
3	6.2	8%	11	24(.5)	6%
4	5.9	8%	12	39	5%
5	6.2	8%	13	52	19%
6	6.7	9%	14	--	---
7	7.1	8%	15	--	--
8	8.3	8%			

Run no. 6

Mirror position	d.c.signal (mV.)	Noise-to-signal ratio	Mirror posn.	d.c.signal (mV.)	Noise-to-signal ratio
1	12	7%	9	9.4	8%
2	5.3	9%	10	13(.5)	7%
3	4.8(5)	8%	11	20	7%
4	4.8	8%	12	32	6%
5	5.0	8%	13	44	16%
6	5.3	9%	14	70	21%
7	5.7	9%	15	--	--
8	6.8	9%			

The most probable reason for the increased effect of aerosol flow noise at small scattering angles is as follows. The particles flowing through the light scattering cell are polydisperse and therefore it is likely that the number of relatively large particles in the incident laser beam will vary with time. Now, the light scattered from large particles is strongly forward-directed. Thus, a temporal variation in the number of large particles in the incident beam will cause large fluctuations in the intensity of the forward-scattered light, which is observed as noise. Since large particles do not scatter strongly at back-scattering angles, or the less acute forward-scattering angles, it is unlikely that noise from this source will be observed in these cases.

From Figs. 2-X to 2-XVII, and also from the work of Maddock (78), it may be seen that the light scattering patterns obtained from fairly polydisperse aerosols exhibit little or no fine structure. Thus, it should be valid to surmise that experimental values such as those obtained at mirror position 5 in Figs. 5-III(a) and (b) are in error, and therefore should be rejected. This was the first criterion adopted to determine the acceptability of data. The second criterion involved the spread of experimental points at a given angular position of a run. Large variations generally correspond to large noise-to-signal ratios, and, in these cases, the readings at the mirror position were rejected.

In Fig. 5-III, the conditions under which each experiment took place are given. Normally, four readings were taken at each mirror position on each scan, and eight scans constituted an experiment. This gives thirty-two readings per mirror position per experiment, which were averaged for the final scattered intensity value. Clearly, the more readings are taken, the more reliable the final result becomes. Examination of the data was also possible to determine where noise was excessive, and thus assist in the decisions on the acceptance or rejection of experimental points.

The noise measurements given here illustrate the difficulties involved

in the application of forward-scattering techniques to the size determination of aggregates of large aerosol particles suspended in a flowing gas. This limitation would appear to apply to any method where a forward-scattered reading is required, such as a dissymmetry method.

(d) The Aerosol Generator (see Section 4.2)

Before embarking on the main experimental work the performance of the aerosol generator was checked. Firstly, samples from the generator outlet were collected in the thermal precipitator, and examined as described in Section 2.4, for a number of initial master solution concentrations. The master solutions were made up to approximately the required concentration, and samples were then analysed accurately by a colorimetric method (acknowledgment is due to the Analytical Services Laboratory). It should be noted that the aerosol takes about 4.5 min. to travel from the generator outlet to the precipitator head (see Section 4.1). The results of these experiments are given in Table 5-3 and Figs. 5-IV to 5-VII. A further experiment, using a gas flowrate of 4.0 l/min., was carried out to check the effect of flowrate on resultant nucleus size. The result of this, illustrated in Fig. 5-VIII, shows that the form of the distribution is similar to that obtained at the higher flowrate.

For each set of conditions corresponding to one of Figs. 5-IV to 5-VIII, five sample grids were taken, and, as far as possible, equal numbers of electron micrographs were taken from each. This is an attempt to reduce statistical errors in sampling.

Table 5-3 gives the main properties of the nuclei distributions obtained, i.e. the modal diameter and spread parameter of the fitted ZOLD distributions, and values of the mass mean diameter obtained from the experimental measurements and from the application of equation (2.9) to the fitted ZOLD parameters. The data points of the histograms, constructed as described in Section 2.4, and the fitted ZOLD curves are given in Figs. 5-IV to 5-VIII. Table 5-3 also gives estimates of the number concentration of the particles in each case, obtained according to equation (2.13). It may be seen from Figs. 5-IV to 5VIII that the data

Table 5-3: Results from analysis of electron micrographs from samples from the aerosol generator outlet.

Illustration in Fig.	Generator flowrate (l/min.)	Solution concentration (%w/w)	No. of particles sized	Fitted ZOLD parameters		Mass mean diameter (μm)		Estimated particle number concn. ($cm.^{-3}$)
				Mode (μm)	Spread	from exptl. data	from ZOLD params.	
5-IV	4.9	0.31	916	0.030	0.59	0.18	0.07	2.66×10^6
5-V	4.9	1.33	593	0.057	0.61	0.41	0.14	2.78×10^6
5-VI	4.9	3.12	947	0.040	0.58	0.25	0.09	2.58×10^6
5-VII	4.9	6.33	552	0.043	0.58	0.31	0.10	*
5-VIII	4.0	1.37	711	0.055	0.73	0.28	0.21	1.33×10^6

* No value obtainable, since parts of the plates showed damaged carbon coats, in areas of which no particles had been deposited.

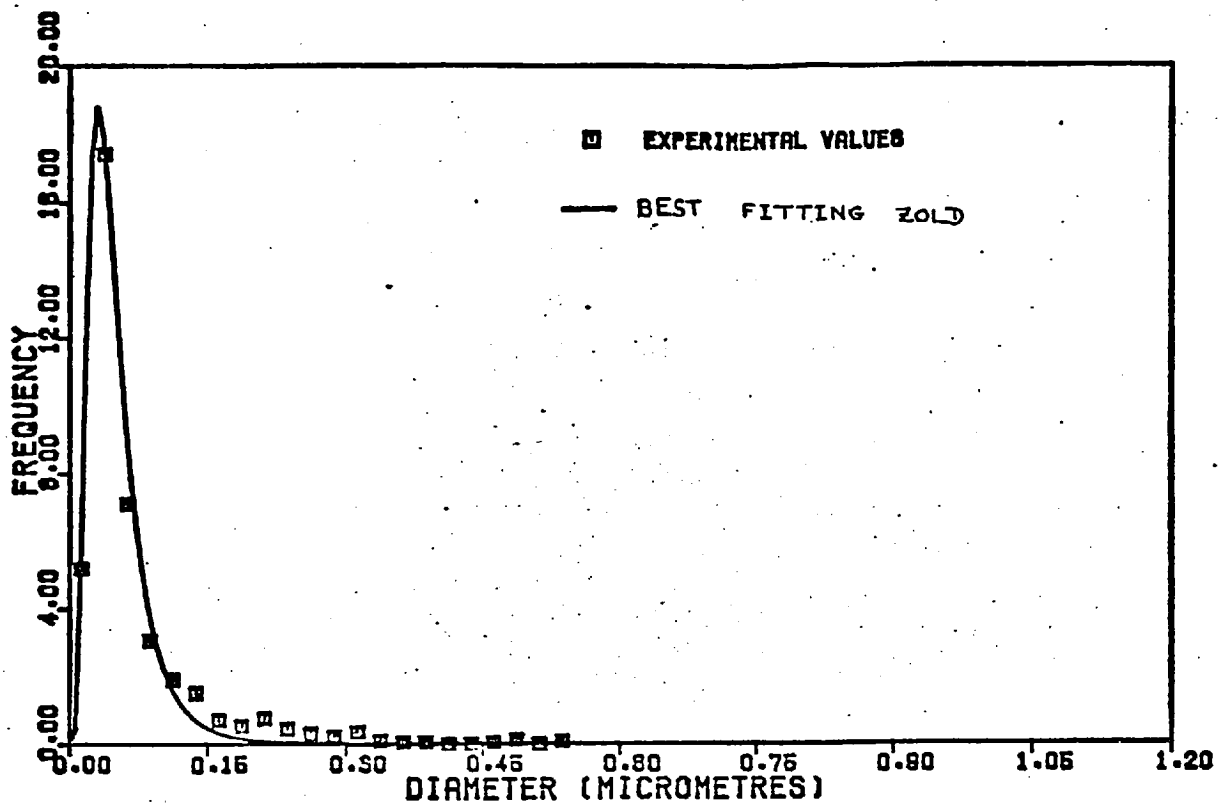

Fig. 5-IV: Distribution of nucleus size from aerosol generator.
Flowrate = 4.9 1/min.
Master solution concentration = 0.31%w/w.

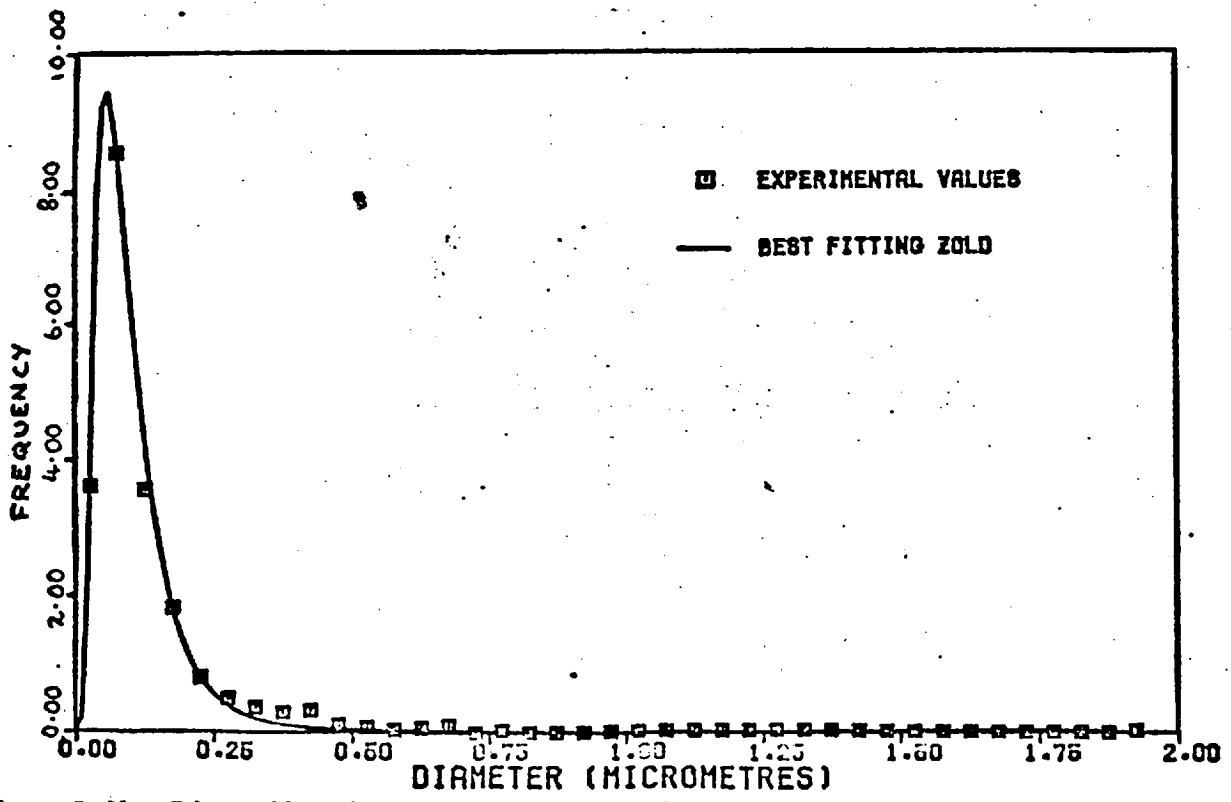

Fig. 5-V: Distribution of nucleus size from aerosol generator.
Flowrate = 4.9 1/min.
Master solution concentration = 1.33%w/w.

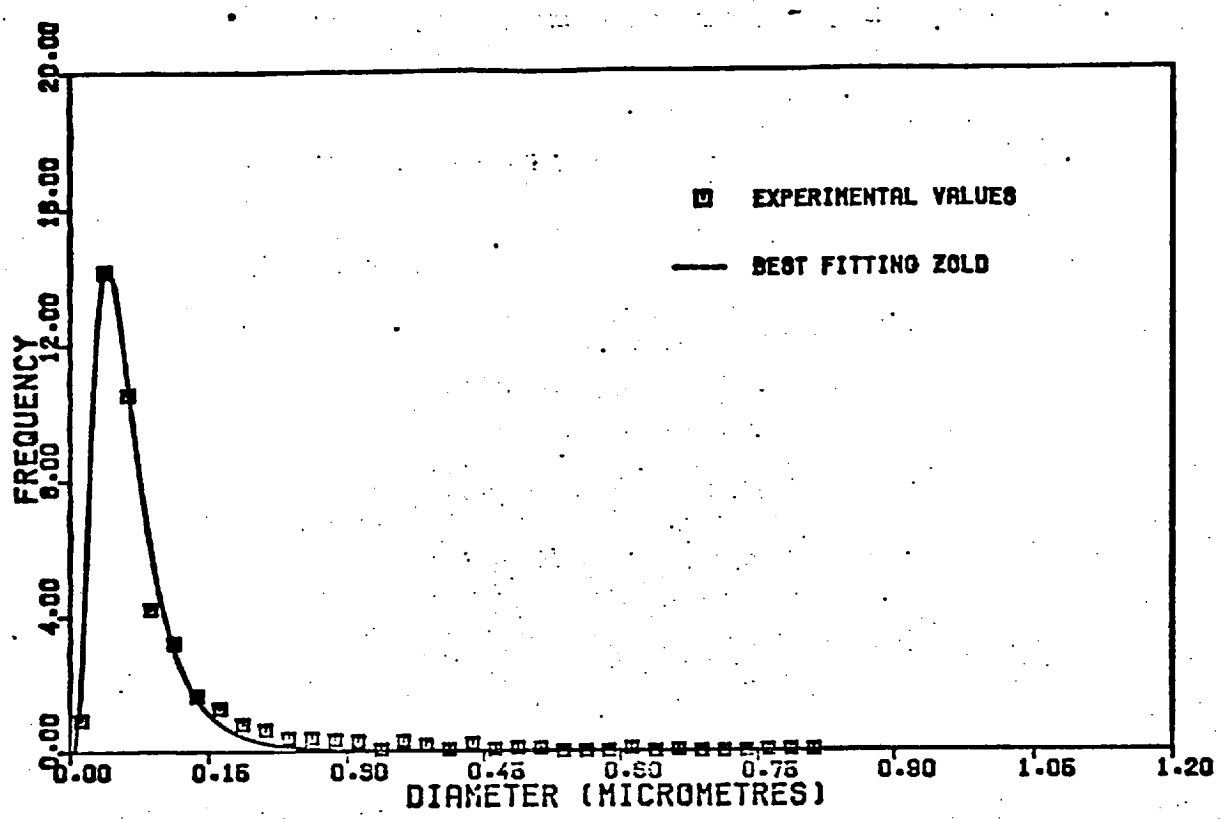

Fig. 5-VI: Distribution of nucleus size from aerosol generator.
Flowrate = 4.9 l/min.
Master solution concentration 3.12%w/w.

Fig. 5-VII: Distribution of nucleus size from aerosol generator.
Flowrate = 4.9 l/min.
Master solution concentration = 6.33%w/w.

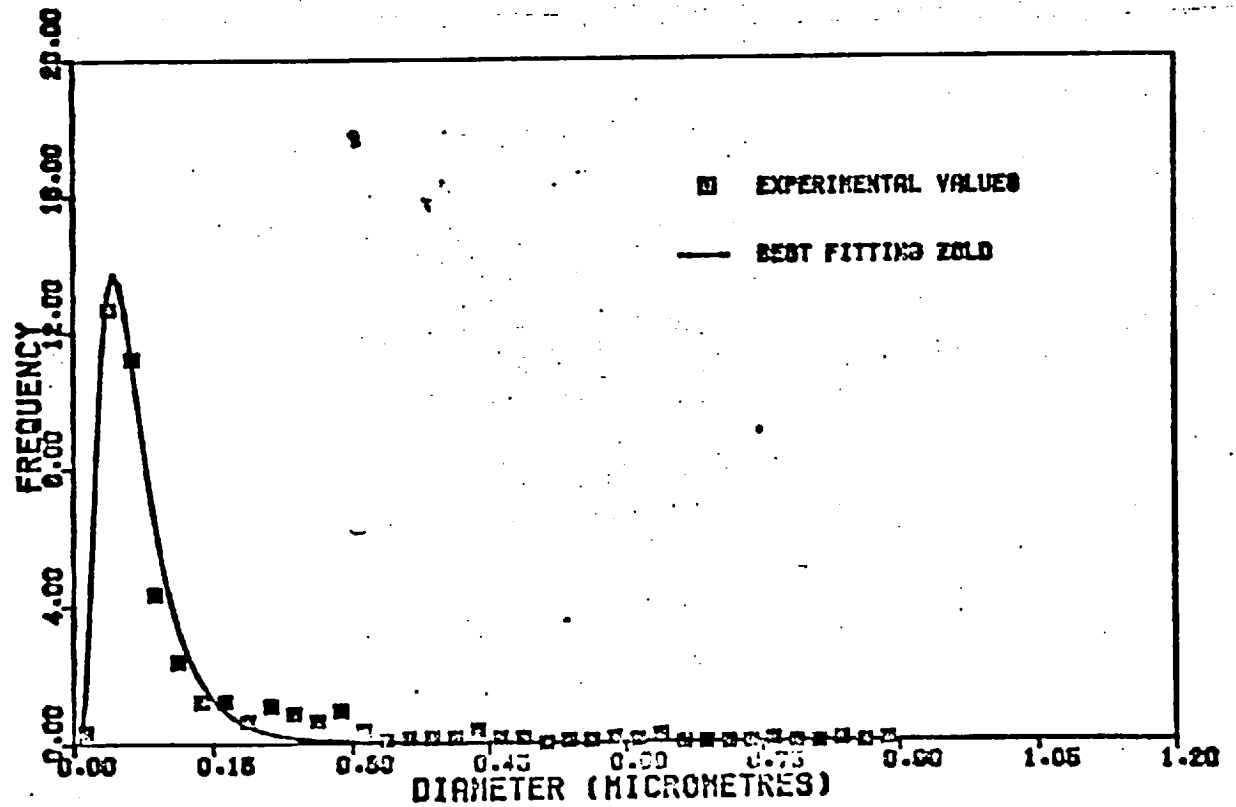

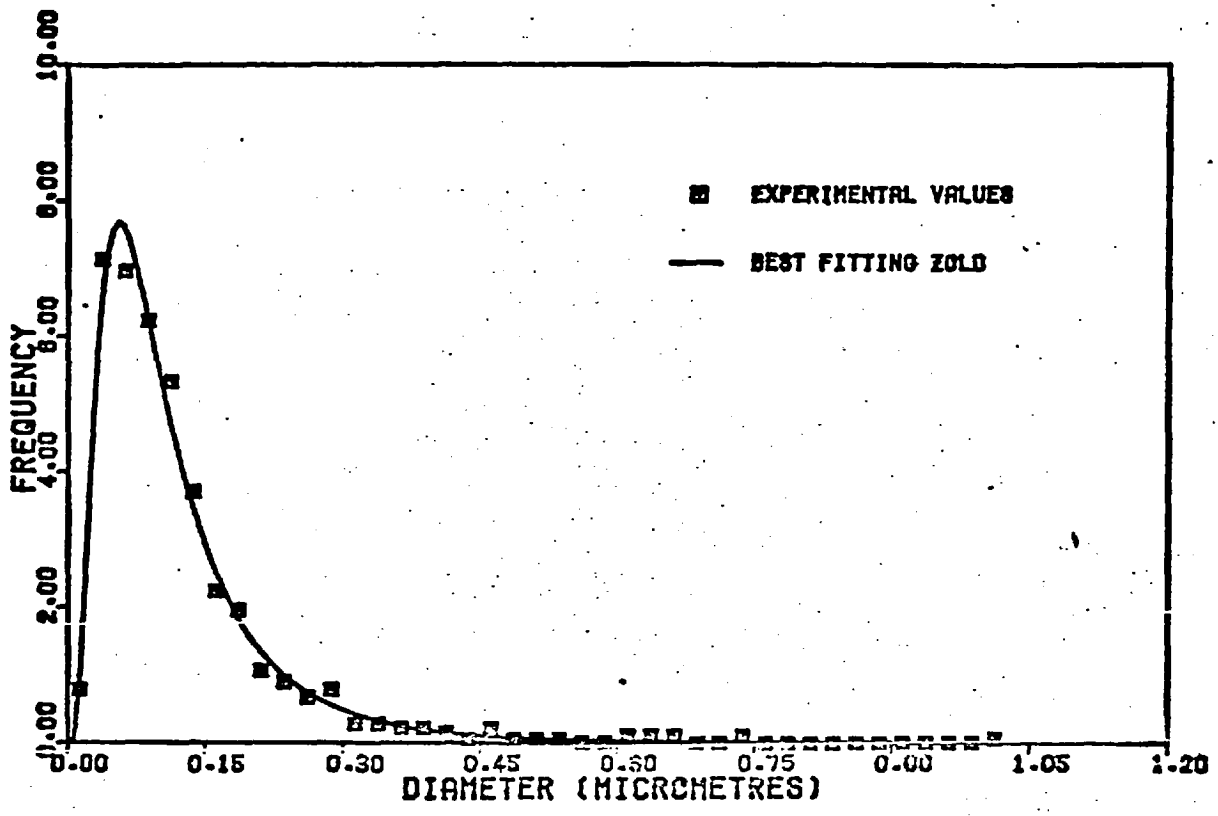

Fig. 5-VIII: Distribution of nucleus size from aerosol generator.

Flowrate = 4.0 l/min.

Master solution concentration = 1.37%w/w.

obtained indicates a good agreement with the ZOLD distribution curve. It is not, however, possible to quantify this agreement since an inadequate number of particles have been sized. However, the agreement appears to be good enough to validate the use of the ZOLD distribution in the light scattering data inversion procedure.

Examination of Table 5-3 indicates that large values of the ZOLD spread parameter and small modal values are fitted to the data. As will be shown in Section 5.2., light scattering results indicate that the spread parameter of the distribution should be smaller than the value obtained from electron microscopy (around 0.3, rather than 0.6). It is difficult to compare the ZOLD parameters obtained directly with the data. However, it is possible to calculate an estimate of the mass mean diameter of the aerosol particles from the sized sample. The standard error in this estimate is known from the number of particles considered. In all cases here, it is less than 4.5%. A second value of the mass mean diameter may be evaluated from the fitted ZOLD parameters. The two values obtained are given together in Table 5-3 for comparison. It may be seen that values calculated from the estimated ZOLD parameters are somewhat lower than those obtained experimentally, indicating that the estimates of the parameters are rather low.

From the values given in Table 5-3, little can be deduced about the variation of mass mean particle diameter with changing master solution concentration. With the exception of the most dilute solution, all values lie in the range of 0.25 - 0.41 μm. The only conclusion that it is possible to draw from these values is that the particle nucleus size is likely to lie in this range if the master solution concentration is in the range between about 1% and 7% w/w. In all cases where the higher aerosol flowrate is used, the estimated spread parameter is around 0.6, though this is probably an overestimate (see Section 5.2). The last column of Table 5-3 contains estimates of the particle number concentration of the aerosol. Good agreement exists between the values at the higher

flowrate. The lower value for the case of the lower flowrate is probably partly due to the different operating conditions in the generator and partly due to the increased residence time in the sampling, permitting more coagulation to take place. The values of the particle number concentration obtained in the first three rows of Table 5-3 were used as a basis for using an initial particle number concentration of 2.6×10^6 cm^{-3} in the solution to the coagulation equation, given in Section 3.4.

Also, the variation with time of the master solution concentration in the generator vessel was measured. Samples were taken periodically from the operating generator. The aerosol flowrate was 4.9 l/min. It would be expected that the manganous sulphate concentration in the generator should increase with time, as the finely divided droplets equilibrate with the surrounding atmosphere more rapidly than the bulk liquid. Thus, a particle formed from the master solution is likely to evaporate rapidly until a concentration/humidity equilibrium is reached. However, much liquid matter is returned to the bulk solution at the first liquid barrier. This will be at least partially evaporated, therefore a more concentrated solution is returned to the generator. The atmosphere above the bulk solution thus becomes more humid than it would be if no atomisation took place, and the tendency for aerosol particles to evaporate to dryness on leaving the generator is reduced.

The results of the analyses of these samples, together with the generator operating time at which they were taken, are given in Table 5-4. The solution concentration does in fact increase slightly, but the effect on the particle size produced is likely to be negligible. This can be seen to be so if the change in master solution concentration is viewed in the context of the results on particle size as a function of solution concentration, given earlier in this sub-section.

Table 5-4: Variation of atomiser master solution concentration with apparatus running time.

Apparatus running time (hr.)	0	0.5	1.0	2.0	3.0	4.0
Solution concentration (%w/w)	2.86	2.86	2.88	2.92	3.00	3.00

5.2. The Behaviour of the Aerosol System in the Absence of Reacting Gas

After the apparatus had been assessed, as described in the previous section, experiments were carried out on the aerosol in the absence of the gas dosing stream. For this purpose, connection 2 in Fig. 4-I was sealed off with a polythene 'policeman', so that the aerosol flowed through the system of reactor tubes. The purpose of this study is twofold. Firstly, comparison of nuclei size data, obtained by electron microscopy, and droplet size data, obtained from light scattering measurements, may be made. This comparison leads to further possibilities of assessing the methods, as well as a guide to the expected manganous sulphate concentration in the droplets. Secondly, the changes in particle size occurring in the reaction vessels due to coagulation and any other phenomena not associated with the reaction may be studied in isolation from the reaction. All of these points will be considered in this section, and all results pertaining to the reacting aerosol/gas system will be dealt with in Section 5.3.

Samples of the aerosol nuclei were collected in the thermal precipitator for each of the six combinations of reactor tubes described in Section 4.1. The procedure used was the same as that for collecting samples from the aerosol generator outlet, five sample grids being collected and the micrographs, as far as possible, being taken in equal numbers from each. The results are given in Table 5-5 and Figs. 5-IX to 5-XIV. It may be seen, from Table 5-5, that for cases of longer residence time in the reactor vessels a fairly small sample has been sized. This is due to the fact that in these cases the population of particles on the grids was found to be very sparse. Some improvement was obtained by taking micrographs at a lower magnification (9,000 X instead of 15,000 X) thus accommodating a larger grid area. From the last column of Table 5-5, it may be seen that the apparent particle number concentration is reduced drastically if seven or more reactor tubes are used. This will be returned to later in this section.

Table 5-5: Results from analysis of electron micrographs. Aerosol flowrate = 4.9 l/min.

Illustration in Fig.	Reaction vessels used	Solution concentration (%w/w)	No. of particles sized	Fitted ZOLD parameters		Mass mean diameter (μm)		Estimated particle number concn. ($cm.^{-3}$)
				Mode (μm)	Spread	from exptl. data	from ZOLD params.	
5-IX	S	2.17	647	0.10	0.60	0.29	0.25	6.53×10^5
5-X	1	2.12	368	0.085	0.72	0.31	0.31	5.54×10^5
5-XI	3	2.20	537	0.10	0.75	0.32	0.41	5.09×10^5
5-XII	7	2.09	302	0.075	1.0	0.42	0.91	1.59×10^5
5-XIII	13	2.14	271	0.22	0.58	0.44	0.51	1.31×10^5
5-XIV	25	2.20	222	0.27	0.54	0.47	0.56	9.10×10^4

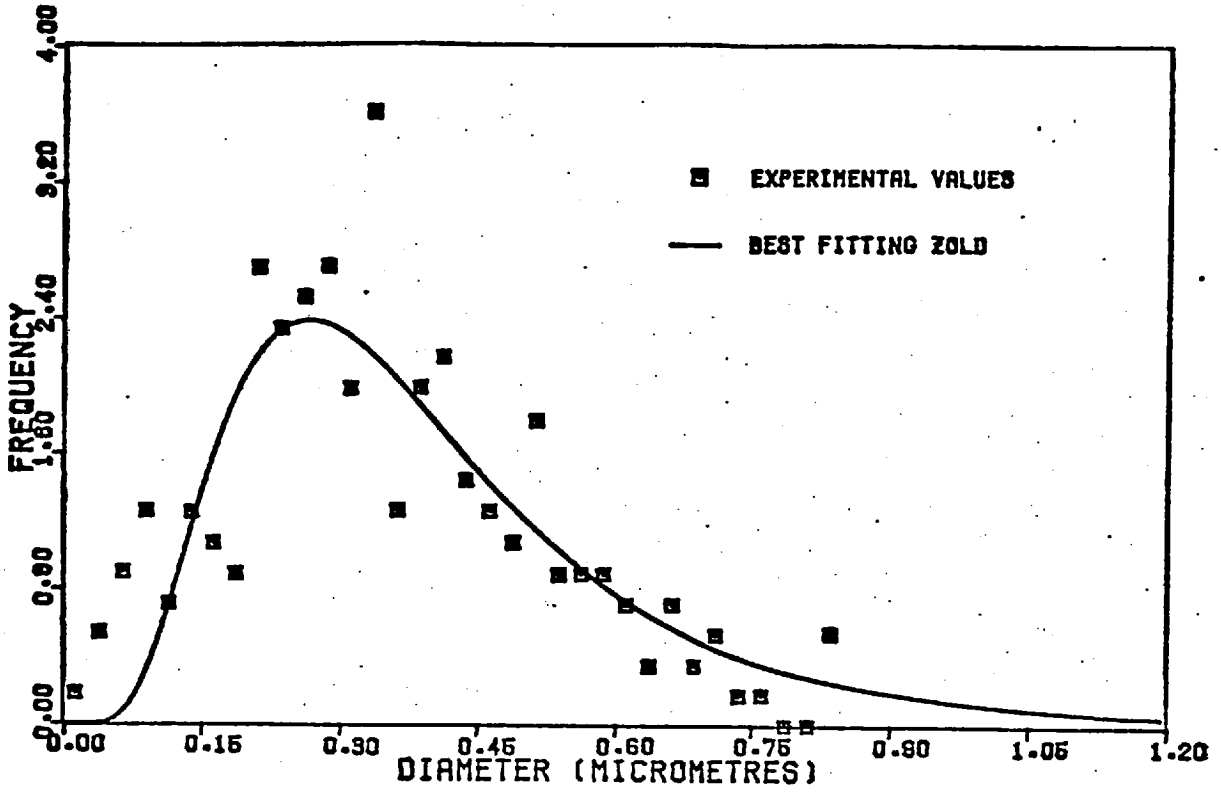

Fig. 5-IX: Distribution of aerosol nucleus size.
Aerosol passed through S tube.
Flowrate = 4.9 1/min.
Master solution concentration = 2.17%w/w.

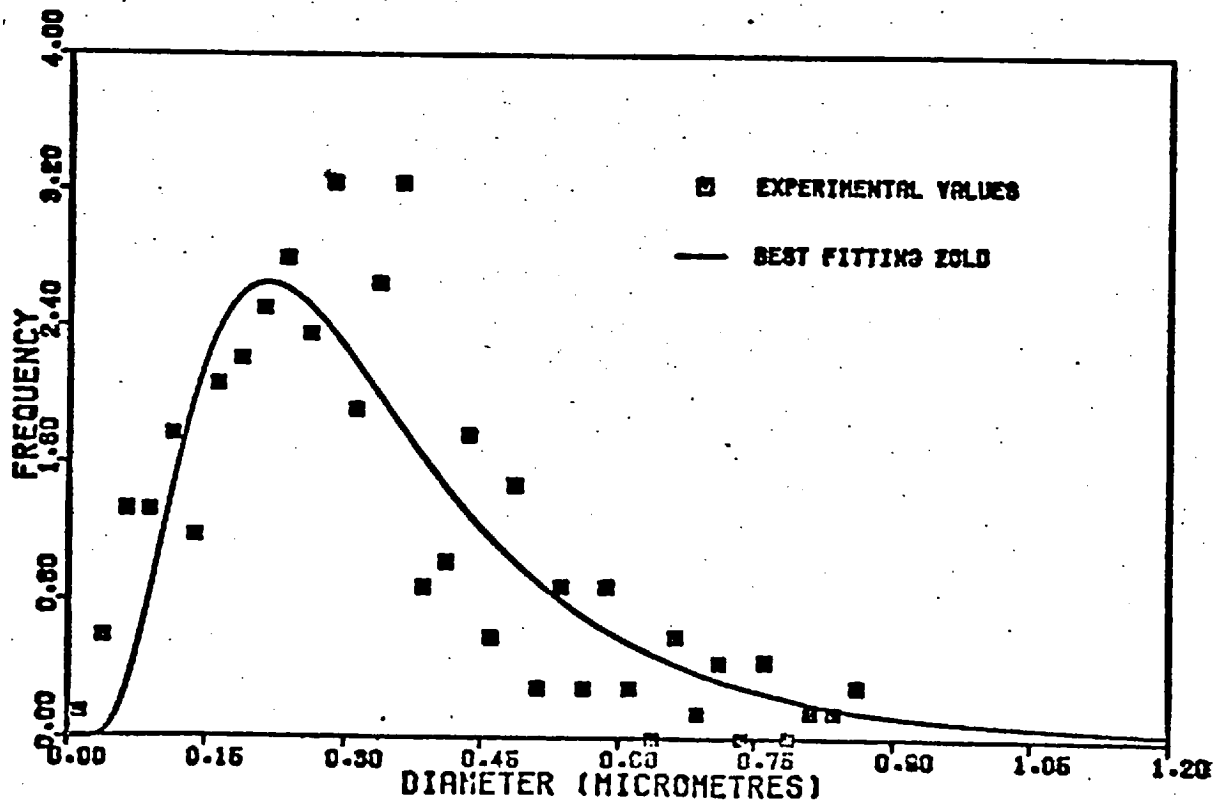

Fig. 5-X: Distribution of aerosol nucleus size.
Aerosol passed through 1 tube
Flowrate = 4.9 1/min.
Master solution concentration = 2.12%w/w

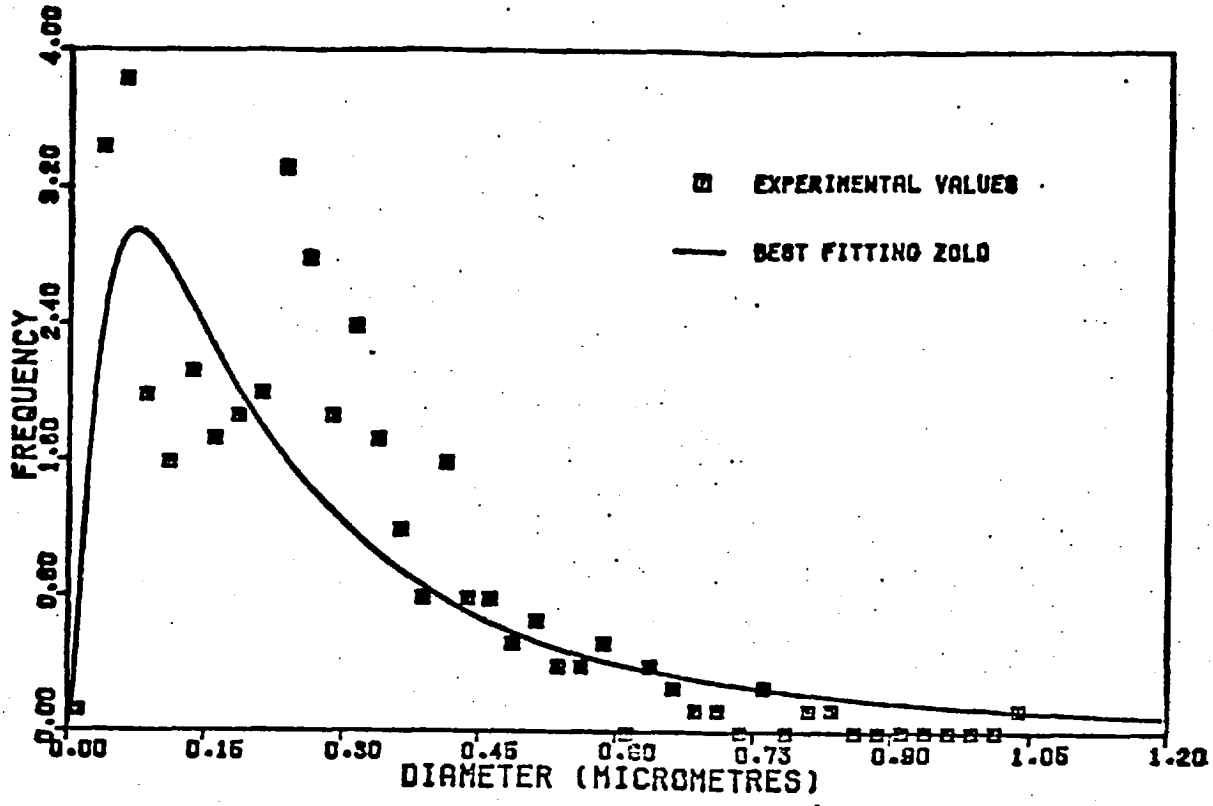

Fig. 5-XI: Distribution of aerosol nucleus size.
Aerosol passed through 3 tubes.
Flowrate = 4.9 1/min.
Master solution concentration = 2.20%w/w.

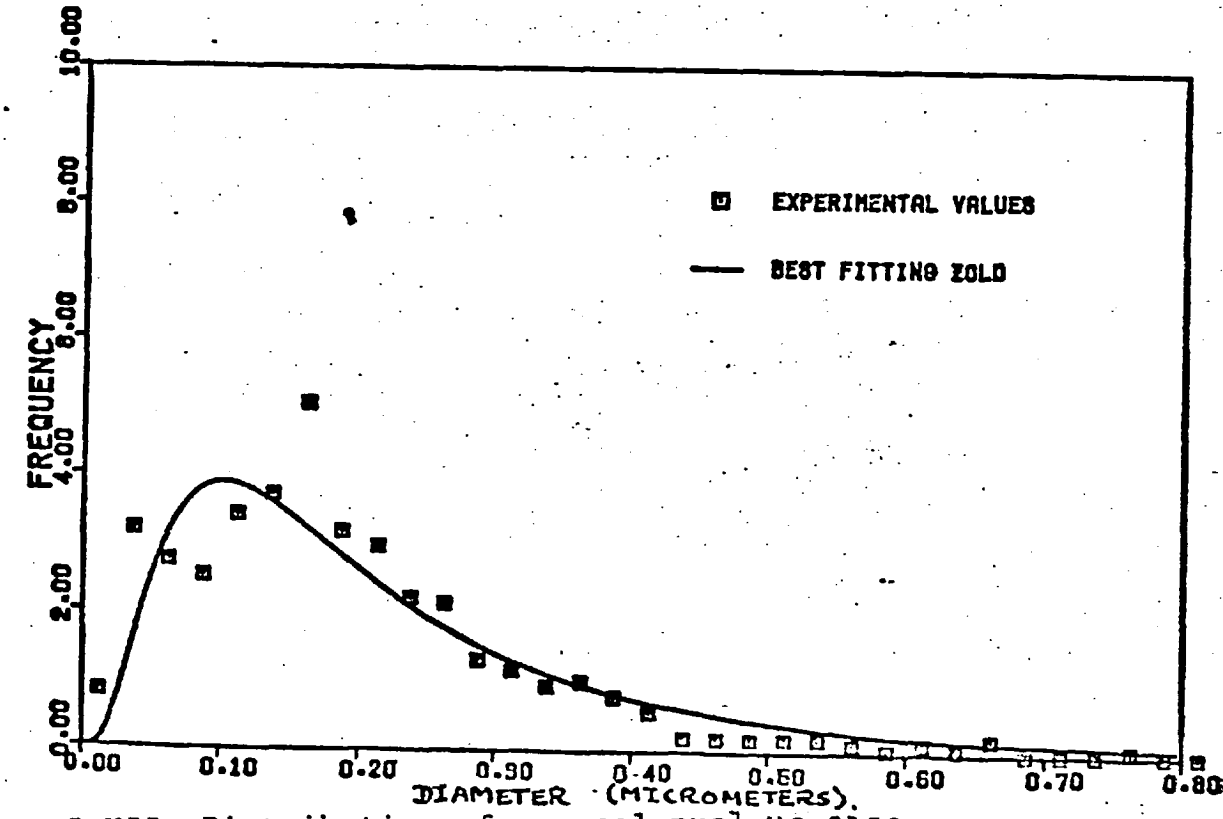

Fig. 5-XII: Distribution of aerosol nucleus size.
Aerosol passed through 7 tubes.
Flowrate = 4.9 1/min.
Master solution concentration = 2.09%w/w.

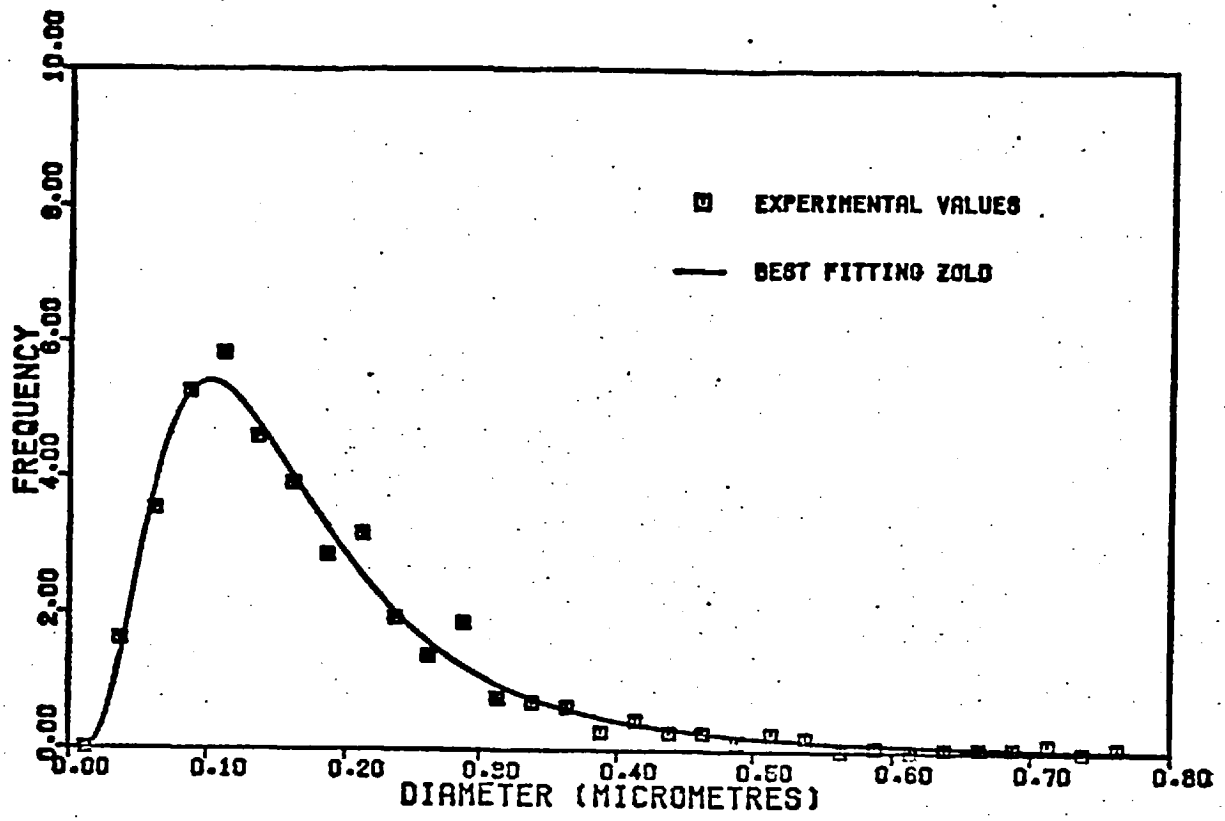

Fig. 5-XIII: Distribution of aerosol nucleus size.
Aerosol passed through 13 tubes
Flowrate = 4.9 l/min.
Master solution concentration = 2.14%w/w.

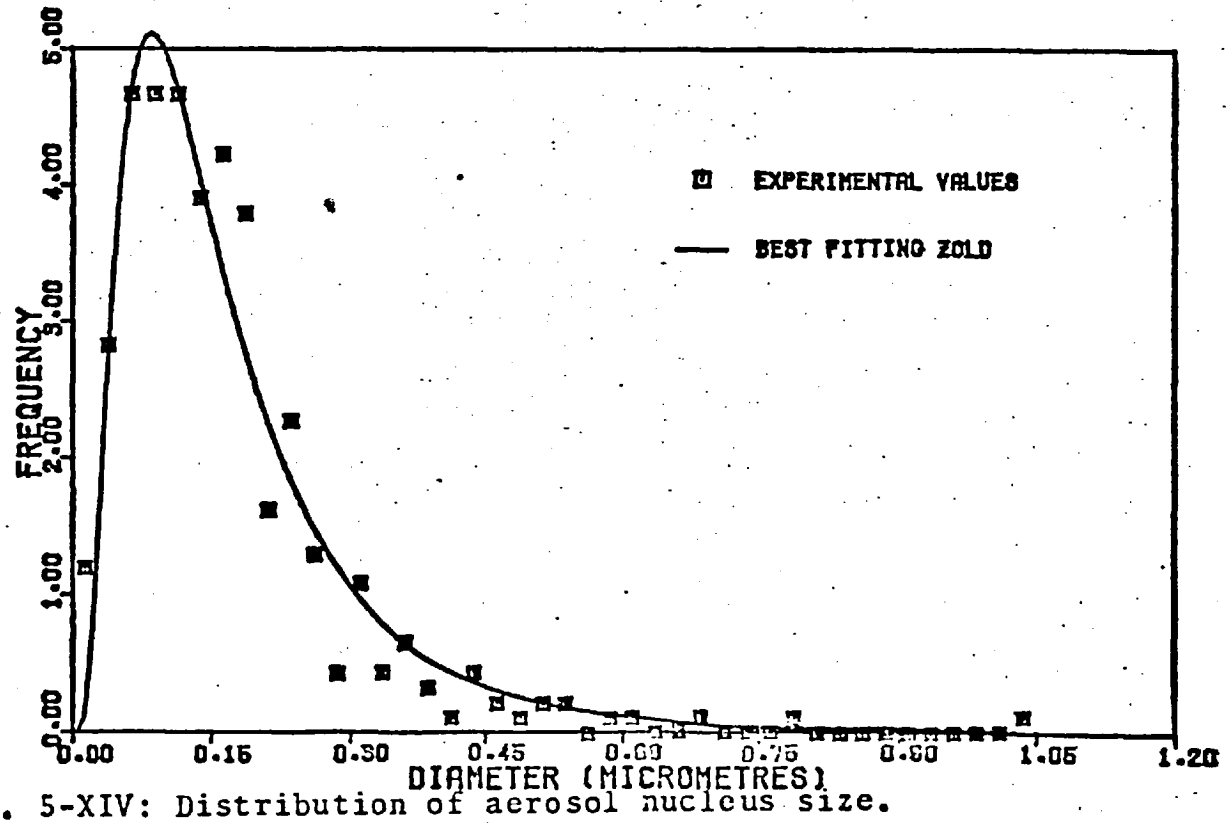

Fig. 5-XIV: Distribution of aerosol nucleus size.
Aerosol passed through 25 tubes.
Flowrate = 4.9 l/min.
Master solution concentration = 2.20%w/w.

Examination of Figs. 5-IX to 5-XIV indicates that the correspondence between the form of the ZOLD function and the experimentally determined histogram deteriorates as the residence time in the reactor system increases. However, no coherent change, such as the consistent development of a second mode, is apparent. There is some evidence of the formation of a bimodal distribution in Figs. 5-XI and 5-XII, corresponding to aerosol residence times of about seven and ten minutes (see Table 4 - 1). When, however, the scatter of points in these cases is considered, the case for the formation of a second mode does not appear strong. Also, the inadequacies of the sampling must be considered; in order to reduce the standard error associated with any given histogram point to below 5%, 400 particles must be sized per histogram interval. This would necessitate the sizing of 10,000 particles per set of conditions. Using the technique described in Section 2.4 this is not a feasible proposition.

Comparison of mass mean diameters obtained from sizing data with those calculated from the fitted parameters using equation (2.9) shows much better agreement than was obtained from the runs of Section 5.1(d). However, a great deal of variation in the relative values of a_{r_1} and σ_0 occurs. This again may be explained by the small sample sizes. The values obtained from the largest sample (reaction tube S used, 647 particles considered) are similar to those in Table 5-3, where relatively large samples have been taken. It is interesting to note that the fitted value of the spread parameter is 0.6 in this case, as in the experiments given in Section 5.1(d).

Light scattering measurements were also taken using the same combinations of reactor tubes. The results are given in Figs. 5-XV to 5-XX, and in Table 5-6. Figs. 5-XV to 5-XX show the light scattering results, with erroneous values removed, corrected according to equation (2.17), and normalised as described in Section 2.5. For each run, the corrected, normalised scattered intensities at each angle are averaged, the averaged light scattering pattern being denoted X.A, where X is the run number. (Since only one experiment has been carried out in run 2,

Eig. 5-XV: Light scattering data for run 1.
Aerosol passed through S tube.
Experiments: ● 1.1; ▲ 1.2;
+ 1.3.
■ Average for run (1.A)

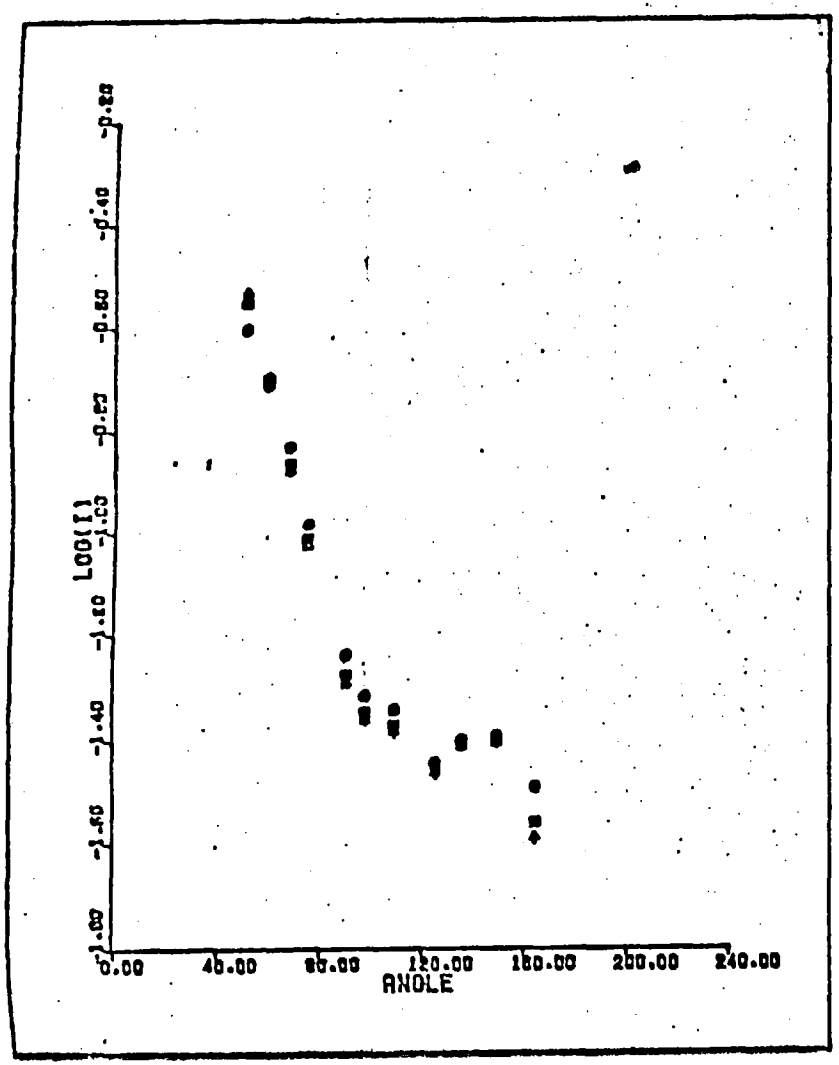

Fig. 5-XVI: Light scattering data for run 2.
Aerosol passed through 1 tube.
Experiment: ■ 2.1

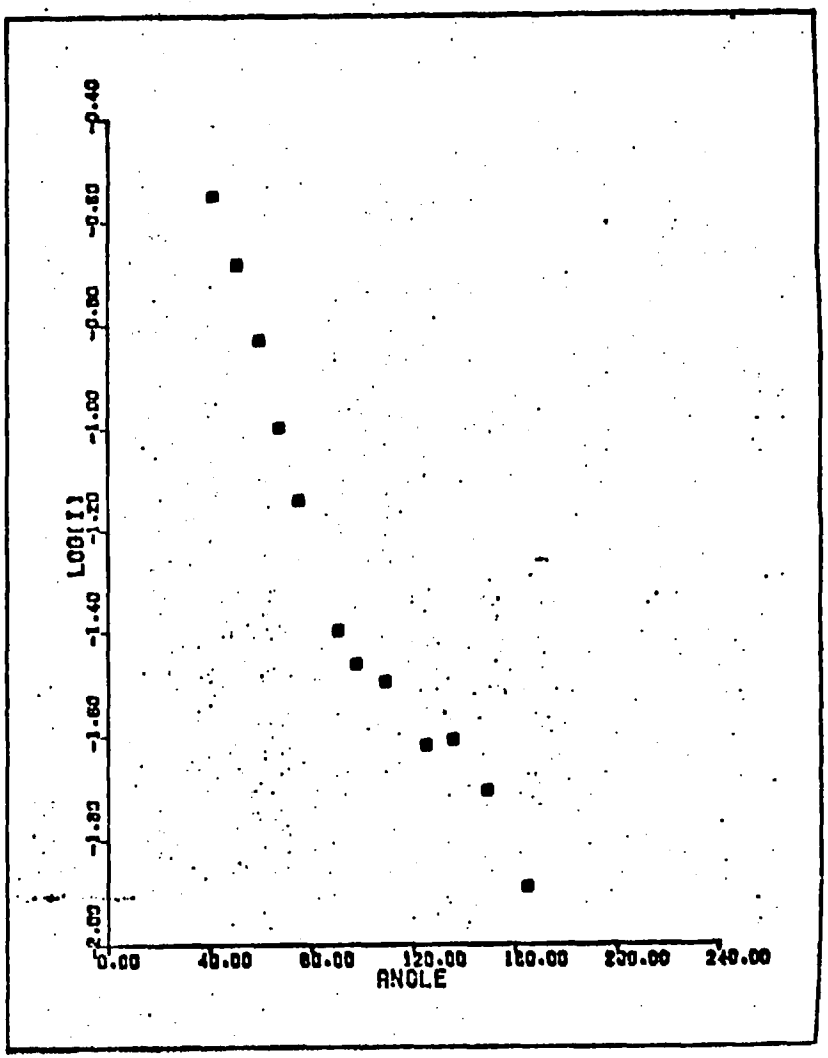

Fig. 5-XVII: Light scattering data for run 3.
Aerosol passed through 3 tubes.
Experiments: ● 3.1; ▲ 3.2
+ 3.3
■ Average for run (3.A)

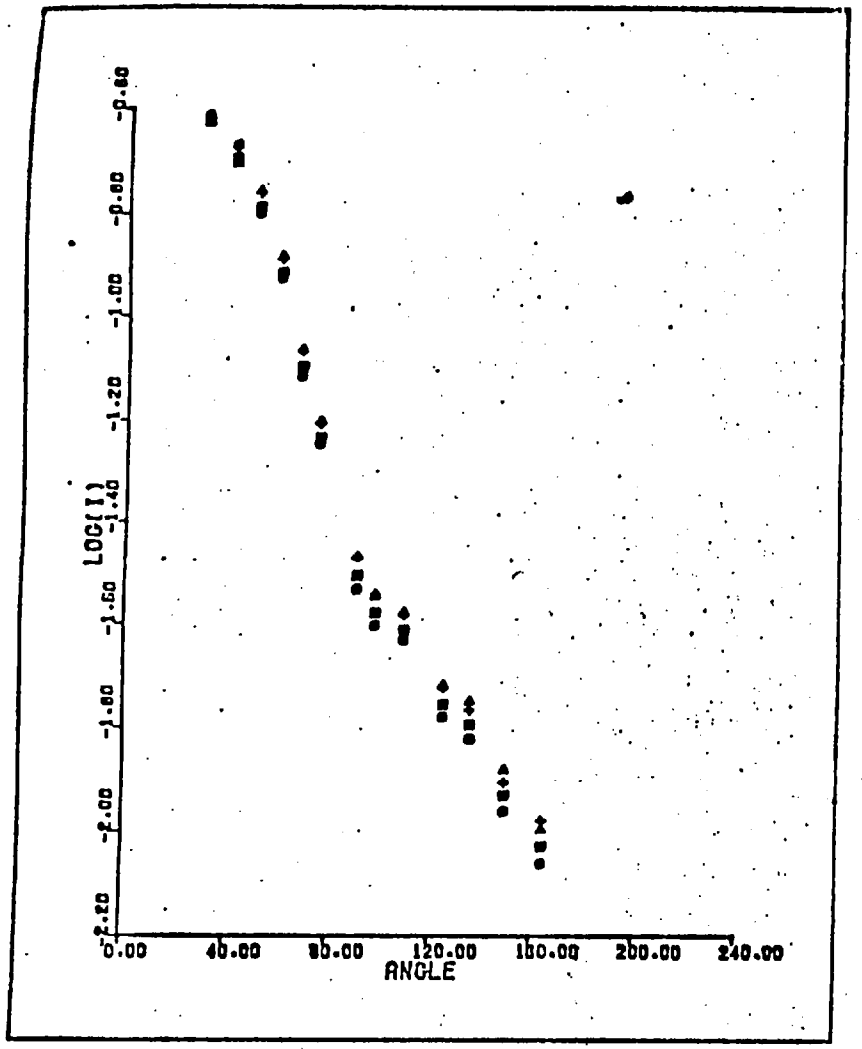

Fig. 5-XVIII: Light scattering data for run 4.
Aerosol passed through 7 tubes.
Experiments: ● 4.1; ▲ 4.2
+ 4.3
■ Average for run (4.A)

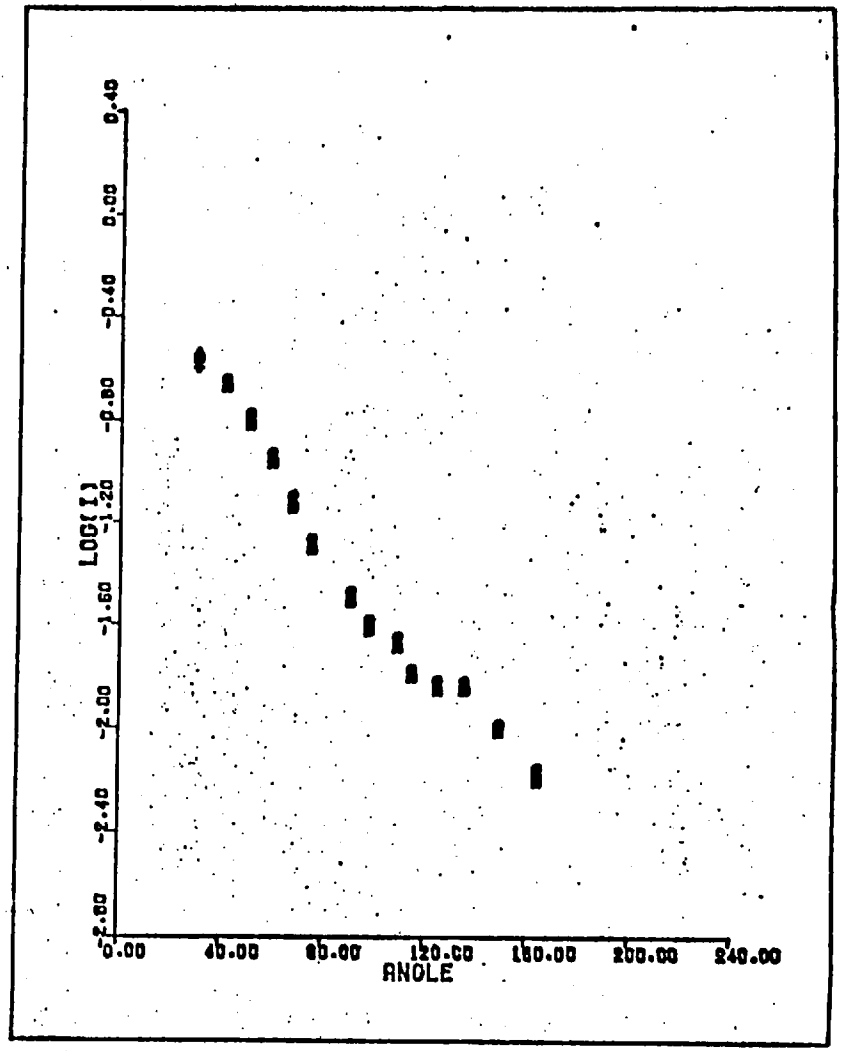

Fig. 5-XIX: Light scattering data for run 5.
Aerosol passed through 13 tubes.
Experiment: ● 5.1; ▲5.2;
+ 5.3; × 5.4
■ Average for run (5.A)

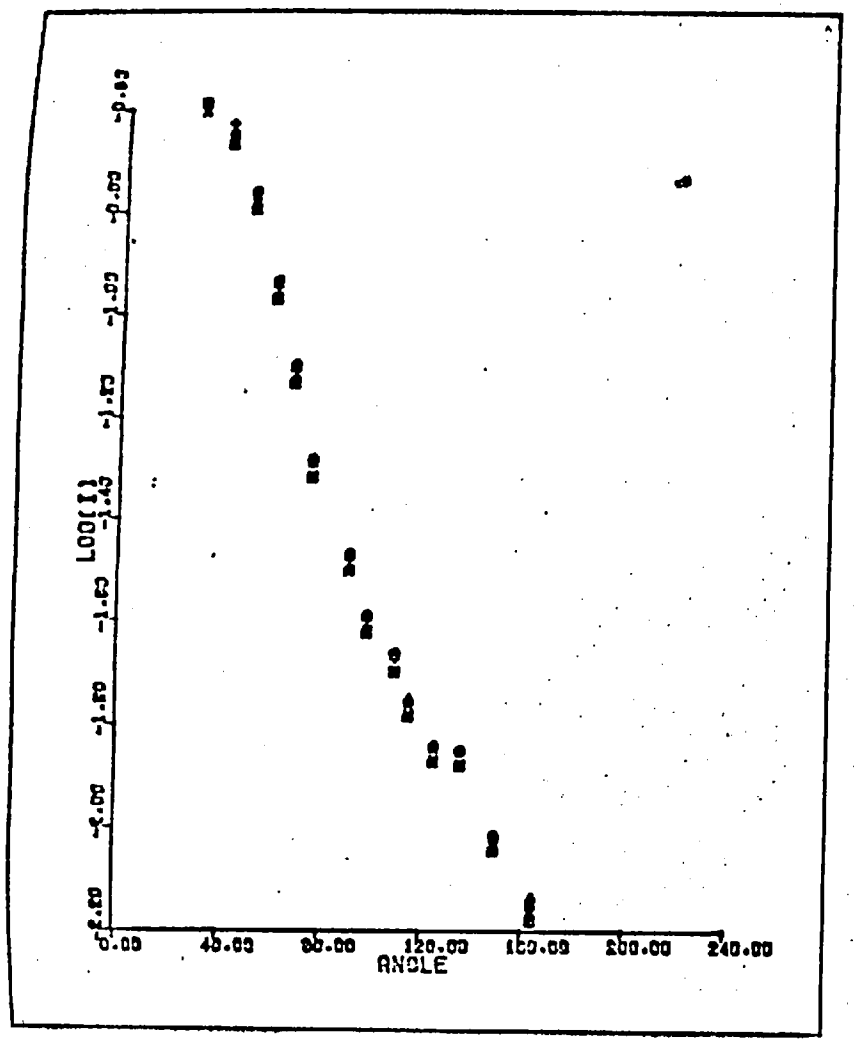

Fig. 5-XX: Light scattering data for run 6.
Aerosol passed through 25 tubes.
Experiment: ● 6.1; ▲6.2
■ Average for run (6.A)

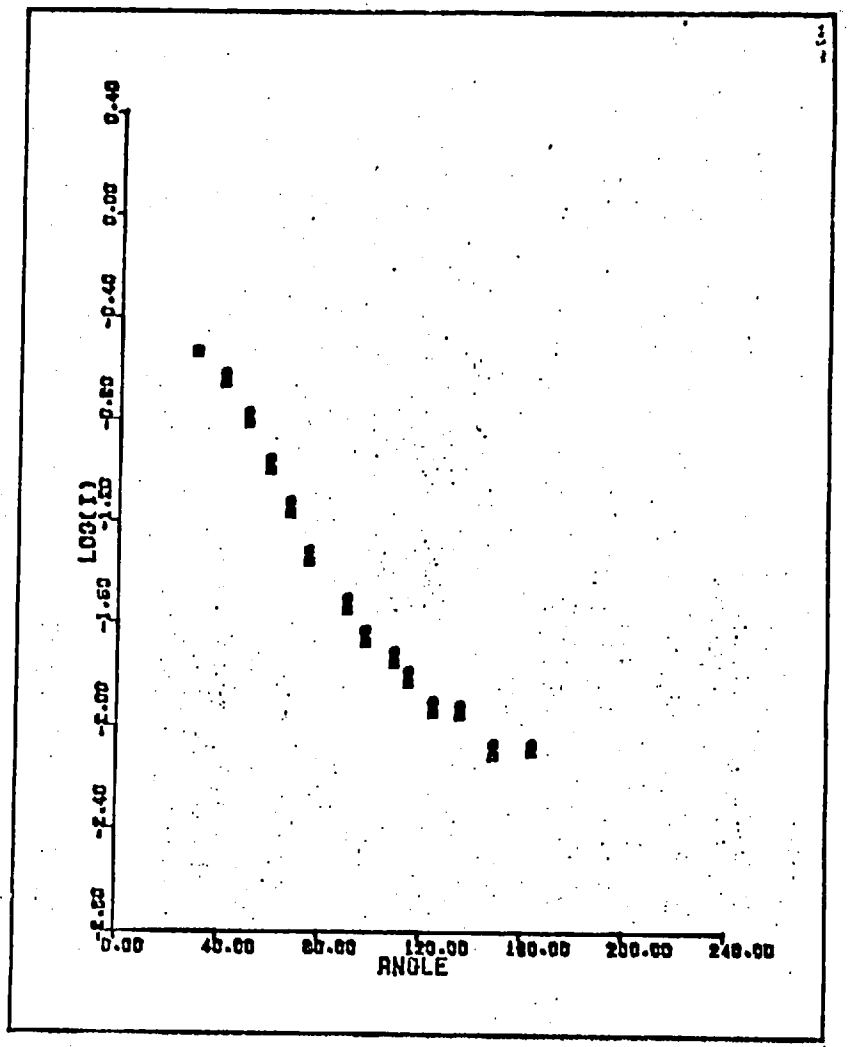

Table 5-6: Results from light scattering runs 1 to 6.
Master solution concentration = 2.5%w/w.

Illustr. in.Fig.	Expt. ref.	Mirror positions rejected	SEARCH starting values (a_m, σ_o)	SEARCH fitted values to data (a_m, σ_o)	Mass mean diameter (μm.)
5-XV	1.1	5,13,14,15	0.2,0.7	0.053,0.790	0.807
			0.1,0.5	0.720,0.214	0.252
	1.2	5,13,14,15	0.2,0.7	0.480,0.354	0.657
			0.1,0.5	0.480,0.354	0.657
	1.3	5,13,14,15	0.2,0.7	0.476,0.359	0.654
			0.1,0.5	0.476,0.357	0.654
	1.A	5,13,14,15	0.2,0.7	0.507,0.339	0.676
			0.1,0.5	0.134,0.646	0.380
5-XVI	2.1	5,14,15	0.2,0.7	0.098,0.579	0.227
			0.1,0.5	0.098,0.579	0.227
5-XVII	3.1	5,15	0.2,0.7	0.233,0.320	0.301
			0.1,0.5	0.233,0.320	0.301
	3.2	5,14,15	0.2,0.7	0.210,0.353	0.287
			0.1,0.5	0.221,0.300	0.277
	3.3	5,14,15	0.2,0.7	0.214,0.349	0.290
			0.1,0.5	0.225,0.296	0.280
	3.A	5,15	0.2,0.7	0.231,0.312	0.295
			0.1,0.5	0.231,0.312	0.295
5-XVIII	4.1	14,15	0.2,0.7	0.234,0.347	0.316
			0.1,0.5	0.234,0.347	0.316
	4.2	15	0.2,0.7	0.227,0.358	0.313
			0.1,0.5	0.227,0.358	0.313
	4.3	15	0.2,0.7	0.244,0.312	0.311
			0.1,0.5	0.244,0.312	0.311
	4.A	15	0.2,0.7	0.235,0.337	0.312
			0.1,0.5	0.235,0.337	0.312

Table 5-6 (continued)

Illustr. in Fig.	Expt. ref.	Mirror positions rejected	SEARCH starting values (a_M, σ_g)	SEARCH fitted values to data (a_M, σ_g)	Mass mean diameter (μm.)
	5.1	14,15	0.2,0.7	0.252,0.320	0.326
			0.1,0.5	0.252,0.320	0.326
	5.2	14,15	0.2,0.7	0.245,0.355	0.326
			0.1,0.5	0.246,0.355	0.326
5-XIX	5.3	14,15	0.2,0.7	0.244,0.357	0.326
			0.1,0.5	0.244,0.357	0.326
	5.4	15	0.2,0.7	0.255,0.301	0.320
			0.1,0.5	0.255,0.301	0.320
	5.A	15	0.2,0.7	0.254,0.307	0.321
			0.1,0.5	0.254,0.307	0.321
	6.1	14,15	0.2,0.7	0.260,0.328	0.340
			0.1,0.5	0.262,0.335	0.347
5-XX	6.2	15	0.2,0.7	0.261,0.335	0.346
			0.1,0.5	0.261,0.335	0.346
	6.A	15	0.2,0.7	0.260,0.328	0.340
			0.1,0.5	0.260,0.328	0.340

no averaging is possible in this case). Since no significant, systematic change in the light scattering pattern with apparatus running time could be detected, the averaged runs have been taken as experiments, the data being processed by the SEARCH technique described in Section 2.5. In theory, they should be statistically more sound than ordinary experiments, since more readings are employed in their evaluation.

In Table 5-6, the mirror positions at which data points were rejected, for reasons given in Section 5.1(c), are given, together with the results of applying the SEARCH data inversion technique. The starting points of (a_m , σ_o) are the same as those used for the substantial part of the testing of the procedure in Section 2.5, viz. (0.2, 0.7) and (0.1, 0.5). Each set of light scattering data is processed using both of these sets of starting values. An interesting fact that can immediately be observed from Table 5-6 is that, in the vast majority of cases, the value assigned to σ_o is around 0.3, half the value obtained from electron microscopy. The values obtained in run 1 are likely to be unreliable owing to the fact that results at four mirror positions have been rejected from each experiment, leaving eleven points on which to fit the ZOLD parameters (see Section 2.5). By and large the modal diameters given in this case are about twice the values given for data from run 3, taken after the aerosol has passed through three reactor tubes. It may be assumed that particle break-up on a scale leading to such results is unlikely, and therefore the results from run 1 are likely to be in error. The results in run 3 are much more self-consistent, more reliable owing to the rejection of fewer data points, and fit in well with results from runs 4, 5 and 6. The parameters in run 2 are also probably in error. As explained in Section 2.5, the rejection of three data points is likely to lead to multi-valued solutions in the minimisation of the objective function of SEARCH (equation (2.16)). Since only one experiment was analysed this theory cannot be checked in this case, but inconsistency with other runs suggests that an erroneous minimum

has been located by the SEARCH procedure. The results obtained from runs 3, 4, 5 and 6 show remarkably good consistency, especially if the value of the mass mean diameter is considered.

Having briefly examined the results from both electron microscopy and light scattering, a comparison of the two will now be made. From the electron microscopy measurements, a value of the mass mean diameter of the nuclei of about 0.29 μm. (Table 5-5) appears reasonable. Thus, the mean nucleus volume, taking account of the shape factor given in Section 5.1(a), would be about 3.4×10^{-15} cm^3. From the light scattering results, we may consider the droplets to have a modal diameter around 0.2 μm. and a spread parameter of about 0.32. The mean droplet volume so obtained would be about 9.0×10^{-15} cm^3. These values would give a solution concentration of above 1.0 g cm^{-3}. This concentration is above the saturation level and clearly not attainable if the particles are to remain in solution. However, as will be shown in Section 5.3, experimental evidence suggests that the particles do remain solution droplets during the experiments. The difference between the values of σ_o obtained from electron microscopy and light scattering has already been pointed out. However, it has been shown in Section 3.3 that volume-proportional particle size changes do not affect the value of σ_o, being reflected only in the modal diameter of the distribution. Therefore, the distributions of nuclei and droplets should have the same value of σ_o. Since statistical problems in the sampling are expected in the electron microscopy measurements, let us assume in the first instance that the value of σ_o is incorrect, and replace it with the value obtained from light scattering. Using the modal diameter given in Table 5-5 and the new value of the spread parameter a value of 0.13 μm. is obtained for the mass mean diameter of the nuclei. Using this value a mean nucleus volume of 3.1×10^{-16} cm^3 is obtained, which corresponds to a solution concentration of 0.11 g. cm^{-3} or 8.9% w/w manganous sulphate ($MnSO_4$) in the droplets. According to Table 3-4(i), the equilibrium relative humidity for this concentration is 98.7%. This is in the range of

humidity determined experimentally by the hygrometer. Also, further evidence that this value is approximately correct was obtained when the humidity of the aerosol stream was reduced by the addition of the gas dozing stream. The results of this experiment will be given in Section 5.3.

Although the acceptance of the value of the modal diameter but not that of the spread parameter yields results in agreement with experiment, the procedure appears rather unsatisfactory and necessitates a further examination of the method of particle sampling used in the electron microscopy. It has already been shown, as in Fig. 2-IV, that the application of direct sample measurement requires a larger sample for a more polydisperse aerosol. In Fig. 5-X, for example, the histogram at large particle sizes has many intervals with no particles, interspersed by two or three intervals containing just one particle. If the relative contribution to the sample volume of the single particle of diameter around 1 μm. is considered in a sample of 368 particles, it is possible to conceive that the value of the mass mean diameter may be overestimated, and that the 'standard error' criterion already discussed need not strictly apply to such estimates. Whereas the ZOLD function allows for the existence of large particles, it is a generalisation, and the distribution of particle volumes obtained from a sample such as that used to plot Fig. 5-X is very different to that illustrated in Fig. 2-II (which shows theoretical particle volume distribution densities calculated from the ZOLD function). Consequently, if the assumption that the aerosol particles (generally present in much larger numbers than the sample size) obey a ZOLD function is to be made, it must be accepted that a volume distribution such as that which would be obtained from the data in Fig. 5-X is unrepresentative, and that a much larger number of particles must be considered for conclusions about particle volume distributions to be drawn. However, the modal diameter in the strictest sense purely corresponds to the commonest particle diameter. Thus, although a better estimate is obtainable from a larger sample, its value estimated from a small sample is less likely to be distorted wildly by random errors caused

by considering particles at the asymptotic large and small ends of the particle size spectrum.

On the other hand, the light scattering signals originate from a cylindrical volume of about 0.25 cm^3 of aerosol, containing of the order of 10^5 particles. Thus, if the particles obey a ZOLD distribution, a fair summation of scattered signals over the distribution should be obtained. Hence, subject to the limitations described in Section 2.5, the parameter values obtained should be acceptable.

In Table 5-7 the results of the light scattering measurements are compared with values obtained from the approximate computer solution of the coagulation equation, described in Section 3.4. For three of the four points compared precise two-figure agreement is obtained. For the fourth point the measured value is rather less than the calculated value, indicating that less coagulation has taken place. Comparing results from light scattering runs 3, 4, 5 and 6 in Table 5-6, a steady increase in the modal diameter appears to have taken place, with no significant change in the spread parameter. From the results in Figs. 3-X and 3-XI (showing the theoretically predicted change in the particle size distribution due to coagulation) it would be expected that a small increase in the spread should occur. However, it must be borne in mind that the light scattering method will only normally give values of the spread parameter accurate to 10% (9). This may be seen if the values obtained in any of the four given runs are examined. Bearing this in mind, the agreement between the values for 3, 7 and 13 reactor tubes in Table 3-7 is remarkably good. If the consistency of results for experiments 6.1, 6.2 and 6.A is considered, it appears likely that the discrepancy between theory and experiment for the case of 25 reactor tubes is due to a systematic rather than experimental error.

Another comparison that can be made is between the values of the particle number concentration. The values estimated from electron microscopy, given in Table 5-5, are somewhat lower than the solution

Table 5-7: Comparison of theoretical & experimental results for the change in mass mean diameter in the absence of sulphur dioxide.

Reactor tubes used	Mass mean diameter as calculated in section 3.4 (μm.)	Mean value of mass mean diameter from light scattering (μm.)
S	(0.28)	--
1	(0.28)	--
3	0.29	0.29
7	0.31	0.31
13	0.33	0.33
25	0.37	0.35

of the coagulation equation predicts, as given in Fig. 3-XII. In the cases involving 7, 13 and 25 reactor tubes the discrepancy runs to an order of magnitude. The agreement between predicted and measured values of the mass mean diameter, recorded in the previous paragraph, suggests that the coagulation does proceed according to the mechanism described in Section 3.4. Therefore the low experimental values of particle number concentration are probably explicable in terms of a removal of particles from the system and/or a deficiency in the method of determining particle number concentration.

It was observed during experimental runs that liquid matter appeared to 'condense' on to the sides of the tubes, particularly the upstream ones. One possible explanation of this is that local fluctuations in temperature lead to regions of supersaturation near to the walls of the vessels. Water vapour then condenses out on to the walls producing the cloudy appearance. However, the effect was more marked in the lower portions of the tubes. It has already been shown (Section 3.5) that sedimentation of particles in the size range under consideration is negligible. But if regions of local supersaturation are created in the presence of particles, the particles will act as condensation nuclei for the excess vapour present. These particles thus become enlarged and their removal by sedimentation may become marked. It was not possible to produce experimental evidence to support this theory, but if the shape of the saturated vapour pressure versus temperature curve for water is examined, it is easy to imagine the difficulties involved in the handling of high humidity atmospheres in environments that are not strictly isothermal.

Another possible contribution to the explanation of the low counts is the variable condition of the carbon coats on the sampling grids. The procedure used to obtain even coats of the required thickness was difficult and delicate, and often incomplete coverage was obtained. Also, the grids underwent some fairly rough treatment during the acquisition of samples; mounting on the precipitator head with 'silver dag', removal,

and treatment in the oven, which tends to deteriorate the film. In some cases, grids had to be rejected, and new samples taken, as no sufficiently large areas of continuous film could be observed for the taking of sample photographs to be feasible.

An interesting feature is the sudden drop, by a factor of five, between the values obtained using 3 and 7 reactor tubes. The results for the sets of S, 1, and 3, tubes, and 7, 13 and 25 tubes, both show a steady, monotonic decrease in the particle number concentration, as would be expected from Fig. 3-XII (which illustrates the decrease of particle number concentration with coagulation time). Statistical errors in the sampling are unlikely to account for discrepancies of this magnitude, since the standard error associated with all estimates is less than 10%. The apparent number concentration drop between the use of S tube and 3 tubes, corresponding to a difference in residence times of about 1.9 min., is from 6.5×10^5 cm^{-3} to 5.1×10^5 cm^{-3}. The corresponding difference in residence times between the use of 3 and 7 reactor tubes is about 3.4 min. Thus, if the rate of decrease in number concentration is maintained, a number concentration of the order of 2×10^5 cm^{-3} would be attained after passage through 7 tubes. This, however, is unlikely to occur, especially if we consider that the decrease would then suddenly fall off to a rate comparable to that calculated from the coagulation mechanism. The simplest explanation appears to be that the result obtained after passage through 7 tubes is in error, and that the true value is somewhat higher. The values for 13 and 25 tubes appear reasonable, since very little deposition of liquid matter on the walls of the vessels was observed beyond about the 10th tube, most of it occurring in the first three.

The fact that the particle number concentration falls off more rapidly than theoretical predictions suggest could explain the low experimental value of the mass mean diameter for the case of maximum residence time (see Table 5-7). The removal of particles from the system slows the rate of coagulation (which is controlled by the probability of

two particles colliding), thus the resultant particle sizes will be smaller than those predicted in the absence of particle loss.

Finally, it is not possible, from results given in this section, to discern any effects of surface charges on the particles. The experimental results are not detailed enough for any definite conclusions to be drawn, save that no significant effect can be observed in this case. Since this phenomenon is not principally under study, no further reference will be made to it.

One factor not considered in this section is the effect of the laminar flowfield, and the consequent distribution of residence times, on the coagulation of the aerosol. This has been considered in detail by Nicolaon et. al. (103). Owing to the relatively small particle size changes occurring in this system, and the good agreement between experiment and theory for the particle size results, the complicated and time-consuming integration of theoretical results over the laminar flowfield will not be attempted, the results given being considered adequate.

5.3. The Behaviour of the Aerosol System in the Presence of Reacting Gas

Having analysed the phenomena occurring in the system in the absence of reacting gas, the phenomenon of the reaction, and the consequent particle growth, will now be considered. Light scattering measurements have been made on the aerosol/gas mixture to obtain particle size data, and measurements of the sulphur dioxide concentration have also been taken in an attempt to monitor the progress of the reaction. Measurements were made using the same combinations of reactor tubes that were used for measurements reported in Section 5.2 (as given in Section 4.1).

A simple qualitative experiment was initially carried out to establish whether or not the oxidation reaction in the droplets takes place. The three 'Millipore' membrane filter holders used in the light scattering sample extraction system (Fig. 4-V(b)) were cleaned thoroughly and refitted with new filters. The parallel arrangement, as illustrated in Fig. 4-V(b), was then assembled and connected to the outlet tube from the reactor vessels. 25 reactor tubes were connected together, giving the arrangement the maximum aerosol residence volume. The throughput of aerosol was assisted by attaching the downstream end of the filtering arrangement to a vacuum pump. The system was run as in the experiments of Section 5.2, with no SO_2 gas dosing stream, for 30 mins., then the filters were removed and placed in sealed Petrie dishes. It was found that, using this arrangement, the flowrate through the filters was less than that through the tubes, and consequently the pressure buildup in the tubes had to be periodically relieved by disconnecting the filters; this is one reason why no quantitative measurements could be obtained. The experiment was repeated with the gas dosing stream in use, giving an initial sulphur dioxide concentration of 63 ppm. in the reactor vessels. On completion, two filters from each of the two runs were treated as follows. 2 ml. of distilled water was added to each, and the filters were allowed to soak for several minutes. A 2 ml. sample of tap water was placed in a separate dish for comparison in the sulphate test. Two control samples were also prepared by soaking clean filters in a manner identical to

that used for the sampling filters. After soaking, the filters were removed and the residual solutions treated as follows:-

(i) To one sample of each type (i.e. one control, one of aerosol without sulphur dioxide and one of aerosol with sulphur dioxide) three drops of BDH Universal Indicator were added. The results were:

(a) Control sample: Greenish-yellow reaction indicating a pH around 6.5.

(b) Sample aerosol without sulphur dioxide: Greenish-yellow reaction indicating a pH around 6.

(c) Sample aerosol with sulphur dioxide: Dark red reaction indicating pH less than 4.

(ii) To the second sample of each type, and to the tap water sample, several drops of freshly prepared barium chloride solution in dilute hydrochloric acid were added.

The results were:

(a) Control sample: Solution remained clear.

(b) Tap water sample: Solution displayed slight milkiness.

(c) Sample aerosol without sulphur dioxide: Solution displayed milkiness slightly more marked than in (b).

(d) Sample aerosol with sulphur dioxide: Precipitate was considerably denser than in (b) or (c).

Test (i) establishes that acid appears in the aerosol which has been exposed to sulphur dioxide. Test (ii) was carried out to ensure that the acidity was not caused simply by sulphur dioxide dissolved in the droplets, since no sulphite precipitate is formed with hydrochloric acid present. The marked increase in the sulphate concentration together with the increased acidity provides sound evidence that sulphuric acid is formed in an appreciable quantity in the droplets.

Since little or no oxidation takes place if particles of solid manganous sulphate only are present, this experiment provides evidence for the assertion made in the previous section that the particles in the reactor vessels are solution droplets. The humidity reading (reported

in the previous section) is in agreement with this fact.

The results of the light scattering experiments with the gas dosing stream in use are given in Figs. 5-XXI to 5-XXXII and Tables 5-8 and 5-9. Runs 7 to 12, given in Figs. 5-XXI to 5-XXVI and Table 5-8, correspond to the use of each of the combinations of reactor tubes already described, with an initial sulphur dioxide concentration of 63 ppm. introduced via the dosing system. (63 ppm. at the mixer outlet, Mx in Fig. 4-I, rather than in the dosing system itself). Runs 13 to 18, in Figs. 5-XXVII to 5-XXXII and Table 5-9, were taken with the gas dosing stream introducing 0.1 l/min. of air free of sulphur dioxide into the system, such that the effects of the change in humidity caused by such an addition of drier gas could be determined. If it is assumed that the manganous sulphate concentration in the droplets in the absence of the dosing stream is 8.9% w/w $MnSO_4$, as calculated in Section 5.2, then the effect of adding the dosing stream should be to increase the equilibrium concentration to 16.5%, neglecting the effect of water vapour evaporating from the droplets. This would result in a reduction in droplet size. Most of the values in Table 5-9 were obtained after the rejection of experimental values at four mirror positions, i.e. by consideration of only eleven data points. This makes the SEARCH data inversion technique unreliable. The best run is No. 17, illustrated in Fig. 5-XXXI, in which values at three mirror positions are rejected. The values of the mass mean diameter obtained in this case are fairly consistent, and indicate a possible result around 0.30 μm. If the above calculation of the increase in the manganous sulphate concentration in the droplets is correct, then, using the data from run 5, Table 5-6, a value of 0.26 μm. would be expected for the mass mean diameter in this case. However, in most of the experiments of run 17 the estimates of the spread parameters are larger than the values obtained in run 5. Using values of the modal diameter in run 5 as a basis, the corresponding modal diameter of the more concentrated particles would be about 0.2 μm. Values obtained for run 17 are in agreement with this figure.

Fig. 5-XXI: Light scattering data for run 7.
Aerosol passed through S tube.
Experiments: ● 7.1; ▲7.2;
+7.3
■ Average for run (7.A)

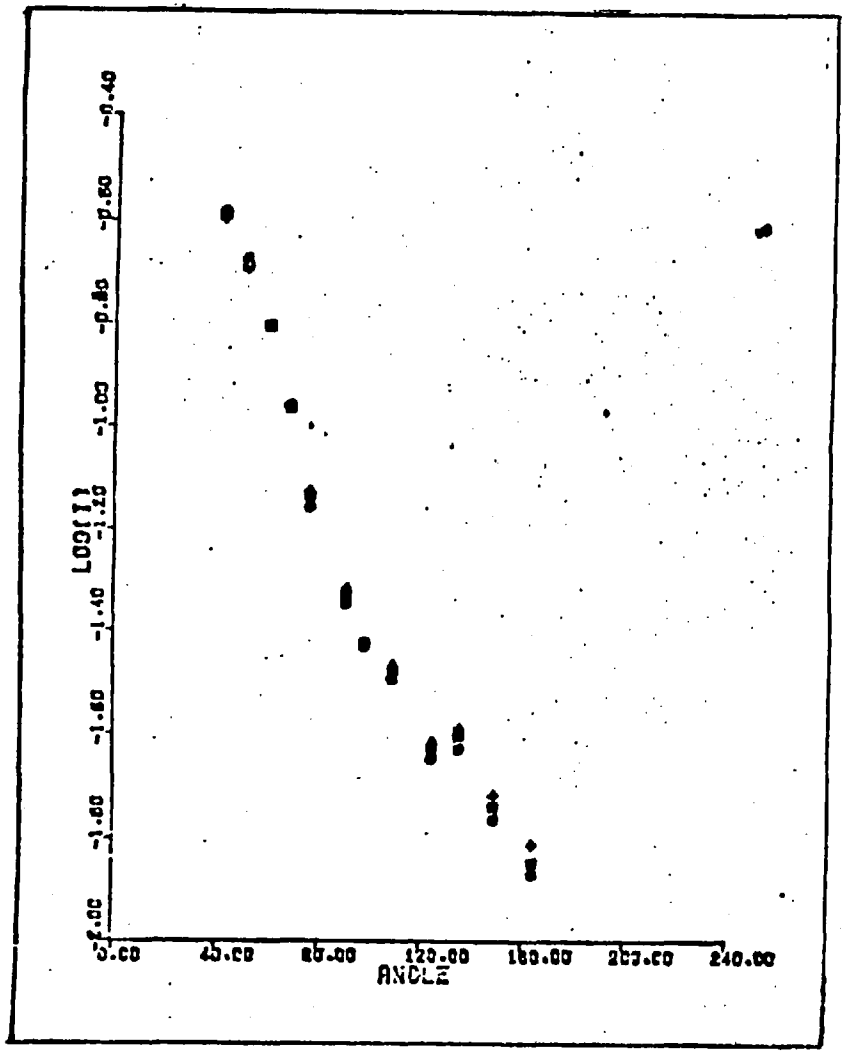

Fig. 5-XXII: Light scattering data for run 8.
Aerosol passed through 1 tube.
Experiments: ● 8.1; ▲8.2;
■ Average for run (8.A)

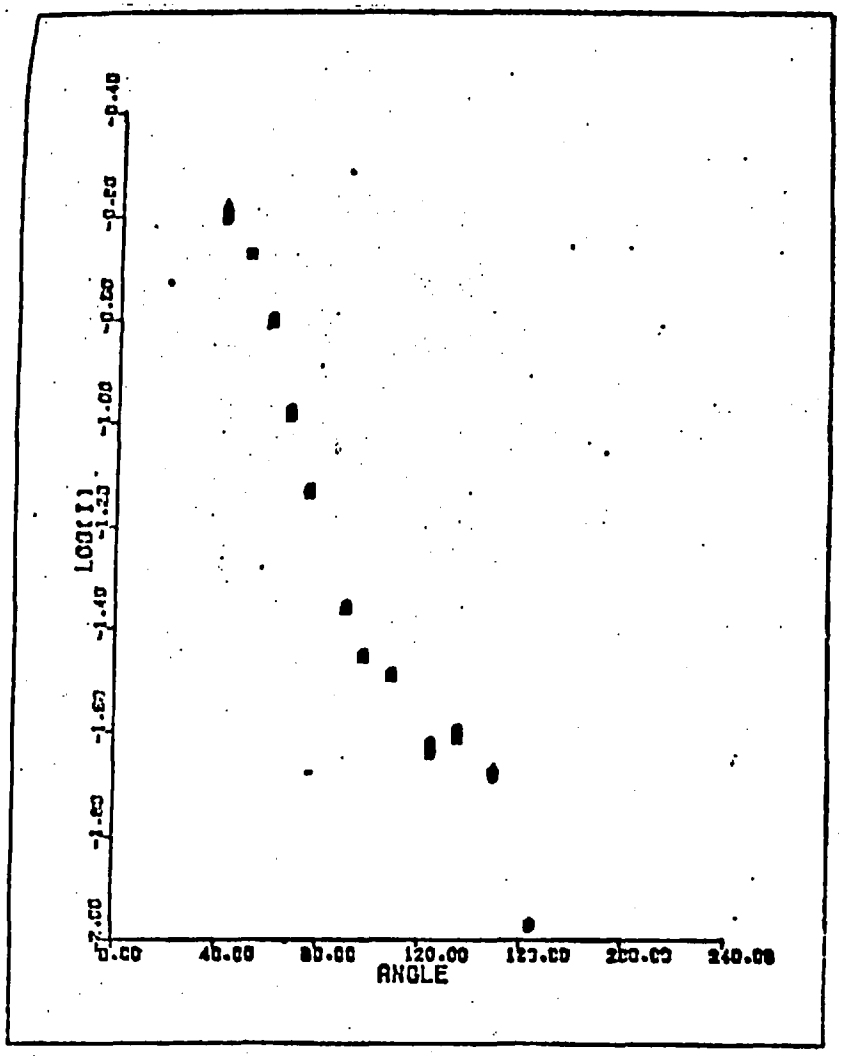

Fig. 5-XXIII: Light scattering data for run 9.
Aerosol passed through 3 tubes .
Experiments: ● 9.1; ▲9.2;
+ 9.3
■ Average for run (9.A)

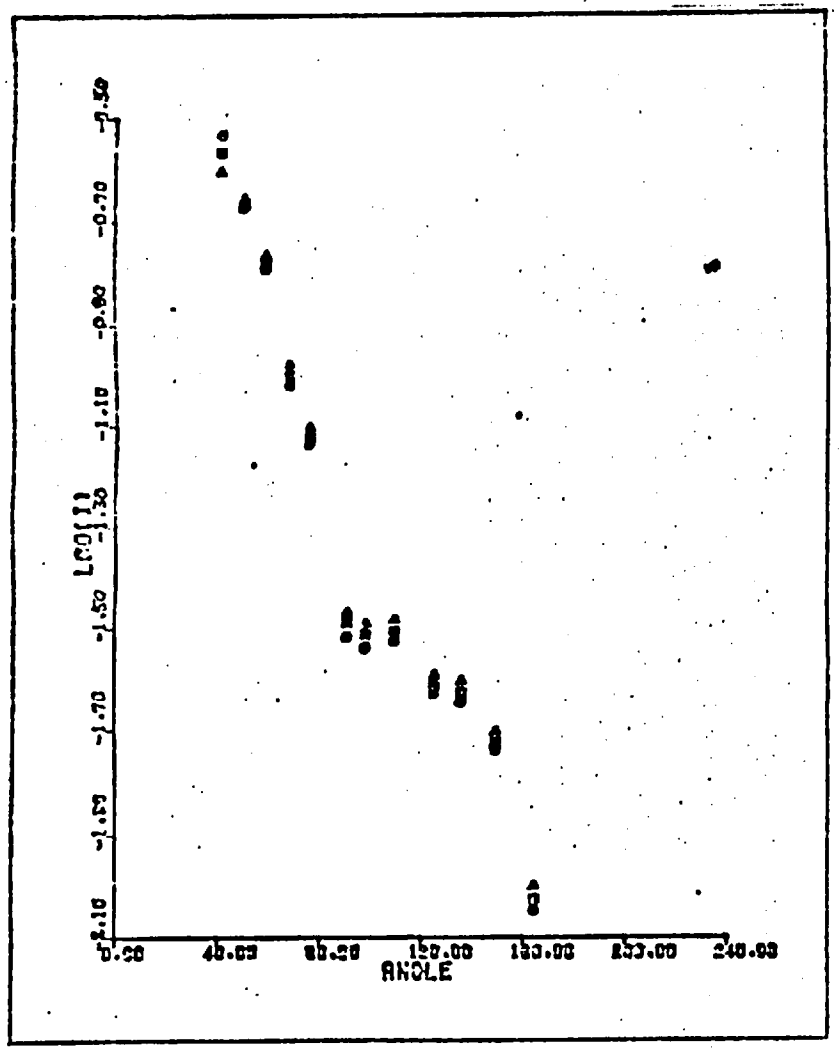

Fig. 5-XXIV: Light scattering data for run 10.
Aerosol passed through 7 tubes.
Experiments: ● 10.1; ▲10.2;
+10.3; ×10.4
■ Average for run (10.A)

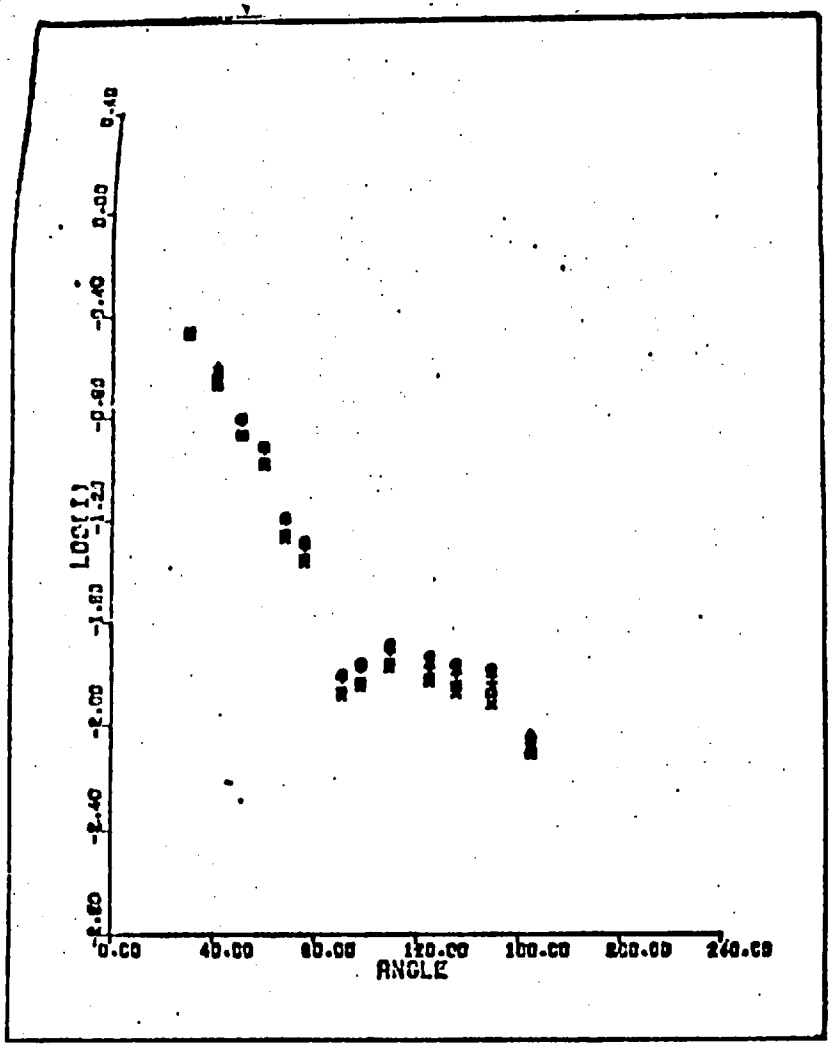

Fig. 5-XXV: Light scattering data for run 11.
Aerosol passed through 13 tubes.
Experiments: ● 11.1; ▲11.2;
+11.3; ×11.4
■ Average for run (11.A)

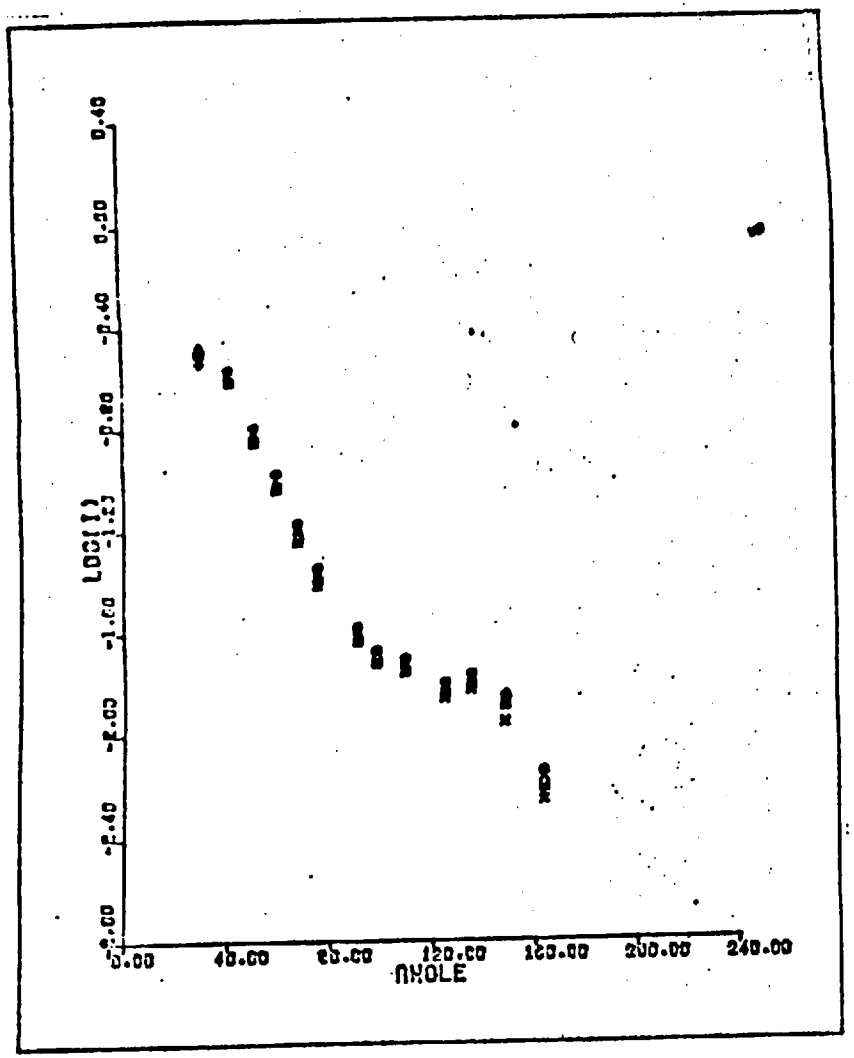

Fig. 5-XXVI: Light scattering data for run 12.
Aerosol passed through 25 tubes.
Experiments: ●12.1; ▲12.2;
+12.3; ×12.4
■ Average for run (12.A)

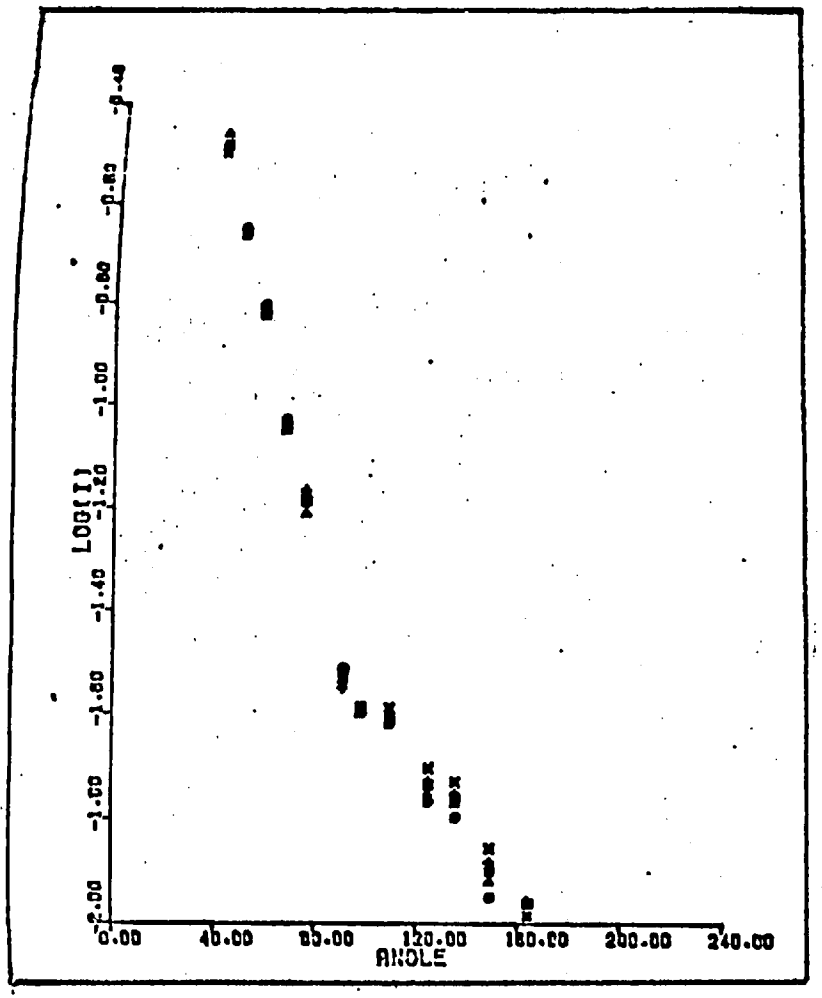

Table 5-8: Results from light scattering runs 7 to 12.
Master solution concentration = 2.5%w/w.

Illustr. in Fig.	Expt. ref.	Mirror positions rejected	SEARCH starting values (a_m, σ_o)	SEARCH fitted values to data (a_m, σ_o)	Mass mean diameter (μm.)
5-XXI	7.1	5.14.15	0.2,0.7	0.181,0.403	0.271
			0.1,0.5	0.181,0.402	0.271
	7.2	5,14,15	0.2,0.7	0.992,0.125	0.959*
			0.1,0.5	0.166,0.416	0.256
	7.3	5,14,15	0.2,0.7	0.921,0.124	0.957*
			0.1,0.5	0.155,0.433	0.248
	7.A	5,14,15	0.2,0.7	0.924,0.125	0.961*
			0.1,0.5	0.167,0.418	0.258
5-XXII	8.1	5,14,15	0.2,0.7	0.926,0.127	0.964*
			0.1,0.5	0.148,0.454	0.248
	8.2	5,14,15	0.2,0.7	0.922,0.136	0.966*
			0.1,0.5	0.111,0.546	0.234
	8.A	5,14,15	0.2,0.7	0.924,0.132	0.965*
			0.1,0.5	0.128,0.501	0.240
5-XXIII	9.1	5,14,15	0.2,0.7	0.130,0.544	0.272
			0.1,0.5	0.130,0.544	0.272
	9.2	5,14,15	0.2,0.7	0.147,0.461	0.250
			0.1,0.5	0.147,0.461	0.250
	9.3	5,14,15	0.2,0.7	0.132,0.515	0.256
			0.1,0.5	0.132,0.515	0.256
	9.A	5,14,15	0.2,0.7	0.126,0.528	0.251
			0.1,0.5	0.126,0.527	0.251
5-XXIV	10.1	5,14,15	0.2,0.7	0.904,0.139	0.949*
			0.1,0.5	0.050,0.702	0.171
	10.2	5.14.15	0.2,0.7	0.051,0.727	0.188
			0.1,0.5	0.050,0.728	0.188
	10.3	5,14,15	0.2,0.7	0.064,0.694	0.213
			0.1,0.5	0.065,0.691	0.214
	10.4	5,15	0.2,0.7	0.140,0.552	0.300
			0.1,0.5	0.140,0.552	0.300
	10.A	5,15	0.2,0.7	0.111,0.597	0.271
			0.1,0.5	0.111,0.597	0.271

Table 5-8 (continued)

Illustr. in Fig.	Expt. ref.	Mirror positions rejected	SEARCH starting values (a_M, σ_g)	SEARCH fitted values to data (a_M, σ_g)	Mass mean diameter (μm.)
	11.1	5,14,15	0.2,0.7	0.182,0.533	0.370
			0.1,0.5	0.182,0.533	0.370
	11.2	5,15	0.2,0.7	0.069,0.699	0.234
			0.1,0.5	0.065,0.709	0.228
5-XXV	11.3	5,15	0.2,0.7	0.081,0.638	0.222
			0.1,0.5	0.080,0.638	0.221
	11.4	5,15	0.2,0.7	0.121,0.568	0.273
			0.1,0.5	0.122,0.567	0.273
	11.A	5,15	0.2,0.7	0.116,0.577	0.265
			0.1,0.5	0.115,0.578	0.265
	12.1	1,5,14,15	0.2,0.7	0.269,0.379	0.385
			0.1,0.5	0.269,0.379	0.385
	12.2	5,14,15	0.2,0.7	0.157,0.675	0.490
			0.1,0.5	0.155,0.677	0.487
5-XXVI	12.3	5,14,15	0.2,0.7	0.104,0.757	0.436
			0.1,0.5	0.104,0.758	0.437
	12.4	5,14,15	0.2,0.7	0.076,0.804	0.382
			0.1,0.5	0.076,0.803	0.381
	12.5	5,14,15	0.2,0.7	0.252,0.406	0.381
			0.1,0.5	0.252,0.406	0.381

Fig. 5-XXVII: Light scattering data for run 13.
Aerosol passed through S tube.
Experiments: ● 13.1; ▲13.2;
+13.3; ×13.4; ♦13.5
■ Average for run (13.A)

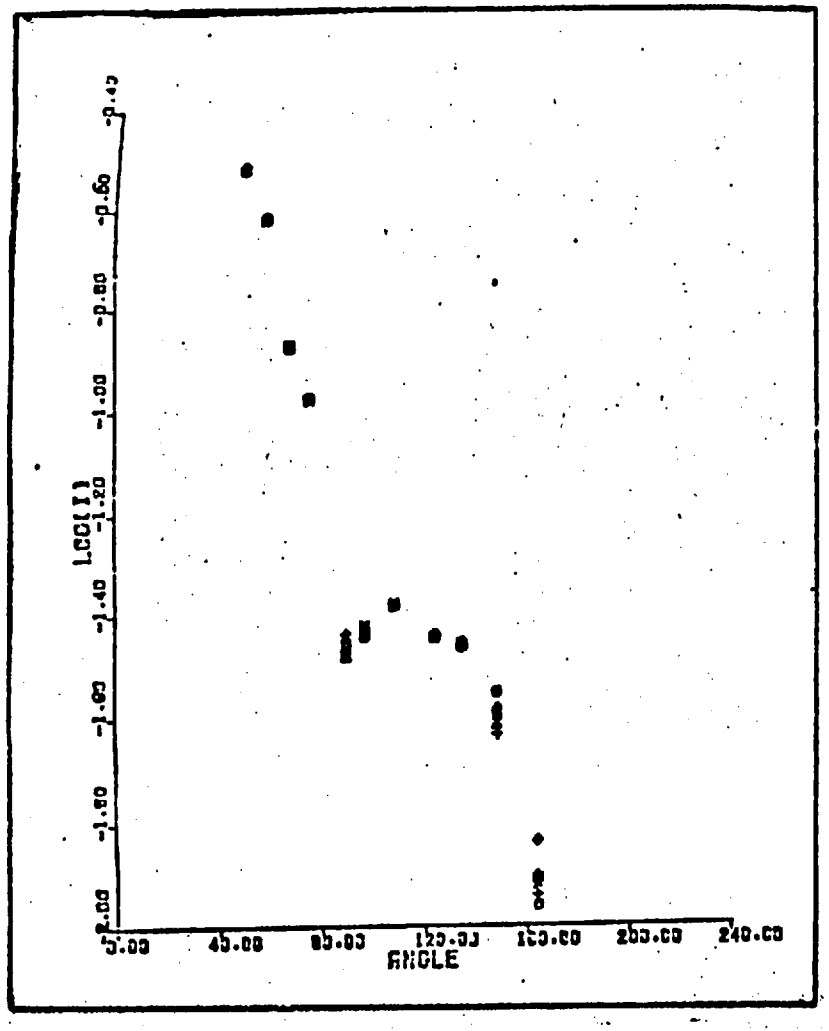

Fig. 5-XXVIII: Light scattering data for run 14.
Aerosol passed through 1 tube.
Experiments: ● 14.1; ▲14.2;
+14.3; ×14.4
■ Average for run (14.A)

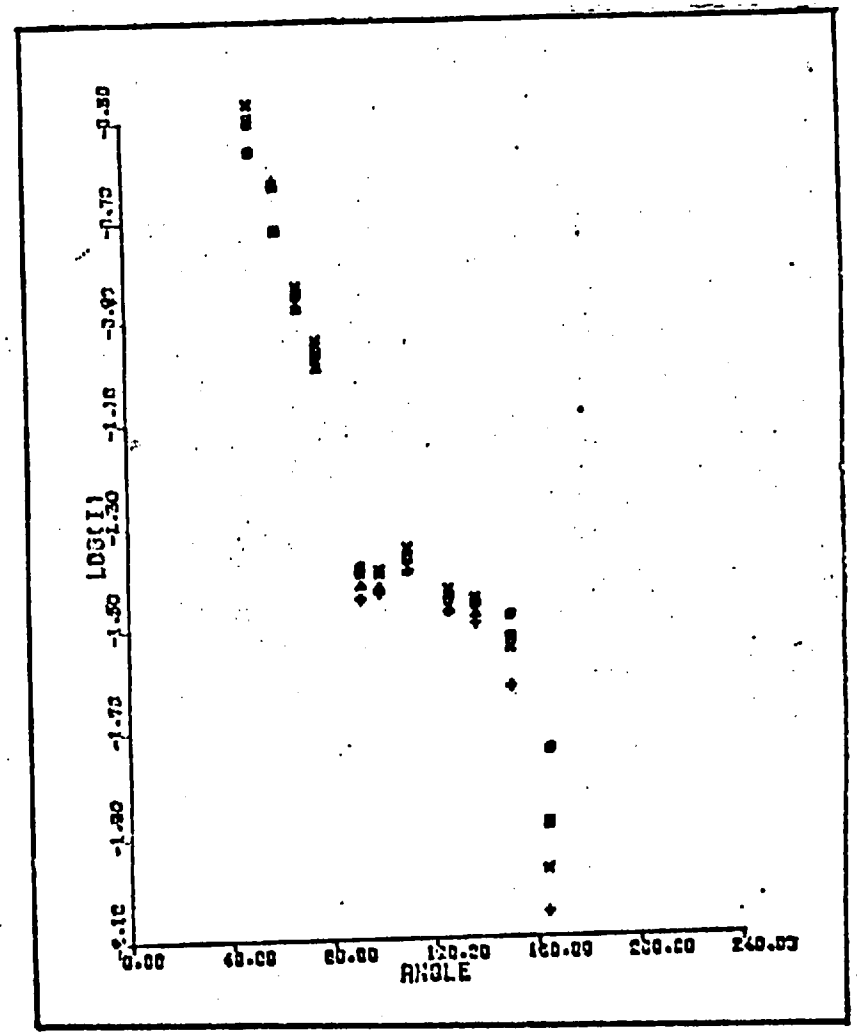

Fig- 5-XXIX: Light scattering data for run 15.
Aerosol passed through 3 tubes.
Experiments: ● 15.1; ▲15.2;
+15.3; ×15.4
■ Average for run (15.A)

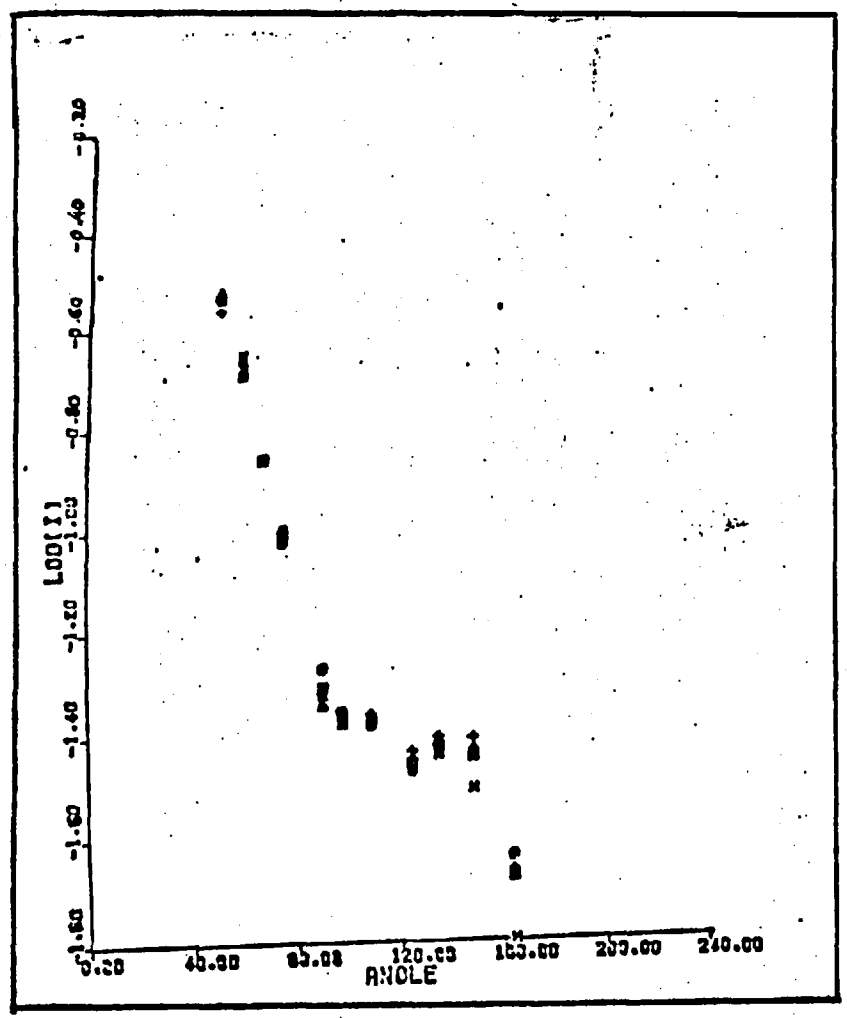

Fig. 5-XXX: Light scattering data for run 16.
Aerosol passed through 7 tubes.
Experiments: ● 16.1; ▲16.2
+16.3; ×16.4; ♦16.5
■ Average for run (16.A)

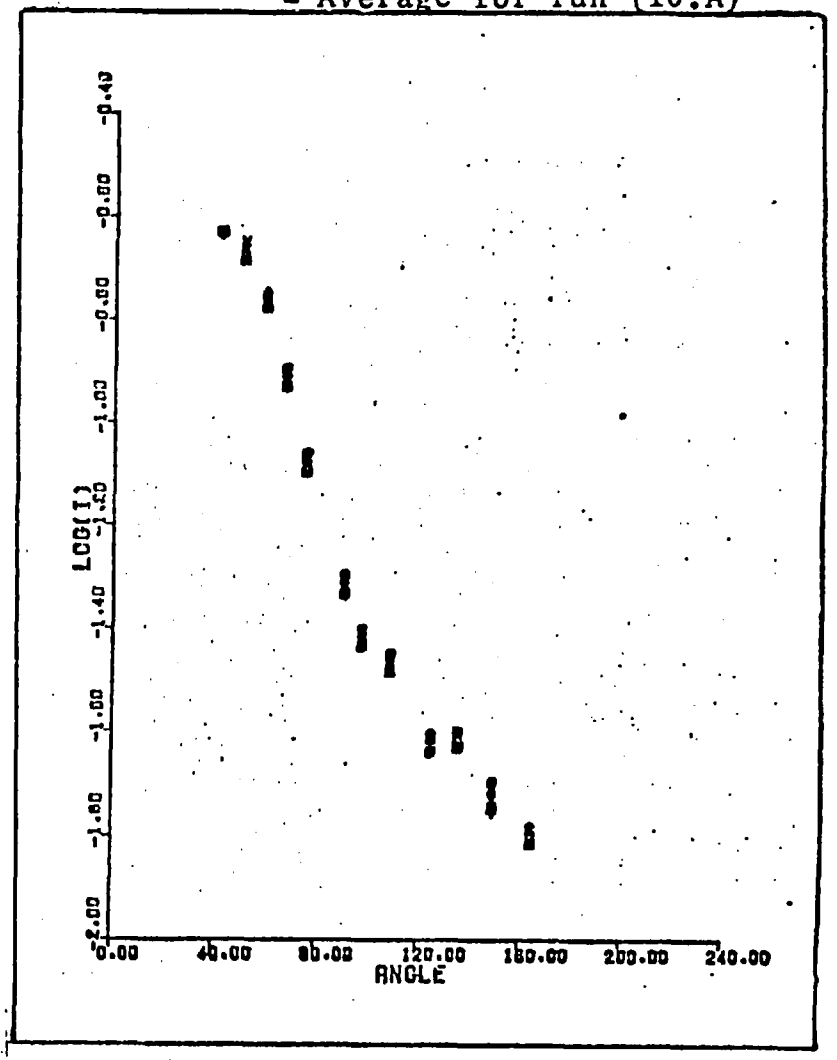

Fig. 5-XXXI: Light scattering data for run 17:
Aerosol passed through 13 tubes.
Experiments: ●17.1; ▲17.2;
+17.3; ×17.4; ♦17.5
■ Average for run (17.A)

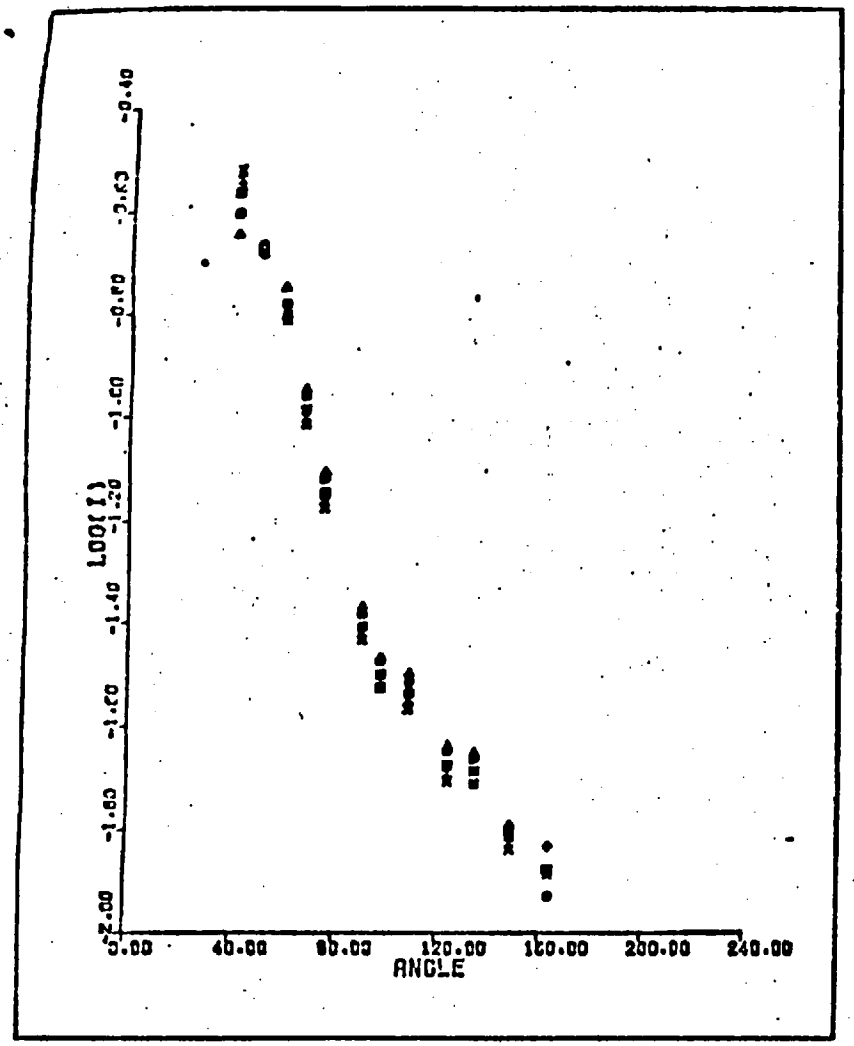

Fig. 5-XXXII: Light scattering data for run 18.
Aerosol passed through 25 tubes.
Experiments: ●18.1; ▲18.2
+18.3; ×18.4; ♦18.5
■ Average for run (18.A)

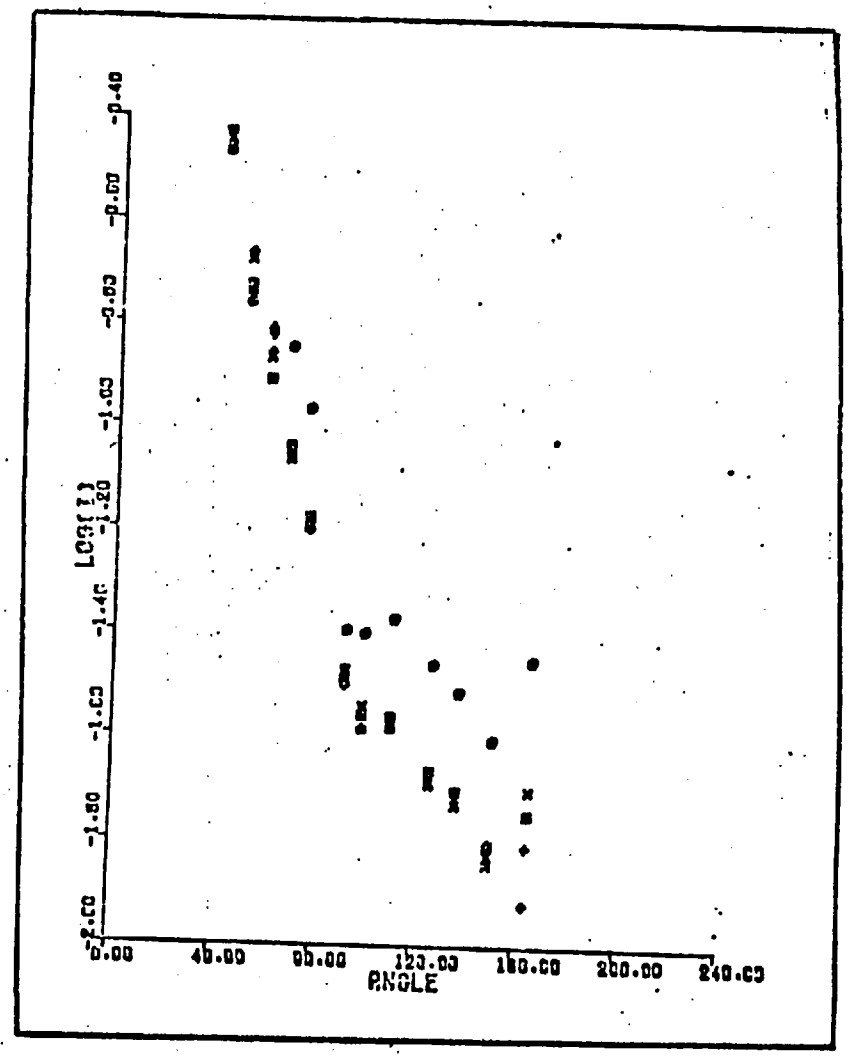

Table 5-9: Results from light scattering runs 13 to 18.
Master solution concentration = 2.6%w/w.

Illustr. in Fig.	Expt. ref.	Mirror positions rejected	SEARCH starting values (a_M,σ)	SEARCH fitted values to data (a_M,σ)	Mass mean diameter (μm.)
	13.1	5,13,14,15	0.2,0.7	0.382,0.385	0.553
			0.1,0.5	0.383,0.383	0.553
	13.2	5,13,14,15	0.2,0.7	0.405,0.351	0.559
			0.1,0.5	0.402,0.361	0.557
	13.3	5,13,14,15	0.2,0.7	0.390,0.367	0.548
			0.1,0.5	0.176,0.527	0.352
5-XXVII	13.4	5,13,14,15	0.2,0.7	0.393,0.372	0.555
			0.1,0.5	0.187,0.527	0.374
	13.5	5,13,14,15	0.2,0.7	0.391,0.359	0.540
			0.1,0.5	0.187,0.531	0.378
	13.A	5,13,14,15	0.2,0.7	0.393,0.371	0.554
			0.1,0.5	0.392,0.372	0.554
	14.1	5,13,14,15	0.2,0.7	0.115,0.624	0.302
			0.1,0.5	0.113,0.626	0.301
	14.2	5,13,14,15	0.2,0.7	0.364,0.398	0.540
			0.1,0.5	0.365,0.398	0.539
5-XXVIII	14.3	5,13,14,15	0.2,0.7	0.348,0.393	0.512
			0.1,0.5	0.349,0.392	0.512
	14.4	5,13,14,15	0.2,0.7	0.452,0.324	0.588
			0.1,0.5	0.050,0.673	0.155
	14.A	5,13,14,15	0.2,0.7	0.408,0.376	0.581
			0.1,0.5	0.108,0.619	0.281
	15.1	5,13,14,15	0.2,0.7	0.455,0.361	0.630
			0.1,0.5	0.104,0.699	0.355
	15.2	5,13,14,15	0.2,0.7	0.446,0.368	0.626
			0.1,0.5	0.446,0.368	0.626
5-XXVIX	15.3	5,13,14,15	0.2,0.7	0.493,0.344	0.663
			0.1,0.5	0.053,0.769	0.232
	15.4	5,13,14,15	0.2,0.7	0.391,0.390	0.572
			0.1,0.5	0.115,0.620	0.301
	15.A	5,13,14,15	0.2,0.7	0.450,0.364	0.627
			0.1,0.5	0.161,0.579	0.394

Table 5-9 (continued)

Illustr. in Fig.	Expt. ref.	Mirror positions rejected	SEARCH starting values (a_M, σ_g)	SEARCH fitted values to data (a_M, σ_g)	Mass mean diameter (μm.)
	16.1	5,13,14,15	0.2,0.7	0.195,0.348	0.264
			0.1,0.5	0.195,0.348	0.264
	16.2	5,13,14,15	0.2,0.7	0.201,0.345	0.268
			0.1,0.5	0.201,0.345	0.268
	16.3	5,14,15	0.2,0.7	0.924,0.116	0.956
			0.1,0.5	0.216,0.329	0.283
5-XXX	16.4	5,13,14,15	0.2,0.7	0.148,0.455	0.248
			0.1,0.5	0.150,0.450	0.249
	16.5	5,13,14,15	0.2,0.7	0.170,0.411	0.258
			0.1,0.5	0.169,0.412	0.258
	16.A	5,14,15	0.2,0.7	0.922,0.117	0.954
			0.1,0.5	0.212,0.335	0.281
	17.1	5,14,15	0.2,0.7	0.220,0.342	0.295
			0.1,0.5	0.220,0.342	0.295
	17.2	5,14,15	0.2,0.7	0.231,0.311	0.294
			0.1,0.5	0.231,0.311	0.294
	17.3	5,14,15	0.2,0.7	0.192,0.443	0.314
			0.1,0.5	0.192,0.443	0.314
5-XXXI	17.4	5,14,15	0.2,0.7	0.195,0.445	0.320
			0.1,0.5	0.195,0.445	0.320
	17.5	5,14,15	0.2,0.7	0.177,0.450	0.294
			0.1,0.5	0.176,0.450	0.294
	17.A	5,14,15	0.2,0.7	0.196,0.407	0.297
			0.1,0.5	0.196,0.407	0.297
	18.1	5,13,14,15	0.2,0.7	0.054,0.615	0.139
			0.1,0.5	0.050,0.626	0.133
	18.2	5,14,15	0.2,0.7	0.196,0.510	0.376
			0.1,0.5	0.196,0.510	0.376
	18.3	5,14,15	0.2,0.7	0.188,0.521	0.371
			0.1,0.5	0.188,0.521	0.371
5-XXXII	18.4	5,14,15	0.2,0.7	0.170,0.543	0.355
			0.1,0.5	0.170,0.543	0.355
	18.5	5,14,15	0.2,0.7	0.189,0.503	0.356
			0.1,0.5	0.188,0.504	0.355
	18.A	5,14,15	0.2,0.7	0.172,0.537	0.354
			0.1,0.5	0.172,0.537	0.354

The results obtained from run 18 (ignoring experiment 18.1 with four mirror positions omitted) show rather low modal diameters and large spread parameters. The values of the mass mean diameter obtained are similar to, or slightly larger than, the values obtained in run 6. Although these results are less reliable than those of run 6, being based on only twelve light scattering data points, their consistency suggests that they do represent the aerosol under the conditions of the run. Owing to the sensitive dependence of manganous sulphate concentration, and hence particle size, on the ambient relative humidity a fluctuation in any of the operating conditions could lead to the result. In fact, the laboratory air temperature was slightly lower than usual during this run. This still does not explain the large spread which could be due to inaccurate SEARCH parameter fitting, or to a spurious change in the atomiser operating conditions.

A similar prediction of low modal diameter and high spread parameter was obtained in run 7, Table 5-8. This run was taken with sulphur dioxide present, but, as will be shown later, the contact time is so short that no growth due to reaction should be observable. The $(\hat{a}_M, \sigma_o)$ values around (0.92, 0.12) will be ignored as a second minimum in the SEARCH objective function (equation (2.16)). The mass mean diameter obtained is around 0.26 μm., the same value as that given by the initial conditions of the coagulation analysis discussed in the previous section. Thus, it appears that initial conditions (a_M, σ_o) of (0.2, 0.32) apply, despite any changes brought about by the introduction of the sulphur dioxide stream. The results from runs 7 to 12 will be discussed later in the context of the reaction and droplet growth.

Thus, it appears that it is not possible to make a definitive statement about the effects of adding the diluent stream. However, in the above calculation, no account was taken of water vapour evaporating from the droplets or the walls of the tubes where liquid was observed to collect (see Section 5.2). It appears reasonable to conclude that it may be expected that the decrease in humidity brought about by the intro-

duction of the dosing stream causes at the most a slight increase in solution concentration (hence reduction in size), far less than that predicted by the calculation given above. The particle size determinant most frequently used for comparisons in this chapter is the mass mean diameter, and examination of values for the three runs discussed above will largely bear out the above statement.

The results of the measurements of the ambient sulphur dioxide concentration are given in Fig. 5-XXXIII. No time co-ordinate has been included as it has already been shown that no definite correlation between apparatus running time and measured values could be found, provided that the apparatus is allowed to stablise for one to one and a half hours (Section 5.1(b)). The representation of experiments is the same as that used in Fig. 5-II, and is intended to give an idea of the sensitivity and accuracy of results obtained by this method.

The results of the gas phase sulphur dioxide analyses are plotted in Fig. 5-XXXIV as a function of aerosol/gas contact time, determined by the number of reactor tubes used. The experimental points represent a weighted average for each run, the weighting factor for any experiment being the number of readings constituting the experiment. (These values are given with the experiments in Fig. 5-XXXIII). Also plotted are the theoretical values obtained by introducing the measured characteristics of the aerosol system at the generator outlet, viz the modal diameter (0.2 μm.), the spread parameter (0.32) and the number concentration (2.6×10^6 cm^{-3}), as the initial conditions in the growth prediction computer programme described in Section 3.3. It was found that if the manganous sulphate concentration in the droplet exceeds 0.4 m.mol cm^{-3} (about 6% w/w) the programme fails to converge. Therefore the concentration of manganous sulphate in the droplets was assumed to be 0.4 m.mol. cm^{-3} for the run. It may be seen from Fig. 5-XXXIV that an obvious disparity exists between theory and experiment. The most probable reason for the sharp drop in the observed sulphur dioxide concentration,

Fig. 5-XXXIII: Results of experiments from sulphur dioxide measurement runs.
Symbols as described in Fig. 5-II (section 5.1)

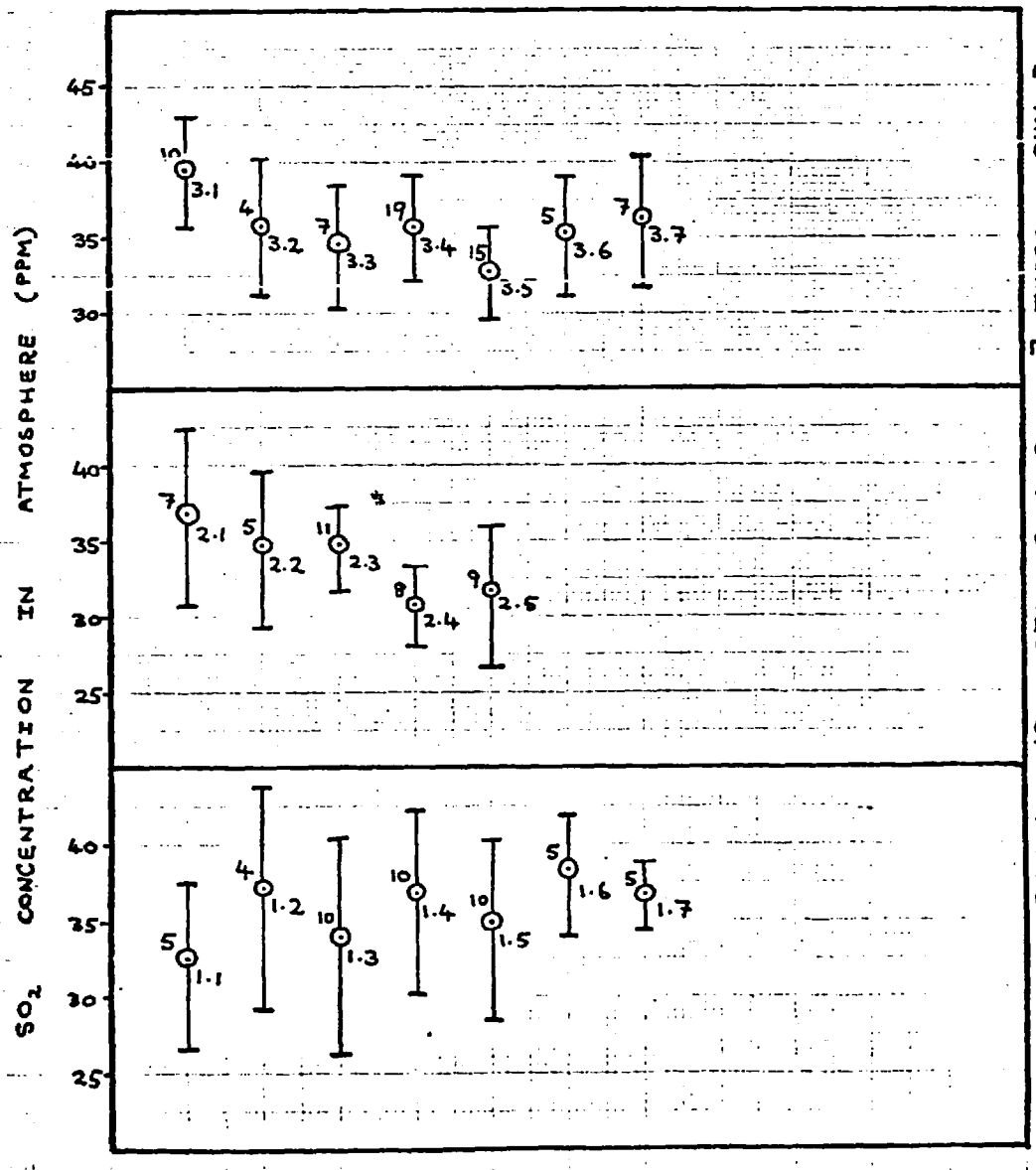

Fig. 5-XXXIII (continued)

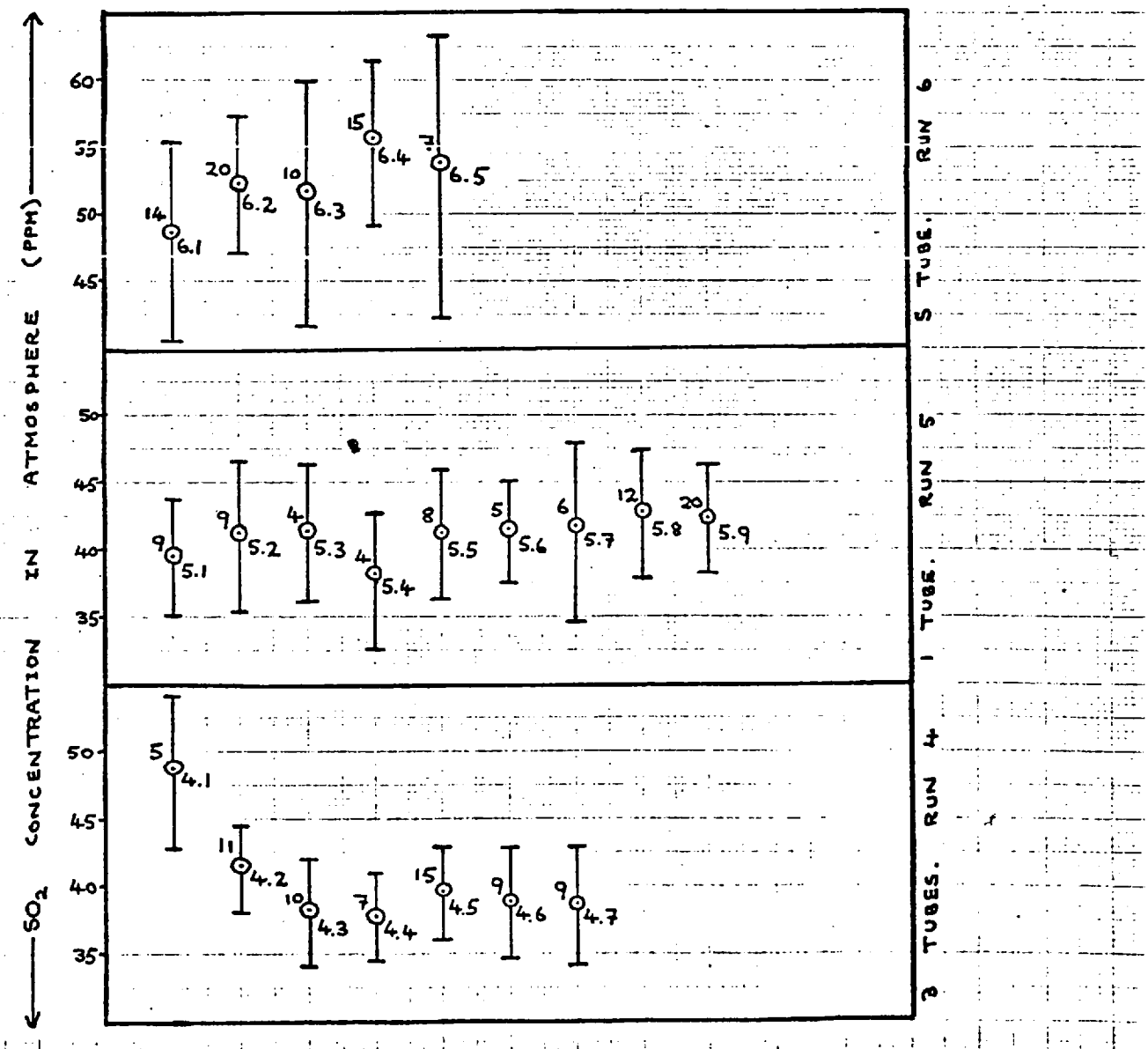

Fig. 5-XXXIV: Comparison of theoretical and experimental values for the sulphur dioxide concentration at the experimentally employed reaction times

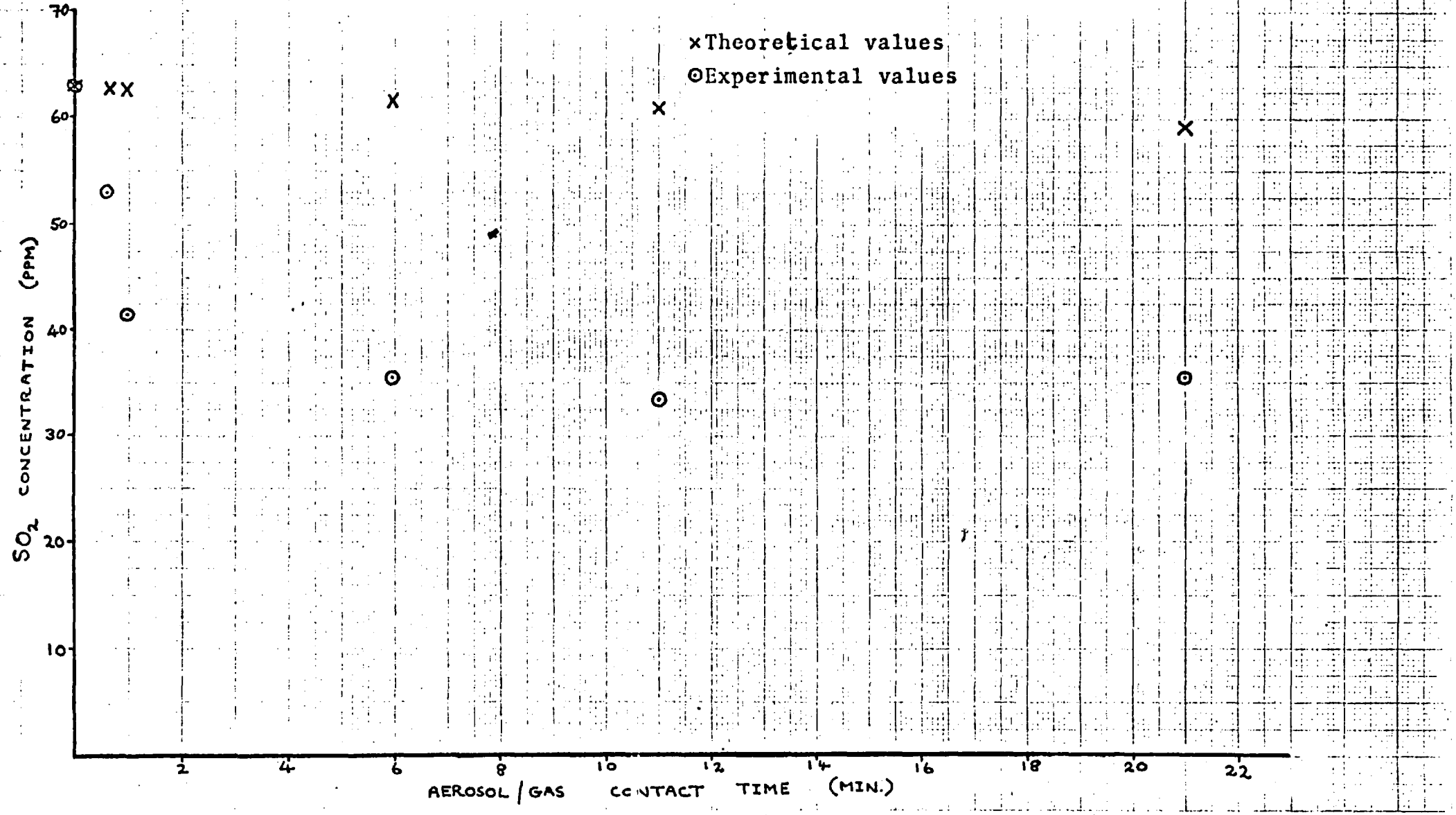

followed by the series of low values, is that the liquid deposited on the sides of the vessels dissolves sulphur dioxide, which may subsequently be oxidised in solution. As noted in Section 5.2 most deposition occurs in the upstream tubes, the region where the decrease in sulphur dioxide concentration is sharpest. The apparent increase in the sulphur dioxide concentration between eleven and twenty-one minutes contact time may be ascribed to experimental error. Examination of the spread of experimental values, as illustrated in Fig. 5-XXXIII, shows that this is the case.

Evidence for the assertion that the deposited liquid accounts for the reduction in sulphur dioxide concentration may be obtained by examining values of the volume fraction of particles in the aerosol. These have been calculated for the case of no dosing stream present, for 3, 13 and 25 reactor tubes, and are tabulated in Table 5-10. These combinations of reactor tubes are the only ones for which reasonably reliable values of both the mass mean diameter and the number concentration are available, as given in Tables 5-7 and 5-5 respectively. The significant decrease in the volume fraction between the 3 and 13 tube cases may be compared with a significant, measurable decrease in the sulphur dioxide concentration. Moreover, the value of the particle volume fraction calculated from the conditions at the generator outlet is 2.34×10^{-2} cm^3 m^{-3}. Thus, the steep initial drop in sulphur dioxide concentration in Fig. 5-XXXIV may be correlated with the apparent extensive loss of particulate matter to the walls of the tubes. By contrast, the loss of material from the stream between 13 and 25 tubes is slight. The experimental data corresponding to these two points effectively show that no measurable change in the sulphur dioxide concentration occurs, which is in agreement with the theoretical predictions.

Discussion of the loss of particulate matter from the system has already been undertaken in Section 5.2. It appears from the results given that it is not possible to monitor accurately the uptake of sulphur dioxide using the method described, and that the most promising method

Table 5-10: Variation of the volume fraction of the aerosol with residence time in the reactor tubes.

No. of tubes used	Mass mean diameter (μm.)	Number concentration ($cm.^{-3}$)	Volume fraction of particles ($cm.^{3}m.^{-3}$)
3	0.29	5.09×10^{5}	6.45×10^{-3}
13	0.33	1.31×10^{5}	2.46×10^{-3}
25	0.35	9.10×10^{4}	2.04×10^{-3}

Table 5-11: Theoretically predicted growth of aerosol particles during reaction.

Reactor tubes used	Modal diameter (μm.)	Mass mean diameter (μm.) (σ_o=0.32)
0	0.200	0.258
S	0.205	0.264
1	0.207	0.267
3	0.217	0.280
7	0.232	0.299
13	0.248	0.320
25	0.270	0.348

is the measurement of the sulphuric acid concentration in the droplets. This, however, has not been attempted here.

Finally, the light scattering results pertaining to the growth of the particles due to formation of sulphuric acid will be discussed. These are presented in Figs. 5-XXI to 5-XXVI and in Table 5-8. The theoretical growth rates obtained by running the particle growth computer programme have been utilised according to equation (3.23) to calculate values of the modal diameter at reaction times corresponding to the use of each combination of reactor tubes. These values, together with values of the mass mean diameter calculated on the basis of a constant spread parameter of 0.32, are given in Table 5-11. It is interesting to note in this case, where the initial particle volume fraction is about 2×10^{-2} cm^3 m^{-3} that the relative values of the reduction in sulphur dioxide concentration and the fractional particle growth are quite different to those obtained in the example of Section 3.3., illustrated in Figs. 3-V to 3-VII, where the initial particle volume fraction is 1.6 cm^3 m^{-3}. The uptake of sulphur dioxide by the aerosol particles is expected to be so low that the loss of sulphur dioxide to the walls of the vessels is unlikely to affect greatly the oxidation rate in the droplets, and the consequent particle growth.

All the pairs of ZOLD parameters obtained from runs 7 to 12 show relatively low modal diameters and high spread parameters when compared with values in Table 5-6. There is also disparity between individual values in most of the tabulated runs. However, the calculated values of the mass mean diameter appear to be relatively consistent, except in cases where obvious error occurs, i.e. where very large modes and small spreads are given. These erroneous values are marked with an asterisk in Table 5-8. Table 5-8 also shows the tendency for the particle size to increase more rapidly than in the coagulation only case discussed in Section 5.2.

In order to compare experimental results with theoretical predictions, the percentage increase in the mass mean diameter with reaction time has

been calculated, for both the theoretical predictions and a selection of results from Table 5-8. The mass mean diameter obtained from the run using the S tube was taken as a standard, and results at higher residence times were calculated as a percentage increase above the standard. The results are given in Table 5-12. It may be seen that, overall, fair agreement exists between the experimental and theoretical growth values. At high residence times the particle size appears to be rather larger than the theory predicts. It would be expected that, if the mechanism of reaction and growth is adequately represented by the scheme proposed in Sections 3.2 and 3.3, the particle size should be larger than predicted to compensate for the effects of coagulation. It may be seen, from Table 5-7, that the percentage growth due to coagulation, occurring between 3 and 25 tubes is of the order of 20%. As explained in Section 3.6 it was not possible to predict the results of the simultaneous coagulation and growth of the aerosol. However, as results in Table 5-12 suggest, (and these only represent a selection of combinations obtainable from Table 5-8) the reaction does lead to substantial particle growth in reasonable agreement with the theory outlined in previous chapters, although precise conclusions are somewhat precluded owing to a lack of knowledge of the behaviour of systems in which coagulation and growth occur simultaneously. A direct comparison of experimental values of the mass mean diameter obtained in the coagulation only and coagulation with growth cases, for 3, 7, 13 and 25 reactor tubes in use, is given in Table 5-13. It may be seen from Tables 5-13 and 5-11 that the effects of growth are likely to show in the values of the ZOLD parameters after residence times corresponding to the use of about 7 to 13 tubes, owing to the limited accuracy of the light scattering technique.

From these values it would appear more logical to ascribe the visible increases in particle size at smaller times to the effects of coagulation. It is not really within the scope of the light scattering method to detect small variations in the modal diameter which would serve to characterise growth in these cases. At large aerosol/gas contact times, the difference is readily apparent and is of an order in agreement

Table 5-12: Comparison of percentage changes in mass mean particle diameter observed from theory with a selection of experimental values.
Percentages refer to percentage growth with respect to particle size obtained in S - tube run.

Source of data/ Diameter using S tube (μm)	Diameter 1 tube		Diameter 3 tubes		Diameter 7 tubes		Diameter 13 tubes		Diameter 25 tubes	
	value (μm)	growth	value (μm)	growth	value (μm)	growth	value (μm)	growth	value (μm)	growth
Theory (table 5-11) 0.264	0.267	1%	0.280	6%	0.299	13%	0.320	21%	0.348	32%
Experiment 7.3 0.248	0.248	0	0.272	9.6%	0.271	9.3%	0.273	10%	0.381	54%
			0.256	3%	0.300	21%	0.370	49%	0.436	76%
Experiment 7.A 0.258	0.248	-3.8%	0.272	5.4%	0.300	16%	0.370	43%	0.381	48%
Experiment 7.1 0.271	0.248	-9.3%	0.272	0	0.300	10%	0.370	36%	0.381	41%

Table 5-13: Direct comparison of mass mean diameters for coagulation only and coagulation with growth.

Reactor tubes	Value for coagulation only	Value for coagulation with growth
3	0.28-0.30 μm.	0.25-0.30 μm.
7	0.31 μm.	0.27-0.30 μm.
13	0.32 μm.	0.37 μm.
25	0.35 μm.	0.38-0.43 μm.

with predictions of the growth from consideration of the chemistry of the system.

It might be expected that the aerosol growth at larger times would slow down owing to the formation of sulphuric acid in the droplets inhibiting the solution of sulphur dioxide and thus decreasing the reaction rate (Section 3.2). The results from runs 11 and 12 indicate that this does not happen to such a degree as to negate the effect of the reaction. (The reason for choosing the apparently least reliable value as representative in run 11 is merely that in other cases the modal diameter is low. In run 10 the highest values are taken as representative. In this case, however, the high values chosen represent the most reliable data sets.) However, the data obtained are not really adequate for quantification of this point, and experiments in bulk solutions appear the simplest way of obtaining accurate data.

Having concluded that the theories of both growth and coagulation fit observed facts reasonably well it is now possible to discuss their relative importance. The coagulation rate is strongly influenced by the number concentration of particles in the aerosol, and the growth due to reaction by the volume fraction of particulate matter. As was noted earlier the particle growth in the experimental system, where the particle volume fraction was low,[4] was much greater than that illustrated in Fig. 3-VII, obtained with a high volume fraction of particles. If the presence of a high volume fraction of particles is incurred by a high number concentration, then it may be assumed that growth due to the reaction may be neglected in comparison with that due to coagulation. If small numbers of large particles are present, giving a large volume of particulate matter, neither coagulation nor growth due to reaction are likely to be appreciable and sedimentation may become significant causing loss of particulate matter. If only a small amount of particulate matter is present, then coagulation is likely to be negligible, and changes in particle size will be determined by the chemical reaction.

5.4. Conclusions

The conclusions of this work will be considered in three groupings; the applicability of the experimental techniques used to the task in hand, the applicability of the theory of chapter 3 to the actual physical situation, and the extension of results to practical situations.

(i) The applicability of the experimental techniques used to the task in hand.

The thermal precipitation/electron microscopy technique of examining the particle nuclei appears satisfactory in so far as it gives particulate deposits of a form predictable from the known amorphous nature of the manganous sulphate hydrate which is stable under sampling conditions. However, this technique suffers from difficulties in particle sizing and counting. These could be overcome by the use of instruments capable of detecting and sizing very small images on a photographic plate. The images would need to be small, since plates would have to be taken at low magnification to ensure the inclusion of an adequate number of particles on a reasonable area of plate. The inadequate sample size is believed to account for much of the error and inconsistency found in results obtained using this technique.

The light scattering technique appears to have produced the best and most reliable experimental results in this work, despite the shortcomings described in Sections 2.5 and 5.1(c). A certain amount of selectivity was involved in comparing results obtained by this technique. However, it is felt that this is justified owing to the tendency of the data inversion calculation to locate erroneous results where a reduced number of light scattering data points are given, as was demonstrated in Section 2.5. The problems necessitating the rejection of the most forward-scattered readings can only really be solved if a more monodisperse aerosol is used, or an alternative to the flow system is devised.

The method of measuring sulphur dioxide concentration is clearly unsuitable for this work. If no absorption into the liquid on the walls of the apparatus had taken place, it would be required to measure sulphur dioxide concentrations around 60 ppm. with an accuracy of about 1 ppm.

for the conditions under which experiments took place. The fact that loss of sulphur dioxide from the system did take place, apparently due to the presence of liquid on the walls of the apparatus, renders any measurement of ambient sulphur dioxide concentration somewhat precarious. As mentioned in Section 5.3, it would appear more fruitful to develop a method of collecting particles e.g. by cascade impaction or electrostatic precipitation, and analysing for sulphuric acid in the liquid phase, if it is required to monitor the uptake of sulphur dioxide by the aerosol.

Another feature that would serve to make results more reliable is the imposition of strict temperature control. During the course of the experimentation the laboratory temperature was monitored, and was rarely found to deviate from 21°C at times when measurements were being taken. The bulkiness of the apparatus prevented the use of normal constant temperature devices, and would necessitate the use of a large enclosure.

(ii) The applicability of the theories of chapter 3 to the actual physical situation.

The light scattering results presented in Section 5.2 (no sulphur dioxide present) show good agreement with predictions from the theory of Brownian coagulation, except at large residence times when the particle number concentration was found to be considerably lower than its predicted value. In this situation, the measured value of the mass mean diameter is lower than the predicted value, as would be expected. No definite explanation of the loss of particulate matter from the system could be found, but it is suspected that this may be due to inadequate temperature control of the high humidity environment, as suggested in Section 5.2.

Although it is difficult to obtain any information from the sulphur dioxide measurements, the trend of results for larger reaction times leads to the conclusion that the uptake rate of sulphur dioxide in the downstream part of the system, where deposition of matter is slight, is of comparable order with that predicted by the theory. The disparity between experiment and theory appears to be mainly due to the absorption of sulphur dioxide in the liquid deposited in the upstream part of the apparatus. Measure-

ments of particle size in the presence of reacting gas indicate that little effect occurs at small contact times, but a marked increase may be observed at large contact times. Again, this is in agreement with the theory, given the accuracy to which the particle size parameters may be measured by the light scattering method. The magnitudes of the observed particle size increases at larger aerosol/gas contact times are also roughly in agreement with theoretical predictions.

Thus, by way of recapitulation, the following characteristics of the aerosol/gas system appear to hold true.

(a) The growth of particles due to reaction, and consequent displacement of the concentration/humidity equilibrium, is reaction rate controlled, the diffusional processes inside the particles occurring relatively rapidly.

(b) The reaction rate in the droplets is predictable using the mechanism given in Section 3.2, with the rate constants of Table 3-2 (second column of values).

(c) The relative importance of growth, due to the reaction, and coagulation in the aerosol/gas system depends on the relative amounts of particulate matter and sulphur dioxide in the system. If the particle volume fraction is relatively low, growth is appreciable. If the particle number concentration is high, coagulation becomes important.

(d) The coagulation process appears to take place as predicted from the theory of Brownian coagulation. Other factors affecting coagulation, such as the presence of surface charges, appear to be relatively unimportant.

(e) The loss of particulate matter from the system is considerably greater than that predicted by the sedimentation equation.

(iii) Extension of results to practical situations.

It has already been pointed out that, in order for sulphur dioxide to be oxidised by solutions of transition metal salts in aerosol form, a high ambient humidity must be present. An effluent plume is likely to satisfy the three conditions of high humidity, appreciable sulphur dioxide concentration, and the presence of particles of transition metal salts.

Foster (31) has noted that sulphur dioxide concentrations of around 2.5×10^3 ppm. are typically present in effluent plumes. As stated in chapter 1, sulphuric acid aerosol has been observed in areas where high concentrations of sulphur dioxide have been present, presumably due to the catalytic oxidation of sulphur dioxide in aerosol particles present.

This work deals with one such reaction, and it may be seen that sulphuric acid concentrations of the order of 1-2 m.mol.cm^{-3} may be attained after a contact time of a half-hour. This is obviously a special case, highly unlikely to occur in nature, with pure reactants being used. However, it has been noted that other metal ions, e.g. Fe^{2+}, Cu^{2+}, and vanadium compounds catalyse the oxidation reaction. Although the effects of these catalysts are weaker than that of manganese (with the possible exception of vanadium!) they may still lead to appreciable concentrations of sulphuric acid in aerosol form.

5.5. Suggestions for Further Work

In this short section, topics for further research, arising out of this project will be enumerated. It is emphasised that these are merely suggestions of avenues which may be investigated and that no feasibility studies concerning them have been carried out by the author of this work.

1. It appears that no quantitative experimental work has been carried out on the relationship between particle size and ambient relative humidity of aerosols of salt solutions. This is presumably due to the difficulties in controlling the very humid environments involved. The development of such a system could lead to the further testing of the fast diffusion theory by the introduction of perturbations in the humidity of the environment and the subsequent measurement of droplet size.

2. Catalysis of the oxidation of sulphur dioxide to sulphuric acid in aerosols of solutions of salts of other transition metals, e.g. Fe^{2+}, Cu^{2+}, could be investigated. These metals are more likely to be present in polluted environments than manganese. Naturally, the slower reaction rate will require a somewhat different experimental design to the one employed here. Experiments in bulk solution may also be necessary to obtain kinetic data for the reaction systems.

3. As indicated in Section 3.6, the theory of simultaneous coagulation and growth is still relatively underdeveloped. A numerical approach to the solution of equation (3.36) needs to be rather more sophisticated than the one attempted in this work.

4. A development of the light scattering method, such that data at forward-scattering angles may be obtained, would be very useful. A method of attaining this would be to substitute a batch sampler for the flow system, coupled with a shortening of the scanning time required by the light scattering apparatus. However, before any such scheme is developed, a check should be carried out of the extent to which Brownian motion of the particulate material contributes to the noise at forward-scattering angles.

REFERENCES

1. Arendt, P. ; Kallmann, H.
Z. Phys. 35 421 (1926)
2. Astakhov, A. Dokl. Akad, Nauk. SSSR.
161 1114 (1965)
3. Axelrod, H. D. ; Pate, J. B. ; Barchet, W. R.
Lodge, J. P. Jr. Atmos. Env. 4 209 (1970)
4. Basset, H. ; Parker, W, G.
J. Chem. Soc. (1951 - II) 1540
5. Born, M. ; Wolf, E. Principles of Optics
Pitman Press (1959)
6. Brock, J. R. J. Coll. Sci. 18 489 (1963)
7. Byers, R. L. ; Davis,J. W.
J. Air. Poll. Contr. Assoc. 20 236 (1970)
8. Carabine, M. D. Chem. Soc. Rev. 1 411 (1972)
9. Carabine, M. D. ; Moore, A. P.
Farad. Symp. Chem. Soc. No. 7
'Fogs & Smokes' p.176 (1973)
10. Cawood, W. ; Whytlaw-Gray, R.
Trans. Farad. Soc. 32 1059 (1936)
11. Chandrasekhar, S. Rev. Mod. Phys. 15 1 (1943)
12. Chapman, H. M. Amer. Medic. Assoc. Arch. Ind. Hyg.
& Occ. Medic. 8 234 (1953)
13. Clark, W. E. ; Whitby, T. K.
J. Atmos. Sci. 24 677 (1967)
14. Copson, R.L. ; Payne, J. W.
Ind. Engg. Chem. 25 909 (1933)
15. Coste, J. H. ; Courtier, J.B.
Trans. Farad, Soc. 32 1198 (1936)
16. Coughanowr, D. R. ; Krause, F. E.
Ind. Engg. Chem. Fund. 4 61 (1965)
17. Coutarel, L. ; Matijević, E. ; Kerker, M. ; Huang, C. M.
J. Coll. Int. Sci. 24 338 (1967)
18. Cunningham, E. Proc. Roy. Soc. Lond.
83A 357 (1910)
19. Dallavalle, J. M. ; Micromeritics
Pitman Publishing (1943)

20. Dautreband, L. Z. Aerosol-Forsch. u. Therapie 2 585 (1953)
21. Dautreband, L. ; Beckmann, H. ; Walkenhorst, W. Arch. Int. Pharmocodyn. et de Thérapie 116 170 (1958)
22. Dautreband, L. ; Highman, B. ; Alford, W. C. ; Weaver, F. L. Arch. Int. Pharmocodyn. et de Thérapie 76 247 (1948)
23. Davies, C. N. Proc. Phys. Soc. (Lond.) 17 259 (1945)
24. Davies, C. N. Aerosol Science Academic Press (1966)
25. Devir (Weinstock), S. E. J. Coll. Int. Sci. 23 80 (1967)
26. Deželić, G. ; Kratohvil, J. P. J. Coll. Sci. 16 561 (1961)
27. Drummond, D. G. (ed.) J. Roy. Micr. Soc. 70 Ch. 4 (1950)
28. Dunning, W. J. The Physical Chemistry of Aerosols (A General Discussion of the Faraday Society) p.9 (1960)
29. Espenscheid, W. F. ; Kerker, M. ; Matijevic, E. J. Phys. Chem. 68 3093 (1964)
30. Firket, J. Trans. Farad. Soc. 32 1192 (1936)
31. Foster, P. M. Atmos. Env. 3 157 (1969)
32. Fraser, D. A. J. Am. Ind. Hyg. Assoc. Quart. 17 75 (1956)
33. Friedlander, S.K. J. Meteor. 17 479 (1960)
34. Friedlander, S.K. J. Meteor. 18 753 (1961)
35. Friedlander, S.K. ; Wang, C. S. J. Coll. Int. Sci. 22 126 (1966)
36. Fuchs, N. A. Z. Phys. 89 736 (1934)

37. Fuchs, N. A. The Mechanics of Aerosols
Academy of Sciences of the USSR.
Institute of Information (1955)
Translated from Russian by MSP. E.
Lachowitz, US Army Chemical Warfare
Laboratories (1958)
38. Fuchs, N. A. Evaporation & Droplet Growth in
Gaseous Media. Pergamon (1959)
39. Fuchs, N. A. ; Sutugin, A. G.
J. Coll. Sci. 20 492 (1965)
40. Gerhard, E. R. ; Johnstone, H. F.
Ind. Engg. Chem. 47 972 (1955)
41. Gillespie, T. Proc. Roy. Soc. (Lond.)
A216 569 (1953)
42. Gillespie, T. J. Coll. Sci. 18 562 (1963)
43. Gmelin. Gmelins Handbuch der Anorganischen Chemie.
8te. Auflage. 'Schwefel'. Teil B, Lieferung 3.
Verlag Chemie, GMBH. Weinheim/Bergstr. (1963)
pp. 1444-1456,1388-1392
44. Green, H. L. ; Lane, W. Particulate Clouds
2nd. Ed. E. Spon, Ltd. London (1964)
45. Green, H. L. ; Watson, H. H. Physical Methods for
the Estimation of the Dust Hazard in
Industry (with Special Reference to the
Occupation of the Stonemason) Ch.III.
The Hot Wire Thermal Precipitator.
Medical Research Council Special Report
No. 199 (1935)
46. Grodzovskij, M. K. Žurnal fiz. chim. (SSSR)
6 478 (1935)
Results given in (43)
47. Hamaker, H. C. Physica 4 1058 (1937)
48. Herdan, G. Small Particle Statistics
New York (Elsevier) (1953)
49. Hidy, G. M. J. Coll Sci. 20 123 (1965)

50. Hidy, G. M. ; Brock, J. R.
J. Coll. Sci. 20 477 (1965)
51. Hidy, G. M. ; Brock, J. R. The Dynamics of
Aerocolloidal Systems
Pergamon Press (1970)
52. Hidy, G. M. ; Brock, J. R. (ed.)
Topics in Current Aerosol Research
(Part 2). Pergamon Press (1972)
53. Hidy, G. M. ; Lilly, D. K.
J. Coll. Sci. 20 867 (1965)
54. Hoather, R. C. ; Goodeve, C. F.
Trans. Farad. Soc. 30 1149 (1934)
55. Huang, C. M. ; Kerker, M. ; Matijević, E. ;
J. Coll. Int. Sci. 33 529 (1970)
56. Hulst, Van de, H. C. Light Scattering by Small
Particles. Chapman & Hall (1957)
57. Johnstone, H. F. Ind. Engg. Chem. 23 559 (1931)
58. Johnstone, H. F. ; Coughanowr, D. R.
Ind. Engg. Chem. 50 1169 (1958)
59. Johnstone, H. F. ; Leppla, P. W.
J. Am. Chem. Soc. 56 2233 (1934)
60. Johnstone, H. F. ; Moll, A. J.
Ind. Engg. Chem. 52 861 (1960)
61. Junge, C. E. Ann. Meteor. 5 Beih. (1952)
62. Junge, C. E. Tellus 5 1 (1953)
63. Junge, C. E. J. Meteor. 12 13 (1955)
64. Junge, C. E. Atmospheric Chemistry. Advances in
Geophysics 4 pp.1-101.
Landsberg, H. E. & Van Miegham, J. (ed.)
(1958)
65. Junge, C. E. J. Atmos. Sci. 26 603 (1969)
66. Kaštanov, L. I. ; Guljanskaja, C. A.
Žurnal. obščej. chim.(SSSR)
6 227 (1936)
Results given in (43)

67. Kaštanov, L. I. ; Ryžov, V. P.
Žurnal. chim. Promyšlennosti (SSSR)
13 1225 (1936)
Results given in (43)
68. Kay, D. H. (ed.) Techniques for Electron Microscopy.
2nd. Ed. Alden Press (1965)
69. Kerker, M. The Scattering of Light and Other
Electromagnetic Radiation.
Academic Press (1969)
70. Kerker, M. ; Daby, E. ; Cohen, G. I. ; Kratohvil, J. P. ;
Matijević, E. J. Phys. Chem. 67 2105 (1963)
71. Knudsen, M. ; Weber, S. Ann. Phys. 36 981 (1911)
72. Köhler, H. Trans. Farad. Soc. 32 1152 (1936)
73. Kruyt, H. R. (ed.) Colloid Science Vol. I.
Elsevier Publishing Co. (1952)
74. Kunkel, W. B. J. App. Phys. 21 833 (1950)
75. Lai, F. S. ; Friedlander, S. K. ; Pich, J. ; Hidy, G. M.
J. Coll. Int. Sci. 39 395 (1972)
76. Low, R. D. H. J. Atmos. Sci. 26 608 (1969)
77. Maddock, J. E. L. Light Scattering by Ammonium
Chloride Aerosols
M.Sc. Thesis. Univ. London (1970)
78. Maddock, J. E. L. A Light Scattering Study of Growth
of Sulphuric Acid Particles.
Ph.D. Thesis. Univ. London (1974)
79. Maron, S. H. ; Elder, M. E.
J. Coll. Sci. 18 107 (1963)
80. Maron, S. H. ; Elder, M. E.
J. Coll. Sci. 18 199 (1963)
81. Maron, S. H. ; Pierce, P. E.
Am. Chem. Soc. Div. Polymer Chem. Preprints
7 733 (1966)
82. Maron, S. H. ; Pierce, P. E. ; Elder, M. E.
J. Coll. Sci. 18 391 (1963)

83. Martynov, G. A. ; Bakanov, S. P.
Solution of the Kinetic Equation for Coagulation. In Deryagin, B. V. (ed.) Research in Surface Forces. Translation by the Consultants Bureau, New York. Vol.I. p.182 (1963)

84. Mason, B. J. The Physics of Clouds Clarendon Press (1957)

85. Mason, B. J. The Physical Chemistry of Aerosols (A General Discussion of the Faraday Society) p.20 (1960)

86. Matteson, M. J. ; Stöber, W. J. Coll. Int. Sci. 23 203 (1967)

87. Matteson, M. J. ; Stöber, W. ; Luther, H. Ind. Engg. Chem. Fund. 8 677 (1969)

88. Mellor, J. W. (ed.) A Comprehensive Treatise on Inorganic & Theoretical Chemistry Vol.XII,pp.401-404 (1932)

89. Melzak, J. A. Quart. J. App. Math. 11 231 (1953)

90. Mie, G. Ann. Phys. 25 377 (1908)

91. Millikan, R. A. Phys. Rev. 22 1 (1923)

92. Mockros, L. F. ; Quon, J. E. ; Hjelmfelt, A. T. Jr. J. Coll. Int. Sci. 23 90 (1967)

93. Moffat, A. J. ; Millan, M. M. Atmos. Env. 5 677 (1971)

94. Moffat, A. J. ; Robbins, J. R. ; Barringer, A. R. Atmos. Env. 5 551 (1971)

95. Montgomery, D. W. Rubber Age 94 759 (1964)

96. Moore, A. P. A Light Scattering Study of the Kinetic Size Distribution Changes of Aerosols. Ph.D. Thesis. Univ. London. (1974)

97. Müller. H. Kolloid-Z. 38 1 (1926)

98. Müller, H. Kolloidchem. Beih. 26 257 (1928)

99. Müller, H. Kolloidchem. Beih. 27 223 (1928)

100. Mc. Donald, J. E. J. Meteor. 10 68 (1953)
101. Nakagaki, M. ; Shimoyama, T.
Bull. Chem. Soc. Japan 37 1634 (1964)
102. Nicolaon, G. A. ; Kerker, M.
Farad. Symp. Chem. Soc.
'Fogs & Smokes' p.133 (1973)
103. Nicolaon, G. A. ; Kerker, M. ; Cooke, D.D. ;
Matijević, E.
J. Coll. Int. Sci. 38 460 (1972)
104. Orr, C. Particulate Technology.
Mc. Millan Co. New York (1966)
105. Orr, C. ; Dallavalle, J. M. Fine Particle
Measurement. Size, Surface, & Pore Volume.
Mc. Millan Co. New York (1959)
106. Orr, C. ; Hurd, K. H. ; Hendrix, W. P. ; Junge, C. E.
J. Meteor. 15 240 (1958)
107. Patterson, H. S. ; Cawood, W.
Proc. Roy. Soc. Lond. A136 538 (1932)
108. Pich, J. ; Friedlander, S. K. ; Lai, F. S.
J. Aerosol Sci. 1 115 (1970)
109. Quon, J. E. ; Mockros, L.F.
Int. J. Air. Wat. Poll. 9 279 (1965)
110. Rayleigh, Lord. Phil. Mag. 12 81 (1881)
111. Reiss, H. J. Chem. Phys. 19 482 (1951)
112. Reiss, H. ; La Mer, V. K.
J. Chem. Phys. 18 1 (1950)
113. Robinson, R. A. ; Stokes, R. H.
Electrolyte Solutions
Butterworth (1959)
114. Sachsse, H. Ann. Phys. 14 396 (1932)
115. Schmauss, A. Meteor. Z. 36 11 (1919)
116. Schmitt, K. H. ; Waldmann, L.
Z. Naturforsch. 15a 843 (1960)
117. Schumann, T. E. W.
Quart, J. Roy. Meteor. Soc. 66 195 (1940)

118. Scott, W. T. J. Atmos Sci. 25 54 (1968)
119. Sedunov, Yu. S. Physics of Drop Formation in the Atmosphere.
Halstead Press (Wiley) (1974)
120. Sherril, M. S. ; Noyes, A. A.
J. Am. Chem. Soc. 48 1861 (1926)
121. Smoluchowski, M. v. Phys. Z. 17 557,585 (1916)
122. Smoluchowski, M. v. Z. Phys. Chem. (Leipzig)
92 129 (1918)
123. Swift, D. L. ; Friedlander, S. K.
J. Coll. Sci. 19 621 (1964)
124. Vasil'ev, S. S. ; Kaštanov, L. I. ; Kastoraskaja, T. L.
Acta. Physicochim. (SSSR) 3 413 (1935)
Results given in (43)
125. Vorha, K. G. ; Nair, P. V. N.
J. Aerosol Sci. 1 127 (1970)
126. Wadden, R. A. A Model of a Growing, Coagulating Aerosol.
Ph.D. Thesis. Northwestern Univ.
(1972)
127. Wadden, R. A. ; Quon, J. E. ; Hulbert, H. M.
Atmos. Env. 8 1009 (1974)
128. Walkenhorst, W. Staub 22 103 (1962)
129. Walkenhorst, W. ; Dautreband, L.
Staub 24 505 (1964)
130. Wallace, T. P. ; Kratohvil, J. P.
J. Polymer Sci. B5 1139 (1967)
131. Walton, W. H. The Application of Electron Microscopy to Particle Size Measurement.
Inst. Chem. Eng. & Soc. Chem. Ind. Symp. on Particle Size Analysis p.64 (1947)
132. Wang, C. S. ; Friedlander, S. K.
J. Coll. Int. Sci. 24 170 (1967)
133. Watson, H. H. Brit. J. App. Phys. 9 78 (1958)
134. Whytlaw-Gray, R. ; Patterson, H. S.
Smoke: A Study of Aerial Disperse Systems
Edward Arnold & Co. (London) (1932)

135. Wiegner, G. ; Tuorila, P.
Kolloid-Z. 38 3 (1926)
136. Williams, D. T. ; Kolitz, B. L.
Appl. Optic. 7 607 (1968)
137. Willis, E. ; Kerker, M. ; Matijević, E.
J. Coll. Int. Sci. 23 182 (1967)
138. Wohlers, H. C. ; Trieff, N.M. ; Newstein, H.
Stevens, W.
Atmos. Env. 1 121 (1967)
139. Zebel, G. Kolloid-Z. 157 37 (1958)

APPENDIX

Calculation of the Equilibrium Vapour Pressure of Solutions of Manganous Sulphate and Sulphuric Acid

According to Low (76), the vapour pressure p over a solution containing an electrolyte, or a mixture of electrolytes, is given by the following form of Raoult's Law:-

$$\frac{p}{p_o} = a_w \qquad (A.1)$$

where p_o is the saturated vapour pressure of pure water at the same temperature and pressure, and

a_w is the water activity of the solution.

McDonald (100) calculated a_w by using empirical Vant Hoff factors for sodium chloride solutions. Low (76), however, has approached the problem in terms of the mean ionic activity coefficients of the dissolved species involved. For a single electrolyte

$$a_w = \exp\left[-w m \nu \Phi\right] \qquad (A.2)$$

where m is the stoichiometric molality of the electrolyte.

$\nu = \nu_+ + \nu_-$ is the total number of moles of ions obtainable from one mole of electrolyte.

$w = (55.51)^{-1}$

Φ is the practical osmotic coefficient of the solution, defined by

$$\Phi = 1 + \frac{\gamma(m)}{m}$$

$$\gamma(m) = \int_1^{\gamma_\pm} m \, d(\ln \gamma_\pm) \qquad (A.3)$$

where $\gamma_\pm$ is the mean ionic activity coefficient of the electrolyte solution.

Thus, if values of $\gamma_\pm$ or Φ are known, it is possible, in principle, to evaluate the water activity of the solution at a given concentration (molality) using equations (A.2) and (A.3). These quantities are

tabulated by Robinson and Stokes (113) for the species considered in this work, i.e. manganous sulphate and sulphuric acid.

In order to obtain interpolated values of Φ, it was necessary to fit one of the tabulated quantities, $\gamma_\pm$ or Φ, to an analytical function of concentration. The quantity chosen for this purpose was $\gamma_\pm$, the mean ionic activity coefficient of the electrolyte under consideration, and the procedure was as follows. The mean ionic activity coefficient used above, defined in terms of solution molality, is related to the rational mean ionic activity coefficient, $f_\pm$, as (113)

$$f_\pm = \gamma_\pm \left[1 + 10^{-3} \nu M m\right] \quad . \quad . \quad . \quad (A.4)$$

where M is the molecular weight of the solvent.

Thus, if the solution is not too concentrated, i.e. m is fairly small, $f_\pm$ may be taken as equal to $\gamma_\pm$.

Now the Debye-Hückel formula for $f_\pm$ is

$$\log_{10} f_\pm = \frac{-A|z_1 z_2|\sqrt{I}}{1 + Ba\sqrt{I}} \quad . \quad . \quad . \quad (A.5)$$

where z_i is the algebraic valency of the ion i. For cations $i = 1$.
For anions $i = 2$.

I is the ionic strength of the solution

$$I = \sum_i \left[c_i z_i^2\right] \quad . \quad . \quad . \quad (A.6)$$

c_i is the concentration of species i in moles per unit volume of solution (molarity)

a is the mean diameter of the ions

A, B are constants, which are functions of temperature and the dielectric constant of the solvent medium. For water at 25°C (113)

$A = 5.115 \times 10^{-1}$ cm$^{3/2}$ m.mol$^{-\frac{1}{2}}$ K$^{3/2}$

$B = 3.291 \times 10^{7}$ cm$^{\frac{1}{2}}$ m.mol$^{-\frac{1}{2}}$ K$^{\frac{1}{2}}$

In equation (A.5) the numerator gives the effect of the long-range coulomb forces between the ions, while the denominator shows how these are modified by short-range interactions, represented in the crudest

possible model, taking the ions to be non-deformable spheres of equal radii. In any real solution there will also be short-range interactions between ions and solvent molecules to consider, as well as short-range interactions between ions which cannot be represented by the fixed-spheres model. Robinson and Stokes (113) have asserted that these are likely to be of a type giving an approximately linear variation of $\log_{10} f_{\pm}$ with concentration. Hence, it should be possible to include them, in a highly empirical fashion, by adding to the right-hand side of equation (A.5) a term linear in concentration (113), viz.

$$\log_{10} f_{\pm} = \frac{-A|z_1 z_2|\sqrt{I}}{1 + Ba\sqrt{I}} + bI \qquad \cdot \quad (A.7)$$

Equations of this type are normally capable of fitting experimental data reasonably up to at least 1 molal solutions. More terms may be added, containing higher powers of I, for higher concentrations. Finally, if $\gamma_{\pm} (= f_{\pm})$ is given by an equation of the form of (A.7), then, from equation (A.3) (113)

$$1 - \Phi = \frac{A'|z_1 z_2|\sqrt{\sum_i z_i^2}\sqrt{m}}{3} f\left\{ Ba\sqrt{\sum_i z_i^2}\sqrt{m} \right\} - \frac{1}{2} b \sum_i z_i^2 \cdot m \qquad \cdot \quad (A.8)$$

where $A' = A \ln 10$

and

$$f(x) = \frac{3}{x^3}\left[(1+x) - 2\ln(1+x) - \frac{1}{1+x}\right]$$

Thus, using tabulated data (113), values of the parameters a and b of equation (A.7) were obtained by numerically fitting this data to the equation, using a least-squares method to obtain an optimum fit. Values of Φ were then calculated using equation (A.8), and compared with published values. It was assumed that $f_{\pm} \approx \gamma_{\pm}$ and $m_i \approx c_i$; both of these approximations are justified provided the solutions do not become too concentrated. The least squares estimates of a and b for each

solute are given below:-

Manganous sulphate: Data for m = 0.1 to 2 m.mol. cm^{-3} fitted.

$$a = 3.837 \times 10^{-8}, \quad b = -1.630 \times 10^{-2}$$

Sulphuric Acid: Data for m = 0.1 to 5 m.mol. cm^{-3} fitted.

$$a = 1.825 \times 10^{-8}, \quad b = 4.828 \times 10^{-2}$$

For manganous sulphate, the maximum percentage error between the fitted values of $\gamma_{\pm}$ and the actual tabulated values was 9%. This occurred at m = 0.1 m.mol. cm^{-3}. The error in the predicted value of the osmotic coefficient Φ reached a maximum of 16.5% at m = 0.7 to 0.8 m.mol. cm^{-3}. For sulphuric acid, the maximum percentage error in the prediction of $\gamma_{\pm}$ was 11.5%, which occurred at m = 0.1 m.mol. cm^{-3}.

The error decreased rapidly from m = 0.1 m.mol. cm^{-3} to m = 0.3 m.mol. cm^{-3}, and, for solution molarities above 0.5 m.mol. cm^{-3}, dropped to under 2%. The maximum error for Φ was just under 8%, occurring at m = 0.5 m.mol. cm^{-3}. Values of Φ outside the molarity range of 0.2 to 2 m.mol. cm^{-3} fitted with errors of less than 1%.

The theory of solutions of mixed electrolytes is rather more complex than that for single components (113). Also, no published data appears to be available on the activity coefficients of solutions containing manganous sulphate and sulphuric acid together. Consequently, it was decided to approximate the combined effects by multiplying together the water activities that would be obtained if each electrolyte is considered as being the only solute in solution. The procedure is consistent with the form of the Gibbs-Duhem equation used by Low (76) to derive equation (A.2). It should be noted, however, that the presence of a second electrolyte affects relationships such as equation (A.4), in that the correction term must be summed over all electrolytes present. This tightens the constraint that the solutions must be fairly dilute for it to be valid to assume that $f_{\pm} \approx \gamma_{\pm}$